Harmonic Optimization of different Distributed Generation (DG) units connected to Micro grid

Thesis Submitted By

Krishna Sarker

Doctor of Philosophy (Engineering)

Department of Electrical Engineering

Faculty Council of Engineering and Technology

Jadavpur University

Kolkata, India

2019

Index No. 298/14/E

1. Title of the thesis

Harmonic Optimization of different Distributed Generation (DG) units connected to Micro grid

2. Name Designation & Institution of Supervisor/s

Prof. Debashis Chatterjee

Electrical Engineering Department
Jadavpur University
Kolkata-700032, West Bengal, India

Prof. Swapan Kumar Goswami

Electrical Engineering Department
Jadavpur University
Kolkata-700032, West Bengal, India

3. List of Research International Journal Publication

(i) Krishna Sarker, Debashis Chatterjee, S. K. Goswami. An optimized co-ordinated approach for harmonic minimization of Doubly Fed Induction Generator connected micro-grid system. International Journal of Electrical Power &Energy Systems, Elsevier, vol. 64, pages 58-70, January 2015.

(ii) Krishna Sarker, Debashis Chatterjee, S. K. Goswami. Grid integration of photovoltaic and wind based hybrid distributed generation system with low harmonic injection and power quality improvement using biogeography-based optimization, Renewable Energy Focus, Elsevier, Volume 22, pages 38-56, Publication date 2017/12.

(iii) Krishna Sarker, Debashis Chatterjee, S. K. Goswami. A Modified Harmonic Minimization Technique for Doubly Fed Induction Generators with Solar-wind Hybrid System using Biogeography-based Optimization, IET Power Electronics, Issue ISSN 1755-4543, DOI: 10.1049/iet-pel.2017.0818, pages 58-70, Publication date 2018/3/23.

List of Communicated/ to be communicated International Journal

(i) Krishna Sarker, Debashis Chatterjee, S. K. Goswami. A Modified PV-Wind-PEMFCS Based Hybrid UPQC System with Combined DVR/STATCOM Operation by Harmonic Compensation. International Journal of Modelling and Simulation, Taylor and Francis.

(ii) Krishna Sarker, Debashis Chatterjee, S. K. Goswami. BBO-Based Multilevel Inverter for Photovoltaic-Fed Dynamic Voltage Restorer. Electrical Engineering, Springer Publishers.

(iii) Sayan Paramanik, Krishna Sarker, Jayanti Sarker, Debashis Chatterjee, S. K. Goswami. Grid Integration and Power Quality Improvement of Smart Grid. IEEE, Smart Grid.

4. *List of Patents:* Nil

5. *International Conference Publication*

(i) Sayan Paramanik, Krishna Sarker, Debashis Chatterjee, S. K. Goswami. Smart Grid Power Quality Improvement Using Modified UPQC. 3rd international conference,"2019 Devices for Integrated Circuit" DevIC 2019.

(ii) Sayan Paramanik, Krishna Sarker, Biswajit Mahantty, Avijit Chakraborty, Debashis Chatterjee, S. K. Goswami. Smart Wireless Distribution for Micro Grid System. 3rd international conference,"2019 Devices for Integrated Circuit" DevIC 2019.

CERTIFICATE FROM THE SUPERVISOR/S

This is to certify that the thesis entitled "**Harmonic Optimization of different Distributed Generation (DG) units connected to Micro grid**" submitted by **Mr. Krishna Sarker**, who got his name registered on 2nd May, 2014 for the award of Ph.D. (**Doctor of Philosophy in Engineering**) degree of **Jadavpur University** is absolutely based upon his own work under the supervision of **Prof. Debashis Chatterjee** and **Prof. Swapan Kumar Goswami** and that neither his thesis nor any part of the thesis has been submitted for any degree/diploma or any other academic award anywhere before.

Prof. Debashis Chatterjee
(debashisju@yahoo.co.in)
Supervisor
Department of Electrical Engineering
Jadavpur University
Kolkata-700032, West Bengal, India

Prof. Swapan Kumar Goswami
(skgoswami_ju@yahoo.co.in)
Supervisor
Department of Electrical Engineering
Jadavpur University
Kolkata-700032, West Bengal, India

Prof. (Dr.) Sakti Prasad Ray
(spray1949@gmail.com)
External Examiner
Department of Electrical Engineering
IIEST, Shibpur
Kolkata-711103, West Bengal, India

DEDICATION

I wish to dedicate this thesis to my parents, Mr. Binay Sarker and Ms. Nisha Sarker. Their unending love, support, and continuous guidance made the completion of this thesis possible. I want to extend my deepest thanks and appreciation to my wife Ms. Jayanti Sarker (Bhattacharjee). Also thanks my family members Dilip Sarker, Sailesh Sarker, Kamana Sarker and others for their never-ending support and kindness.

ACKNOWLEDGEMENTS

I would like to express my sincere gratitude to my supervisor Prof. Debashis Chatterjeeand, Prof. Swapan Kumar Goswami, for their guidance, encouragement, and support throughout the course of this work. It was a precious learning experience for me and I am proud to be one of their students. In fact, their backbone to my research carrier. From strong support of supervisors, I have gained not only extensive knowledge, but also careful research thoughts.

I extend my appreciation to the Head of the Department of Electrical Engineering for providing me with the necessary infrastructures to complete my research work. Also, I am indebted to him who provided me all official and laboratory facilities.

I am grateful to my Doctoral Scrutiny Members, Prof. Samarjit Sengupta, Prof. S. Paul, Dr. A. Das, and Dr. Sunita Halder nee Dey, for their valuable suggestions and comments during this research period.I also thank the other members of the Department of Electrical Engineering and all the fellow research scholars of Power System Simulation Laboratory and Electric Drives Laboratory of the Department of Electrical Engineering for their helpful advice, encouragement, continuous support and creating a friendly atmosphere.

I am especially indebted to my colleagues in the power electronics and power system group. I would like to specially thank Mr. Avijit Chakraborty, who helped me in implementing my real time experiments. We share each other a lot of knowledge in the field of power electronics and power system. I would also thank my beloved wife Jayanti Sarker (Bhattacharjee) for his valuable thoughts in my research carrier. I would also like to thank my beloved Mr. Arunava Chatterjee, the other members of the team, Mr. Shibaji Chatterjee, Mr.Sajib Chakraborty, for extending their technical and personal support making my stay pleasant and enjoyable.

This section would remain incomplete if I don't thank all the lab assistants of JU and SMIT, without whom the work would have not progressed. I would like to thank my student Mr. Sayan Paramanik for helping me. Lastly, with the deepest love, I would be grateful to my beloved Father, Mother, and all my families who supported and encouraged me all the time, no matter what difficulties are encountered.

Krishna Sarker Date:

Declaration

I hereby declare that the work which is being presented in the thesis entitled "**Harmonic Optimization of different Distributed Generation (DG) units connected to Micro grid**" in partial fulfillment of the requirements for the award of the degree of ***DOCTOR OF PHILOSOPHY*** (Ph.D) submitted to the Department of Electrical Engineering of **Jadavpur University, Kolkata**, **India** is an authentic record of my own work under the supervision of **Prof. Debashis Chatterjee** and **Prof. Swapan Kumar Goswami**, Department of Electrical Engineering. I have not submitted the matter embodied in this thesis for the award of any other degree or diploma of the university or any other institute.

_____

Krishna Sarker Date:

Harmonic Optimization of different Distributed Generation (DG) units connected to Micro grid

Table of Contents

List of Abbreviations

Abbreviations	Full Form
AC	Alternating Current
APF	Active power filters
BBO	Biogeography-Based Optimization
BESS	Battery energy storage system
BJT	Bipolar junction transistors
CES	Capacitor energy storage
CHBMLI	Cascaded H-Bridge Multilevel Inverter
PMU	Phasor Measurement Unit
CSA	Cuckoo Search algorithm
CSI	Current Source Inverter
CVCF	Constant voltage and constant frequency
DC	Direct Current
DCC	Diode-Clamped Converter
DCE	Direct Current Electricity
DCI	Diode Clamped Inverter
DCMG	Direct Current Micro-grid
DE	Distributed energy
DERs	Distributed Energy Resources
DFIG	Doubly-fed Induction Generator
DG	Distributed Generation
D-STATCOM	Distribution-STATCOM
DVR	Dynamic Voltage Restorer
EMI	Electromagnetic interference
EPQ	Electric Power Quality
ESD	Energy Storage Device
FACTS	Flexible AC Transmission System
FC	Fuel cell
FCC	Flying Capacitor Converter
FCMLI	Flying Capacitor Multi Level Inverter
FET	Field-effect transistor
FSIG	Fixed Speed Induction Generator
GA	Genetic Algorithms
GSA	Gravitational Search algorithm
GSC	Grid-side Converter
GTO	Gate turn-off thyristor
HIS	Habitat suitability index
HVAC	High Voltage Alternate Current

HVDC	High Voltage Direct Current
IEEE	Institute of Electrical and Electronics Engineers
IGBT	Insulated-gate Bipolar Transistor
IGT	Insulated-gate thyristor
IPFC	Interline power flow controller
MG	Micro-grid
MLI	Multi-Level Inverter
MPTT	Maximum Power Point Tracking
NPC	Neutral-Point-Clamped Converter
NPC-MLI	Neutral-Point-Clamped Multilevel Inverter
PCC	Point of common coupling
PEMFC	Proton exchange membrane fuel cell
PF	Power factor
PLL	Phase Locked Loop
PMSG	Permanent Magnet Synchronous Generator
PSO	Particle Swarm Optimization
PVPs	Photovoltaic panels
PWM	Pulse Width Modulation
RES	Renewable Energy System
RSC	Rotor-side Converter
SHE	Selective Harmonic Elimination
SIV	Suitability index variable
SMES	Superconducting magnetic energy
SPWM	Sinusoidal Pulse Width Modulation
STATCOM	Static Synchronous Compensator
SVC	Static var compensator
SVM	Space-Vector Modulation
THD	Total Harmonic Distortion
UPFC	Unified Power Flow Controller
UPQC	Unified Power-Quality Conditioner
UPS	Uninterruptible power supplies
VCO	Voltage controlled output
VSI	Voltage-Source Inverter
WT	Wind Turbine

List of Nomenclature or Symbols

Nomenclature or Notations	Full Form
P_{mod}	Habitat modification probability.
K_{eep}	Elitism parameter.
I	Maximum immigration rate.
E	Maximum emigration rate.
dt	Step size for numerical integration.
m_{max}	Maximum mutation rate.
P_{mutate}	Mutation probability.
λ_{lower}	Lower bound for immigration probability per gen.
λ_{upper}	Upper bound for immigration probability per gen.
μ_{lower}	Lower bound for emigration probability per gen.
μ_{upper}	Upper bound for emigration probability per gen.
S_{max}	Maximum species count.
P_{size}	Total population size.
G_{max}	Maximum number of generation.
Num_{var}	Number of variable.
P_{count}	Species count probability of each habitat.
m_d	Modulation index
V_{an}	Output phase voltage of the inverter
α	Switching angles
F(α)	Objective function
N_{solar}	No of solar cell
V_{nom}	Nominal voltage
L_m	Inductance
V_0	Output DC voltage
V_{dc}	DC voltage of DVR
C_{dc}	DC link capacitance
Z	Leakage impedance
f_s	Frequency

K_p	Regulator gain
V_{mp}	Voltage at $P_{\max}$
I_{mp}	Current at $P_{\max}$
$P_{\max}$	Maximum power
L_f	LC Filter inductance
C_f	LC Filter capacitance
f_c	Cut of frequency
Q	Quality factor
V_{DVR}	DVR series voltage
b_n	Amplitude of different harmonic orders
V_{inj}	DVR injected voltage
V_{sag}	Sag voltage

LIST OF FIGURES

LIST OF TABLES

ABSTRACT

This thesis presents an improved configuration of Micro-grid with different DGs units. At the same time, the proposed DG control unit improves the overall power quality. The different inverter configurations used in this thesis with PV, DFIGs for reactive power controlling purpose with different configurations of FACTS devices. The Matlab simulations and different soft-computing optimization techniques along with hardware implementations are used in the proposed system. The proposed micro-grid is very simple, controllable, with low loss and reduced cost.

Due to effect of Harmonics, there will be a problem regarding distortions in voltage and current waveforms. The electrical harmonic generally refers to a part of an undulation of a grid frequency with multiple of the basic, in general 50 Hz. At steady state condition, the harmonics present in the supply voltage waveform are usually within specified limit but during unusual conditions, e. g fault, unbalance, the harmonics are present in the micro-grid or smart micro-grid as harmonic level increases due to abnormalities in voltage waveform. A typical measurement of the degree of presence of harmonics in micro-grid is Total Harmonic Distortion (THD) of grid voltage, which is calculated by IEEE as follows: is that the squared sum of magnitude of the harmonics present as a percentage of the fundamental magnitude.

Power Quality problems are malformed or collapsed the grid system and required mitigation for the customers according to IEEE 519. The IEEE suggested practices and necessities for harmonic management in electrical grid or micro-grid Systems, is that the commonplace for harmonics.

The cause of harmonics are any type of power electronic loads or non-linear loads in the electrical system, leading to non-sinusoidal distorted current from drawn from a sinusoidal supply. Samples of loads generating harmonics are: any type of FACTS device, AC or DC motor drives, discharge furnaces, different type of inverters, variable frequency drives and switch-mode power providers like computers, lighting ballasts, and gear of industrial electronics etc.

In this thesis elimination of inter-harmonics or sub-harmonic, which are not multiple of the fundamental frequencies is also introduced. The serious issues of having distorted grid voltage and current waveforms are unwanted tripping of the system, unscheduled shutdown of the grid or micro-grid/smart grid. Moreover, due to higher harmonic losses, the grid efficiency reduces resulting in out sizing of the electrical cables, transformers, circuit breakers with shorter the lifetimes of the equipment. For power quality improvement, mitigation of harmonics or reduction of harmonics are the common issues and as a result a minimum 15% capital cost and a 10% additional expenses required for passive or active filter, inverter switching for 6,12,18 pulses with Pulse Width Modulation (PWM) and AC line reactors in series etc.

A micro-grid or smart micro-grid is a confined to a small area and combination of clean electricity generation, power storage, and system load units that generally works in synchronism with customary centralized network, with the maximum flexibility that the unit as a entire may be cut off from the central grid and may continue operation as an isolated small grid hence the name of micro grid. When the micro-grid operate bi-directionally, with monitoring

and controlling by PMU, smart meters, flow meters, power electronics FACTS devices then the micro-grid converted into the advance micro-grid or smart grid. The supply resources may consist of reciprocating locomotive generator sets, different micro turbines, fuel cells, wind driven induction generator, photovoltaic and other small-scale renewable generators, storage device, and controllable end-use loads. Electrical coordination loads are day-by-day increasingly becoming the very sensitive in character because of the augmented use of modern power electronic and new technological micro controller based devices, programmable logic controllers (PLC), energy efficient lighting and Supervisory Controlled and Data Accusation (SCADA) system. Maintaining the superior excellence of electrical power as recommended in IEEE 1547, IEC, EN, CIGRE Wg 36-05, NRS, stipulation as have thus become compulsory. Harmonic elimination and minimization therefore is an extremely essential issue is respect of the operation of the micro grid.

The main aim of this thesis is to explore optimum ways to reduce the targeted order of harmonics in order to cater better quality of electrical power to the end users. In this thesis the method of harmonic reduction to improve the power quality is explored in details. The switching angles are computed off-line through a suitable soft computing technique. The obtained switching angles will be stored in microcontroller memory for on-line application using 'mixed model' equation for low memory usage. In the current state, doubly-fed induction generator (DFIG), PV, wind, PEMFCS is used as the DG source and harmonic elimination of individual as well as combined units has been studied. Conversely for power quality improvement we studied the FACTS controller like DVR, SVC, STATCOM, UPQC etc. This FACTS controller maintains the overall power quality, active and reactive power, power interruption, negative sequence current etc.

The objective of this thesis is to find out different construction of micro-grids, DFIGs; different type of FACTS devices for improved the grid performance. This strategy includes the reduction of system loss, improvement of the voltage profile, increase the transmission and distribution capacity, the overall harmonic minimization with low cost and minimum loss. The proposed work increases the system stability with better quality of power. The advanced controller FACTS devices and different inverter topology control the critical loads. In this circumstance various soft computing techniques are used for inverter, FACTS and micro-grid control purpose.

In this thesis the DFIGs connected micro-grid demonstrate and control by biogeography based optimization (BBO) based harmonic elimination switching technique. The lower order harmonics are independently eliminated in each DFIG outputs conversely the higher order harmonics are eliminated in such a way that the harmonics generated by one source is eliminated by the other after generating the same order of harmonics in opposite phase. The DFIG connected inverters excited power mainly obtained from a wind or PV panel. Projected work consequently supported and the total harmonic distortion (THD) in the output is found to be within the specific set limit. This new technique implement for improve the voltage and current harmonics in a micro-grid system with near to the ground switching loss.

This thesis explains photovoltaic (PV) based Dynamic Voltage Restorer (PV-DVR) to diminish the voltage sags, voltage swells, flickers and harmonics for small or medium standard voltage suburban or residential micro-grid system. The proposed PV-DVR system consists of a selected harmonic elimination and moderation PWM (SHEAM-PWM) multilevel inverter system for the PV module, step-up DC–DC boost converter, and a series injection

transformer. The voltage generated from the PV module is connected to the multilevel inverter through a step-up DC-DC converter. For the switching methods assumed that the dc sources are equal or unequal (varying) to one another. The multilevel inverter is chosen to reduce the switching losses as low number of switching of individual converters can reduce overall voltage THD to a considerable amount and achieve high dynamic performance. For the multilevel SHEAMPWM inverter, the optimum switching angles are computed off line to eliminate the lower order harmonics. Biogeography-Based Optimization (BBO)-based SHEAM-PWM technique is employed for this purpose. The proposed method is simulated considering a practical system and the results indicate that the voltage harmonics are highly reduced by the proposed technique.

This thesis investigates the combined operation and performance of the doubly fed induction generator (DFIG) and powerful custom power devices such as dynamic voltage restorer (DVR), static compensator (STATCOM) and unified powr quality conditionar (UPQC) with common distributed generation (DG) systems. Improved multilevel inverter based topologies for DVR, STATCOM and UPQC operations using DFIG and PV are proposed in this chapter. The proposed technique can efficiently mitigate the power quality problems e.g. voltage sag, swell, flicker, reactive power, voltage interruption, unbalance neutral current, voltage and current harmonics etc. in the distribution system. The proposed DG connected three phase multilevel converter for photo voltaic (PV) system reduces filtering requirements, increases redundancy and enables transformerless interface with grid. Biogeography-Based Optimization (BBO) technique is applied for calculating the exact switching angles for the inverter at each modulation index considering low total harmonic distrotion (THD) for the output voltage. The performance of the UPQC mode is compared with both DVR and STATCOM modes. For the proposed topology, the simulation studies with MATLAB are presented which show that the proposed DFIG and PV based UPQC performs significantly better than the DG-DVR and DG-STATCOM combinations.

The electrical power quality issues are of the major concern in the present scenario of critical loads. In this research work considerable advancement is achieved to overcome such power quality issues e.g. sag, swell, under voltage, over voltage, harmonic issues etc. for the domestic and industrial consumers.

Chapter 1

Introduction of the MGs, DGs, Inverters, FACTS and Proposed Work

Chapter 1

1.1 Chapter Overview

The following chapter serves various ideas of the proposed analysis of research purpose. This chapter learns on special grid technologies with grid up gradation. The challenge of Micro-grid formulates the inspiration to make Smart grid systems. It communicates the construction or planning of different grids with high security confronts and power quality improvement. The following chapter also serves several introductory materials on different type of inverter topology with some advantage and disadvantage.

For lot of advantages the FACTS technology need to install latest power system (grid, micro-grid and smart grid). Using this smart technology we tend to maintain and advance the already installed system and new smart system to boost the system potency, most capability, harmonic optimization, real power and correct reactive power manage, system voltage and coordination current related uncontrolled any problem, application of renewable. For energetic and fashionable applications of FACTS strategy is that the technical benefits addressing in transient constancy, dampening, and emergency needed electrical voltage management and acceptable voltage stability. The new technological power electronics FACTS devices are necessary when there is require responding to energetic (dynamic or fast-changing) system circumstances. In fashionable life the facility of power systems must give easy or need to provide simple, reliable, stable, secure, completely controllable, economic (low loss and low price with high efficiency), and high-quality power with deregulated atmosphere it is imagine that FACTS controllers participate awfully necessary role.

1.2 Thesis Research and Step

The great scientist Nikola Tesla is the father of AC electricity. Technologically developed the power grid and for modification of global warming the environmental pollution with C emission reduction is very essential. So the new and fresh carbon less green energy is very essential for power discovery which is accessible in great amount for availability. To overcome all the challenges the researchers are introduced the advanced technological micro-grid to smart grid operations.

1.3 About Micro-grids

Figure 1.1 shows the schematic representation of a micro-grid [1, 2, 3, 4]. Micro-grids are miniature versions of the conventional power grid. They consist of power generation, distribution, and controls units such as switch gears and voltage regulation. Modern electrical micro grid or a limited power grid is a collection of any type electricity sources and loads that usually works or associated to and synchronous with the traditional electrical power network, but can also separate to "island mode" — and utility independently as bodily and/or economic conditions dictate. The modern micro-grids are known as distributed, decentralized, dispersed, and embedded or constituency energy generation system.

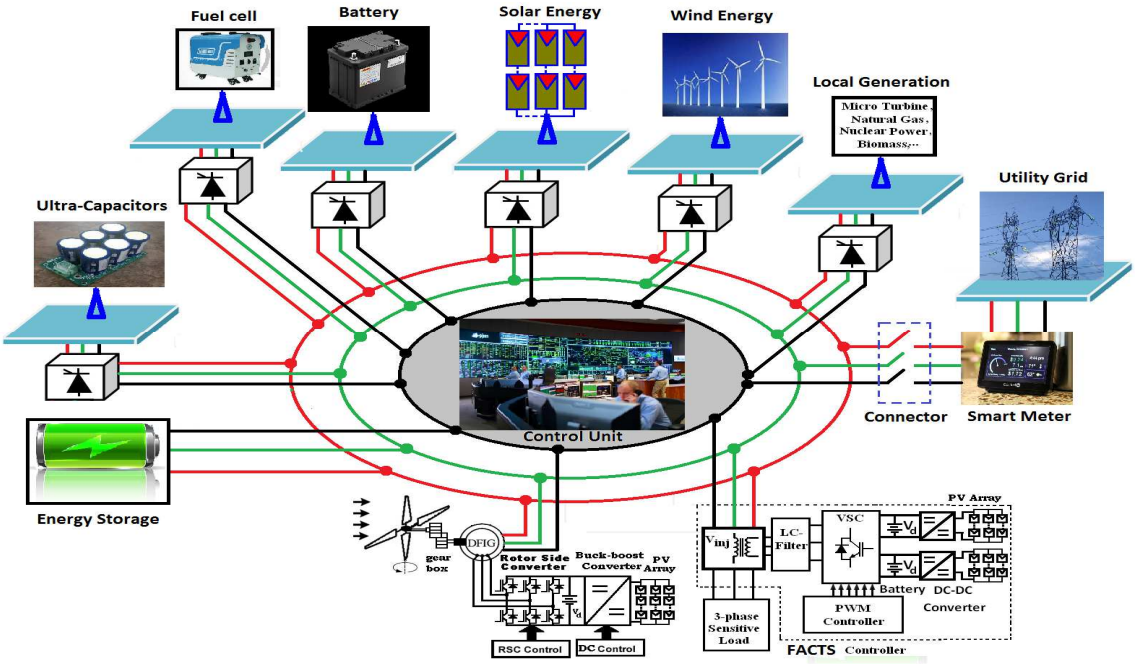

Figure 1.1 A typical scheme of micro grid with renewable energy resources in grid-connected mode

1.4 Types of Micro-grids

1.4.1 There are different types of micro-grids (i) Customer micro-grids or true micro-grids (µgrids) (ii) Utility or community micro-grids or milli-grids (mgrids) (iii)Virtual micro-grids (vgrids) (iv) Remote power systems (rgrids) (v) Campus Environment/Institutional Micro-grids (vi) Remote "Off-grid" Micro-grids (vii) Military Base new Micro-grids and (viii) most practical Commercial and Industrial (C&I) Micro-grids

1.4.2 DC Micro-grid

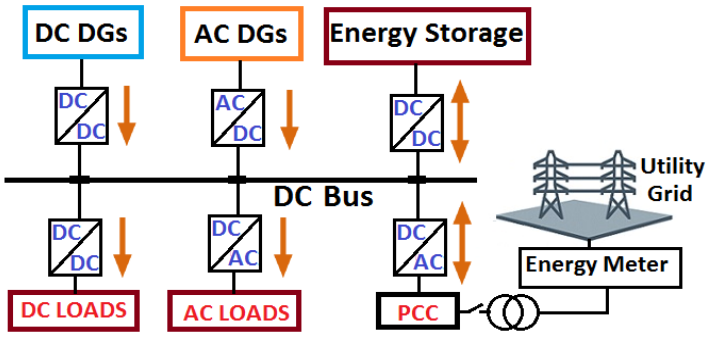

Figure 1.2 General structure of DC micro grids system.

Compare to ac the dc micro-grids [5, 6] is more economical and cheaper alternative. In the present life the LEDs are rising as a favorite alternative for high efficiency illumination, and they glow on DC power and growing global consumption of electricity by DC devices. The appropriate output of DERs (Distributed Energy Resources) like

most significant PV, fuel cells and other DC foundation is DC, for wind power or any ac electrical source, using most multifaceted power electronics switching devices, DC power can be gained. The universal configuration of DC micro-grid system is illustrated in Figure 1.2.

- **Generation of DC power mainly (a)** Fuel cell (b) Solar PV panels **(c)** Micro wind turbines (d) Rectifier connected to a utility grid.
- **DC electrical storage system mainly (a)** Battery **(b)** Super capacitor.
- **DC power distribution** -Wiring and control
- **DC gadgets like (a)** Laptops **(b)** Telephones **(c)** Satellite TV controllers
- **DC lighting** -i.e. LEDs.
- **Controls or Monitoring by**-Wireless/ Wired/ Virtual/ Cloud Based.

On the other side the low carbon and fuel cell familiarity transfer network DC micro-grid connected component are accessible in market like Moixa Energy, Horizon Fuel Cell, BOC, Sun Microsystems, Philips has embraced.

- **Advantages of DC Micro-grids**

The advantages of a dc micro grid can be classified into three primary categories: (i) System Efficiency –high (ii) Reliability of Power-free and (iii) Safety-high (iv) Operation is simple.

1.4.3 AC micro-grid system

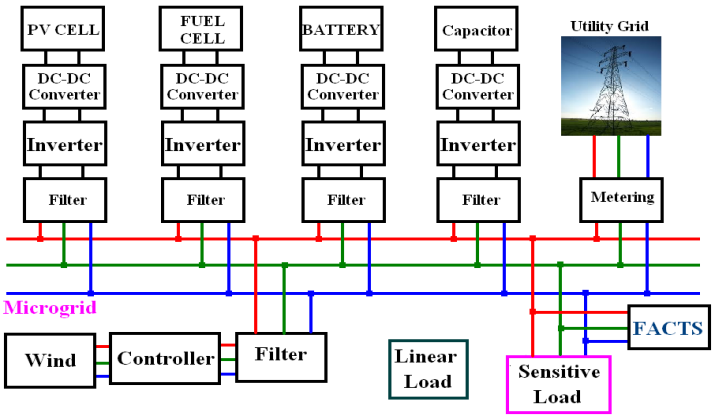

Figure 1.3 General structure of AC micro grids system

In Figure 1.3 shows in the general arrangement of an AC micro-grids system. The AC micro-grid [7] system is the most common, versatile and most significant ingredient in contemporary power grid. The ac micro-grid is basically straightforward, more controllable, more stable, more flexible and high efficiency based utilizable network. AC micro-grid consist of the most universal part of the point of common coupling (PCC) which is usually located as the only power crossing point between a micro-grid and utility grid. The renewable DGs supported on ac micro-grid systems are usually operated, controls and maintains by the ability of power electronic converters with distributed control. The most common green and fresh renewable DGs sources wind extract the power from the natural

environment which is generating the ac power by proper controlling. The other renewable DGs sources PV, extract the maximum power from sunlight and convert the electrical ac power by power electronics converter and this power generation mainly depends on instant environmental circumstances. The modern high-performance power electronics device provides instant support to monitor the grid, MGs and smart grid.

1.4.4 Hybrid Micro-grid System

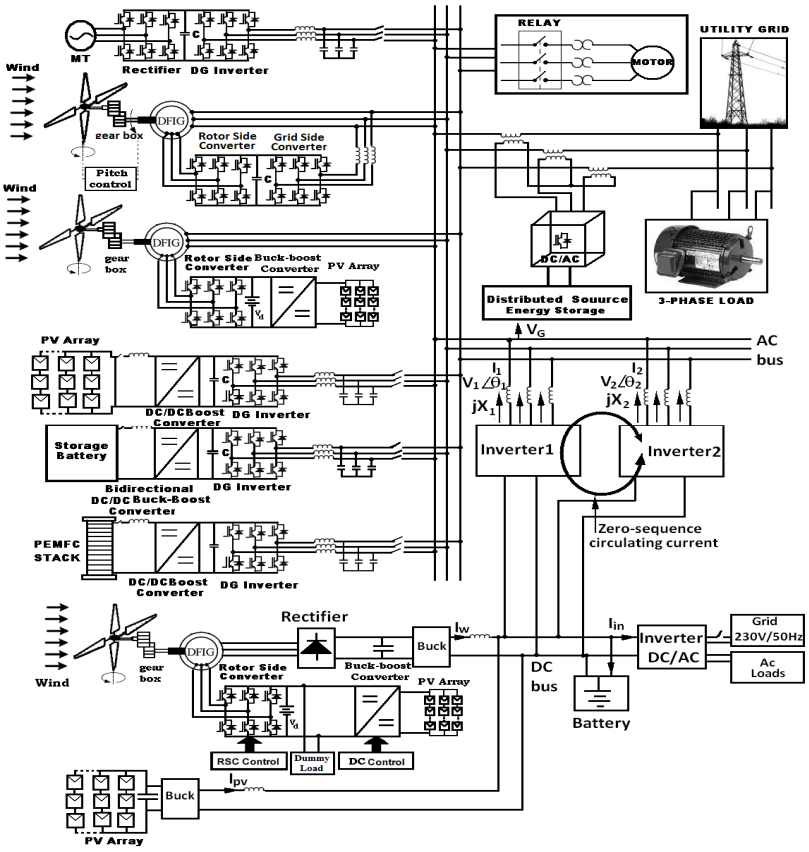

Figure 1.4 General structure of Hybrid Micro-grid System with control

The Figure 1.4 is shows a general arrangement of Hybrid Micro-grid System [8, 9] where ac and dc both are connected to a single network. When the set of distributed generation sources and interrelated loads with universal control methods is associated within a clearly specific electrical periphery the coordination is named Hybrid or combination Micro-grid System. The hybrid micro-grid operates different type ac or dc loads and DGs with power electronic controller.

1.5 Basic Components in Micro-grids

Basic Components in micro-grid are

i. **Local generation-**Local generation basically present's different type of electrical generation source that gives electric power to the consumer. These electrical sources are in two most important groups

   a. **Thermal energy sources** - Diesel generators

   b. **Renewable generation sources** - wind turbines, Solar, Fuel cells

ii. **Consumption-** It merely refers to parts that consume electricity that vary from single devices to lighting, utility of buildings, business centers, etc. within the case of governable hundreds, the electricity consumption may be changed in demand of the network.

iii. **Energy Storage devices-** In micro-grid system, the energy storage system performs multiple operations, such as ensuring PQ improvement, frequency control, voltage regulation, backup power providing for the grid and playing vigorous role for reliability & cost optimization.

iv. **Point of common coupling (PCC)-** For a micro-grid system the PCC is the junction of an electric network where a micro-grid is linked to a central grid. For remote sites sometimes the PCC is not present in the micro-grid system and this type of system is called isolated micro-grids.

v. **Controls units-** The control units control the overall systems for high efficiency**.**

1.6 Advantages of Micro-grid

(i) Micro grid is a way to integrate wind, solar, and hydroelectricity, etc; to the main grid in small-scale power distribution network (ii) Micro grid is capable of operations in grid-connected modes, stand-alone modes or both. In the MGs in islanded mode, generates real and reactive power (iii) By proper maintenance MGs improve the ability of power quality, system efficiency, economics, and resiliency (iv) During emergency, power shortage period or power interruption period the MGs provides complete solution to supply the power in the main grid (v) MGs can separate (in peak load periods prevents utility grid) and isolate independently from the central grid during disturbance and it is controlled locally by the society (vi) Micro-grid encourages the utilization of the most inventive renewable energy sources wherever the outsized land use impacts are avoided and CO_2 Emissions are reduced.

1.7 Disadvantages of Micro-grid

The main disadvantages of the MGs are (i) due to different DGs the voltage, required frequency and power i.e. resynchronization with utility grid (ii) some times more space required due to battery banks (iii) installation cost is high (iv) reverse power flows (Bidirectional power flows) at low voltages, may lead to protection coordination complications, unpredicted power flow patterns, distribution of fault current , & voltage control (v) Stability issues is the main factor for local oscillations, small-disturbance stability, transient issues (vi) Low inertia in the system can lead to severe frequency deviations (vii) Uncertainty of generation is also one of the major problems.

1.8 Type of DGs

The types of DGs are (i) Wind power based Doubly-fed induction generator (DFIG) (ii) Photovoltaic type renewable generators (iii) Micro turbines (MT) (iv) Fuel cell (FC) (v) Storage devices (vi) Biomass (vii) Tidal (viii) Wave (ix) Geothermal (x) Hydro-electric (xi) Distributed cogeneration source (i.e. steam turbines, natural gas-fired, fuel-cell, micro-turbines or reciprocating engines) etc.

1.8.1 Wind Turbines with DFIG

Wind turbine based DGs consist of rotor that extracts kinetic energy from the wind and converts it into a rotating movement; this is then rehabilitated into electrical energy by the DFIG [10] through a low-speed shaft, a high-speed shaft and a gearbox. Figure 1.5 exemplifies the arrangement of a DFIG where the stator windings are directly connected to the grid and the rotor winding is associated with the network via a back-to-back power electronic converter. The rotor aspect converter regulates the active and reactive power injected by the DFIG and therefore the grid aspect converter controls the voltage at the DC link.

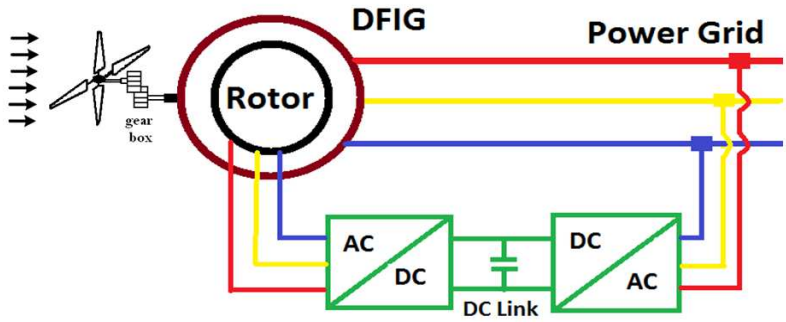

Figure 1.5 Doubly fed induction generator.

DFIG is attractive and popular due to its flexibility in variable speed range and lower cost. The DFIGs rotor operates at a variable speed in order to optimize the tip-speed ratio and the rotor speed is controlled to operate within a variable speed range centered on the generator synchronous speed. Therefore the generator system operates in both a sub-synchronous and super-synchronous mode, typically between ± 30% of synchronous speed.

1.8.2 Conventional and Proposed DFIG with Wind

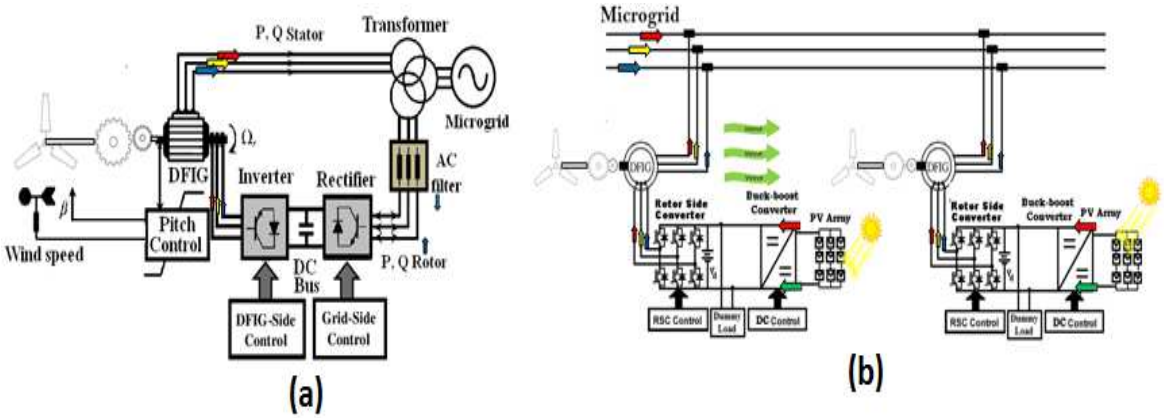

Figure 1.6 Doubly fed induction generator configuration for (a) conventional (b) proposed.

Figures 1.6 illustrate the conventional and proposed DFIG configuration. Where for proposed micro-grid connected DFIG configuration consists (i) the stator of both the DFIGs are directly connected to 50 Hz micro grid (ii) the PV panel output is connected to the rotor through a dc to dc converter in series with a three-phase bridge inverter (rotor side converter) (iii) Photovoltaic (PV) systems provide green & renewable energy (iv) A battery V_d is incorporated between the two converters which stores of the extra energy from the PV panel when the rotor side power demand is less than PV panel output, acting as a dc source in the absence of sun light to inject the power to the rotor and Storing of the recovered power coming from the machine at super-synchronous speed etc.

1.8.3 Types of Wind Turbine Generator Technologies

(i) **Squirrel Cage Induction Generators (SCIG):** this is driven by fixed-speed and stall-regulated wind turbines. SCIG has simple, robust construction and power by controlling, power control capability; but efficiency is low for low variable speed control, flicker, and no reactive control.

(ii) **Induction Generators with variable external rotor resistance:** this is driven by a variable-speed, pitch regulated wind turbines where the main advantages are variable speed, fast control and low harmonics but the efficiency is medium.

(iii) **Doubly-Fed Induction Generators (DFIG)**: the DFIG is driven by variable-speed and pitch regulated wind turbines. Where the main **advantages** are higher efficiency and reactive power control but the disadvantages are (i) needs slip rings, also it requires frequent maintenance (ii) has limited fault ride through capability and needs protection schemes (iii) have complex control schemes (iv)harmonics (where only 25% of output power goes through converters).

(iv) **Synchronous Induction Generators** (SIG): SIG operates with full converter interface (back-to-back frequency converter), driven by variable-speed, pitch regulated wind turbines. The main advantages are variable speed, fast control and low harmonics but efficiency is medium.

1.8.4 Configurations of Wind Turbine

The wind turbine system has two configurations.

1.8.4.1 Fixed-speed Wind Turbines

In this system, the generator is connected directly to the grid and the rotor speed is always fixed. The construction and operations are simple but efficiency is high at a particular wind speed also being robust and low cost. Due to wind instability the power variation is an important factor, which affects the power quality of the grid. On the other hand, the major disadvantages are an unmanageable reactive power consumption and mechanical stress.

1.8.4.2 Variable-Speed Wind Turbines

Variable speed doubly fed induction generator (DFIG) is most commonly used. By controlling the variation of wind speed with generator speed and the generator torque the power quality is increased. For improvement of power quality and reduction of mechanical stress on the wind turbine, power electronics converter controls the generator speed against wind variations.

1.9 Advantages of DFIG for Micro-grid Operation

The maim advantages of the DFIG for micro-grids are (i) Variable-speed and higher efficiency (ii) Grid Integration is straightforward (iii) Active and Reactive power control (iv) Enough reactive power support for steady-state and post-fault conditions, a mix of static (e.g. switched capacitor banks) and dynamic reactive compensation (e.g. SVCs and STATCOMs) is often used while integrating large wind farms to transmission systems (v) The DFIG technology allows extracting maximum energy from the wind for low wind speeds by optimizing the turbine speed, while minimizing mechanical stresses on the turbine during gusts of wind (vi) The optimum turbine speed producing maximum mechanical torque to generate maximum power (vii) RSC is to extract maximum power with independent control of active and reactive powers with controlling direct and quadrature axis rotor currents respectively (viii) The grid side converter (GSC) can provide reactive power. The control of this GSC is for mitigating the harmonics produced by the nonlinear loads (x) the characteristics of DFIG are high efficiency, flexible control and low investment (xi) power factor control can be implemented in this system (xi) DFIG is simple in construction and cheaper than a PMSG.

1.10 Photovoltaic Energy

Micro-grid connected photovoltaic system is electricity generation from solar PV systems that is linked with utility network which enclosed PV array or solar cells to exchange sunlight into electricity.

The series or parallel connected Solar cells build PV array. DC-DC high or low step up converter is used to increase or decrease the output voltage of PV cell depending upon the weather condition. A battery is used to store the solar energy which supplies the voltage to three phase inverter in absence of sunlight. MPPT [11, 12] controller is connected which is capable of maximum power extraction from PV array. Total harmonic distortion (THD) is reduced by using inverter switching technique and various converter models we apply in simulation purpose. In Figure 1.7 illustrate the simple PV based micro-grid configuration.

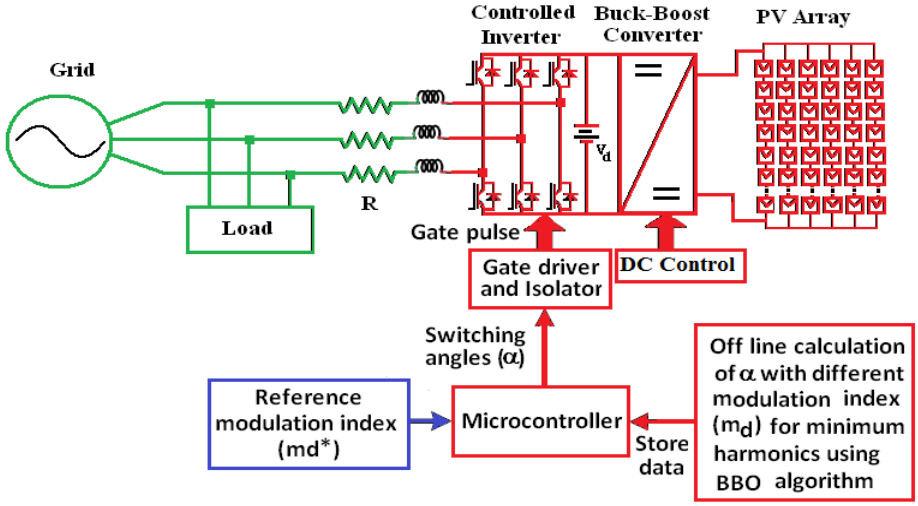

Figure 1.7 Configuration of simple PV based micro-grid system

A MPPT controller is important to increase the output efficiency energy of PV array. Different types of MPPT algorithm have been discussed, such as open circuit voltage (OC), incremental conductance (INC), perturbs and observation (P&O) etc. Among all of these methods P&O method is most popular. To amplify or decrease the output voltage of the PV array a DC-DC converter or, buck-boost converter is used depending upon the temperature and solar irradiance by controlling technique. In this thesis, there are various techniques for pulse width modulation, buck-boost converter, filter, MPPT algorithm control are used. The generated PV power we apply in DC bus and AC bus related Proposed Photovoltaic based Micro-grids system, DFIG, DVR, STATCOM, and UPQC etc

The different methods to utilized solar energy i.e. (a) Direct Methods (b) Thermal (c) Photovoltaic and (d) Indirect Methods (like, Water power, Wind, Biomass, Wave Energy, Ocean Temperature differences and Marine Currents).

The PV array output is totally dependent on temperature and solar irradiation, therefore a battery is essential to store the energy and running the grid during the absence of sunlight.

1.11 Power Quality Improvement of Micro-grid Systems

Power Quality (PQ) [13, 14]: The increase of power electronics application, computers and microprocessors or microcontroller systems has resulted in power quality issues involving transient and other disturbances in voltage magnitude, waveform and frequency.

The Power Quality problems are categorized as follows

(i) Transient problems (a) Impulsive (b) Oscillatory.

(ii) Short and Long duration variations (a) Interruptions (temporary interruption, long-term outage and momentary interruption) (b)Voltage Sag (dip) (c) Voltage Swell

A. Voltage unbalance
B. Waveform distortion (1) DC offset (ii) Harmonics distortion (iii) Inter-harmonics (iv) Voltage Notching (v) Noise
C. Voltage Flicker
D. Power frequency variations
E. Voltage fluctuation

In this thesis the more details about these problems and solution are discussed in chapter 1 to 6 and established the improvement of PQ by proposed SHE-PWM, FACTS [15-18] controllers and Custom Power Devices (CPD). The main FACTS control devices are based on VSC i.e. Shunt connected Distribution static compensator (STATCOM), Series connected Dynamic Voltage Restorer (DVR), Combined shunt and series connected Unified Power Quality Conditioner (UPQC) used for improving PQ and all the FACTS devices controlled by PWM switching and improve micro-grid efficiency. The series connected CPD & DVR can operate as a source voltage reaching, harmonic isolator, providing voltage regulation, load balancing and active and reactive power controller. A series shunt connected FACTS device UPQC as the combination of series connected DVR and shunt connected STATCOM.

From the source currents, a STATCOM is used to eliminate the harmonics and providing reactive power compensation which is improving the power factor and adjust the load bus voltage.

1.12 Different type of Inverter and Different Switching Technique

Inverter [19, 20, 21] convert DC wattage into AC wattage at desired output voltage and frequency. There are mainly two universal type of inverters according to the scenery of input supply

I. Voltage supply electrical converter or Voltage Source Inverter (VSI)

II. Current supply electrical converter or Current Source Inverter (CSI)

1.12.1 Voltage Source Inverter (VSI) or Voltage Fed Inverter (VFI) Consists

a. Minimum one DC supply or stiff DC voltage supply that could also be a battery, fuel cell, PV cells or alternative common d. c. source.

b. Small and negligible impedance.

c. Commutation is very simple.

d. A common dc link for ac to dc or dc to ac at an adjustable frequency.

e. The input to the electrical converter is provided by a ripple free dc voltage.

1.12.2 Current Source Inverter (CSI) or Current Fed Inverter (CFI)

a. Input DC source impedance is high.

b. No generation of radio-frequency interference in CSI.

These inverters are two types

A. Load commutated Current Source Inverter

B. Force commutated Current Source Inverter

1.13. Types of Voltage Source Inverters: The voltage source inverters are mainly of two types

i. Single phase voltage source inverters

ii. Three phase voltage source inverters

To manage the output voltage of one part or single phase inverters are frequently to survive the variation of dc input voltage. For industrial and domestic applications the voltage regulation is incredibly vital for maintaining of continuous voltage and frequency. At input terminals a voltage supply electrical converter has stiff d.c. voltage. It's appropriate for single and multi-motor drives.

1.13.1 Single Phase Half-bridge Inverter

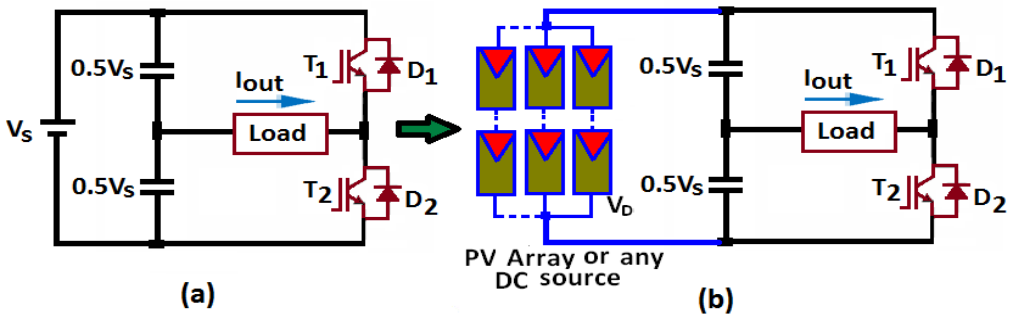

Figure 1.8 Single Phase Half-Bridge Inverter

The representation of control circuit diagram for a single phase half-bridge electrical converter configuration is illustrated in Figure. 1.8 (a) and (b). The load side of the half-bridge electrical inverter is either resistive, inductive or both. At approximately 50% duty cycle, this type of electrical converter is operated by controlling switching S_1 and S_2 as an alternative and this gate commutated power electronics component as BJTs, GTO, MOSFETs, IGBT, MCT etc. The semiconductor unit transistor T_1 conducts within $0 < t < \pi$ and for higher voltage supply Vs/2 the load part is subjected Vs/2. T_2 is gated on at $t = \pi$ and therefore the semiconductor unit transistor T_1 is commutated. Transistor T2 is conducting when the period $\pi < t < 2\pi$ and due to the lower voltage source Vs/2 the load voltage is (-Vs/2).

1.13.2 Single Phase Full-bridge Inverter

Figure 1.9 (a) & (b) shows the power circuit diagram of a single phase full-bridge electrical inverter. When the input voltage is connected across T_1 and T_2 the input voltage appears across the load. The switching states for single-phase full-bridge VSI as shown in Table 1.1.

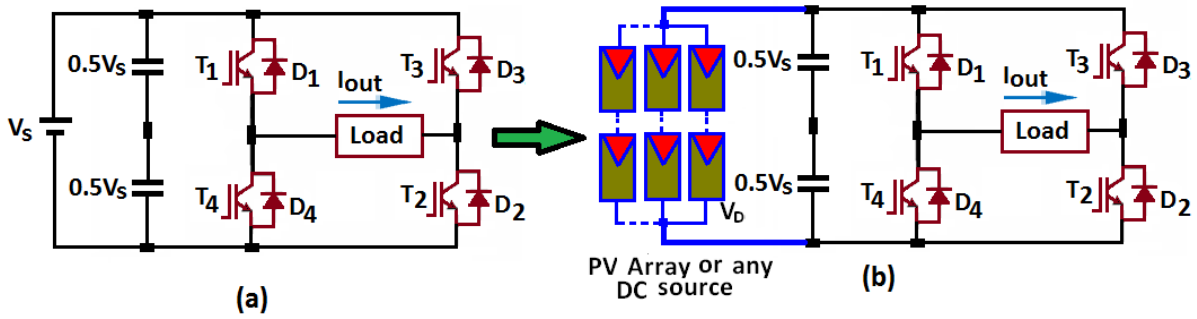

Figure 1.9 Single-Phase Full-Bridge Inverter (a) without renewable (b) with renewable.

Table 1.1 Switching states 1-phase full bridge VSI

Stat	Switching states				V_{out}	I_{out}	
No.	S1	S2	S3	S4		$I_{out}>0$	$I_{out}<0$
1	ON	ON	OFF	OFF	Vs	S1 and S2 conduct	D1 and D2 conduct
2	OFF	OFF	ON	ON	-Vs	D4 and D3 conduct	S3 and S4 conduct
3	ON	OFF	ON	OFF	0	S1 and D3 conduct	D1 and S3 conduct
4	OFF	ON	OFF	ON	0	D4 and S2 conduct	S4 and D2 conduct
5	OFF	OFF	OFF	OFF	-Vs	D4 and D3 conduct	
6	OFF	OFF	OFF	OFF	Vs		D1 and D2 conduct

These two types of inverters are controls by most efficient method as

A. Single-pulse width modulation (B) Multiple-pulse width modulation (C) Sinusoidal-pulse width modulation (D) Modified sinusoidal-pulse width modulation (E) Phase displacement control.

1.13.3 Three Phase Voltage Source Inverters

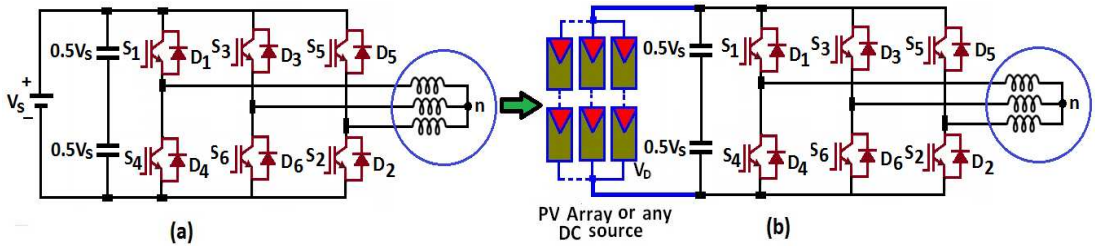

Figure 1.10 The facility of a power circuit diagram for three phase electrical bridge inverter utilizing six IGBTs (a) without renewable (b) with renewable.

For three phase projected inverters a six steps bridge is employed by using logical six switches and at the same time two switches are used for every phase. Figure 1.10 (a) & (b) show the basic circuit diagram of a three-phase bridge electrical converter. Using a most versatile six-step bridge electrical converter, the gate pulse signals are managed and therefore the controlling modes are 120^{o} and 180^{o}, however these two schemes operate in 60-degree intervals. Sometimes a large condenser (capacitor) is associated at the input terminal to formulate the constant DC input and suppress the harmonics fed to the source.

1.13.3.1 Three Phase 180^{o} Conduction Mode Voltage Source Inverter: By Figure 1.10, each transistor conducts for 180^{o} of a cycle. For this case at a time three transistors remain on at any instant. In Table 1.2 shows the three phase 180^{o} conduction mode voltage source inverter switching states.

Table 1.2 Three-phase VSI switching states, for 180^{o} conduction mode.

Stat	Switching states						Vab	Vbc	Vca
No.	S1	S2	S3	S4	S5	S6			
1	ON	ON	OFF	OFF	OFF	ON	Vs	0	-Vs
2	ON	ON	ON	OFF	OFF	OFF	0	Vs	-Vs
3	OFF	OFF	ON	ON	OFF	OFF	-Vs	Vs	0
4	OFF	OFF	ON	ON	ON	OFF	-Vs	0	Vs
5	OFF	OFF	OFF	ON	ON	ON	0	-Vs	Vs
6	ON	OFF	OFF	OFF	ON	ON	Vs	-Vs	0
7	ON	OFF	ON	OFF	ON	OFF	0	0	0
8	OFF	ON	OFF	ON	OFF	ON	0	0	0

1.13.3.2 Three Phase 120^{o} Conduction Mode Voltage Source Inverter: For this case each transistor conducts for 120-degree conduction mode of a cycle and requires six steps of each 60-degree. A three-phase voltage control inverter may be considered as three single-phase inverters where the output of each single-phase VSI is shifted by 120-degree. The most commonly used techniques for three-phase VSIs are (i) Sinusoidal PWM (ii) 60-degree PWM (iii) Third-harmonic PWM (iv) Space vector modulation.

1.14 Performance Parameters of Inverters:

An inverter ideally should give sinusoidal output voltage but in practical the inverter output are non-sinusoidal and contain basic and different harmonic components. The performance of power electronics inverters is evaluated in general by (a) Harmonic Factor of n^{th} harmonic (HF) (b) Total harmonic distortion (THD or % of THD) (c) Distortion Factor (DF) (d) Lowest order harmonics (LOH) etc.

1.15 Inverter Classification According to the Wave-Shape of the Output Voltage:

According to the nature of output voltage waveform the inverter can be classified as: (i) Square-wave inverter (ii) Quasi- Square wave inverter (iii) Pulse-width modulation (PWM) inverter.

Thyristor Inverter classification:

The thyristor inverters are classified in two types and the categories are: (I) according to the method of commutation (II) according to the connection.

According to the method of commutation, the SCR inverters are mainly of two types (A) Line commutated inverters (B) Forced Commutated inverters

According to connections- the inverter can be classified as (i) Series connected inverters (ii) Parallel connected inverters (ii) Bridge inverters. **Also the bridge inverters are two types, as: (a)** Half-bridge inviter **(b)** Full-bridge inverter

1.16 Concept of Multilevel Inverters

Multilevel inverters [22, 23] have found wide range of industrial applications as well as research application. Within the most up-to-date few years, the MLI latest technologies have been reported for a lot of contributions and establish the newest state of the art and trends of the technology to produce readers with a comprehensive and perceptive review. MLI applications are increasing recently for different systems as they have (i) Increased overall power ratings (ii) Improved harmonic performance (iii) The electromagnetic interference (EMI) emission reduced etc.

The construction of multilevel converter topologies and management strategies is dependent on the electrical converter styles or inverter designs. For harmonic management within the low-pass filters are applied to permit the fundamental harmonic component of the output waveform. For MGs system application of power electronic systems are required to promise for the power allotment and the energy quality with high efficiency. The primary concepts of MLIs are (a) Inverters control technology is very flexible (b) More feasible (c) More reliable (d) Low cost and more simple (d) Control the low to higher power-quality and (e) May or may not be needed an additional power filters. Therefore the multilevel converter topology concept is the challenging issue for micro-grid and smart-grid right now. The multilevel converter topologies is generally bi-directional switches, that why the multilevel VSC can work in both rectifier and inverter modes. It is the very important view that when the number of levels reaches infinity, the output THD approaches zero.

The different multilevel converter structures have been applied in domestic and industrial applications. In our thesis, we applied mainly DFIGs, MGs, PVs, PEMFCS, and FACTSs etc.

1.17 Concept of Classical Two-Level Inverters

The main topology for two-level VSI is illustrated in Figure 1.11, where the inverter converts a fixed DC voltage to three-phase AC voltage. Six groups of active switches control the gate signals which are depending on the dc operating voltage. For low power applications the classical inverters are excellent-quality, but for high-power levels multilevel technology offers the merits of a good alternative for power applications.

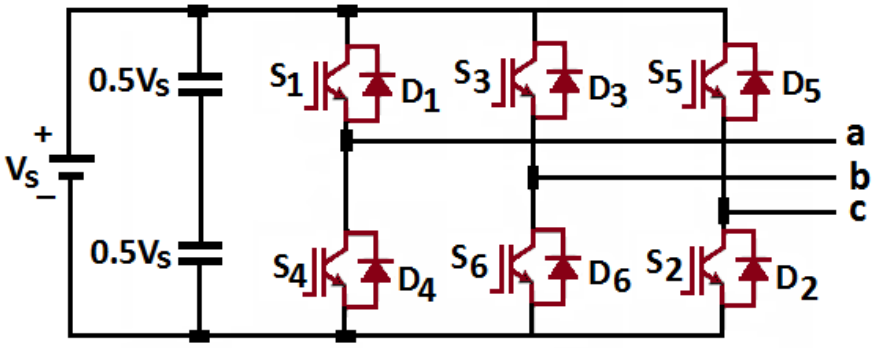

Figure 1.11 Basic diagram of a two-level, 3-phase VSC.

1.18 Analysis of Three-Level Inverter

Three level inverters are more applicable for harmonic optimization. This type of inverters can be utilized for applications, such as PV, wind, PEMFCS, active power filter, FACTS compensator and industrial drive for sinusoidal and trapezoidal current applications. By varying the input DC voltage a variable output voltage can be obtained. Pulse-width-modulation (PWM) control is very important for this type of inverter. The power rating is high compared to two level inverters. The construction of a three-level NPC inverter is shown in Figure 1.12. From Figure 1.12 the switching operating states are shown in Table 1.3 which can represent the status of the switches in the three-level NPC inverter. When the switching state is '1', it is indicated that S_1 and S_2 'on' and S_3 and S_4 'off' for inverter leg A.

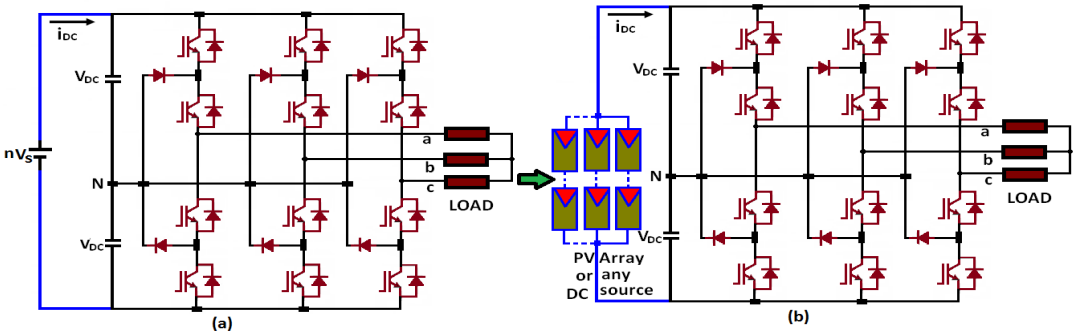

Figure 1.12 Three-level NPC inverter (a) without renewable (b) with renewable.

Which means the voltage of the inverter terminal is +V. When the switching state is '-1' the lower two switches are 'on', which means the neutral point is -V. When switching state '0', it indicates that the inner two switches S_2 and S_3 are connected and V =0 through the clamping diode, depending on the direction of the load current.

Table 1.3 Switching states for three level inverter with phase-A

Switching State	Phase A switching state				Inverter Terminal Voltage
	S1	S2	S3	S4	Vaz
1	ON	ON	OFF	OFF	V
0	OFF	ON	ON	OFF	0
-1	OFF	OFF	ON	ON	-V

1.19 A Brief Review of Multilevel Inverters

A. Diode clamped Multi-level inverters
B. Flying capacitors based Multi-level inverters
C. Neutral point inverters Multi-level inverters
D. Cascaded H-bridges multilevel converter with separate dc sources
E. Cascaded H-bridges converter with single dc sources
F. Cascaded H-bridges converter with unequal dc sources
G. Hybrid Cascaded H-bridges multilevel converter with single dc sources
H. Cascade MLI with single dc source by employing single phase transformer
I. Hybrid cascade multilevel with bottom three leg inverter
J. Multi-level inverters with varying DC sources

Although each type of conventional and proposed multilevel converters has various advantages and disadvantage and due to their structures and some important they may be suitable for specific application. The inverter dc input mainly battery, PV, PEMFCS, IGs etc.

1.19.1 Neutral Point Clamped Multilevel Inverter (NPC-MLI)

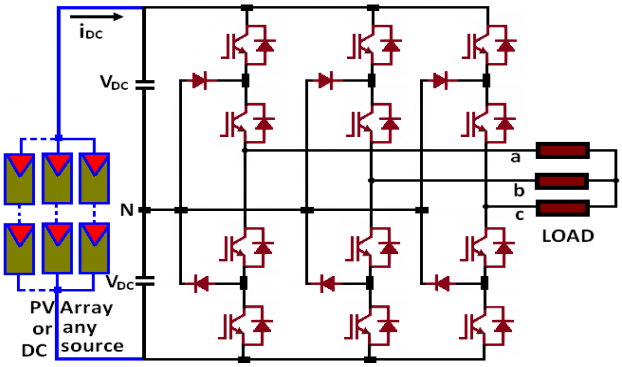

Figure 1.13 Three-level neutral point clamped power circuit

NPC-MLI topology is a modified of two traditional two-level VSCs. Figure 1.13 shows the NPC-MLI construction. This configuration connected by one positive and another negative side of the converter. Moreover to get the proper phase output response two clamping diodes are interlink through a neutral point N and the dc-link voltage is

separating in two divisions. At this instant the NPC-MLI gives, (i) Double power rating (ii) The middle-of-the-dc-voltage point enables the production of a zero voltage stage (iii) Getting a special voltage levels (iv) The gate controlling signal is of digital or binary form which is representing by **0** for the OFF state of the switch and by 1 for the ON state.

ADVANTAGES The capacitance requirements is minimum (b) The DC-link capacitors may be pre-charged as a collected facility (c) The efficiency is high (d) High applicable for renewable energy (e) simple, reliable and flexible (f) it's controlled the reactive and active power flow (g) The overall control technique is very simple due to its back-to-back configuration (h) The filter is unnecessary due high level and harmonics distortion is so.

DISADVANTAGES are (a) Number of required clamping diodes are enlarged (b) The DC-link capacitors control is difficulty (c) At power flow state the controlling technique is becoming more difficult (iv) neutral point synchronization not easy.

1.19.2 Flying Capacitor Multilevel Inverter (FC-MLI)

When the flying capacitors are connected at position of clamping diodes the NPC-MLI are converted to FC-MLI. Figure 1.14 shows the different level of construction for FC-**MLI** topology and there output voltage response.

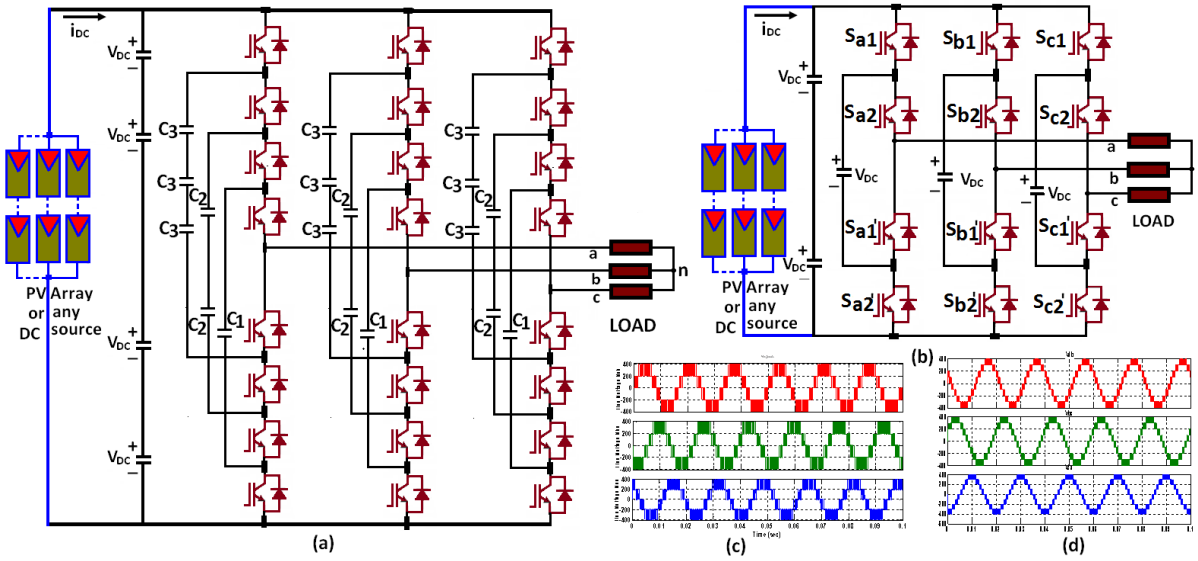

Figure 1.14 The schematic diagram of a (b) five-level capacitor clamped inverters topology (a) three-level flying capacitor power circuit (c) and (d) output of the inverters.

To produce the zero voltage stage the load cannot be directly connected to the neutral of the converter. The DC-link are connected as a chain and at the same time the flying capacitor are connected with positive or negative bar and with opposite polarity .The zero voltage level is obtained by proper synchronization of flying capacitors and the dc-link voltage. Between the nearest two adjoining capacitors the increment of voltage gives the degree of the voltage steps in the output waveform. For huge quantities of connected storage capacitors the major problem in this type of

inverter is synchronization. Voltage rating of every capacitor provided that the used is the equal as that of the central power switch.

Advantages (i) Not required extra clamping diodes (ii) At list one dc supply is required for matching the FC (iii) Cost and loss is low (iv) Construction of series capacitor the performance compare to diode clamped are improved (v) Power flow (reactive, real) can be managed (vi) By lots of abundance of capacitors permits the converter to traverse through tiny amount outages and totally different voltage sags (vii) Using FACTS technology this type of inverter can be control total grid system (viii) Inverter gives the equivalent output voltage level.

Disadvantages (i) complication of modulation (ii) Difficulties encountered whereas trailing the electrical energy levels for each of the capacitors (iii) Pre-charging of all capacitors at identical voltage level along with startup brings a lot of complications (iv) poor switching utilization (v) the start-up is difficult (vi) the potency is poor (x) The structure isn't modularized and hulking and as a result for higher voltage levels packaging is complicated.

Applications of Flying Capacitors Multilevel Inverter are (i) With Direct Torque Control the Induction motor be able to manage (ii) Control of static Var invention (iii) For AC/DC or DC/AC application (iv) Diminish the harmonics effect when the harmonic distortion is far above the ground.

1.19.3 Cascaded H-Bridge Multilevel Inverter (CHB-MLI)

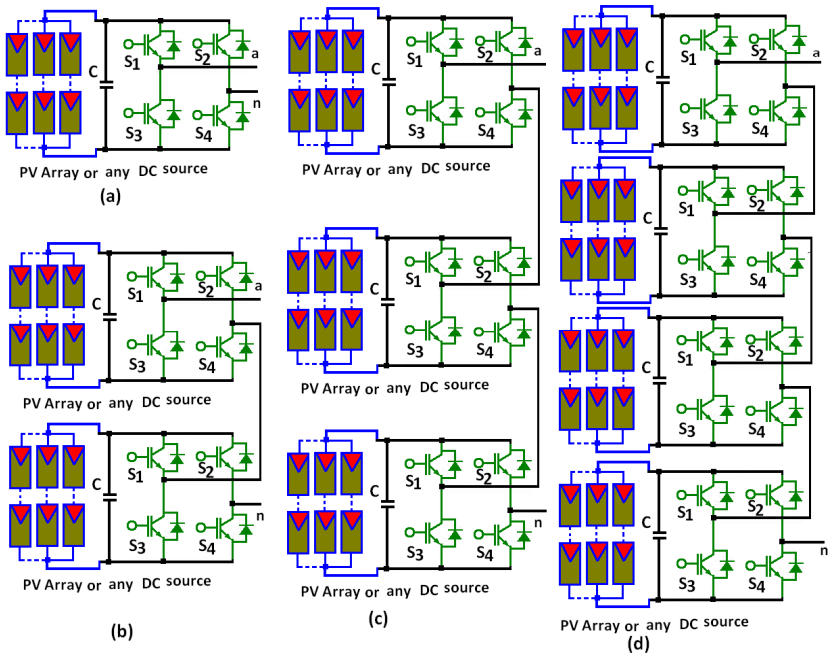

Figure 1.15 (i) Cascaded H-bridges multilevel inverter using (a) one dc sources (b) two dc source (c) three dc source and (d) four dc source.

Cascaded H-bridges multilevel inverter is associated in a chain sequence of n-number (n=2,3,4…) similar pattern. The Single-phase **CHB-MLI** topology structure is demonstrated in Figure 1.15 (i) (a-d). In this case for AC voltage

output, we used individual dc for inverter input. Choice of suitable inverter switching each H-bridge generates dissimilar three voltages which are $+V_{dc}$, 0, and $-V_{dc}$. The inverter output voltage is $+V_{dc}$ when control switch S_1 and S_4 activate, on the other hand the voltage is $-V_{dc}$ when inverter switch S_2 and S_3 are operate or else the output voltage level is 0 when the switches of inverter is S_1 and S_2 otherwise the switches S_3 and S_4 are congested. In example, a MLI can construct a maximum of 11 distinct levels for output of inverter phase voltage for five separate dc sources. Cascade seven levels three phase star connected multilevel inverter topology illustrates in Figure 1.15 (ii). In Figure 1.16 shows the voltage output of cascaded H-bridges multilevel inverter.

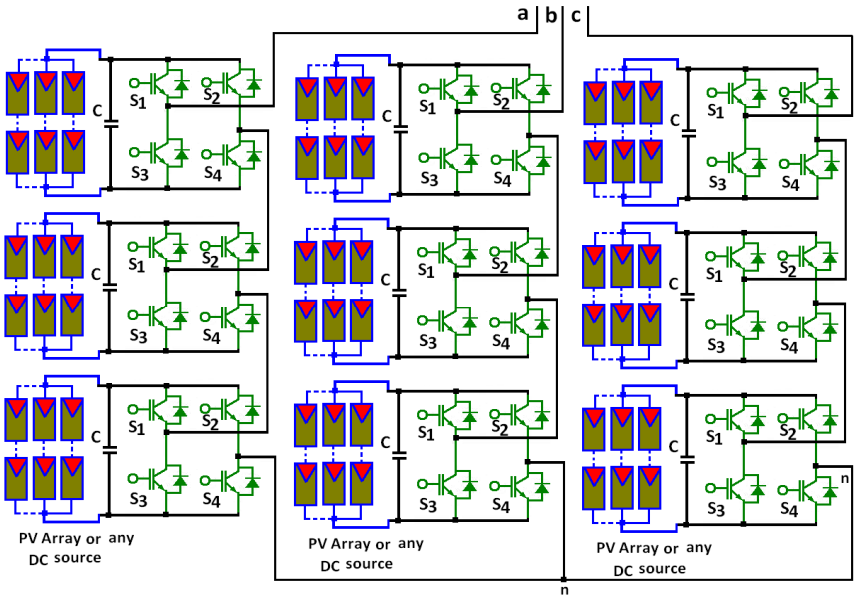

Figure 1.15 (ii) Details of conventional three phase multi-level cascade inverter (Y-configuration)

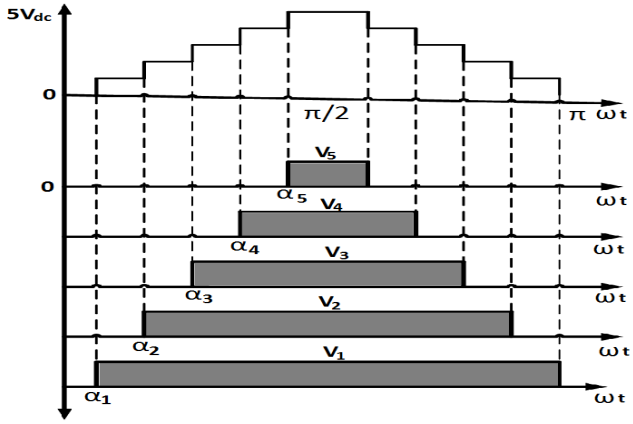

Figure 1.16 Voltage output of cascaded H-bridges multilevel inverter

Advantages and Disadvantages of CMLI

Advantages (i) Low switching loss, low cost and the regulation is simple but high (ii) with a lesser amount of number of components the identical number of voltage levels can be accomplish (iii) minimum quantity of components needed for CMLI (iv) the reliability is maximum (v) The separate DC sources provides segregation of between sources of every unit (vi) the total output voltage added and individual unit is small and therefore anxiety on individual devices gets minimized (vii) for topological view the flexibility is high and hence additional suitable to reconfigure in case of happening of fault (viii) the probable of electric shock is not as much (ix) soft-switching can be used in this type of construction (x) each voltage is equivalent to total output phase where the switching redundancies survive (xi) The harvest voltage and power levels is superior (xii) MLI control the Staircase waveform quality, Common-mode (CM) voltage , Input current, Switching frequency, Efficiency etc.

Disadvantages (i) Used for real power alteration necessities the different dc resource uses are comparatively inadequate (iii) Owing to separate dc supply the function is narrow (iii) Purpose of 3-phase scheme the switching is more switches than a more conformist inverter.

Application of CMLI

Principally the separate DC based inverters are applicable for (i) ac to dc or dc to ac actual power applications, renewable energy application, fuel cell, biomass, photovoltaic, wind, Motor drives, Active filters, electrical vehicle drives, DC power supply utilization, Power issue compensators, and back to back frequency link systems, static power unit generation, FACTS, and traction drive in electrical vehicles.

1.19.4 Diode-Clamped Multilevel Inverter (DCMLI)

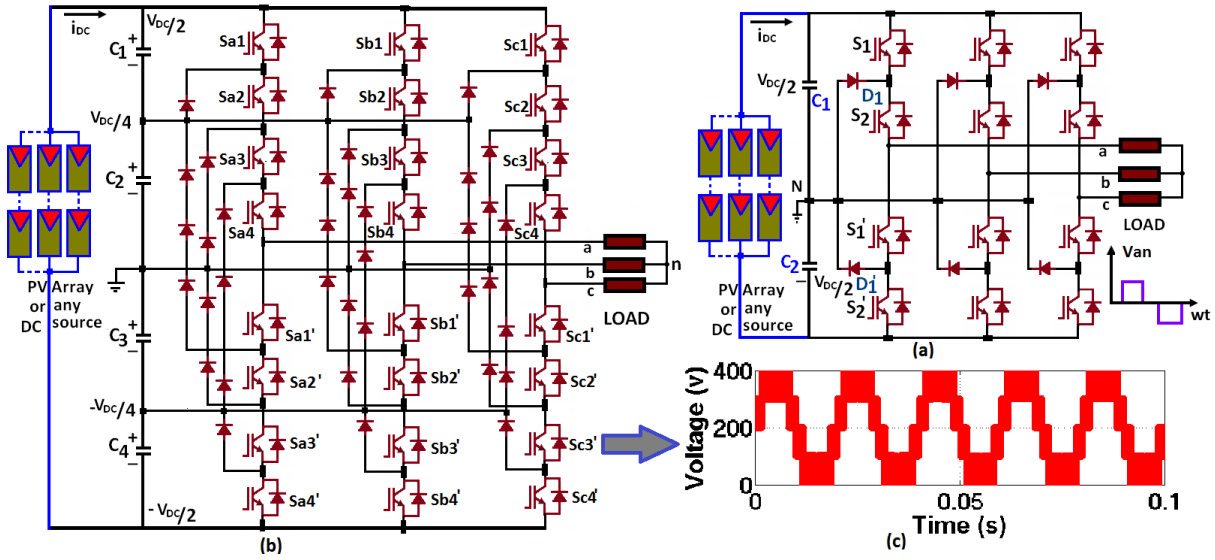

Figure 1.17 Topology of the diode-clamped inverter (a) three-level inverter, (b) five -level inverter (c) phase voltage output

DCMLI is that the most ordinarily used structural topology, to accomplish steps within the output voltage and to clamp the dc bus voltage the diode is employed because of as the clamping device. A three-level DCMLI topology consists of two diodes for access to mid-point voltage and two pairs of switches that are works during

a complimentary mode. By series connected two capacitors, C_1 and C_2 split into three voltage levels from DC bus voltage. From Figure 1.17 the full dc link voltage V_{dc} and therefore the regulated middle voltage half the dc link voltage that is $V_{dc}/2$. For three-level electrical converter the switching state is summarized in Table-1.4.

Table-1.4 Switching states in one leg of the three-level diode clamped inverter

Switch Status	State	Pole Voltage
S1=ON,S2=ON S1'=OFF,S2′=OFF	S=+ve	Vao=Vdc/2
S1=OFF,S2=ON S1'=ON,S2′=OFF	S=0	Vao=0
S1=OFF,S2=OFF S1'=ON,S2′=ON	S=-ve	Vao=-Vdc/2

The number of required diodes and conjointly the quantity of switching devices will increase for the high level, and build the arrangement unfeasible to implement. Generally for a p level DCMLI, for every one leg 2(p-1) switching devices, (p-1) * (p-2) clamping diodes and (p-1) dc-link capacitors are necessary.

Advantages:

The following advantages of the DCMLI are (i) DCMLI will be operated at high potency with the elemental frequency (ii) electrical capacitor will be pre charged along at the specified voltage level (iii) By connecting phases of electrical converter with common DC link, the capacitance demand will be reduced (iv) the control methodology is easy (v) the harmonic magnitude, %THD can reduced by rising the number of level and minimize the filtering cost (vi) the connected capacitors may be pre-charged as a group (vii) potency is extremely high (viii) can be used as back to back inverters (ix) Less number of devices is needed as compared to cascaded H-Bridge topology (x) Switching redundancy is flexible for balancing the voltage (xi) Real and reactive power is controlled by this kind of electrical converter

Disadvantages are (i) Excessive clamping diodes area mostly needed when the number of inverter levels is far above the ground (ii) it's strongly difficult to manage the actual power flow of individual multilevel converter (iii) the storage capacitor number is very unnecessary (iv) Flow of real power is tough for single electrical converter as intermediate DC levels can tend to discharge and overcharge while not precise observance and overall control (v) System isn't versatile, reconfiguration of electrical converter cannot be done on incidence of fault and as a result this topology isn't redundant, i.e., if any switch gets broken, the entire converter gets offline.

Applications of Diode Clamped Multilevel Inverter: (a) static VAR compensation applications and other and FACTS control system (b) Variable speed motor drives (c) High and medium voltage scheme interconnections (d)

all type of DC and AC voltage transmission lines (e) This topology is well suited for variable speed drive with high power medium voltage motor.

1.19.5 Cascade H-Bridge Multilevel Inverter with Unequal DC Voltage Sources

In CMLHBI could also be introduced by equal and unequal DC voltages power cells. In Figure 1.18 shows the development of unequal dc voltages. This structure for three-cell electrical converter is construct thirteen level voltage wave shape i.e., 6V, 5V, 4V, 3V, 2V, V, 0, –V, –2V,–3V,–4V,–5V,–6V.

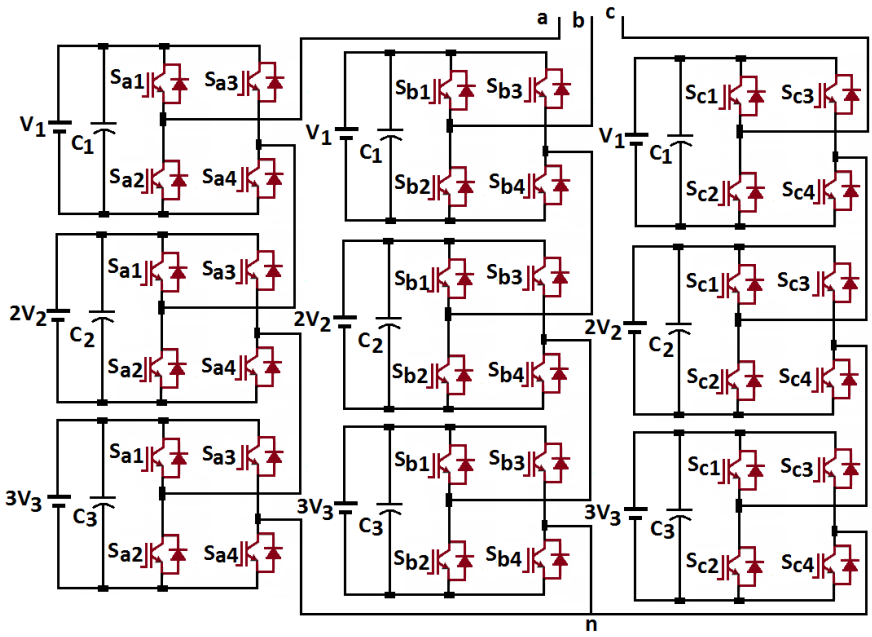

Figure 1.18 Cascade multilevel converter with minimum number of dc sources

Merits are (i)Total reliability of the scheme is improved significantly (ii)The cost is less and construction is very simple (iii) Modularity is finite (iv) For simple manufacturing with flexibility this is applicable in PV, wind, FACTS system (v) Easily control the real and reactive power purpose.

Demerits

- Complex switching because switching pattern design becomes much more difficult.
- For poor THD of the output voltage this kind of topology has restricted industrial applications.

1.19.6 Hybrid Cascade Multilevel With Bottom Three Leg Inverter

The three-phase hybrid structure of multilevel converter topology is showing in Figure 1.19. The bottom side 3-leg consists of one DC supply. The input of the H-bridge will use a PV, wind, IG, capacitor, battery or alternative dc power supply. The switching strategy is very easy and it's depending on whether it is necessary to charge or not it's essential to charge the capacitor. This sort of electrical converter simply controlled the harmonic magnitude and improves the power quality with ability. These inverters are generally used in utility interface applications with PV, Wind, FACTS, energy storage device etc.

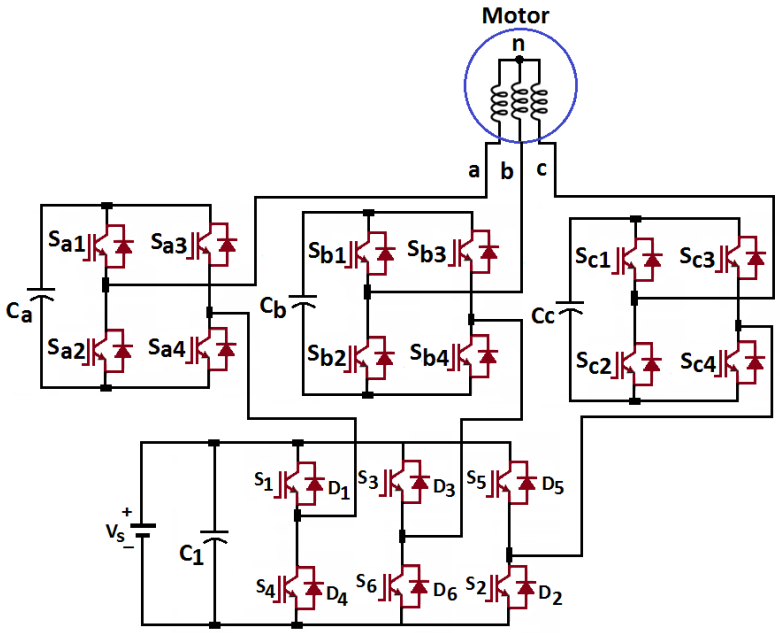

Figure.1.19 Hybrid cascade multilevel Bottom Three Leg Inverter with single dc-source

Merits: Simple construction, Low Cost effective, the Packaging is much easier, Improvement in reliability is effectiveness, High application in renewable energy purpose, actual and reactive power control practically improved and for FACTS application (i.e. STATCOM, DVR, UPQC etc.) it is highly relevant.

Demerits

- The switching pattern is complex
- The modulation index range is narrow.

1.19.7 Hybrid Cascade H-Bridge Multilevel Inverter with Single DC Source:

In Figure 1.20 shows the hybrid cascade H-Bridge construction of MLI with renewable energy supported single DC supply. This configuration of MLI contained electric battery or fuel cell with an output voltage of Vdc for the primary H-bridge (H1). On the opposite side for the second bridge, the input dc supply is capacitor. The output voltage of the primary H-bridge and resulting H-bridge is V1 and V2 severally. During this configuration, the choice of electrical capacitor values is incredibly necessary.

Merits: More reliability, cost is low, efficiency high, applicable in FACTS and renewable energy system, contained low harmonics and also the power quality are high.

Demerits

- For large discharging time and small charging time the modulation index range is thin.

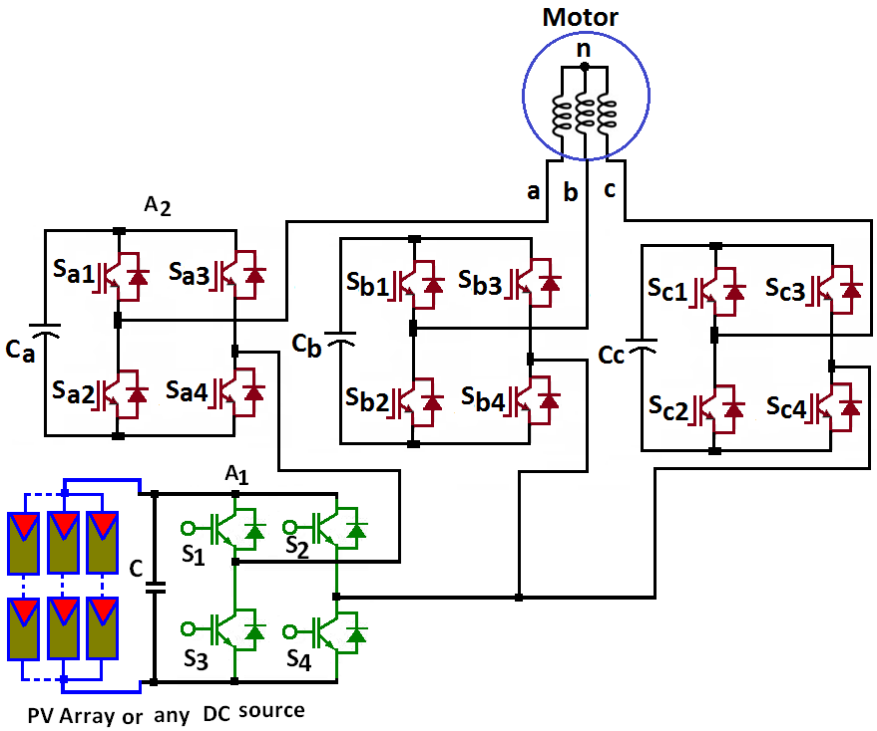

Figure 1.20 Hybrid cascade H-bridge multilevel inverter with single dc-source

1.19.8 Cascade H-Bridge Multilevel Inverter by Employing Single Phase Transformers

Figure 1.21 shows a high performance Cascade H-Bridge Multilevel Inverter which is constructed by single phase transformers with single dc source (i.e. battery, PV, IG, PEMFCS etc). For utility interfacing applications these special type of converter are broadly used.

Advantage are -Single DC supply, for single phase transformer the voltage is added and stepped, the overall system is simple, reliable, flexible and low cost, versatile, applicable in renewable energy system**,** the output waveform is smooth, can control the real and reactive power, for FACTS (i.e. STATCOM, DVR, UPQC etc.) it is very much applicable.

Demerits

- The switching pattern is multifaceted.
- The modulation index range is slender.

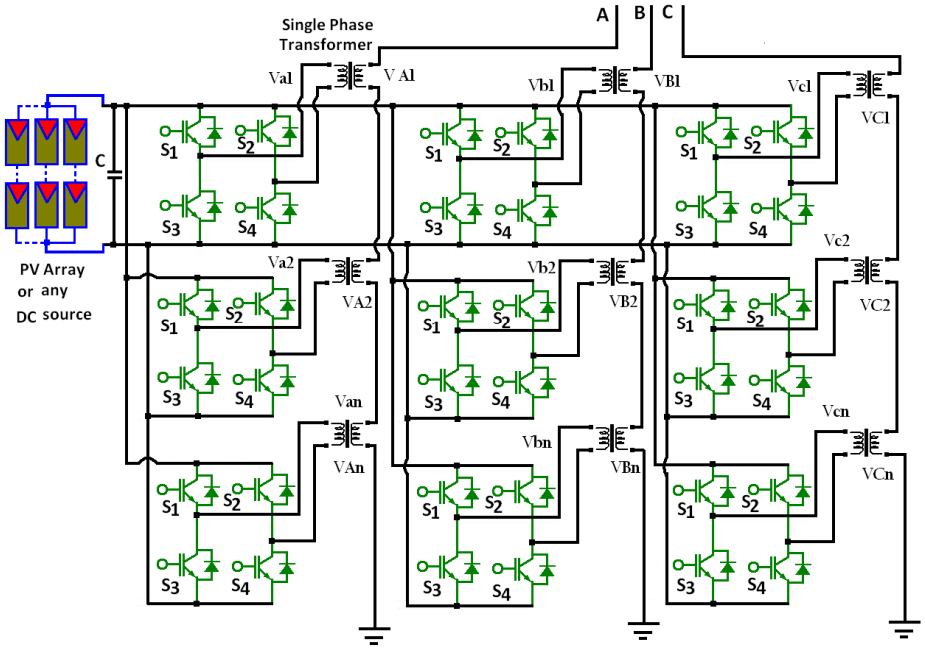

Figure.1.21 Details of cascade multilevel inverters with Single dc source by employing single phase transformers

1.19.9 Cascade Multilevel Inverter with Cascade Transformers

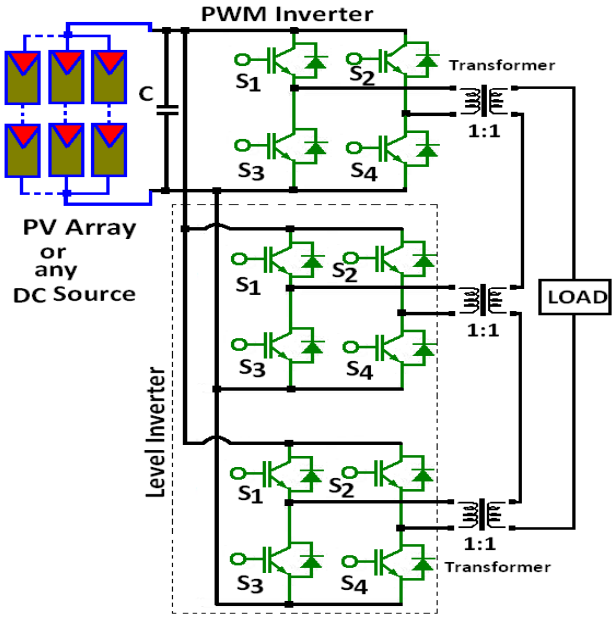

Figure 1.22 Details of Cascade multilevel inverter with Single dc source by employing cascade transformers

In Figure 1.22 illustrates the construction of cascade multilevel inverter with cascade transformers. The innovative structure is extremely applicable in PV, wind and alternative renewable energy system. For construction of cascade

transformer on secondary we can exchange the power from ac utility, from comparatively low dc voltages by itself. It's the superfluous deserves that no output filter needed due to transformers. For fundamental switching mode the switching losses are very low and the efficiency is very high.

Advantages: (i) single DC supply (b) trouble-free, reliable, and low price (iii) potency is higher (d) modularity degree is high (e) perfectly manage the real and reactive power (f) highly applicable DFIG, FACTS and other renewable.

Disadvantages:

- The complexity in switching scheme is high.
- To generate a higher number of voltage levels the excessive numbers of switching components are required.
- Waveforms are poor quality because of the third harmonic component and usage of many switching components.

1.19.10 Cascade Multilevel Inverter with Single DC Source by Using Three Phase Transformers

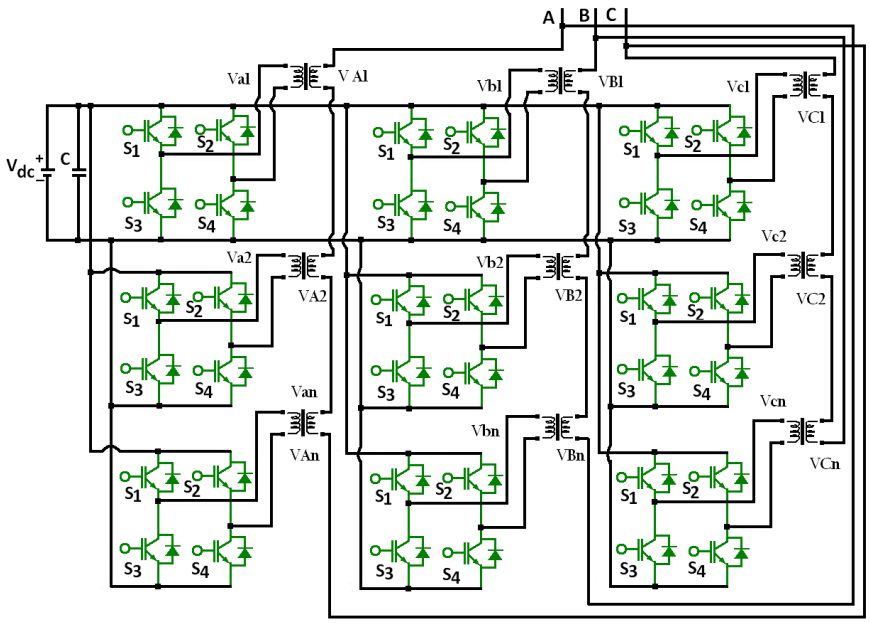

Figure 1.23 Cascade multilevel inverter employing three-phase transformers with single dc source.

In Figure 1.23 shows the configuration of the cascade multilevel single DC source with three phase transformers connected inverter. These types of inverters are generally similar to the NPCMLI type and this configuration mostly used in transmission and distribution system. Recently this inverter are used in FACTS control system for reactive power and power quality improvement purpose. This type of inverter is highly appreciated because the harmonic present is very low. The adjustment of three phase transformers and PWM operation the voltage and current waveform are more accurate and similar to the NPC-MLC performance.

Advantage: (i) The switching pattern is very simple and acceptable (ii) It is applicable in FACTS (like STATCOM, SSSC, DVR, UPQC etc.), renewable energy, domestic and industrial purpose (iii) This type of inverter greatly progress the power superiority (iv) The harmonic magnitude is very low (v) Number of switching is reducing per cycle and the switching loss is very low (vi) The number of DC source is single and the number of capacitor is very low (vii) Easily applicable in photovoltaic, wind power and other grid connected system (viii) This type of inverter reduces in voltage and current hazard (ix) The common-mode disturbance is preferred level.

Disadvantage:

i. For 3-phase transformer the overall cost and total size is slightly amplified.

1.20 Harmonic Elimination Switching Schemes [24, 25, 26, 27]

Description: For increasing the power electronics device, non-linear load, presence of variable electric loads on the power system the voltage and current waveforms assume non-sinusoidal shape. As a result the different magnitude and phase related sine waveform distorted and the frequencies that are multiples of power-system main frequency.

Causes: Typical sources: when the electric machines functioning higher than the knee of the magnetization curve (magnetic saturation), welding machines, arc furnaces, PWM, rectifier load, and application of DC brush motors.

Consequences: Possibility of the amplified resonance, in 3-phase systems the neutral overload, overheating of all the electrical cables and apparatus, loss of efficiency in electric machines, at communication systems the electromagnetic interference, in measuring purpose the errors occurs when using average reading meters, trouble of tripping the thermal protections, malfunction the PMU, flow meter, smart meter etc.

Appropriate solution: Using active and passive filter, k-rated transformers can minimized the harmonic distortions, delta-wye transformers, PWM switching, increasing the size of conductors can help reduce impedance and thus the harmonic distortion, the power electronics FACTS controller (STATCOM, UPQC, UPFC, DVR etc) control the harmonic.

Modern power-electronics based equipment, like rectifier, choppers, and inverters produces current and voltage harmonics throughout the inverter switching time. These harmonics introduce the instrumentation or equipment that the connected to a similar system through conduction and by radio interference.

Presence of harmonics within the electrical inverter system leads to the following disadvantages:

a) Due to the extreme heating the harmonics current reduces the load caring capability.
b) Without proper regulation and control in power side the harmonics can affect their operation and can results system malfunctioning.
c) In presence of harmonic current on the sensitive or critical loads produce pulsation torque.
d) Harmonics currents increase the loss within the ac system.

By harmonics minimization, these effects can be minimized. Harmonic elimination is an important issue in inverter switching schemes. By reduction of harmonics contents or by wave-shape improvement the system performance can be improved. Switching schemes used in practice are,

A. 180-degree switching operation

B. 120-degree switching operation
C. Bipolar switching operation
D. Unipolar switching operation
E. 60-degree modulation switching operation
F. Virtual Stage PWM switching operation
G. Multi level switching operation

1.21 Flexible Alternating Current Transmission System (FACTS)

Flexible Alternating Current Transmission System (FACTS) [15-18, 94-100] is a most recent integrated innovative idea based on smart power electronic switching converters and fully energetic controllers to improve the whole system operation and power transfer capability moreover because the responsibility, reliability, security, stability, and power superiority. From first to last the years there has been an augmentation in the enormous quantity of power transfers and electric utility power transmission facilities all over the world are not openly permitted to progress due to the various kind of ecological, land-use and authoritarian pressures that arise. At the same time the foremost outcome upholds in electric power transmission, asymmetrical power capability tradition, and disagreeable parallel pathways or loop movements are being well-knowledgeable. The operational coordination becomes very difficult to supervise finally becomes the comprehensive there is improve in power transfer. In case of enormous electric power movements this complexity of the whole manage on the scheme becomes extremely feeble and the electrical required power transport can become insecure. The USA utility industry Electric Power Research Institute (EPRI) at first dealing in joint research and development arm, has nowadays decided to furnish power electronics based Flexible AC Transmission System (FACTS) technology, a healthy solution for the above mentioned problems. When the capacity of electrical power flow is massive the multipurpose power electronic solid states devices, FACTS are utilized to stay in ensure the total grid systems and protect the overall system troubles. The US researchers of EPRI have been invested in FACTS both in stipulations of its significance values and capability. The advance FACTS generally progress the Micro-grid prospective, active and reactive power management, to regulate the voltage and to add to the lower voltage systems' plus points. Now the FACTS are straightforwardly apply in micro grid, grid and smart grid and improved the system constancy or reliability. Near the beginning of 1960s the development of thyristor technology had started growing. Power electronics switching based on thyristors are a key component in controlling the automatic components in active and reactive power compensation systems. The electrical pulse is transformed by fiber optics at ground potential directly to control the electronics thyristor gate. For this electronic equipment the different triggering technique reduces the number of electronic and electrical components in the thyristor valve and, also improves the reliability and eliminates all the electromagnetic compatibility problems. The thyristors can block voltages up to 8-kilovolts and carry current up to 4,200 amperes.

- The FACTS is power-electronic idea based mostly advance controllers, which improve the capacity or capability of transmission and distribution networks.

- The energetic FACTS controllers operate without any risking extremely fast and increase the secure in operating limits with stability.
- The solid-state switching devices completely manage the electrical power flows on the lines to protect with highest margin of safety.
- The modern FACTS controllers transmit mostly required electrical power with high superiority at a smallest amount of operating expense and increased the value of overall transmission assets.
- Through low interruption–rating isolators the faulted DC line can be discontinue.
- The FACTS controllers control line-to-ground fault clearing without employ of any circuit breakers.
- The speedy controllers control the transient constancy of the systems through active-power damping.

1.21.1 Static Synchronous Compensator (STATCOM)

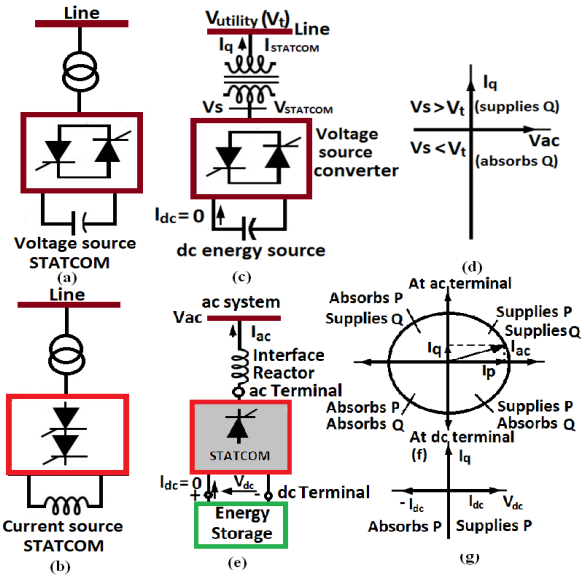

Figure 1.24 Schematic diagram of STATCOM for (a) Voltage source (b) current source (c) a power circuit (d) reactive power exchange (e) with an energy-storage device of suitable capacity (f) power circle and (g) power exchange.

Figure 1.24 illustrations the demonstration of STATCOM for (a) Voltage source (b) current source(c) a power circuit (d) reactive power exchange (e) with an energy-storage device of suitable capacity(f) power circle and (g) power exchange. The Sullivan substation 100-MVA STATCOM is first installed the Tennessee Valley Authority (TVA) in 1995. STATCOM is a shunt connected powerful FACTS regulator and it has the most common uniqueness to that of synchronous condenser however it's no inertia. STATCOM connected to a line generally without any transformer and consists of a solid state voltage supply or current supply inverter however typically voltage supply is most popular. This special type of arrangement either provides or draws the reactive power at the purpose of point of common coupling while not any large capacitor banks or external reactors at a more rapidly rate compared with synchronous motor condenser. It matches a capacitive or an inductive

reactance at the purpose wherever it is connected because this type of regulator injects the current almost in quadrature with the line voltage.

1.21.1.1 Harmonic Performance of STATCOM

The shunt connected STATCOM consists of IGBT based semiconductor switches with anti-parallel diodes as shown in Figure 1.25.The converter output waveform is shown in Figure 1.26 which is producing balanced three quasi-waveforms with given frequency.

For distorted waveforms of voltage and current due to harmonic effect induces the system abnormality, freeloading losses and affects the control accuracy in measurement instruments and sometimes the control and protection equipment. For harmonic elimination a proper switching technique (like120°,180°, bipolar, unipolar and modified unipolar etc.) can be selected to mitigate the harmonic and high-frequency problem.

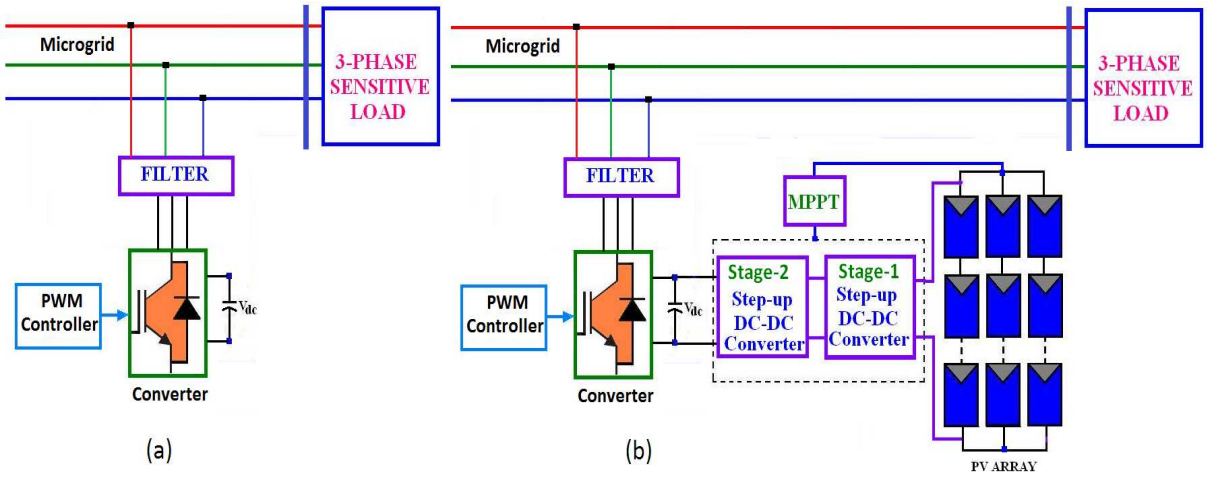

Figure 1.25 Configuration of VSC based STATCOM (a) conventional (b) proposed

The output of the STATCOM line & phase voltages are V_{ab} ,V_{bc},V_{ca} and V_{an}, V_{bn}, V_{cn}respectively. The Fourier analysis of STATCOM is as:

$$V_{ab} = a_0 + \sum_{n=1}^{\infty}\left(a_n \cos(n\omega t) + b_n \sin(n\omega t)\right)$$

The phase voltage waveform of a 3-phase bridge inverter is a quasi-square wave. The wave form has quarter-wave symmetry and due to the quarter-wave symmetry, we get

$a_0 = 0$for all n , and $a_n = 0$, for all even n

also, $b_n = \frac{2}{\pi}\int_0^{\pi} V_{dc} \sin(n\omega t)\, d(\omega t)$ for all odd $'n'$

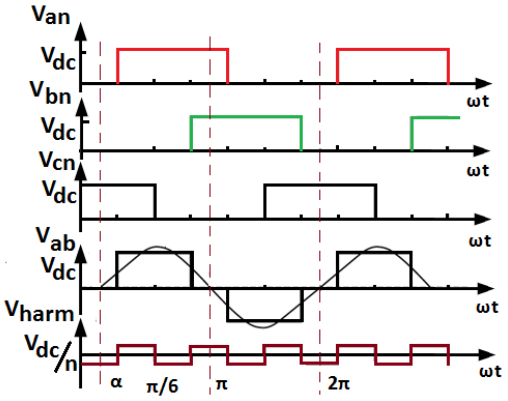

Figure 1.26. The output waveforms of the STATCOM for 180-degree conduction mode

$$b_n = \frac{2}{\pi}\int_{\alpha}^{\pi-\alpha} V_{dc}\sin(n\omega t)\,d(\omega t)$$

$$= \frac{2V_{dc}}{n\pi}\cos(n\alpha)$$

Therefore

$$V_{ab} = \sum_{n=1,3,5,7,\cdots}^{\infty} \frac{4V_{dc}}{n\pi}\cos(n\alpha)\sin(n\omega t)$$

For better quality of power and to reduce the harmonic generation, different type of converter configurations and converter-switching techniques are recommended in this chapter.

1.21.2 Custom Power Dynamic Voltage Restorer (DVR)

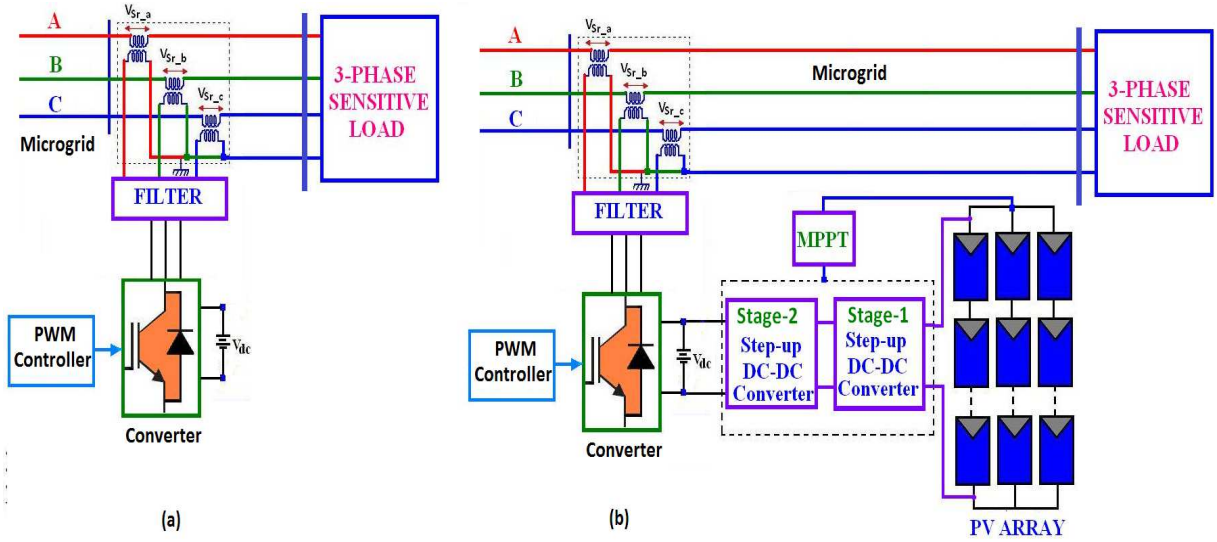

Figure 1.27 Configuration of Dynamic Voltage Restorer (DVR)

Custom power FACTS control device, DVR is a flexible series connected restricted compensator. DVR can protect the sensitive load against voltage unbalanced. The DVR enhanced the power superiority for voltage dip mitigation. The compensator DVR operate only abnormal condition by switching technology where the normal voltage or unaffected load voltages conditions the DVR is stationary and performs no switching to reduce losses. The DVR detects the voltage dip and injects the absent measuring voltage until the energy storage and absolutely drained or returned to customary voltage levels. The synchronism time with the supply is very short and the injected voltage for every phase can be controlled autonomously in magnitude and phase at the same time the zero sequence effect can be eliminated.

The compensator DVR controls the positive sequence, negative sequence, zero sequence in the supply voltages. This compensator compensate the symmetrical and non-symmetrical voltage dips which is cases for different kind of sensitive loads and control voltage sags, voltage swells, flickers, harmonics etc. The basic configuration of the DVR has converter, filter, injection transformer, DC-link and energy storage, By-pass equipment, disconnection equipment, energy storage etc. The main objectives are to amplify the capability of consumption of distribution feeders, decrease the losses and progress power quality at the load bus. In the smart distribution system, the uncompensated sensitive or nonlinear loads introduce the harmonic within supply voltages. To mitigate this issues caused by poor quality of power supply, series connected DVR compensators are used to optimize the power excellence. The Duke installation in U.S.A. in August 1996 initial used the DVR application and therefore the evaluation of 2 MVA with 660 kJ of energy storage with 50% compensating voltage sag rating period of 0.5 second (30 cycles). Figure 1.27 shows the DVR configuration.

The DVR has mainly two working modes.

1. Standby operation mode or short circuit operation (SCO) mode- in this case the magnitude of voltage injected is zero.
2. Boost operation mode which menace when the compensator device DVR inserts a necessary voltage of suitable magnitude and phase to re-establish the pre-fault load bus voltage.

The DVR can

- Protect the sensitive loads from short duration voltage dips
- Compensate voltage sags, voltage swells, flickers, harmonics, and transients mainly compensation for the harmonics and unbalance in the source voltage.
- Improve reliability and power quality.
- Progress the power factor on the supply side (at PCC)
- The real and reactive power Generating or absorbing by proper way

The different issues of power quality with highlighting put on voltage dips and power quality issues are

- Voltage / current unbalance, power system harmonics, interruption/ over voltage/ under voltage, voltage sag, voltage swells, flickers etc, power system transients, power frequency disturbances, outage, ringing waves.

1.21.3 Unified Power Quality Conditioner (UPQC)

The unified power quality conditioner (UPQC) is a most multitalented power quality improvement power electronics switching based custom power device. The UPQC construction is similar to another versatile FACTS device unified power flow conditioner (UPFC). The UPQC contains one series and another shunt connected voltage supply inverters (VSIs) which are coupled to a typical dc energy storage element. The series connected VSI control the voltage sags, swells flicker, voltage unbalance, spike and harmonics and also mitigates the supply side instability. The Series connected completely different type of converter connected to take care or maintain of the load voltages level that is balanced and distortion free. The shunt connected inverter compensates, mitigates the current quality problems, power factor problems, load harmonic currents, load unbalance, reactive power problems etc. The overall construction of the UPQC is shown in the Figure 1.28. The total UPQC model control by various control loops like voltage control loop, current control loop, voltage and current unbalance measuring control loop, switching control loop, PLL control loop etc.

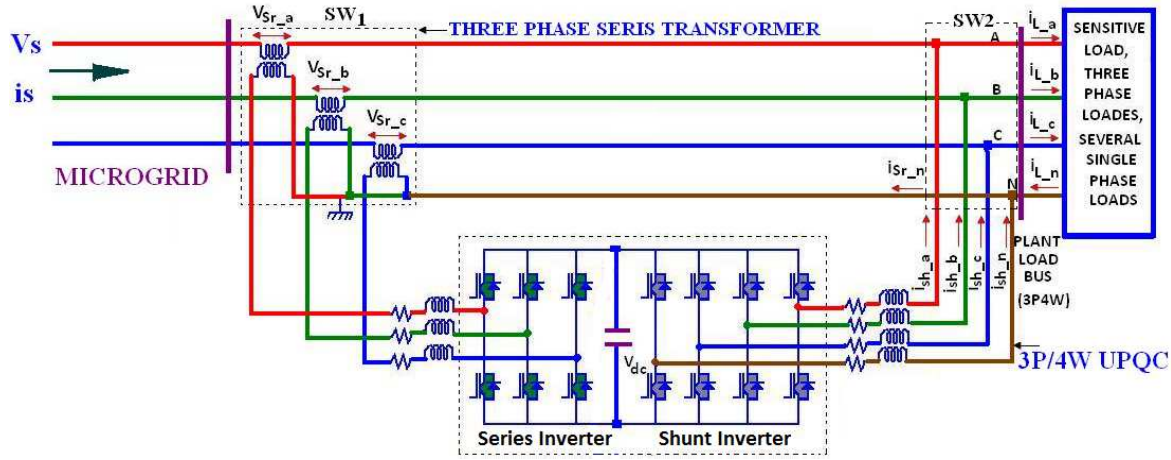

Figure. 1.28 Basic model of 3-phase 4-wireUPQC configuration

By active power management and minimum VA loading control the UPQC work as an in-phase process. The voltage injection through series converter, construction of quadrature voltage injection and load angle control mode or the power angle facility control mode of operation that mitigates the power superiority problems in grid, micro-grid and sensible grid or smart grid systems.

Control Objectives of UPQC

The shunt path of the converter provide the subsequent management objectives

A. To steady the supply currents and voltages by initiating negative and zero progression mechanism desired by the load
B. To regulate the harmonics within the load current by inserting the specified harmonic currents.
C. To regulate the ability issue or power factor by injecting the specified reactive current (at elementary frequency)
D. To supervise the bus voltage of DC side

The series path converter has the subsequent supervision objectives

a. To sense of balance the voltages at the load bus by injecting negative and zero sequence voltage to complete those contributions within the supply.
b. To manage the amount of voltage for load bus by boosting the required real and reactive essentials at normal frequency on the availability aspect which is concerning on the power factor issue (PFI).
c. At the contribution port to handle the PFI of the UPQC is restricted by the shunt connected power electronics converter.

   The application of the UPQC is for

   - Distributed generation such as wind generation, PV power, micro-grid, smart grid, grid etc.

1.22 Outline of the Thesis

The organization of the thesis is outlined as follows

Chapter 1 explains the introduction, Research Background, About Micro grids, Microgrid Definitions, Basic components in micro grids, Advantages of micro grid, Disadvantages of micro grid / Challenges, DG units like Wind, Photovoltaic Energy, MPPT control Hydropower, PEMFCS, Geothermal energy, Bio energy Micro grid Control , Power Quality improvement of micro grid system, Motivation of the proposed work. DG controls Methodologies, where we discussed Different type of inverter and different switching technique. Concept of multilevel inverters, Concept of classical inverters and medium or high power inverters, Traditional multilevel inverters i.e. NPC-MLI, FC-MLI, CHB-MLI, BLMLI. Also we discuss the conventional and proposed Harmonic Elimination Technique. Presents the PQ issues with reactive power compensation through FACTS devices. This chapter, we discussed the advances in Power-Electronics Switching Devices, Principles and Applications of Semiconductor Switches, What is Flexible AC Transmission (FACTS), Why Compensation Techniques are used in Power system?, Controllability of micro-grid, grid and smart-grid system. This chapter covers the different Type of FACTS controller.

Chapter 2 cover the Proposed BBO based selected harmonic elimination technique for DFIGs connected to a micro-grid, where we construct a new model of micro-grid configuration and control of micro-grid strategies also we connect a new switching technique with 180º Mode of operation for Quasi sine wave switching, and 120^0 mode of operation for quasi sine wave switching. We measured the Different standards for voltage and current harmonics and the proposed switching control the harmonic level and also proposed switching applied Co-ordinated approach for harmonics elimination. Proposed Harmonic Elimination Principle control the switching angles using BBO algorithm. Simulation and experimental results for 180º Switching mode of operation and 120^0 switching mode of operation control the harmonic and system the power quality. The simulation & experimental Results verified the grid code.

Chapter 3 describes speed dependent stator harmonics elimination of DFIG through Proposed RSC switching where the proposed work are basic idea of DGs, DFIG and stator side harmonic. In this chapter we proposed a

DFIG based System configuration. In this DFIG system we discussed step by step the Harmonic Analysis for Stator and Rotor Currents. Another proposed work Rotor Speed dependent Stator Harmonics. Here we calculate the harmonics for rotor speed dependent stator harmonic at 1 to 3000 rpm. The switching mode is 180^0, $120^{0.}$ Proposed Harmonic Elimination Principle using BBO Algorithm successfully controls the harmonic magnitude and power quality. This chapter we control the Sub-harmonic. The key emphasis of the work the proposed on-line Control Scheme.

Chapter 4 Proposed Performance of DFIG, DVR, STATCOM, UPQC with common DG systems and Biogeography-Based Optimization. Where we discussed the Importance of DG, DFIG, STATCOM, DVR, UPQC in power system. Studies the proposed system micro-grid configuration. Existing and Proposed Switching Strategies mainly the suggested harmonic elimination method for multilevel inverter. Comparative study of different conventional and proposed soft-computing techniques. Also Studies Effect of variation of free parameters with BBO. The Simulation Results for Proposed and Conventional Inverter PV based DC-DC Converter, for STATCOM, DVR, and UPQC with Filter concluded that the power quality is best for UPQC. Performance Comparison of the proposed DFIG-PV system under UPQC, DVR and STATCOM modes verified the UPQC performance. Experimental Result and Discussion are verified the simulation results.

Chapter 5 Proposed Photovoltaic (PV) based DVR, Where we discussed Proposed micro-grid configuration with DVR, Existing and Proposed Switching Strategies, Multilevel inverter operation, Proposed Elimination of Harmonic Principle Using BBO Algorithm, Proposed multilevel inverter with varying DC sources, DVR operating states, Simulation Results for multilevel Inverter, Simulation Results for DVR and filter, Resistive load with balanced & unbalanced mitigation of voltage sag, swells for nonlinear load, Placement of capacitors near a DVR, Voltage Flicker suppression and Induction Motor Load operation.

Chapter 6 Proposed Three phase PV-wind- PEM- FCS-HCBLMI- based DVR, STATCOM and UPQC topology with SVPWM Proposed FACTS Connected Micro-grid Configuration, The new configuration of the proposed PV-wind-PEMFCS based DVR, STATCOM and UPQC, Optimal Predictive Multilevel PV-wind-PEMFCS-based DVR, STATCOM and UPQC Control System with SVPWM Algorithm, Different Level Proposed Multilevel Inverter Topology, Proposed Space Vector Pulse Width Modulation Switching control strategies, SVPWM simulation output results, Simulation Results for DVR, STATCOM and UPQC with Filter, Proposed PV-wind- PEMFCS based DVR simulation results, Proposed PV-wind- PEMFCS based UPQC simulation results, Compare to the performance of the PV-wind- PEMFC-UPQC, PV-wind- PEMFC -DVR and STATCOM,

Chapter 7 discussed the Conclusions and Future Research

Appendix of the thesis

Reference of the thesis

Chapter 2

Proposed BBO based selected harmonic elimination technique for DFIGs connected to a micro-grid

Chapter 2

2.1 Chapter Overview

This chapter illustrates the biogeography based optimization (BBO) based selected harmonic elimination technique for DFIGs connected to a micro-grid. The lower order harmonics are individually eliminated in each DFIG outputs but the higher order harmonics are eliminated in such a way that the harmonics generated by one source is eliminated by the other after generating the same order of harmonics in opposite phase. The switching angles are computed off-line and stored in microcontroller memory in the form of look-up tables for on line application. The excitation power for the inverters is obtained from a photovoltaic (PV) panel. Proper simulations are executed for the proposed theory and subsequently supported by investigational verifications. Both the simulation and experiments agree well with the analytical formulation. The total harmonic distortion (THD) in the output is found to be within the stipulated limit.

2.2 Basic idea of DGs, DFIGs, and Harmonic Elimination

Micro-grid systems with induction generator as one of the distributed sources of generation (DG) are widely being introduced for production of electrical power. The doubly fed induction generators (DFIG) are becoming increasingly popular for such scheme to generate electricity at constant voltage and frequency from a variable speed wind turbine. The DG units [28], connected to micro grid [29] operate either in parallel with the large utility grid or in the islanding mode, while providing continuous power to multiple loads and end-users. The most popular configuration of micro grid having DFIG wind energy conversion system along with the PV generation modules is shown in Figure 2.1. The rotor side is fed with a three level quasi-sine wave supply generated from a simple bridge inverter, while the stator side is directly connected to the micro grid. The dc input to the inverter is from a group of PV panels. The output from the PV panels is buffered through a set of batteries which absorb the excess power from the PV panels or the generated power from the rotor of the DFIG when the speed goes above the synchronous speed. The last part of the power converter operates as rectifiers. To reduce the switching losses while having a simple control circuit, a six-step switching technique [30, 31, 32] is widely used in thyristor based inverters both in the rotor and grid side. The six-step switching technique contains all odd harmonics except triple-n harmonics. The harmonic current components present in the rotor circuit induce corresponding harmonics in the stator, resulting in pulsating torques.

Micro-grids operate at distribution voltage levels. During the past few decades, electrical system loads have been increasingly becoming sensitive in nature because of the increased use of power electronic and computer controlled devices. Maintaining stipulated quality of power as recommended in IEEE 1547, IEC, IEEE 519, EN, CIGRE WG 36-05 specifications as have thus become mandatory. Harmonic elimination therefore is a very important issue is respect of the operation of the micro-grids.

The elimination of specific harmonics from a given output voltage waveform generated by voltage source inverter using pulse width modulation (PWM) has been widely dealt in literature [33, 34, 35, 36]. These methods are known as selected harmonic elimination (SHE) or programmed PWM techniques. The SHE problem becomes complex and computation intensive with the increase of number of harmonics to be eliminated. The method given in [37,38, 39, 40] uses PWM technique while in [41, 42, 43] a space vector topology is used for this purpose. Both these techniques are having high switching losses. Harmonic analysis of DFIG can be found in [44]. Harmonic elimination problem is a set of non-linear transcendental equations. The solution approach of this problem by eliminating selected harmonics while obtaining the required fundamental component of output focused in [45,46], has become a great challenge. The rapid convergence of Newton iteration is achieved in [47, 48] by predicting initial values. Multiple solutions to the SHE problem are focused in [47, 48] while [49] presents an optimization technique to minimize the harmonics. The recent trend in optimization technique which is becoming very popular uses population of points instead of a single point. For instance, Genetic Algorithm (GA) has been used to the solution of SHE problem [50, 51, 52, 53, 54]. [55, 56, 57] describe the application of the Particle swarm optimization technique (PSO). But none of these techniques are implemented in a DFIG-based converter switching application. Various control strategies are also proposed for micro grids connected with DFIGs [58, 59].

This chapter presents an optimization approach for harmonic minimization technique of DFIG connected to micro grid. Combination of PV panel and wind generator in the micro-grid system with two inverter switching schemes have been proposed. Since the inverters connected to the micro-grid handle bulk amount of power, a lesser number of switching per cycle is advantageous for satisfactory operation and reduced switching losses. The combinations of different switching with BBO [60] based harmonic optimization are applied for this purpose. In the proposed scheme, the frequency and phase of one inverter is so chosen as to counter balance the selected order of harmonics generated by the other inverter in the micro-grid system. Thus, a wider band of harmonics can be reduced to a considerably low magnitude with less number of switching for either of the inverters. Proper simulations and experiments are performed on practical inverters which support the theoretical formulations.

2.3 Proposed Micro-grid Configuration

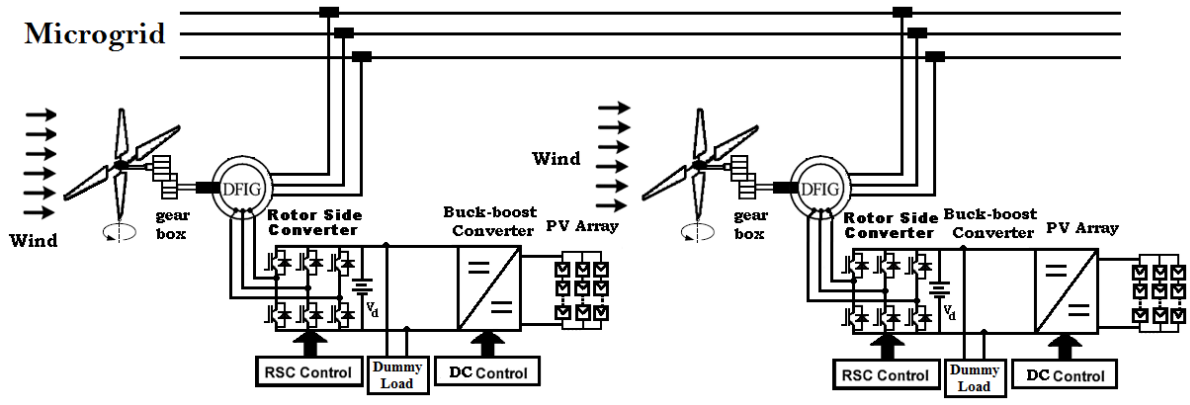

Figure 2.1. Schematic diagram of a DFIG based wind generation.

The block diagram of the proposed AC micro-grid system is shown in Figure 2.1.The stator of both the DFIGs is directly connected to 50 Hz micro grid. The PV panel output is connected to the rotor through a dc to dc converter in series with a three-phase bridge inverter (rotor side converter). Solar power generated from photo-voltaic (PV) cells is gaining increased importance as a renewable source due to advantages such as the absence of fuel cost, little maintenance and no noise and wear due to absence of moving parts. A battery V_d is incorporated between the two converters and it provides various advantageous requirements like storing of the extra energy from the PV panel when the rotor side power demand is less than PV panel output, acting as a dc source in the absence of sun light to inject the power to the rotor, storing of the recovered power coming from the machine at super-synchronous speed etc. To reduce inverter switching losses, the output voltage of the inverter is generally a quasi-sine wave as shown in Figure 2.2 (for 180° conduction mode) and Figure 2.4 (for 120° conduction mode). The dummy load is used to absorb the excess power during super synchronous speed condition. Harmonic analysis of the phase voltage waveform gives all the odd *n*th harmonic of $n = 6k \pm 1$ with $k = 0,1,2,3,\cdots$. The harmonics analysis for the six-step inverter output and the proposed PWM wave form with extra switching is performed for comparison.

2.4 Existing and Proposed Switching Strategies

The DFIG rotor voltage waveform fed from inverter is generally a quasi-sine wave to reduce switching losses in the semiconductor devices. The inverters can be switched under both 180° and 120° mode of operation, which can introduce harmonics of $(6k \pm 1)$ order in the rotor voltage waveform. In the proposed technique both these modes are suitably modified to substantially reduce harmonics which is shown in the following analysis.

2.4.1 180° Mode of Operation

2. 4.1.1 Quasi Sine Wave Switching

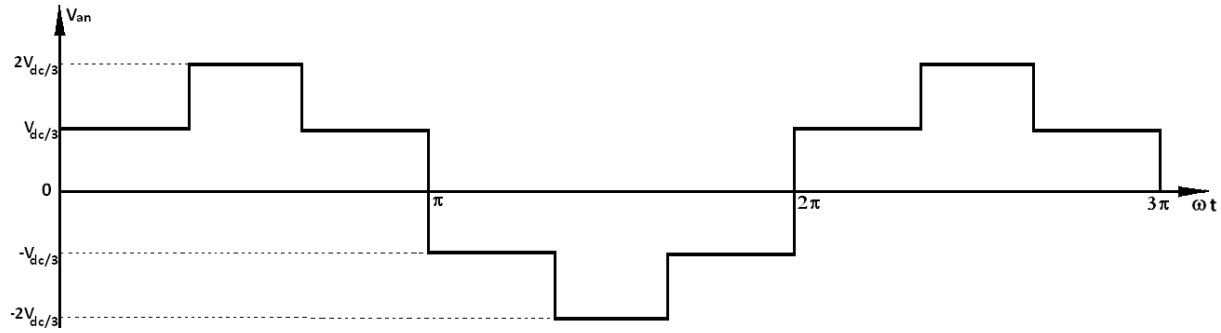

Figure 2.2 Three-phase six-step Quasi-sine waveforms of 180° switch conduction phase voltage applied to the rotor.

The output phase voltage of the inverter is a quasi-sine wave as shown in Figure 2.2 for one of the three phases. The instantaneous phase voltage (180° conduction mode) V_{an} can be expressed in a Fourier series,

$$V_{an} = \frac{a_0}{2} + \sum_{n=1}^{\infty} \left(a_n \cos(n\omega t) + b_n \sin(n\omega t) \right) \tag{2.1}$$

The phase voltage waveform of a 3-phase bridge inverter is a quasi-square wave. The wave form has quarter-wave symmetry, thus, we get

$$a_0 = 0 \text{ for all } n, \text{ and } a_n = 0, \text{ for all even } n$$

and

$$\text{also, } b_n = \frac{4}{\pi} \int_0^{\pi/2} e(\omega t) \sin(n\omega t)\, d(\omega t) \text{ for all odd } 'n'$$

$$\text{or, } b_n = \frac{4}{\pi} \left[\int_0^{\pi/3} \frac{V_{dc}}{3} \sin(n\omega t)\, d(\omega t) + \int_{\pi/3}^{\pi/2} \frac{2V_{dc}}{3} \sin(n\omega t)\, d(\omega t) \right]$$

$$= \frac{4V_{dc}}{3n\pi} \left[\left[\cos(n\omega t) \right]_{\pi/3}^{0} + 2 \left[\cos(n\omega t) \right]_{\pi/2}^{\pi/3} \right]$$

$$= \frac{4V_{dc}}{3n\pi} \left[1 - \cos\left(\frac{n\pi}{3} \right) + 2\cos\left(\frac{n\pi}{3} \right) - 2\cos\left(\frac{n\pi}{2} \right) \right]$$

$$\text{but, } \cos\left(\frac{n\pi}{2} \right) = 0 \text{ for all odd } n,$$

The n^{th} harmonic component can be mathematically expressed as

$$b_n = \frac{4V_{dc}}{3n\pi} \left[1 + \cos\left(\frac{n\pi}{3} \right) \right] \tag{2.2}$$

And $\phi_n = \tan^{-1}\left(\frac{a_n}{b_n} \right) = 0$

From equation (2.2) it can be observed that the triple-n harmonics $(3, 9, 12, 15, \cdots)$ can be automatically cancelled for balanced three-phase system. Therefore, the triple-n harmonics are not chosen for elimination in the phase voltages. Hence, the resulting output voltage from the stator contains harmonics which is fed to the micro-grid. The harmonic analysis of the phase voltage waveform gives the n^{th} harmonic as, $n = 1, 5, 7, 11, 13, 17, \cdots$

or, $n = 6k \pm 1$ for $k = 1, 2, 3, 4, \cdots$

2.2.1.2 Proposed Switching Strategy

For six-step quasi-sine waveforms of 180° conduction, the phase voltage switching pattern is shown in Figure 2.3 with five switching angles in quarter cycle. It can be shown that the n^{th} harmonic can be eliminated by a proper choice of switching angles α. The Fourier series of output voltage waveform can be represented by equation (2.1).

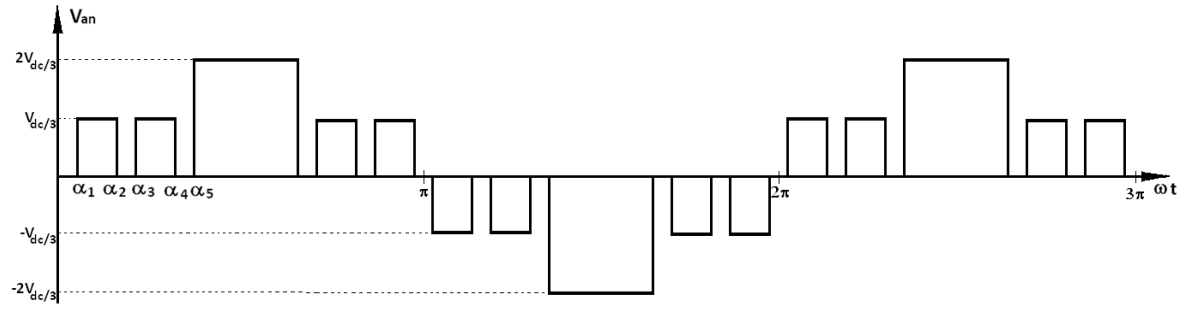

Figure 2.3 Three-phase six-step Quasi-sine waveforms of 180° switch conduction phase voltage switching pattern with five (α_1 to α_5) switching angles.

The phase voltage waveform of a 3-phase bridge inverter has quasi-sine wave symmetry, thus the even harmonics are absent and we can write,

$$a_0 = 0 \text{ for all } n, \text{ and } a_n = 0, \text{ for all even } 'n'$$

$$\text{then, } V_{an} = \sum_{n=1,5,7,\cdots}^{\infty} b_n \sin(n\omega t)$$

$$\text{or, } b_n = \frac{1}{\pi}\int_0^{2\pi} V_{an} \sin(n\omega t)\, d(\omega t)$$

$$= \frac{4V_{dc}}{3n\pi}\left[\cos n\alpha_1 - \cos n\alpha_2 + \cos n\alpha_3 - \cos n\alpha_4 + 2\cos n\alpha_5 - 2\cos n\pi/2\right]$$

$$b_5 = \frac{4V_{dc}}{3\times 5\times \pi}\left[\cos 5\alpha_1 - \cos 5\alpha_2 + \cos 5\alpha_3 - \cos 5\alpha_4 + 2\cos 5\alpha_5\right]$$

$$\cos n\pi/2 = 0 \text{ for } n = 1,5,7,11,\cdots, \ (6n \pm 1)$$

$$= \frac{4V_{dc}}{3n\pi}\left[\cos n\alpha_1 - \cos n\alpha_2 + \cos n\alpha_3 - \cos n\alpha_4 + 2\cos n\alpha_5\right]$$

Thus the general equation of b_n can be written as,

$$b_n = \frac{4V_{dc}}{3n\pi}\left[-\sum_{k=1}^{m}(-1)^k \cos(n\alpha_k) - 2\sum_{k=m+1}^{N}(-1)^k \cos(n\alpha_k)\right] \quad (2.3)$$

For 5-switching, the mathematical statement of these circumstances is then

$$\begin{cases} \cos\alpha_1 - \cos\alpha_2 + \cos\alpha_3 - \cos\alpha_4 + 2\cos\alpha_5 = \mathrm{M} \\ \cos 5\alpha_1 - \cos 5\alpha_2 + \cos 5\alpha_3 - \cos 5\alpha_4 + 2\cos 5\alpha_5 = 0 \\ \cos 7\alpha_1 - \cos 7\alpha_2 + \cos 7\alpha_3 - \cos 7\alpha_4 + 2\cos 7\alpha_5 = 0 \\ \cos 11\alpha_1 - \cos 11\alpha_2 + \cos 11\alpha_3 - \cos 11\alpha_4 + 2\cos 11\alpha_5 = 0 \\ \cos 13\alpha_1 - \cos 13\alpha_2 + \cos 13\alpha_3 - \cos 13\alpha_4 + 2\cos 13\alpha_5 = 0 \end{cases} \quad (2.4)$$

The $5^{th}, 7^{th}, 11^{th}$ and 13^{th} harmonics would be eliminated if $b_5 = b_7 = b_{11} = b_{13} = 0$. These equations can be solved iteratively to calculate the angles $\alpha_1, \alpha_2, \alpha_3, \alpha_4, \cdots, \alpha_k$. A selection of the converter switching angles gives some degree of freedom in minimizing certain harmonics as well as reducing the THD, which directly affects the AC micro grid.

2.4.2 120^0 Mode of Operation

2. 4.2.1 Quasi Sine Wave Switching

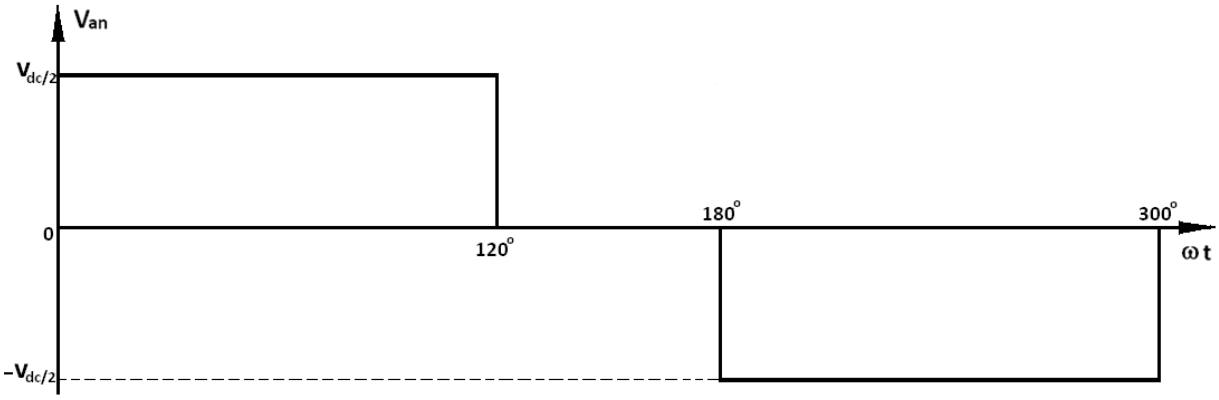

Figure 2.4 Three-phase Quasi-sine waveforms of 120° switch conduction phase voltage applied to the rotor.

The instantaneous phase voltage in Figure 2.4 (120° conduction mode) V_{an} can be expressed in a Fourier series, in equation (2.1). The wave form has quarter-wave symmetry (even harmonics are absent). Due to the quarter-wave symmetry, we get

$$a_0 = 0 \text{ for all } n, \text{ and } a_n = 0, \text{ for all even } n$$

$$\text{or, } b_n = \frac{4}{\pi}\int_{\pi/6}^{\pi/2} \frac{V_{dc}}{2}\sin(n\omega t)\, d(\omega t) \text{ for all odd } 'n'$$

$$= \frac{2V_{dc}}{n\pi}\left[\cos(n\omega t)\right]_{\pi/2}^{\pi/6}$$

$$= \frac{2V_{dc}}{n\pi}\left[\cos\left(\frac{n\pi}{6}\right) - \cos\left(\frac{n\pi}{2}\right)\right]$$

The n^{th} harmonic component can be mathematically expressed as

$$b_n = \frac{2V_{dc}}{n\pi}\sin\left(\frac{n\pi}{2}\right)\sin\left(\frac{n\pi}{3}\right), \text{ where } \sin\left(\frac{n\pi}{3}\right) = \cos\left(\frac{n\pi}{6}\right)$$

Now, $c_n = \sqrt{a_n^2 + b_n^2} = \frac{2V_{dc}}{n\pi}\sin\left(\frac{n\pi}{2}\right)\sin\left(\frac{n\pi}{3}\right)$ (2.5)

and $\phi_n = \tan^{-1}\left(\frac{a_n}{b_n}\right) = 0$

From the equation (2.5) we can observe that the triple-n harmonics $(3,9,12,15,\cdots)$ are zero.

Hence, the harmonics present are given by, $n = 1,5,7,11,13,17,\cdots$

or, $n = 6k \pm 1$, for $k = 0,1,2,3,4,\cdots$

2.4.2.2 Proposed Switching Strategy

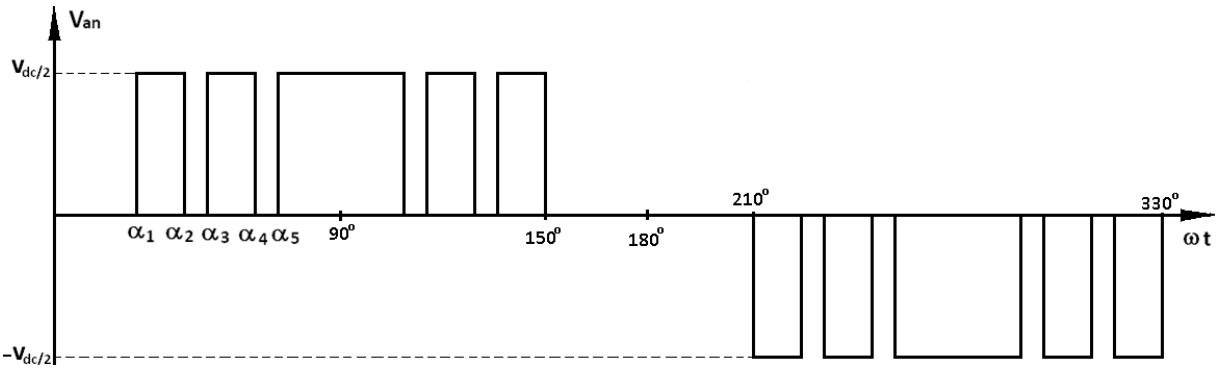

Figure 2.5 Three-phase six-step Quasi-sine waveforms of 120° switch conduction phase voltage switching pattern with five switching angles and starting point 30°.

Generalized six-step Quasi-sine waveforms of 120° switch conduction phase voltage waveform is depicted in Figure 2.5. The phase voltage waveform of a 3-phase bridge inverter is a quasi-square wave. The wave form has quarter-wave symmetry. In this case the isolated neutral-phase voltages are also six-step waveforms with the fundamental component phase-shifted by $\pi/6$ from that of the respective line voltage. Also, in this case, the triple-n harmonics are suppressed.

$a_0 = 0$ for all n, and $a_n = 0$, for all even $'n'$

$$b_n = \frac{1}{\pi}\int_0^{2\pi} V_{an}\sin(n\omega t)\,d(\omega t)$$

The expression for b_n can be written as,

$$b_n = -\left(\frac{2V_{dc}}{n\pi}\right)\sum_{k=1}^{m}(-1)^k\cos(n\alpha_k) \tag{2.6}$$

For 5-switching, the mathematical statement of these circumstances is then

$$\begin{cases}\cos\alpha_1-\cos\alpha_2+\cos\alpha_3-\cos\alpha_4+\cos\alpha_5=\mathrm{M}\\ \cos5\alpha_1-\cos5\alpha_2+\cos5\alpha_3-\cos5\alpha_4+\cos5\alpha_5=0\\ \cos7\alpha_1-\cos7\alpha_2+\cos7\alpha_3-\cos7\alpha_4+\cos7\alpha_5=0\\ \cos11\alpha_1-\cos11\alpha_2+\cos11\alpha_3-\cos11\alpha_4+\cos11\alpha_5=0\\ \cos13\alpha_1-\cos13\alpha_2+\cos13\alpha_3-\cos13\alpha_4+\cos13\alpha_5=0\end{cases} \tag{2.7}$$

The $5^{th}, 7^{th}, 11^{th}$ and 13^{th} harmonics would be eliminated if $b_5 = b_7 = b_{11} = b_{13} = 0$.These equations can also be solved iteratively and the switching angles $\alpha_1, \alpha_2, \alpha_3, \cdots, \alpha_\kappa$ can be computed. The selection of the converter switching angles gives some degree of freedom in minimizing certain harmonics as well as reducing the THD, which directly affects the AC micro grid.

2.5 Different Standards for Voltage and Current Harmonics

TABLE 2.1 Summary of IEEE 1547, IEC 61726 and IEC 61000-3-2 class D individual current harmonic

ISSUE	IEEE1547	IEC61727	IEC 61000-3-2	
Nominal Power	30kW	10kW	class D	
Harmonic	(2-10) 4.0 %	(3-9) 4.0 %	harmonic	I_h (A)
current (order - h)	(11-16) 2.0 %	(11-15) 2.0 %	order (h)	
limits	(17-22) 1.5 %	(17-21) 1.5 %	3	2.3
	(23-34) 0.6 %	(23-33) 0.6 %	5	1.14
	(>35) 0.3 %		7	0.77
	Even harmonics in these ranges shall be less than 25% of the odd harmonic limits listed		9	0.4
			11	0.33
Maximum current THD		5.00%	13	0.21
	less than 0.5% of rated output	less than 1.0% of	15	0.15
DC current injection	current	rated output current	:	:
Frequency range for			39	15/h
normal operation	59.3 Hz to 60.5 Hz	50±1	Equipment input current ≤ 16 A per phase	

TABLE 2.2 Summary comparison of individual harmonic voltage between different standards and guidelines for LV and MV.

	LV-Harmonic	MV-Harmonic Voltages (% of fundamental or declared voltage)								
	IEC	IEC	IEC	IEC	IEC	CIGRE	EN	NRS	ER G5⁄4	ANS/IEEE
Harmonic	61000-2-2	61000-2-4	61000-2-4	61000-3-6	61000-2-12	WG 36-05	61000-3-2	0482:2003	:2001	519:1992
Order		class 2	class 3	:1996	:2003		EN 50160			
h	$\%V_h$	$\%V_h$	$\%V_h$	$\%V_h$	$\%V_h$	$\%V_h$	$\%V_h$	$\%V_h$	$\%V_h$	$\%V_h$
Voltage level	≤1 kV	1 to 35 kV	1 to 35 kV	1 to 35 kV	1 to 35 kV	1 to 35 kV	1 to 35 kV	1 to 35 kV	1 to 35 kV	120V to 69 kV
2	2	2	3	1.6	2	2	2	2	1.5	3
3	5	5	6	4	5	3	5	5	3	3
4	1	1	1.5	1	1	1	1	1	1	3
5	6	6	8	5	6	6	6	6	3	3
6	0.5	0.5	1	0.5	0.5	0.5	0.5	0.5	0.5	3
7	5	5	7	4	5	5	5	5	3	3
8	0.5	0.5	1	0.4	0.5	0.5	0.5	0.5	0.4	3
9	1.5	1.5	2.5	1.2	1.5	1.5	1.5	1.5	1.2	3
10	0.5	0.5	1	0.4	0.5	0.5	0.5	0.5	0.4	3
11	3.5	3.5	5	3	3.5	3.5	3.5	3.5	2	3
12	0.2	0.2	1	0.2	0.46	0.2	0.5	0.2	0.2	3
13	3	3	4,5	2.5	3	3	3	3	2	3
14	0.2	0.2	1	0.2	0.43	0.2	0.5	0.2	0.2	3
15	0.3	0.3	2	0.3	0.4	0.5	0.5	0.3	0.3	3
16	0.2	0.2	1	0.2	0.41	0.2	0.5	0.2	0.2	3
17	2	2	4	1.6	2	2	2	2	1.6	3
18	0.2	0.2	1	0.2	0.39	0.2	0.5	0.2	0.2	3
19	1.5	1.5	4	1.2	1.76	1.5	1.5	1.5	1.2	3
20	0.2	0.2	1	0.2	0.38	0.2	0.5	0.2	0.2	3
21	0.2	0.2	1	0.2	0.3	0.5	0.5	0.2	0.2	3
22	0.2	0.2	1	0.2	0.36	0.2	0.5	0.2	0.2	3
23	1.5	1.5	3.5	1.2	1.41	1.3	1.5	1.5	1.2	3
24	0.2	0.2	1	0.2	0.35	0.2	0.5	0.2	0.2	3
25	1.5	1.5	3.5	1.2	1.27	1.5	1.5	1.5	0.7	3
26	0.2	0.2	1	0.2	0.34	0.2	0.5	0.2	0.2	3
27	0.2	0.2	1	0.2	0.34	0.2	0.5	0.2	0.2	3
28	0.2	0.2	1	0.2	0.33	0.2	0.5	0.2	0.2	3
29	0.63	0.63	3.07	1.06	1.06	1.32	0.63	0.63	0.63	3
30	0.2	0.2	1	0.2	0.33	0.2	0.5	0.2	0.2	3
31	0.6	0.6	2.97	1.006	0.97	1.24	0.6	0.6	0.6	3
$6n\pm1$	0.2+12.5/h	0.2+12.5/h	$5*\sqrt{\frac{11}{h}}$	0.2+25/h	2.27*(17/h)-0.27	0.2+32.5/h	0.2+12.5/h	2.27*(17/h)-0.27	0.2+0.5*(25⁄4)	3
order	$h\le 40$	$h\le 40$	$h\le 40$	$h\le 40$	$h\le 50$	$h\le 40$	$h\le 40$	$h\le 40$	$h\le 40$	all order
THD up to 40th	$\le 8\%$	$\le 8\%$	$\le 10\%$	≤ 6.5	$\le 8\%$	$\le 8\%$	$\le 8\%$	$\le 8\%$	$\le 4\%$	$\le 5\%$

A number of Grid code specifications have been proposed to standardize the norms for maintaining the quality of the wave forms in power system. The proposed system is able to meet utilities regulations, IEEE 1547 and IEC standards. For this system, the current harmonic injection in to the grid must not exceed 5%, with limitations imposed on individual harmonics as a percentage of the fundamental component according to IEEE and IEC standards [40, 61]. In this thesis, implementation of a BBO-based SHE-PWM method using the least possible switching frequency to satisfy different grid codes IEC 61000-2-2, IEC 61000-2-4 class 2, IEC 61000-2-4 class 3, IEC 61000-2-6, CIGRE JWGC4.07, EN 61000-3-2 and 110 kV grid CIGRE [62, 61, 63, 64, 65, 66, 67] is presented. This thesis proposes a BBO-based optimization technique to calculate the switching angles both for 120-degree and 180-degree switching modes of the PWM inverter satisfying the grid codes of harmonic requirement for both low and medium grid voltage level. This technique is also used to reduce the no. of switching per cycle to as minimum as possible while maintaining THD requirement according to grid codes. The different grid codes for harmonic requirements in a micro grid system are shown in Table 2.1 and Table 2.2 respectively. The harmonics up to 40^{th} are mitigated to satisfy the current and voltage harmonic standards grid codes from both individual harmonics and THD point of view.

2.6 Proposed Co-ordinated Approach for Harmonics Elimination

The proposed technique for harmonic elimination employs multiple switching within quarter cycle of the inverter output, instead of normal six-step quasi sine wave output. A wide range of harmonic elimination requires more number of switching per quarter-cycle. This increases switching losses due to higher switching frequency and imposes a limit on the inverter rating. Thus, efforts should be made to reduce as many harmonics as possible with lesser number of switching for better inverter efficiency. The lower order harmonics are individually eliminated in each DFIG outputs but the higher order harmonics are eliminated in such a way that the harmonics generated by one source is eliminated by the other after generating the same order of harmonics in opposite phase. Thus for a micro grid consisting of several DFIGs acting as DG sources, only one of the rotor side inverters for DFIGs can be programmed to operate at higher switching frequencies. The other inverter can have lower number of switching eliminating only the targeted lower order harmonics.

2.6.1 Proposed Harmonic Elimination Principle

Conventional SHE-PWM techniques involve elimination of unwanted order harmonics and to control the amplitude of the fundamental component. A typical output voltage waveform of an inverter as illustrated in Figure 2.2 and Figure 2.4 comprises of harmonics and the output function $V(t)$ can be represented as

$$V(t) = \sum_{n=1}^{\infty} \left(a_n \cos n\alpha_n + b_n \sin n\alpha_n \right) \tag{2.8}$$

Having the quarter-wave symmetry of the output voltage, the even harmonics are eliminated $\left(a_n = 0\right)$ and only odd harmonics are existing. The first quadrant switching angles range is

$$0 < \alpha_1 < \alpha_2 < \alpha_3 < \cdots < \alpha_m < (\pi/2)$$

For any odd harmonics, equation (2.3) and (2.6) can be extended till k^{th} term, where m is the number of variables related to switching angles from α_1 through α_m of the first quadrant. In selected harmonic elimination, b_1 is taken as the required value for fundamental component and the other coefficients associated with the harmonics to be vanished are equated to zero.

The equations (2.4) and (2.7) are applied to find the appropriate switching angles $\alpha_1, \alpha_2, \alpha_3, \cdots, \alpha_m$ by which the fundamental component M (in p.u.) can be controlled and the non-triple-n odd harmonics i.e. $5^{th}, 7^{th}, 11^{th}, 13^{th}$ and n^{th} are vanished. Here the permissible switching angles are within 0° to 90° .Generally, there is one condition for fundamental voltage control and $N-1$ conditions for eliminating the positive-sequence harmonics i.e. the $(6n+1)$ harmonics and negative-sequence or the $(6n-1)$ harmonics. In order to eliminate N harmonics, $N+1$ angles need to be found and the above sets of equations are to be solved. The proposed method is to improve the quality of power supplied to the micro grid from different DG units. The proposed THD minimization technique in the AC micro-grid is verified with the help of two interfacing inverters of DG1 and DG2 shown in Figure 2.1. The DG1 unit produces the $(6n \pm 1)$ order harmonics while the DG2 unit produces the same order harmonics having equal magnitudes but opposite phase. The selected lower order harmonics (phase and line) for 3-switching are 5^{th} and 7^{th}, for 4-switching are $5^{th}, 7^{th}$ and 11^{th}, for 5-switching are $5^{th}, 7^{th}, 11^{th}$ and 13^{th}, for 6-switching are $5^{th}, 7^{th}, 11^{th}, 13^{th}$ and 17^{th} and for 7-switching are $5^{th}, 7^{th}, 11^{th}, 13^{th}, 17^{th}$ and 19^{th} order. All these harmonics are eliminated by optimizing the switching angle through minimization of the objective function $F(\alpha)$ in (10). The corresponding coefficients b_5, b_7 (for 3-switching); b_5, b_7, b_{11} (for 4-switching); b_5, b_7, b_{11}, b_{13} (for 5-switching); $b_5, b_7, b_{11}, b_{13}, b_{17}$ (for 6-switching) and $b_5, b_7, b_{11}, b_{13}, b_{17}$, b_{19} (for 7-switching) are individually equated to zero. When DG1 is programmed to eliminate any of the harmonic sets as mentioned over, the remaining higher order harmonics will be present in the voltage injected by DG1 to the micro-grid. In the proposed technique, some of the selected higher order harmonics can be counter balanced by the dominant harmonics generated in opposite phase by the BBO-based SHE-PWM inverter of DG2 set. Thus, when these two inverters (DG1 and DG2) are connected to the grid in parallel, the corresponding selected higher order harmonics are also reduced from the grid voltage waveform besides eliminating the lower order harmonics. These converters are able to improve the quality of the supply voltage and extend the benefits of power electronics into both the electrical transmission and distribution networks.

2.6.2 Determination of the Switching Angles Using BBO Algorithm

In the proposed method, the harmonic elimination problem is converted to optimization problem and the switching angles are found out offline to contribute minimum voltage THD. The %THD of the output voltage can be computed

using (2.9). Biogeography-Based Optimization technique is a relatively recent heuristic method to solve different optimization problems. In the present work we apply BBO to find the optimum switching angles of the converters. The reasons for obtaining the solution using BBO are the followings:

i. BBO is a relatively new technique, and has not yet been explored extensively to solve energy systems problem, particularly the problem of converter switching.
ii. Unlike the other metaheuristic techniques, BBO does not require unreasonable amount of computational effort [60].
iii. Application of BBO is rather straight forward, requires less tuning of its parameters.

$$\%THD = \left[\frac{1}{b_1^2} \sum_{n=5}^{\infty} (b_n)^2 \right]^{1/2} \times 100 \tag{2.9}$$

Where $n = 6k \pm 1$ for $(k = 1, 2, 3, 4, \cdots)$

The equation (2.9) of the voltage THD is considered as the objective function $F(\alpha)$ for optimization. In order to proceed with the minimization, an objective function describing a measure of effectiveness of eliminating selected order of harmonics while maintaining the fundamental at a pre-specified value must be defined. To minimize the overall THD in the output voltage waveform, this objective function $F(\alpha)$ has to be minimized with the constraints of selected harmonic elimination and the optimum switching angles are obtained by optimizing equation (2.10). Mathematically, the problem can be formulated as follows

$$\text{Minimize } F(\alpha) = F(\alpha_1, \alpha_2, \alpha_3, \cdots, \alpha_m) \tag{2.10}$$

$$\text{Subject to: } 0 < \alpha_1 < \alpha_2 < \alpha_3 < \cdots < \alpha_m < (\pi/2); \tag{2.11}$$

$$b_1 = \mathrm{M}, b_5 \le \varepsilon_1, b_7 \le \varepsilon_2 \text{ and } b_n \le \varepsilon_n \tag{2.12}$$

Where b_1 is the fundamental amplitude and $\varepsilon_1, \varepsilon_2, \cdots, \varepsilon_n$ are the permissible limits of individual harmonics which are chosen very close to zero for the more significant selected low-order harmonics. In the present problem, each search point of the population is composed of the switching angles per quarter cycle α_1 through α_m. To start the search procedure, the switching angles are randomly generated satisfying the conditions of equation (2.11) for the chosen number of population. Using these random values, individual harmonics are computed which represents the fitness of the search point. The best combination of angles among the population of search points up to present iteration is called the elite or best solution for the variables α_1 through α_m. At each iteration, new search points are generated from the current search points and the information regarding the best solutions is found out by using the

BBO. Using the terminology of the BBO, consider the probability P_s that the habitat contains exactly S species. P_s changes from time t to time $t+\Delta t$ as follows:

$$\mathrm{P}_s\left(t+\Delta t\right)=\mathrm{P}_s\left(t\right)\left(1-\lambda_s\Delta t-\mu_s\Delta t\right)+\mathrm{P}_{s-1}\lambda_{s-1}\Delta t+\mathrm{P}_{s+1}\mu_{s+1}\Delta t \tag{2.13}$$

Where λ_s and μ_s are the immigration and emigration rates when there are S species in the habitat. We assume that Δt is small enough so that the probability of more than one immigration and emigration can be ignored. Taking the limit of equation (2.13) as $\Delta t\to 0$ gives equation (2.14). For each habitat, update the probability of its species count using equation (2.14) and compute each habitat suitability index (HSI). HSI is satisfies the suitability index variable (SIV) constraints.

$$\dot{\mathrm{P}}_s=\begin{cases}-\left(\lambda_s+\mu_s\right)\mathrm{P}_s+\mu_{s+1}\mathrm{P}_{s+1} & S=0\\ -\left(\lambda_s+\mu_s\right)\mathrm{P}_s+\lambda_{s-1}\mathrm{P}_{s-1}+\mu_{s+1}\mathrm{P}_{s+1} & 1\le S\le S_{\max}-1\\ -\left(\lambda_s+\mu_s\right)\mathrm{P}_s+\lambda_{s-1}\mathrm{P}_{s-1} & S=S_{\max}\end{cases} \tag{2.14}$$

We can arrange the $\dot{\mathrm{P}}_s$ equations (for $S=0,\cdots,n$) into the single matrix equation is

$$\dot{\mathrm{P}}=\mathrm{AP} \tag{2.15}$$

For the straight line curves shown in [21], we have

$$\mu_k=\frac{\mathrm{E}k}{n}\ \text{and}\ \lambda_k=\mathrm{I}\left(1-\frac{k}{n}\right) \tag{2.16}$$

Where, μ_k and λ_k are emigration and immigration rate and k number of species. The maximum possible immigration rate to the habitat is I and the maximum emigration rate is E.

Now, consider the special case E=I, in this case, we have

$$\lambda_k+\mu_k=\mathrm{E} \tag{2.17}$$

The steady state value for the probability of the number of each species is given by equation (2.18)

$$\mathrm{P}\left(\infty\right)=\frac{V}{\sum_{i=1}^{n+1}V_i} \tag{2.18}$$

Where, v is the eigen vector.

The mutation rate m is inversely proportional to the solution probability and is given by equation (2.19)

$$m(S) = m_{\max}\left(\frac{1-\mathrm{P}_s}{\mathrm{P}_{\max}}\right) \tag{2.19}$$

Where $m_{\max}$ (maximum mutation rate) is a user-defined parameter. This equation makes high habitat suitability index (HSI) solutions.

Application of BBO for solving the SHE-PWM problem can be summarized as follows:

The system of nonlinear equations in m variables to be optimized can be represented as

$$f_j(\alpha_1, \alpha_2, \alpha_3, \alpha_4, \cdots, \alpha_m) = 0, \quad j = 1, 2, 3, \cdots, m \tag{2.20}$$

These m equations are obtained for the problem by equating equations (2.3) and (2.6) to zero for any harmonics desired to be eliminated.

BBO representation of the problem is shown in Figure 2.6.

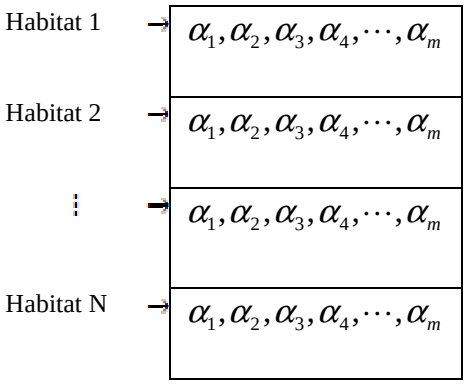

Figure 2.6 BBO representation of the problem**.**

Collection of one set of switching angles, $\alpha_1, \alpha_2, \alpha_3, \cdots, \alpha_m$ form a solution set of the problem. This solution set is termed as a 'habitat' in BBO. Number of the set of habitat N is nothing but the number of the population of the population based optimization algorithms. In BBO it is called the eco-system.

Habitat Suitability Index (HSI) indicates the quality of the solution set. For the problem being considered, HSI is represented by the total harmonic distortion (THD) value generated by the solution set.

Equation (2.20) is written in vector notation as

$$f(\alpha) = 0 \tag{2.21}$$

Where

$f = [f_1, f_2, f_3, f_4, \cdots, f_m]^T$, an $m \times 1$ matrix

$\alpha = [\alpha_1, \alpha_2, \alpha_3, \alpha_4, \cdots, \alpha_m]^T$, an $m \times 1$ matrix

Equation (2.21) can be solved by using a BBO technique, where the nonlinear equations give an approximate solution. The steps involved in computing a solution are as follows.

The switching angle matrix,

$$\alpha^j = [\alpha_1^j, \alpha_2^j, \alpha_3^j, \alpha_4^j, \cdots, \alpha_m^j]^T \tag{2.22}$$

The nonlinear system matrix,

$$f^j = \begin{bmatrix} \cos(\alpha_1^j) - \cos(\alpha_2^j) + \cos(\alpha_3^j) - \cos(\alpha_4^j) + \cos(\alpha_5^j) \\ \cos(5\alpha_1^j) - \cos(5\alpha_2^j) + \cos(5\alpha_3^j) - \cos(5\alpha_4^j) + \cos(5\alpha_5^j) \\ \cos(7\alpha_1^j) - \cos(7\alpha_2^j) + \cos(7\alpha_3^j) - \cos(7\alpha_4^j) + \cos(7\alpha_5^j) \\ \cos(11\alpha_1^j) - \cos(11\alpha_2^j) + \cos(11\alpha_3^j) - \cos(11\alpha_4^j) + \cos(11\alpha_5^j) \\ \cos(13\alpha_1^j) - \cos(13\alpha_2^j) + \cos(13\alpha_3^j) - \cos(13\alpha_4^j) + \cos(13\alpha_5^j) \end{bmatrix} \tag{2.23}$$

And

$$\left[\frac{\partial f}{\partial \alpha}\right]^j = \begin{bmatrix} -\sin(\alpha_1^j) + \sin(\alpha_2^j) - \sin(\alpha_3^j) + \sin(\alpha_4^j) - \sin(\alpha_5^j) \\ -5\sin(5\alpha_1^j) + 5\sin(5\alpha_2^j) - 5\sin(5\alpha_3^j) + 5\sin(5\alpha_4^j) - 5\sin(5\alpha_5^j) \\ -7\sin(7\alpha_1^j) + 7\sin(7\alpha_2^j) - 7\sin(7\alpha_3^j) + 7\sin(7\alpha_4^j) - 7\sin(7\alpha_5^j) \\ -11\sin(11\alpha_1^j) + 11\sin(11\alpha_2^j) - 11\sin(11\alpha_3^j) + 11\sin(11\alpha_4^j) - 11\sin(11\alpha_5^j) \\ -13\sin(13\alpha_1^j) + 13\sin(13\alpha_2^j) - 13\sin(13\alpha_3^j) + 13\sin(13\alpha_4^j) - 13\sin(13\alpha_5^j) \end{bmatrix} \tag{2.24}$$

The corresponding harmonic amplitude matrix,

$$b = \begin{bmatrix} M & 0 & 0 & 0 & 0 \end{bmatrix}^T \tag{2.25}$$

The statement of algorithm is shown as follows

i. Guess a set of values for α (a^j with $j=0$) ; call them

$$\alpha^0 = [\alpha_1^0, \alpha_2^0, \alpha_3^0, \alpha_4^0, \cdots, \alpha_m^0]^T \tag{2.27}$$

ii. Determine the value of

$$f\left(\alpha^0\right) = f^0 \tag{2.28}$$

iii. Linearize (2.21) about α^0.

$$f^0 + \left[\frac{\partial f}{\partial \alpha}\right]^0 d\alpha = 0 \tag{2.29}$$

Where

$$\left[\frac{\partial f}{\partial \alpha}\right]^0 = \begin{bmatrix} \frac{\partial f_1}{\partial \alpha_1} & \frac{\partial f_1}{\partial \alpha_1} & \cdots & \frac{\partial f_1}{\partial \alpha_m} \\ \frac{\partial f_2}{\partial \alpha_1} & \frac{\partial f_2}{\partial \alpha_1} & \cdots & \frac{\partial f_2}{\partial \alpha_m} \\ \vdots & \vdots & \vdots & \vdots \\ \frac{\partial f_m}{\partial \alpha_1} & \frac{\partial f_m}{\partial \alpha_1} & \cdots & \frac{\partial f_m}{\partial \alpha_m} \end{bmatrix} \tag{2.30}$$

Evaluate at α^0 and $d\alpha = [d\alpha_1, d\alpha_2, d\alpha_3, d\alpha_4, \cdots, d\alpha_m]^T$

iv. Solve (2.29) for $d\alpha$.

v. Repeat (updated) (i to iv)

$$\alpha^{j+1} = \alpha^j + d\alpha^j \text{ or, } \alpha^1 = \alpha^0 + d\alpha^0 \tag{2.31}$$

vi. The process is repeated until (2.21) is satisfied to the desired degree of accuracy. If the previous method converges, it will give a solution to (v21). In case of divergence from the initial guess, it is necessary to make a new initial guess. The process is a trial and error method. The correct solution must satisfy the condition (2.11)

The switching angles corresponding to minimum voltage THD for varying modulation index $\left(m_d\right)$ are stored as look-up table in the memory of the DSP for online application. The elite values are updated after every iteration. The

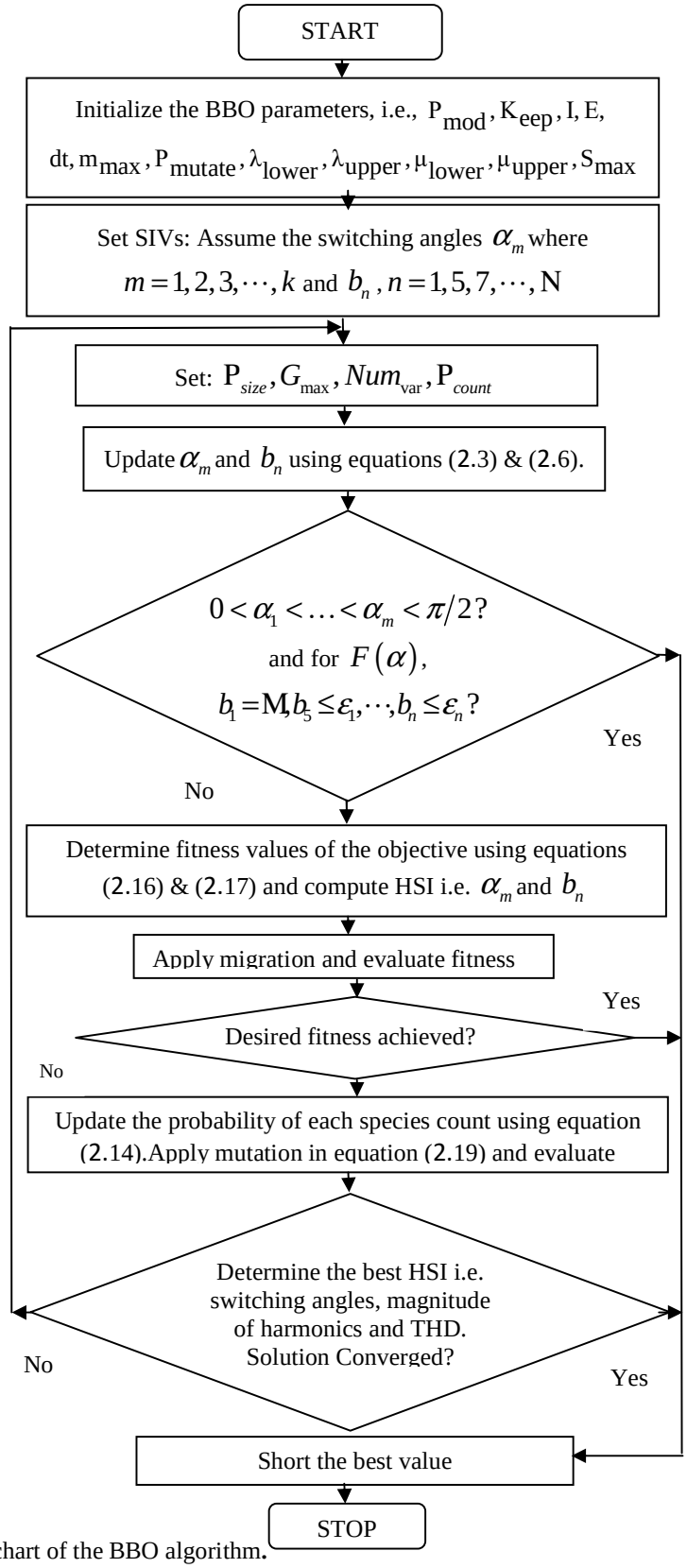

Figure 2.7 Flowchart of the BBO algorithm**.**

process is repeated until the convergence is obtained. The process terminates if the changes in the fitness values between consecutive iterations are less than a given tolerance, or the fitness values do not change for a number of iterations, or the permissible number of iteration runs are completed. A flowchart of the BBO algorithm for optimized switching is shown in Figure2.7.

2.7 Simulation and Experimental Results

The proposed scheme has been simulated in MATLAB 7.8/Simulink environment for both 120° and 180 °switching mode of inverter. Both these modes are separately simulated and the results are shown separately.

2.7.1 180° Switching Mode of Operation:

The simulation results for switching angles considering three switching per quarter cycle with varying modulation index (m_d) for the BBO-based SHE-PWM inverter are shown in Figure 2.8. During computation, the objective function $F(\alpha)$ as defined by (2.10) is optimized to obtain minimum voltage THD. The coefficients b_5 and b_7 corresponding to the amplitudes of 5^{th} and 7^{th} harmonics are set to zero. The coefficient b_1, which is the amplitude of the fundamental voltage, has been set as per the desired m_d. The dominant harmonics that appear after eliminating up to 7^{th} harmonic by the above technique are the $11^{th}, 13^{th}, 17^{th}$ and 19^{th} harmonics of which the amplitude of the latter is found to be much more significant in this case. Figure 2.9 shows the switching angles for 180-degree conduction for 5-switching per quarter cycle. The higher switching frequency reduces the overall voltage THD as evident from Figure 2.8 and 2.9. Figure2.10 shows the plot of minimum weighted THD for output voltage (up to 31st order of harmonics) with varying m_d, for 3, 4, 5, 6 and 7-switchings per quarter cycle.

When DG1 is set to eliminate 5^{th} and 7^{th} harmonics, it will generate the higher order harmonics of $11^{th}, 13^{th}, 17^{th}$ and 19^{th} for which DG2 inverter is to be switched to eliminate them. The amplitude variation of the dominant $11^{th}, 13^{th}, 17^{th}$ and 19^{th} harmonics with phase angle at different modulation indices is calculated and with proper selection of phase angles to generate the required $11^{th}, 13^{th}, 17^{th}$ and 19^{th} harmonics in opposite phase at different m_d. Therefore, if a micro grid consists of n no. of DFIGs, only one inverter is to be switched at higher frequencies to eliminate the unwanted $11^{th}, 13^{th}, 17^{th}$ and 19^{th} harmonics generated by the others but all the other inverters can have lower switching frequencies to eliminate the 5^{th} and 7^{th} harmonics only. The overall weighted THD for BBO-based SHE-PWM inverter combination is computed. The comparison of weighted voltage THD for the individual BBO-based SHE-PWM inverter, combined BBO-based SHE-PWM inverter is shown in Figure 2.11 and Figure 2.12. In Figure 2.11 individual 3-switching and 5-switching THD along with the combination of 3 and 5 switching for two inverter are shown, from which it is evident that the latter considerably reduces the overall voltage

THD of the micro-grid. In Figure 4.12 the individual 3-switching and 7-switching THD along with the combination of 3 and 7switching for two inverters are shown, from which it is also evident that the latter considerably reduces the overall voltage THD of the micro-grid.

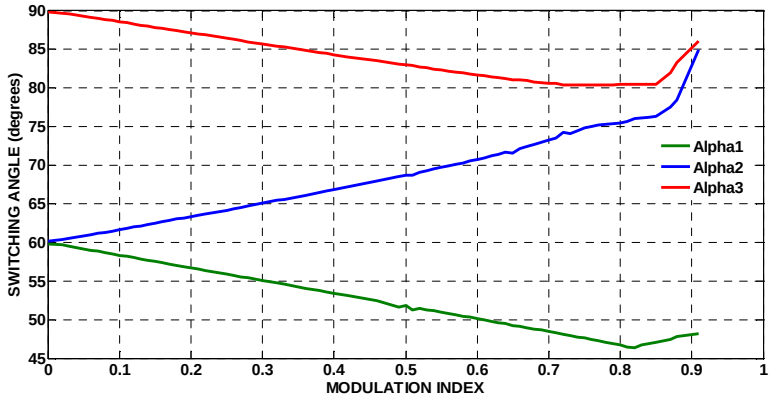

Figure 2.8 180-degree conduction mode for phase voltage, Modulation Index Vs. 3-Switching angles (degrees).

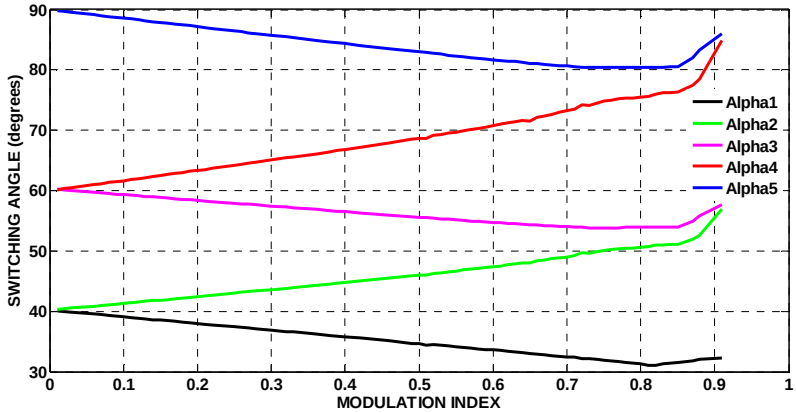

Figure 2.9180-degree conduction mode for phase voltage, Modulation Index vs. 5-Switching angles (degrees).

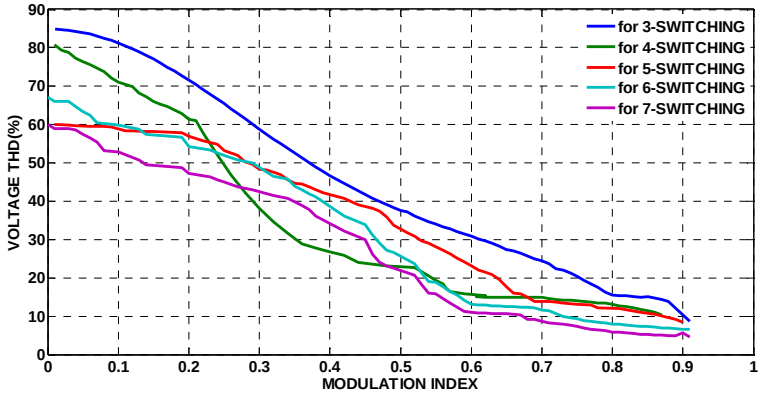

Figure 2.10 180-degree conduction mode for phase voltage Minimum Voltage THD (%) Vs. Modulation Index.

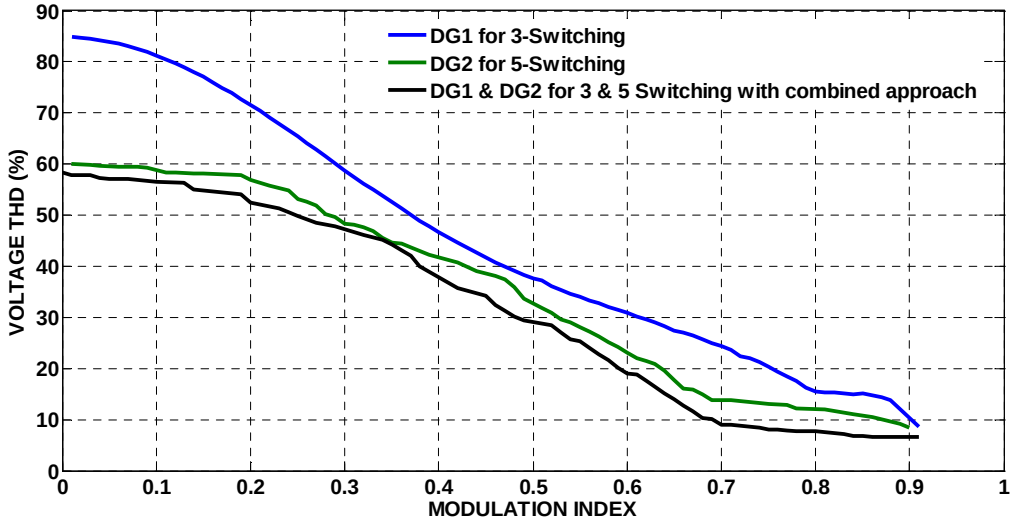

Figure 2.11 Simulated voltage THD for BBO-based inverters with individual 3 and 5 switching and combined switching.

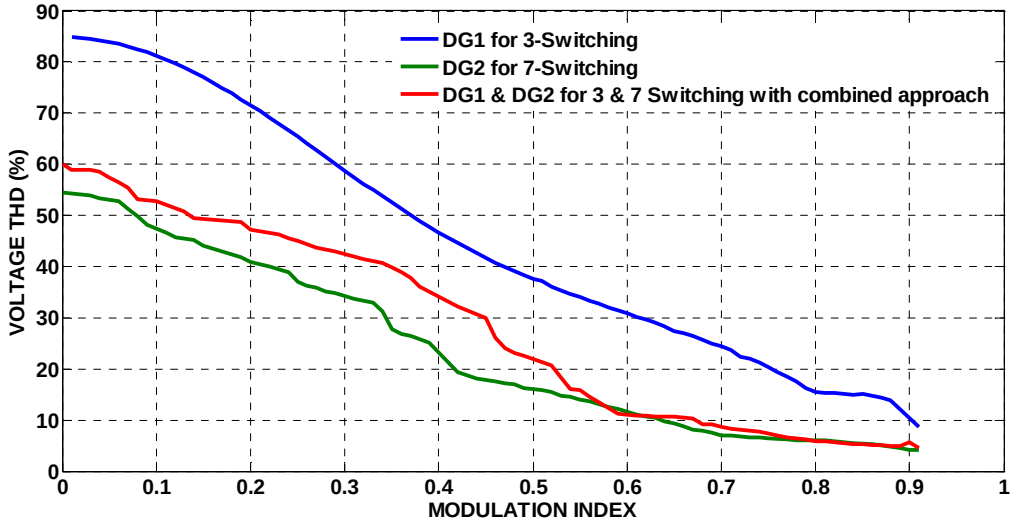

Figure 2.12 Simulated voltage THD for BBO-based inverters with individual 3 and 7 switching and combined switching.

2.7. 2 120^0 Switching Mode of Operation:

The simulation results with three and five switching per quarter cycle with varying modulation index (m_d) for the BBO-based SHE-PWM inverter are shown in Figures. 2.13 and 2.14 respectively. In this mode also the higher switching frequency reduces the overall voltage THD. The plot of minimum weighted THD for output voltage (up to

31st order of harmonics) with varying m_d , for 3, 4, 5, 6 and 7-switchings per quarter cycle is shown in Figure 2.15. The comparison of weighted voltage THD for the individual BBO-based SHE-PWM inverter, combined BBO-based SHE-PWM inverter is shown in Figure 2.16. In Figure 2.16 the individual 3-switching and 5-switching THDs along with the combination of 3 and 5 switching for two inverter as shown, from which it is evident that the latter considerably reduces the overall voltage THD of the micro-grid.

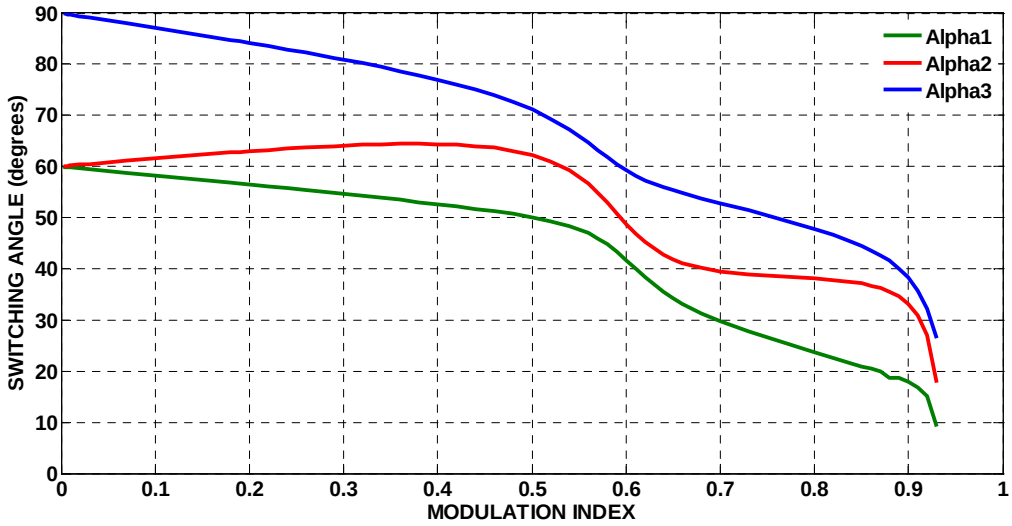

Figure 2.13 120-degree conduction mode for phase voltage, Modulation Index Vs. 3-Switching angles (degrees).

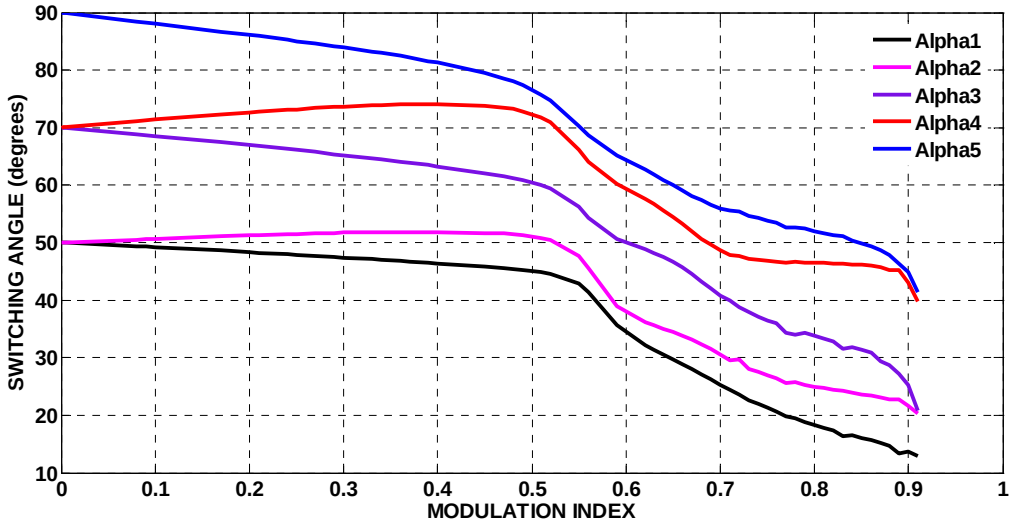

Figure 2.14 120-degree conduction mode for phase voltage, Modulation Index Vs. 5-Switching angles (degrees).

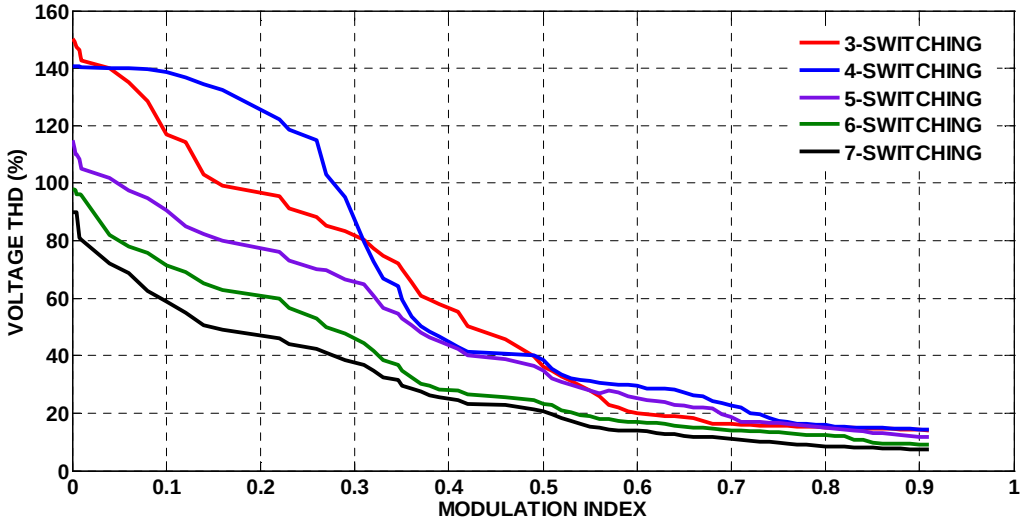

Figure 2.15120-degree conduction mode for phase voltage Minimum Voltage THD (%) Vs. Modulation Index.

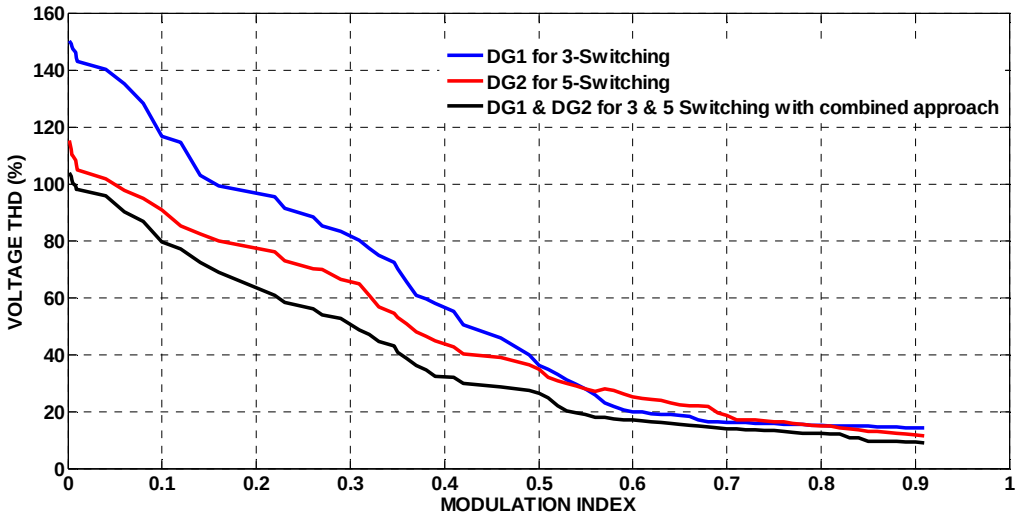

Figure 2.16 Simulated voltage THD for BBO-based inverters with individual 3 and 5 switching and combined switching.

2.8 System Implementation:

Figure 2.1 shows the laboratory version of the experimental set up used for verification of the proposed scheme. The system used for the experiment consists of two DFIGs connected in a micro grid which supplies a common load. The rotor side of each DFIG is fed from an inverter connected to a converter controlled solar array. The stator of the DFIG is directly connected to the micro grid. The specifications of the DFIG, solar panel and the battery are shown in Table 2.3.

Table 2.3 Parameters of the experimental system:

Micro grid Specification		DFIG Specification				Solar panel Specification	
		Stator Parameters		Rotor Parameters			
Vgrid	415 V	V_s	415 V	V_r	110 V	Rated power	2 kW each
f_s	50 Hz	Δ-Connected		Y-Connected		Voltage	110 V
Rated Capacity	5 kVA	f_s	50 Hz	R_r	1.5 Ω	Battery	1000 AH
		P	2.2 KW	L_{lr}	10 mH		
5^{th}, 7^{th}	As per	I_s	4 A	I_r	14 A		
11^{th}, …	grid	R_s	1.2 Ω	N_r	1450 rpm		
harmonic	codes	L_{ls}	10 mH				
voltage		L_m	300 mH				

2.9 Experimental Results:

The proposed method of harmonic elimination is experimentally verified with the scheme described in Figure 2.1. The DFIG is run at a speed of 1560 rpm with the quasi-square wave switching in 180^0 mode in the rotor side. The corresponding harmonic spectra for rotor and stator voltage are shown in Figure 2.17 (a) and 2.17 (b) respectively. The rotor and stator voltage waveforms before harmonic elimination are shown in Figures. 2.18 (a) and 2.18 (b). The modified stator voltage after elimination of 5^{th} and 7^{th} rotor harmonics are shown in Figure 2.18 (c). Then the proposed control strategy is also applied for 120^0 switching mode at the same speed of the generator and the obtained harmonic spectra and the corresponding voltage waveforms are shown in Figures. 2.19 (a), (b) and Figures. 2.20 (a), (b) and (c) respectively. Both the switching modes are verified as any of these techniques can be used to control the rotor side converter during DFIG operation. The harmonic spectra of the rotor voltage and the corresponding stator voltage after elimination of 5^{th} and 7^{th} rotor harmonics for m_d =0.9 at 1560 rpm rotor speed are shown in Figure 2.21 (a) and 4.21(b) for 180° switching while those for 120° switching are shown in Figures. 2.22(a) and 2.22(b) respectively. Figures. 2.23 (a) and 2.23(b) show the stator voltage harmonic spectra after the proposed combination of both 3-switching and 5-switching technique of the rotor side converter for the two DFIGs connected to the common micro grid for both 180° and 120° operation. Inspection of Figure 2.17 to Figure 2.23 shows a considerable improvement in the stator voltage harmonic spectra with the proposed control strategy. As more number of harmonics are eliminated by the combination of 3 and 5 switching the grid harmonics are substantially reduced. Figure 2.24 shows the current waveform of the micro grid feeding a load of 1 kVA at 0.8 pf. lag both before and after the proposed harmonic elimination.

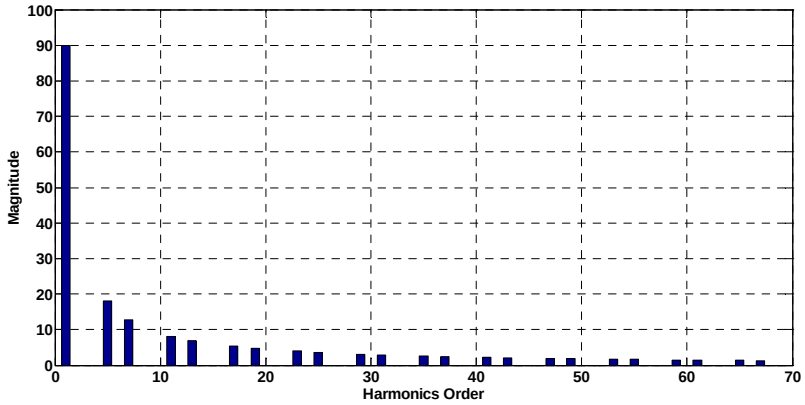

Figure 2.17. a Harmonics spectra of the output voltage of rotor side converter for 180-degree mode without harmonic elimination.

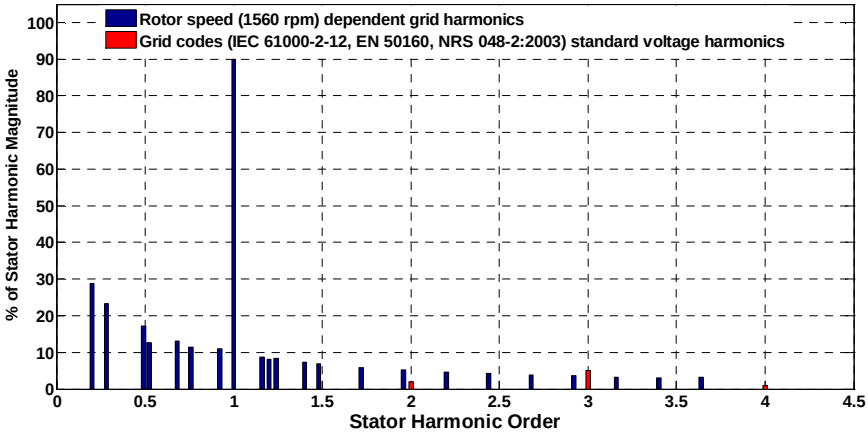

Figure 2.17.b Harmonics spectra of the stator voltage for 180-degree mode with grid codes without harmonic elimination at 1560 rpm.

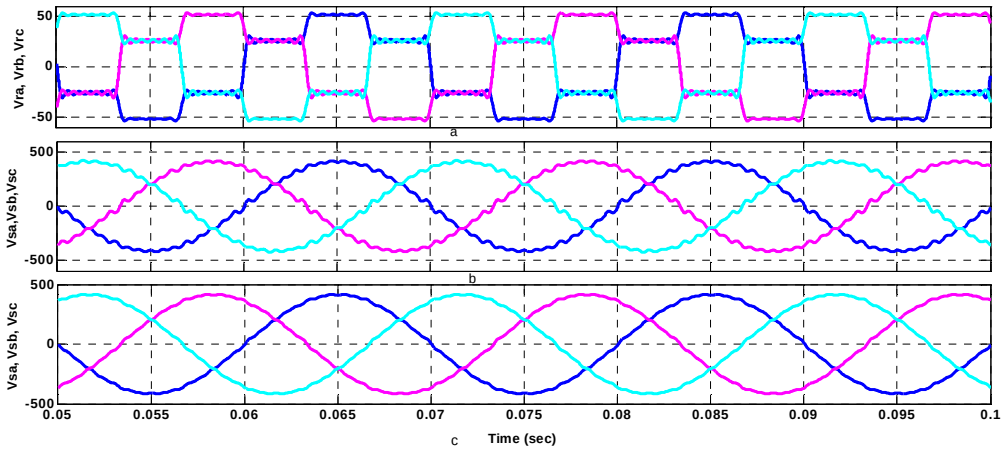

Figure 2.18 DFIG with quasi-sine rotor injection 180-degree conduction mode. (a) Phase a, b, c rotor voltage without harmonic elimination. (b) Phase a, b, c stator voltage without harmonic elimination. (c) Phase a, b, c stator voltage after 5^{th} and 7^{th} rotor harmonics eliminated.

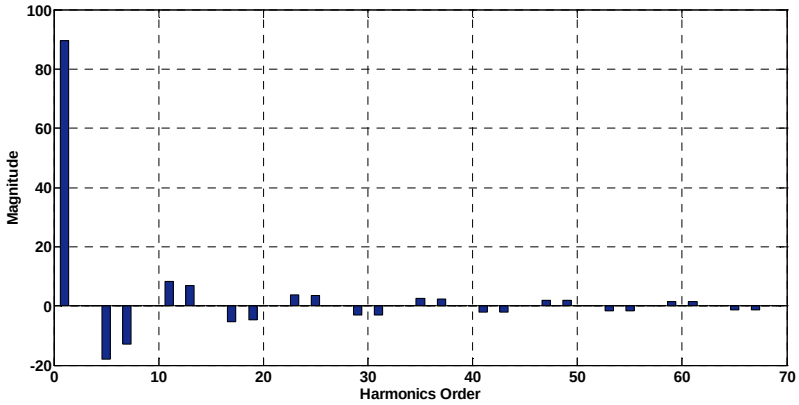

Figure 2.19. a Harmonics spectra of the output voltage of rotor sider converter for 120-degree mode without harmonic elimination.

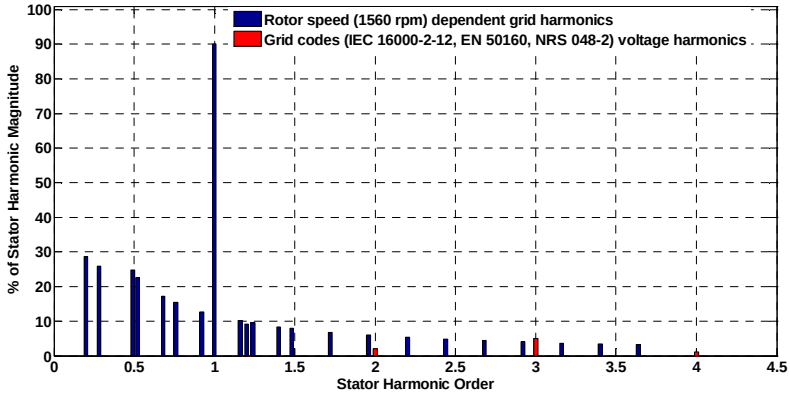

Figure 2.19. b Harmonics spectra of the stator voltage for 120-degree mode with grid codes without harmonic elimination at 1560 rpm.

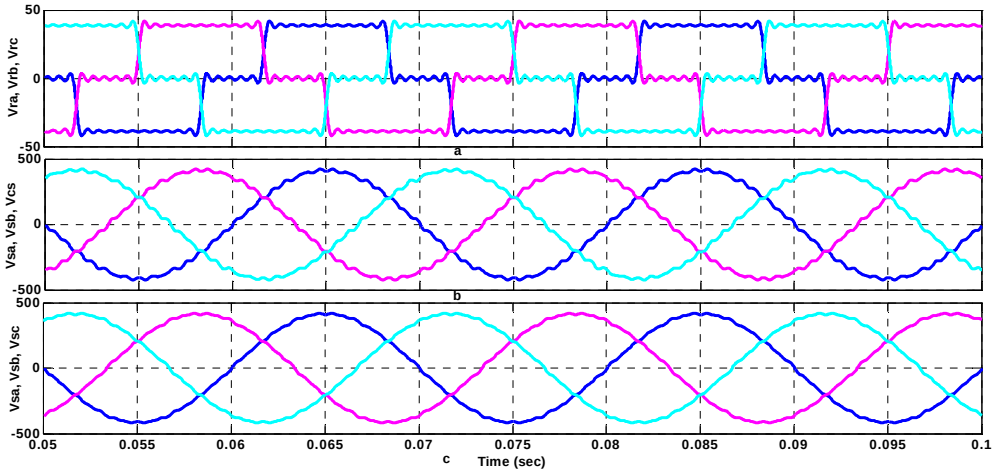

Figure 2.20 DFIG with quasi-sine rotor injection 120-degree conduction mode. (a) Phase a, b, c rotor voltage with harmonics without harmonic elimination. (b) Phase a, b, c stator voltage without harmonic elimination. (c) Phase a, b, c stator voltage after rotor harmonics up to 31st order eliminated.

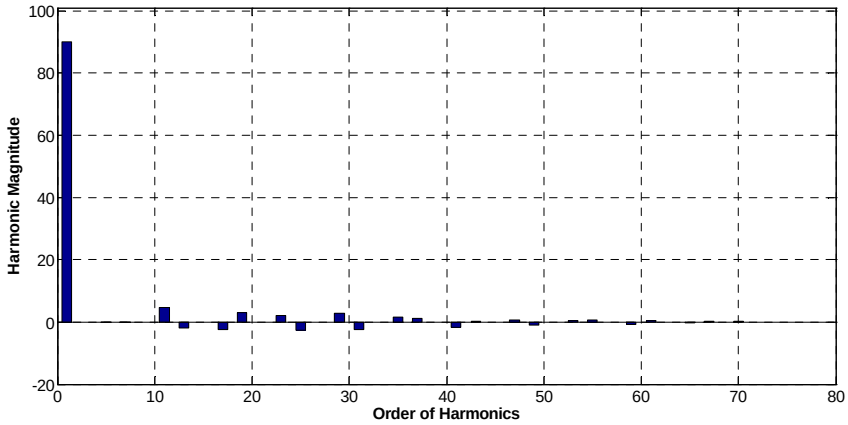

Figure 2.21. a Harmonics spectra of the rotor input voltage for 180-degree conduction mode at m_d =0.9 with 5th and 7th harmonics eliminated.

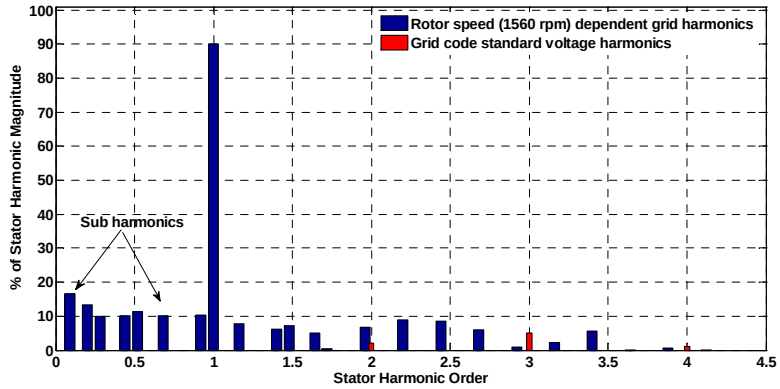

Figure 2.21.b Harmonics spectra of the stator voltage for 180-degree mode with grid codes at 1560 rpm at m_d =0.9 after 5th and 7th rotor harmonics eliminated.

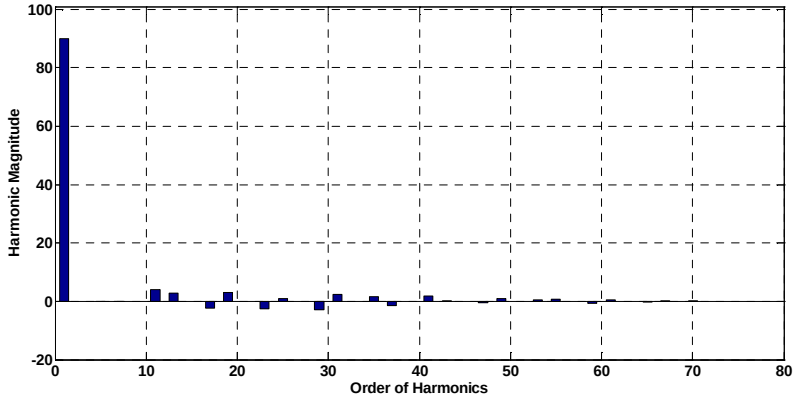

Figure 2.22. a Harmonics spectra of the rotor output voltage of 120-degree conduction mode at m_d =0.9 with 5th and 7th harmonics eliminated.

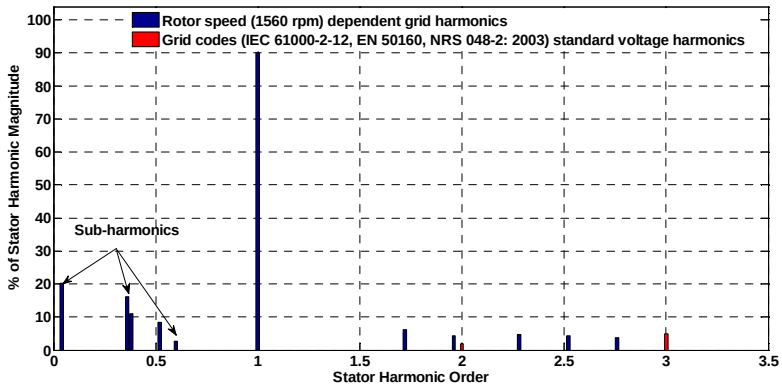

Figure 2. 22.b. Harmonics spectra of the stator voltage of 120-degree conduction mode with m_d =0.9 with 5th and 7th rotor harmonics eliminated at 1560 rpm.

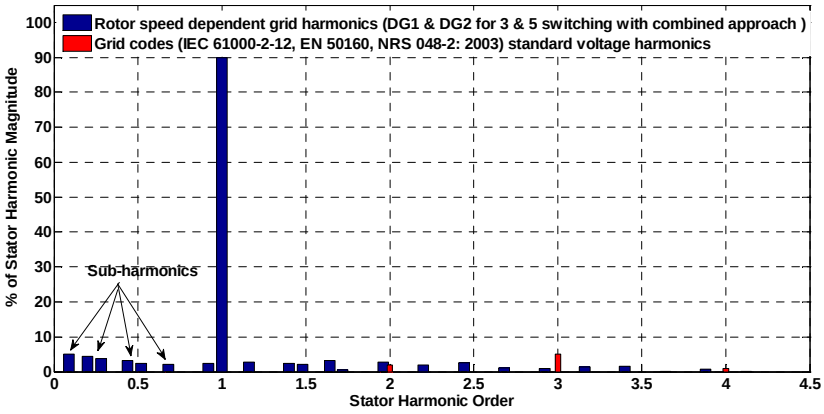

Figure 2.23.a. Harmonics spectra of the stator voltage for 180-degree mode with grid codes at 1560 rpm at m_d =0.9 after DG1and DG2 for 3 and 5 switching with combined approach.

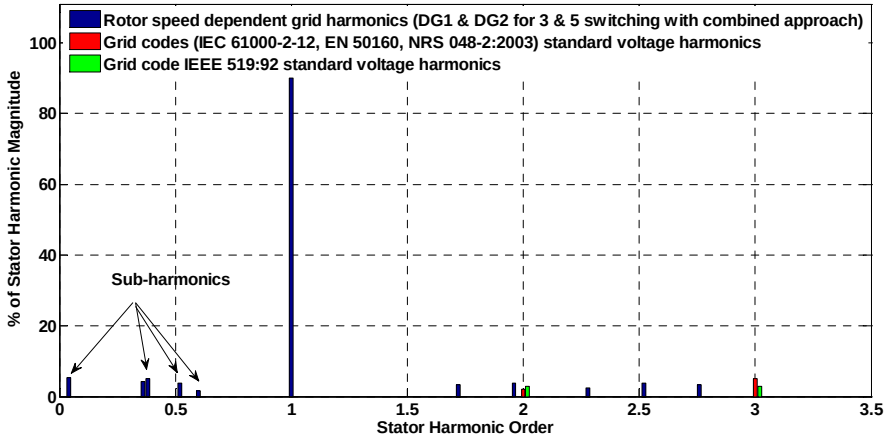

Figure 2.23.b. Harmonics spectra of the stator voltage for 120-degree mode with grid codes at 1560 rpm at m_d =0.9 after DG1and DG2 for 3 and 5 switching with combined approach.

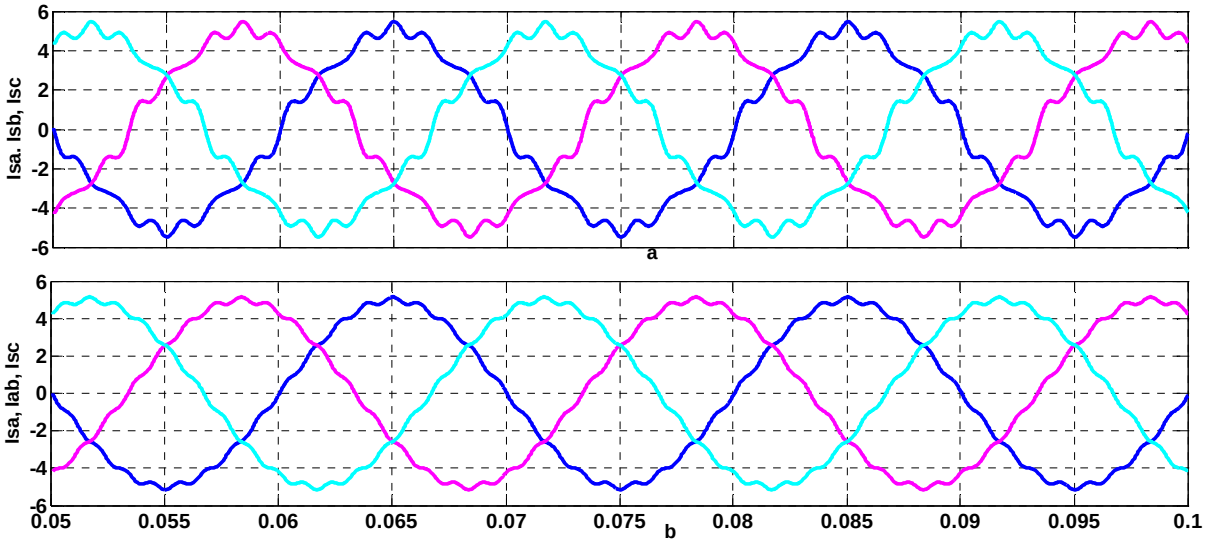

Figure 2. 24 The output of the DFIG with quasi-sine rotor injection 180-degree conduction mode for (a) Phase a, b, c stator current with IEEE 1547 standard harmonics (c) Phase a, b, c stator current up to 19^{th} rotor harmonics eliminated.

2.10 Conclusion

A new method for reduction of voltage harmonics in a micro-grid system consisting of DFIG as multiple DG sources is proposed. The BBO-based SHE-PWM control of rotor side inverters is employed for this purpose. The selected lower order harmonics of the rotor output voltage e.g. 5^{th} and 7^{th} are eliminated by BBO-based SHE-PWM technique. The switching angles eliminating lower order harmonics at different modulation indices are computed by the BBO algorithm and stored in a DSP as look-up table for online application. The other PWM inverter connected to the micro grid is also controlled by BBO-based SHE-PWM technique in such a way to suppress higher order harmonics including 11^{th}, 13^{th}, 17^{th}, and 19^{th} order which are generated by other inverters besides eliminating its own lower order harmonics. Thus, the overall voltage THD in the micro-grid is minimized. The total switching losses of the inverters are lower compared to the situation when all the inverters are switched to eliminate both lower and higher order harmonics. The proposed scheme can be efficiently employed for online control of any number of inverters connected with the micro-grid system supplied from different DG sources.

Chapter 3

Proposed Speed Dependent Stator Harmonics Elimination of DFIG through Proposed RSC switching

Chapter 3

3.1 Chapter Overview

This chapter develops a framework for optimization of rotor side converter (RSC) switching to eliminate lower order harmonic injection of a doubly fed induction generator (DFIG) connected to grid. A biogeography based optimization (BBO) technique is used for this purpose. Three level inverters operating in either 120° or 180° modes at slip frequency are usually employed for the RSC to reduce switching losses. Non-sinusoidal rotor injected voltages by RSC generates undesirable stator harmonics based on operating rotor speed. Induced harmonics in stator are analyzed and computed. A new switching strategy is developed to reduce stator harmonics at different speeds. A BBO based technique is used to compute the switching angles off-line controlled to minimum injected harmonics at closed intervals of modulation indices. These angles are stored in processor memory for on-line application using mixed model equations which have low memory usage. Various simulations are executed supported by suitable experiments with a practical machine for verification of the proposed model which provided satisfactory results.

3.2 Introduction and basic idea of DGs, DFIG and stator side harmonic

In modern life, the possibility of an electric system based on renewable energy is drawing increased attention with the increase in continuous consumption of fossil fuels leading to energy crisis and environmental pollution problems. Therefore, as substitutions of fossil fuels, the "green" and "low carbon" power becomes the insistent need of electric power system and the ultimate outcomes of the ongoing research are solar power, wind power etc. The grid connected DFIG schemes are becoming increasingly popular to get a constant voltage and constant frequency (CVCF) ac output from a variable speed wind turbine. Doubly-fed induction generators (DFIG) fitted with bi-directional inverters at the rotor side are key components of distributed generation systems (DGSs) and micro-grids (MGs). The major advantage of variable-speed DFIGs is that their annual energy capture is about 5% greater than the fixed speed technology [68]. When the wind speed changes, the rotor speed will change, and hence the rotor injection frequency should also be adjusted. The rotor of a DFIG is directly fed with a variable frequency and variable magnitude three-phase voltage. The injected ac voltage to the rotor usually comes from a DC/AC bridge converter shown in Figure 3.1. The performance is studied when the rotor-injected voltage is a three level quasi-sine wave. A six-step switching (which possess $(6n \pm 1)$ harmonics) technique which results in a quasi-sine voltage is generally applied to the rotor circuit to reduce the converter switching losses. Non-sinusoidal rotor voltages cause rotor harmonics which in turn generates undesirable stator harmonics depending on rotor speed. Micro-grids operate at distribution voltage levels. The electrical loads are becoming increasingly sensitive and polluting in nature with the augmented usage of power electronic and computer controlled devices. Therefore, it has become mandatory to maintain stipulated quality of power as recommended indifferent international standards e.g. IEEE 1547, IEC, EN, CIGRE WG 36-05, NRS [69]. Harmonic elimination has therefore become a very important issue with respect to the operation of the micro-grids. Moreover, this issue has become more relevant with the introduction of micro grid connected DGs with renewable energy sources requiring strong power electronic control. One of such popular DGs is a hybrid generation scheme with DFIG based wind energy conversion system and PV panels, which is shown in Figure 3.1. The stator side of the DFIG is directly connected to the utility grid while the rotor side is fed from a three level PV connected inverter beside the grid. The PV panel output is supported with a battery to absorb the excess power from the PV panels or from the DFIG rotor during super synchronous operation. The preliminaries for the harmonics generated by quasi sine wave three level inverters are furnished in [70]. In [71, 72], the technique for

elimination of specific harmonics from a given output voltage waveform using pulse width modulation (PWM) has been discussed. The selected harmonic elimination based pulse width modulation (SHE-PWM) scheme with a lower number of switchings is also shown in [73]. The SHE-PWM method has usually no control over the non-eliminated harmonics, which can increase to higher values. Moreover, the process becomes complex and computation intensive with increased number of harmonics to be eliminated. The six-step switching technique [68, 73] is widely used in thyristor based inverters in order to reduce the switching losses with a simple control circuit. The six-step switching technique introduces quasi-sine ac voltages containing all odd harmonics except triple-n harmonics in the rotor line voltage. The harmonic rotor currents can induce speed dependent stator current harmonics, which can result in pulsating torques. The harmonic elimination for selected order of harmonics along with required fundamental component has been discussed in [30, 34, 35, 74, 75]. In [32,76], rapid convergence with Newton iteration is shown by predicting suitable initial values. Multiple solutions to the SHE problem are also discussed in [46, 77], while [47, 78] represent an optimization technique for particular objective function to minimize the required harmonics. Also Genetic Algorithm (GA) technique has been introduced in [79, 80] to speed up solution of SHE problem. In [81], Particle swarm optimization technique (PSO) technique is proposed, while in [82] a modulation-based PWM method is employed for this purpose. The works in [60, 83, 84] discuss the harmonics issues in rotor and stator sides of DFIG. But none of these techniques address DFIG-based converter switching modification for reduction or control of stator side harmonics.

This chapter develops a framework for optimization of rotor side converter (RSC) switching for a doubly fed induction generator (DFIG) connected to grid. When the rotor side converter is switched to provide conventional quasi-sine voltage to rotor, various speed dependent stator harmonics can be generated to pollute the grid voltage. Thus a modified rotor side inverter switching scheme is proposed in this chapter to reduce the overall stator voltage THD. The rotor side inverter is fed from a solar PV panel cascaded with a DC-DC buck-boost converter, battery and capacitor. Since the inverters connected to the grid system are subjected to handle bulk amount of power, a lesser number of switching per cycle is advantageous for satisfactory operation and reduced switching losses. Optimization based technique is applied to calculate the switching angles of the RSC to reduce injected harmonics. In the present approach, a BBO based [85] algorithm is used to compute the switching angles leading to elimination of selected lower order harmonics and reduction of higher order harmonics. In the present approach, the BBO algorithm searches for optimum set of switching strategies to contribute the minimum THD at all permissible modulation indices. The method is found to be effective for both 120° and 180° switching techniques for RSC switching. The switching angles are computed offline and the combination of switching angles corresponding to minimum voltage THD at sufficiently close points of modulation indices with consideration of linearity between two successive points are stored in a digital signal processor (DSP) memory for online application. Various simulations and experiments in a practical 3 KW DFIG validate the proposed concept.

3.3 Proposed DFIG System Configuration

The block diagram of the DFIG system with proposed control technique is shown in Figure 3.1.The stator of the DFIG is directly connected to grid at line frequency. The DFIG is mechanically coupled with a wind turbine through gearbox. The wind turbine is also having pitch angle control facility for speed control of the turbine-generator assembly. The RSC actually controls the active and reactive power flow from the DC link to the generator which is demonstrated in Figure 3.1. During sub-synchronous mode the active power is fed from the dc bus to the rotor. On the other hand, during super-synchronous mode of operation, the active power is extracted from the rotor to the dc bus which is used to charge the battery and supply other dc loads. The reactive power is controlled in such a way so that the stator operates near unity power factor. The battery can also

be charged from the solar panel in this mode. The DC link voltage V_d is controlled in MPPT mode by the DC-DC converter which is fed from the solar panel.

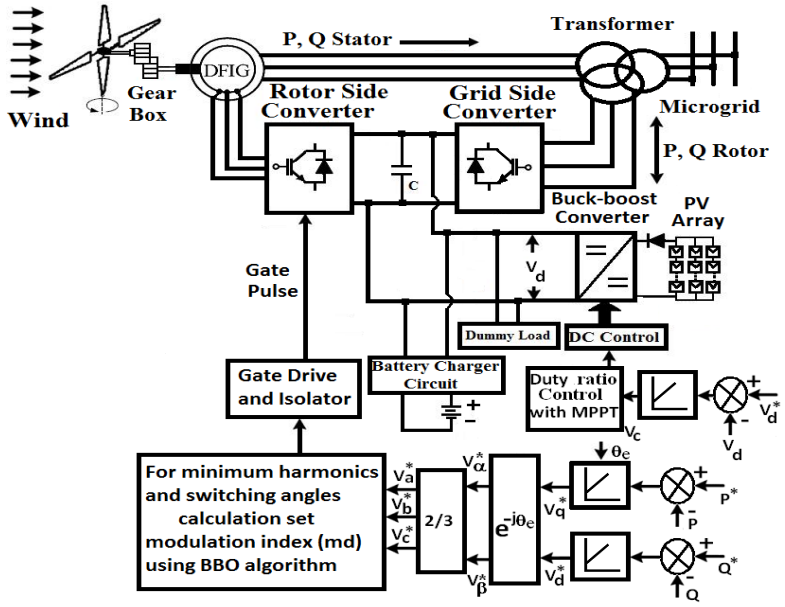

Figure 3.1 Schematic diagram of a DFIG based wind generation

The optional battery connected between the two converters can serve the purpose of storing the extra energy from the PV panel when the rotor side power demand is less than PV panel output. Moreover, this can act as a stand by dc source in the absence of sun light to inject power to the rotor. Also the same can store the recovered power from rotor during super-synchronous operation. In case of the battery gets fully charged, the excess power from the PV panel or the RSC can be fed back to grid through the grid side converter (GSC). The DC-DC converter provided with PV panel uses maximum power point tracking (MPPT) to get the maximum possible power from the PV array etc. Inverters feeding the rotors of the DFIGs handle high current. Thus the devices will have high current stress both during switching and continuous conduction. Since the conduction current cannot minimized as it is decided by the load, the switching losses should be reduced. Thus, output voltage of the rotor side inverter is generally chosen to be a quasi-sine wave with either 120° or 180° [86] switching modes allowing least no. of switching per cycle. Harmonic analysis of the stator circuit with quasi-sine rotor voltage injection is investigated. The six-step switching [52, 87] introduces $(6n\pm1)$ harmonics in the injected rotor voltages which results in a non-sinusoidal stator voltage waveform.

3.4 Harmonic Analysis for Stator and Rotor Currents

Harmonics in the three phase systems have different phase sequence depending on the order of harmonic. The rotor current contains harmonics of order $(6n+1)$ which have positive sequence and harmonics of order $(6n-1)$ which have negative sequence. The positive sequences are defined by $(6n+1)f_r$ i.e. $7f_r, 13f_r, \cdots$ and the negative sequences are defined by $-(6n-1)f_r$ i.e. $-5f_r, -11f_r, \cdots$ .Therefore, the following stator side harmonic components can be observed in the stator current: $f_r + f_m$, $-5f_r + f_m$, $7f_r + f_m$, $-11f_r + f_m$ and $13f_r + f_m$ etc. The lowermost order harmonic (LOH) observed is $|5f_r - f_m|$ .The fifth harmonic of the rotor current produces rotor flux which rotates at five times the

fundamental rotor frequency in the opposite direction. The fifth harmonic rotor flux reacts with the fundamental flux to produce a pulsating torque at six times the rotor fundamental frequency which is – 6 f_r . Similarly, the seventh harmonic rotor field produces a pulsating torque at six times the fundamental frequency i.e. 6 f_r . The stator induced voltages due to the rotor injected harmonics can be formulated by $\left[1+(i-1)s\right]f_s$ and $\left[1-(i+1)s\right]f_s$ where $i=6n+1$ for forward and $i=6n-1$ for backward fields.

The harmonics of the order $3+6.n$, where $n = 0,1,2,3,\cdots$ are zero sequence components and they will not be present in the line voltages. The interaction between the rotor flux harmonics and the fundamental flux in the air-gap also introduces sub-harmonic currents in the stator. The introduction of the sub-harmonics depends on the speed of the rotor and these also are responsible for stator voltage distortion. Therefore, the aim should be to eliminate these undesirable harmonics from the stator induced voltages in the working speed range of the DFIG. The rotor-side converters should ensure that the injected rotor voltage at slip frequency produces a constant stator frequency of 50 Hz. A sinusoidal input at the rotor side removes the problem. The RSC operating in 6-step mode injects harmonics to the rotor circuit. These harmonics reaches the stator terminals from rotor side as analyzed in [31, 45, 88-90]. This phenomenon can also cause speed ripple depending on the inertia of the machine and other operating conditions [91]. In [92] adaptive filtering technique has been used to partially remove this problem. Different PWM techniques can be used to control the frequency and amplitude of the output of the rotor-side converter. But producing a near sinusoidal voltage requires high switching frequency which is undesirable due to high switching losses in the inverter. For quasi-sine wave switching [86] the $(6n-1)^{th}$ harmonics produces negative sequence harmonics and the corresponding rotor voltage are given by (3.1).

$$\begin{cases} V_{an} = \mathrm{Im}\left(\dfrac{2V_{dc}}{\pi}\dfrac{1}{6n-1}e^{j(6n-1)\omega t}\right) \\ V_{bn} = \mathrm{Im}\left(\dfrac{2V_{dc}}{\pi}\dfrac{1}{6n-1}e^{j(6n-1)\omega t}e^{j(2\pi/3)}\right) \\ V_{cn} = \mathrm{Im}\left(\dfrac{2V_{dc}}{\pi}\dfrac{1}{6n-1}e^{j(6n-1)\omega t}e^{-j(2\pi/3)}\right) \end{cases} \tag{3.1}$$

Similarly the $(6n+1)^{th}$ harmonics are positive sequence harmonics and the rotor voltages are given by in Eq. (3.2).

$$\begin{cases} V_{an} = \mathrm{Im}\left(\dfrac{2V_{dc}}{\pi}\dfrac{1}{6n+1}e^{j(6n+1)\omega t}\right) \\ V_{bn} = \mathrm{Im}\left(\dfrac{2V_{dc}}{\pi}\dfrac{1}{6n+1}e^{j(6n+1)\omega t}e^{j(2\pi/3)}\right) \\ V_{cn} = \mathrm{Im}\left(\dfrac{2V_{dc}}{\pi}\dfrac{1}{6n+1}e^{j(6n+1)\omega t}e^{-j(2\pi/3)}\right) \end{cases} \tag{3.2}$$

3.5 Rotor Speed dependent Stator Harmonics

It is already shown that the six-step switching of RSC introduces a number of rotor voltage harmonics, which in turn generate stator voltage harmonics. The stator voltage harmonics generated from rotor harmonics depends on the rotor speed. The stator frequency f_s is to be kept constant at 50 Hz irrespective of the rotor speed. The rotor speed f_m (mechanical

frequency in Hz) changes with wind speed. The rotor injection frequency f_r is so adjusted to keep the stator frequency f_s constant. For the injected rotor harmonics order of $(6n+1)$, the order of stator frequency generated is $((6n+1)\,f_r + f_m)$ with n=1,2,…. Similarly for rotor harmonics injection of order $(6n-1)$, the generated stator frequency will be $(-(6n-1)\,f_r + f_m)$. The fundamental component can be observed in the stator current at a frequency of $(f_r + f_m)$. Then the total stator harmonics observed has frequency of $|(6n \pm 1)\,f_r \pm f_m|$.If the machine has *P* poles and the rotor speed in rpm is N_r , then the frequency of the rotor voltage to be injected is given by $f_r = f_s - f_m = s\,f_s$ where $f_m = PN_r/120\,Hz$ and the slip is given by $s = (N_s - N_r)/N_s$.

A four pole 3KW DFIG is considered for the present case for which the synchronous speed is 1500 rpm. Considering a maximum operating slip of ± 30%, the possible approximate rotor speed range of the DFIG can be between 1000 rpm to 2000 rpm. If the rotor speed is 1000 rpm, the corresponding rotor mechanical frequency is 33.33 Hz and the rotor injection frequency is $16.667Hz$. If the rotor injected harmonic order is 13^{th}, the rotor injected frequency is $216.67Hz$. The injected 13^{th} harmonic rotor voltage generates a stator frequency of (216.67+33.33) Hz or $250\,Hz$ in the forward direction. Hence the generated stator harmonic order is 5^{th} in forward direction. For the 17th harmonic rotor injected frequency, the rotor supply frequency $-283.334Hz$ i.e. 283.33Hz in reverse direction. Hence the 17^{th} order rotor injected harmonic develops a stator frequency of (-283.33+33.33) Hz or 250Hz in reverse direction. Hence the stator harmonic order is -5^{th} or 5^{th} in reverse direction. In the same way, for a rotor speed of 1250 rpm the corresponding mechanical frequency is 41.67 Hz and the rotor injection frequency is 8.33 Hz. For the 5th order rotor injected harmonic, the rotor injected frequency is (5x8.33) Hz =41.67 Hz in the opposite direction to the rotation. Therefore, the generated stator harmonic frequency is (41.67-41.67) Hz= 0 Hz, which has the significance of no stator harmonic or dc injection to the stator.

Table 3.1 Generated stator harmonics due to presence of rotor harmonics at various rotor speeds

Rotor harmonic order	Rotor speed (rpm)	Generated stator harmonic order	Rotor harmonic order	Rotor speed (rpm)	Generated stator harmonic order	Rotor harmonic order	Rotor speed (rpm)	Generated stator harmonic order	Rotor harmonic order	Rotor speed (rpm)	Generated stator harmonic order
	1000	-1*		1000	-7*		1000	5		1100	-7*
5th	1250	0		1125	-5*		1500	1		1200	-5*
	1500	1		1375	-1*		1625	0		1400	-1*
	1750	2		1500	1	13th	1750	-1*		1500	1
	1500	1		1750	5					1700	5
7th	1750	0	23rd	1875	7		1000	-5*		1800	7
	2000	-1*					1500	1	29th	2000	11
				1125	7	17th	2000	7			
	1250	-1*		1250	5					1000	11
	1375	0		1500	1		1000	7		1200	7
11th	1500	1		1875	-5*		1250	4		1300	5
	1875	4	25th	2000	-7*	19th	1500	1		1500	1
	2000	5					1750	-2		1550	0
							2000	-5*		1600	-1*
									31st	1800	-5*

* The negative sign indicates that the generated frequency has opposite sequence

Thus the stator generated harmonics due to different rotor injected frequencies corresponding to different wind speeds can be calculated and some of them are shown in Table-3.1.The negative sign for the harmonics shown in Table-3.1 indicates that the generated harmonics are in opposite direction. The harmonic content of stator voltage shown in Table-3.1 reveals that the rotor harmonic elimination is very much required for the rotor side inverter in order to suppress lower order stator voltage harmonics at different speed. Hence, BBO-based SHE-PWM technique is developed to calculate switching angles to reduce specific lower order rotor harmonics from rotor voltage. The angles are calculated off-line and stored in processor memory for on-line application.

3.6 Existing and Proposed Switching Strategies

The RSC of DFIG is generally switched under either 180° or 120° mode of operation which injects quasi-sine voltage waveform to the rotor circuit. In the proposed technique both these modes are suitably modified to substantially reduce injected harmonics which is shown in the following analysis.

3.6.1Operating mode of180^{0}

3.6.1.1 Existing Quasi sine wave 180-degree switching operation

In Figure 3.2 shows the basic circuit diagram of the three phase bridge inverter, which contained six power switches and six freewheeling control diodes. The inverter switching controller generates the preferred output voltage and current waveform. Figure 3.3 shows the waveform diagram of the 180-degree conduction mode which is operate 180-degree switch in each period, phase shift is 60-degree, at a time the two upper and one lower switch operate, the output voltage always quasi-square wave.

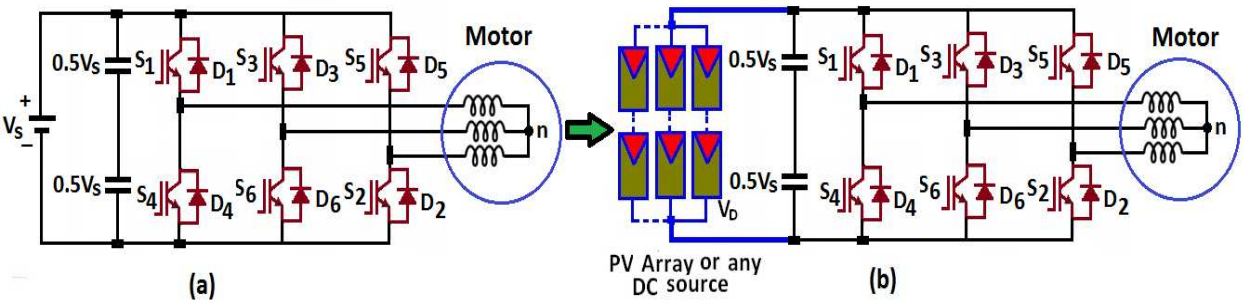

Figure 3.2 Three phase inverter for 180-degree switching conduction (a) without renewable (b) with renewable

The instantaneous line voltage V_{ab}, V_{bc} and V_{ca} can be expressed as equation (3.3) which is shifted by $\pi/6$ and even harmonics are zero.

$$V_{ab} = \sum_{n=1,3,5,\cdots}^{\infty} \frac{4V_{dc}}{n\pi} \cos(n\pi/6) \sin n(\omega t + \pi/6)$$

$$V_{bc} = \sum_{n=1,3,5,\cdots}^{\infty} \frac{4V_{dc}}{n\pi} \cos(n\pi/6) \sin n(\omega t - \pi/2) \quad (3.3)$$

$$V_{ca} = \sum_{n=1,3,5,\cdots}^{\infty} \frac{4V_{dc}}{n\pi} \cos(n\pi/6) \sin n(\omega t - 7\pi/6)$$

The phase voltage for 180-degree conduction mode as (4) is

$$V_{aN} = \sum_{n=1,3,5,\cdots}^{\infty} \frac{4V_{dc}}{\sqrt{3}n\pi} \sin(n\pi/3) \sin(n\omega t)$$

$$V_{bN} = \sum_{n=1,3,5,\cdots}^{\infty} \frac{4V_{dc}}{\sqrt{3}n\pi} \sin(n\pi/3) \sin n(\omega t - 2\pi/3) \tag{3.4}$$

$$V_{cN} = \sum_{n=1,3,5,\cdots}^{\infty} \frac{4V_{dc}}{\sqrt{3}n\pi} \sin(n\pi/3) \sin n(\omega t - 4\pi/3)$$

The instantaneous phase voltage (180° conduction mode) V_{an}, V_{bn} and V_{cn} are expressed in Fourier series as (3.5),

$$V_{an} = \frac{a_0}{2} + \sum_{n=1}^{\infty} \left(a_n \cos(n\omega t) + b_n \sin(n\omega t) \right) \tag{3.5}$$

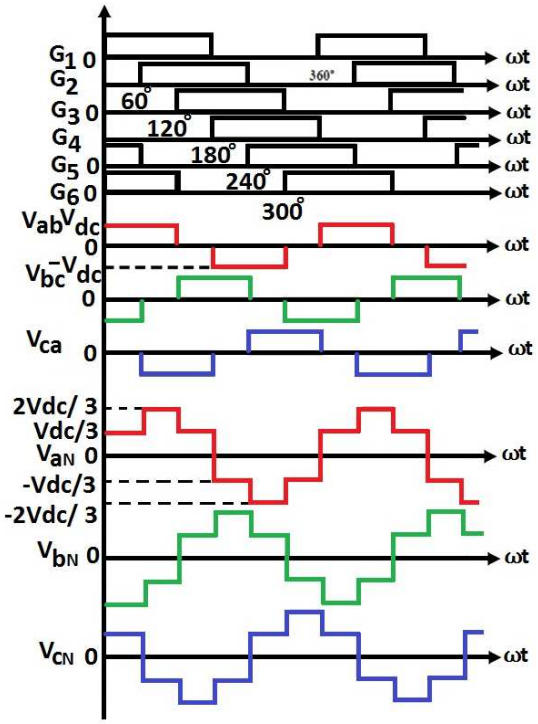

Figure 3.3 The overall output waveform for 180-degree switching conduction.

The phase voltage waveform of a 3-phase bridge inverter is a quasi-square wave. The wave form has quarter-wave symmetry, due to the quarter-wave symmetry, we gat

$a_0 = 0,$ for all n, and $a_n = 0$, for all even n

The phase voltage equation (3.5) becomes (3.6)

$$V_{an} = \sum_{n=1}^{\infty} b_n \sin(n\omega t) \tag{3.6}$$

And the harmonics coefficient b_n can be expressed as

$$b_n = \frac{4}{\pi} \int_0^{\pi/2} e(\omega t) \sin(n\omega t)\, d(\omega t) \text{ for all odd } 'n'$$

or, $$b_n = \frac{4}{\pi} \left[\int_0^{\pi/3} \frac{V_{dc}}{3} \sin(n\omega t)\, d(\omega t) + \int_{\pi/3}^{\pi/2} \frac{2V_{dc}}{3} \sin(n\omega t)\, d(\omega t) \right]$$

$$= \frac{4V_{dc}}{3n\pi}\left[\left[\cos(n\omega t)\right]_{\pi/3}^{0} + 2\left[\cos(n\omega t)\right]_{\pi/2}^{\pi/3}\right]$$

$$= \frac{4V_{dc}}{3n\pi}\left[1 - \cos\left(\frac{n\pi}{3}\right) + 2\cos\left(\frac{n\pi}{3}\right) - 2\cos\left(\frac{n\pi}{2}\right)\right]$$

but, $\cos\left(\frac{n\pi}{2}\right) = 0$ for all odd n,

The n^{th} harmonic component can be mathematically expressed as

$$b_n = \frac{4V_{dc}}{3n\pi}\left[1 + \cos\left(\frac{n\pi}{3}\right)\right], \text{ and the phase angle } \phi_n = \tan^{-1}\left(\frac{a_n}{b_n}\right) = 0 \quad (3.7)$$

The harmonic analysis of the phase voltage waveform gives the n^{th} harmonic as, $n = 1, 5, 7, 11, 13, 17, \cdots$

or, $n = 6k \pm 1$ for $k = 1, 2, 3, 4, \cdots$

From (3.6) and (3.7) we get the final phase voltage i.e (3.8).

$$V_{an} = \sum_{n=1}^{\infty} \frac{4V_{dc}}{3n\pi}\left[1 + \cos\left(\frac{n\pi}{3}\right)\right]\sin(n\omega t) \quad (3.8)$$

Harmonic phase voltage for V_{an} with 180° conduction mode as (3.9)

$$V_{n(phase)} = 0.63662V_{dc}\left[\frac{1}{1}\sin(1\omega t) + \frac{1}{5}\sin(5\omega t) + \frac{1}{7}\sin(7\omega t) + \frac{1}{11}\sin(11\omega t) + \frac{1}{13}\sin(13\omega t) + \cdots\right] \quad (3.9)$$

From equation (3.7) the calculated harmonics is observed as Table 3.2 and from Table we can observe that the triple-n harmonics (3, 9, 12, 15, …) are zero. The harmonic spectrum for and phase voltage is shown in Figure 3.4 (a) and (b).

Table 3.2 Generated harmonics for 180-degree conduction from (3.7) with multiplying V_{dc}.

Harmonic Order	1	5	7	11	13	17	19	23	25
Harmonic Magnitude (%)	63.662	12.732	9.0946	5.7875	4.8971	3.7448	3.3506	2.7679	2.5465
Harmonic Order	29	31	35	37	41	43	47	49	53
Harmonic Magnitude (%)	2.1952	2.053	1.818	1.720	1.552	1.480	1.3545	1.2992	1.2012
Harmonic Order	55	59	61	65	67	71	73	77	79
Harmonic Magnitude (%)	1.1575	1.079	1.043	0.979	0.950	0.896	0.872	0.826	0.805

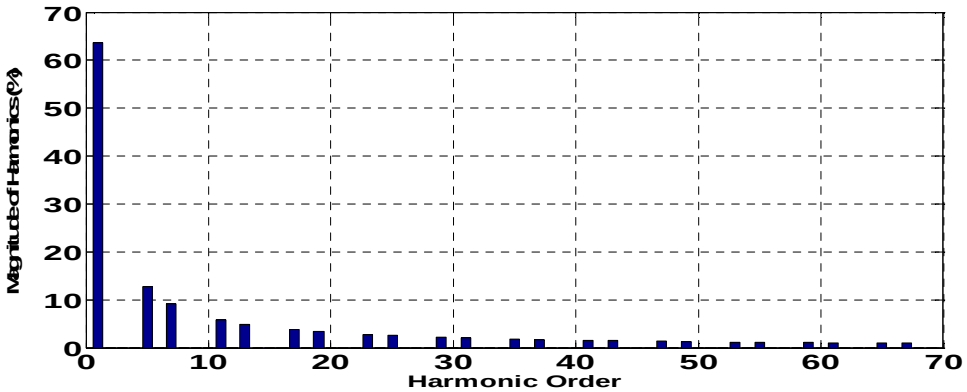

Figure 3.4 (a) The harmonic spectrum for phase voltage

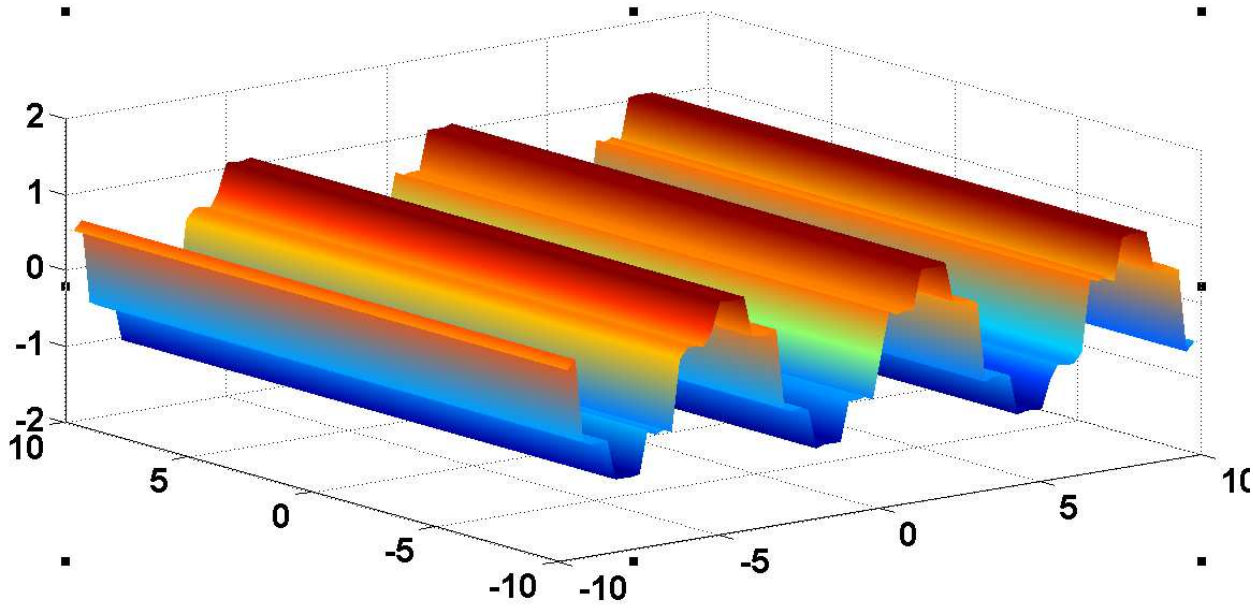

Figure 3.4 (b) The harmonic voltage for V_{an} phase.

3.6.1.2 Proposed SHE-PWM switching Scheme

A three phase six-step quasi-sine 180° switching pattern for phase a, b and c with five switching angles is shown in Figure 3.5.

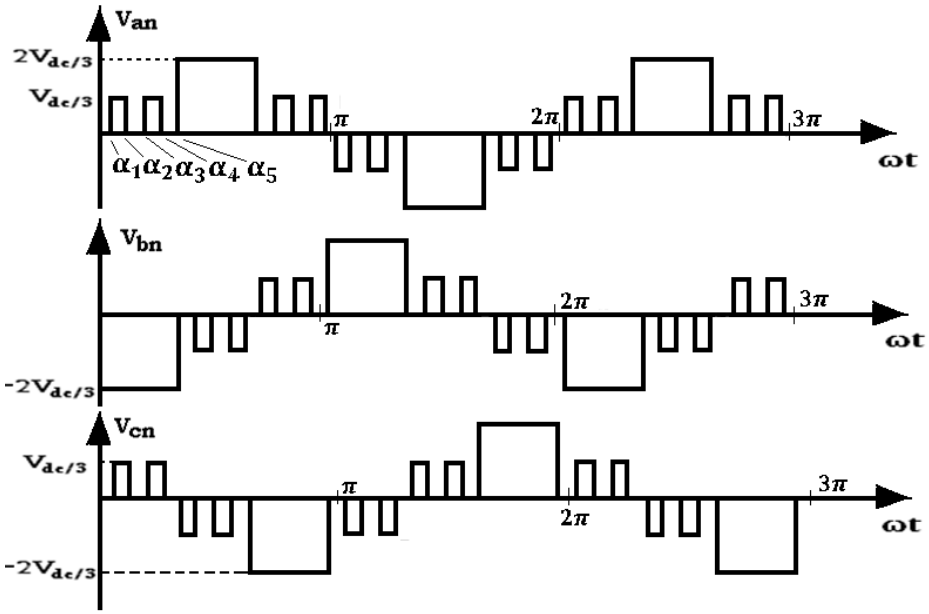

Figure 3.5 A three-phase six-step Quasi-sine waveforms of 180° switch conduction phase voltage switching pattern with five switching angles.

A three-phase six-step Quasi-sine waveforms of 180° switch conduction phase voltage switching pattern with five switching angles indicate that up to 5^{th}, 7^{th}, 11^{th} and 13^{th} order harmonic are eliminated and the higher order harmonics are suppressed by a proper choice of displacement angle α.

The Fourier series of output voltage can be expressed as (3.5)

The phase voltage waveform of a 3-phase bridge inverter is a quasi-square wave. The wave form has quarter-wave symmetry, and due to the quarter wave symmetry

$$a_0 = 0 \text{ for all } n, \text{ and } a_n = 0, \text{ for all even } 'n'$$

$$\text{then}, V_{an} = \sum_{n=1,5,7,\cdots}^{\infty} b_n \sin(n\omega t)$$

$$\text{or, } b_n = \frac{1}{\pi}\int_0^{2\pi} V_{an}\sin(n\omega t)\,d(\omega t)$$

$$= \frac{4}{\pi}\int_0^{\pi/2} V_{an}\sin(n\omega t)\,d(\omega t)$$

$$= \frac{4}{\pi}\left[\int_{\alpha_1}^{\alpha_2} V_{an}\sin(n\omega t)\,d(\omega t) + \int_{\alpha_3}^{\alpha_4} V_{an}\sin(n\omega t)\,d(\omega t) + \int_{\alpha_5}^{\pi/2} V_{an}\sin(n\omega t)\,d(\omega t)\right]$$

$$= \frac{4}{\pi}\left[\int_{\alpha_1}^{\alpha_2} \frac{V_{dc}}{3}\sin(n\omega t)\,d(\omega t) + \int_{\alpha_3}^{\alpha_4} \frac{V_{dc}}{3}\sin(n\omega t)\,d(\omega t) + \int_{\alpha_5}^{\pi/2} \frac{2V_{dc}}{3}\sin(n\omega t)\,d(\omega t)\right]$$

$$= \frac{4V_{dc}}{3n\pi}\left[(-1)\cos(n\omega t)\Big|_{\alpha_1}^{\alpha_2} + (-1)\cos(n\omega t)\Big|_{\alpha_3}^{\alpha_4} + 2(-1)\cos(n\omega t)\Big|_{\alpha_5}^{\pi/2}\right]$$

$$= \frac{4V_{dc}}{3n\pi}\left[\cos n\alpha_1 - \cos n\alpha_2 + \cos n\alpha_3 - \cos n\alpha_4 + 2\cos n\alpha_5 - 2\cos n\pi/2\right]$$

$$\cos n\pi/2 = 0 \text{ for } n = 1,5,7,11,\cdots, \ (6n \pm 1)$$

$$= \frac{4V_{dc}}{3n\pi}\left[\cos n\alpha_1 - \cos n\alpha_2 + \cos n\alpha_3 - \cos n\alpha_4 + 2\cos n\alpha_5\right]$$

Put $n = 1,5,7,11,13,\cdots$ the harmonic coefficient can be easily calculated and which is,

$$b_1 = \frac{4V_{dc}}{3\pi}\left[\cos 1\alpha_1 - \cos 1\alpha_2 + \cos 1\alpha_3 - \cos 1\alpha_4 + 2\cos 1\alpha_5\right]$$

$$b_5 = \frac{4V_{dc}}{3\times 5\times \pi}\left[\cos 5\alpha_1 - \cos 5\alpha_2 + \cos 5\alpha_3 - \cos 5\alpha_4 + 2\cos 5\alpha_5\right]$$

$$b_7 = \frac{4V_{dc}}{3\times 7\times \pi}\left[\cos 7\alpha_1 - \cos 7\alpha_2 + \cos 7\alpha_3 - \cos 7\alpha_4 + 2\cos 7\alpha_5\right]$$

Thus the general equation of b_n can be written as (10),

$$b_n = \frac{4V_{dc}}{3n\pi}\left[-\sum_{k=1}^{m}(-1)^k\cos(n\alpha_k) - 2\sum_{k=m+1}^{N}(-1)^k\cos(n\alpha_k)\right]$$

or

$$V_{an} = \frac{4V_{dc}}{3n\pi}\left[-\sum_{k=1}^{m}(-1)^k\cos(n\alpha_k) - 2\sum_{k=m+1}^{N}(-1)^k\cos(n\alpha_k)\right]\sin(n\omega t) \tag{3.10}$$

For 5-switching, the mathematical statement of these circumstances is then (3.11)

$$\begin{cases} \cos\alpha_1 - \cos\alpha_2 + \cos\alpha_3 - \cos\alpha_4 + 2\cos\alpha_5 = \mathrm{M} \\ \cos 5\alpha_1 - \cos 5\alpha_2 + \cos 5\alpha_3 - \cos 5\alpha_4 + 2\cos 5\alpha_5 = 0 \\ \cos 7\alpha_1 - \cos 7\alpha_2 + \cos 7\alpha_3 - \cos 7\alpha_4 + 2\cos 7\alpha_5 = 0 \\ \cos 11\alpha_1 - \cos 11\alpha_2 + \cos 11\alpha_3 - \cos 11\alpha_4 + 2\cos 11\alpha_5 = 0 \\ \cos 13\alpha_1 - \cos 13\alpha_2 + \cos 13\alpha_3 - \cos 13\alpha_4 + 2\cos 13\alpha_5 = 0 \end{cases} \tag{3.11}$$

The $5^{th}, 7^{th}, 11^{th} and 13^{th}$ harmonics would be eliminated if $b_5 = b_7 = b_{11} = b_{13} = 0$. These equations can be solved iteratively and calculate the $\alpha_1, \alpha_2, \alpha_3, \cdots, \alpha_k$ for low % THD.

Similarly for three switching the phase voltage switching pattern is shown in **Figure 3.6**

For elimination of the $5^{th} and 7^{th}$ harmonics, $b_5 = b_7 = 0$; number of switching angles =3.Three notches per quarter-wave would be required. Equation (3.12) gives the following set of nonlinear simultaneous equations to solve for the angles.

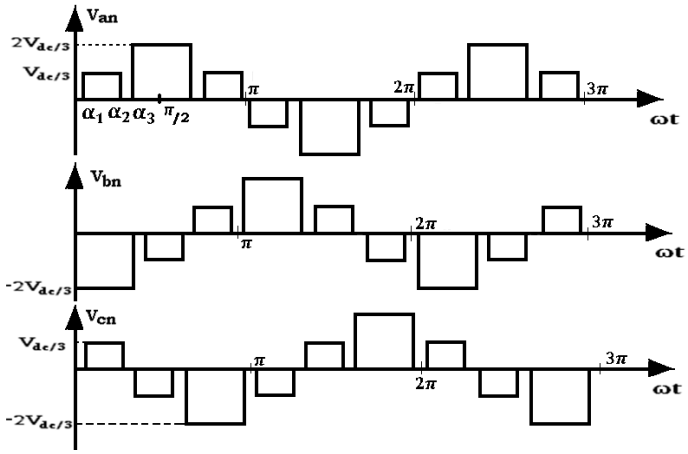

Figure 3.6 A three-phase six-step Quasi-sine waveforms of 180° switch conduction phase voltage Switching pattern with three switching angles.

$$\begin{cases} \cos\alpha_1 - \cos\alpha_2 + 2\cos\alpha_3 = \mathrm{M} \\ \cos 5\alpha_1 - \cos 5\alpha_2 + 2\cos 5\alpha_3 = 0 \\ \cos 7\alpha_1 - \cos 7\alpha_2 + 2\cos 7\alpha_3 = 0 \\ \cos 11\alpha_1 - \cos 11\alpha_2 + 2\cos 11\alpha_3 = 0 \\ \cos 13\alpha_1 - \cos 13\alpha_2 + 2\cos 13\alpha_3 = 0 \end{cases} \quad (3.12)$$

From Figure 3.3 the line voltage waveform of a 3-phase bridge inverter is a quasi-square wave. Due to the quarter-wave symmetry, we gat, $a_0 = 0$ for all n, and $a_n = 0$, for all even n

The general line voltage equation as (3.13)

$$V_{ab} = \sum_{n=1}^{\infty} \left(a_n \cos(n\omega t) + b_n \sin(n\omega t) \right) \quad (3.13)$$

For $a_0 = 0$ for all n, and $a_n = 0$, for all even n, the (3.13) becomes

$$V_{ab} = \sum_{n=1}^{\infty} b_n \sin(n\omega t)$$

And the harmonics coefficient b_n can be expressed as

$$b_n = \frac{4}{\pi} \int_0^{\pi/2} V_{ab} \sin(n\omega t)\, d(\omega t) \text{ for all odd } 'n' \quad (3.14)$$

or, $b_n = \frac{4}{\pi} \int_{\pi/6}^{\pi/2} V_{dc} \sin(n\omega t)\, d(\omega t)$

$$= \frac{4V_{dc}}{n\pi} \left[\cos(n\omega t) \right]_{\pi/2}^{\pi/6}$$

$$= \frac{4V_{dc}}{n\pi}\left[\cos\left(\frac{n\pi}{6}\right) - \cos\left(\frac{n\pi}{2}\right)\right]$$

$$= \frac{4V_{dc}}{n\pi}\sin\left(\frac{n\pi}{2}\right)\sin\left(\frac{n\pi}{3}\right)$$

Here, $\sin\left(\frac{n\pi}{3}\right) = \cos\left(\frac{n\pi}{6}\right)$

Now, the phase angle $\phi_n = \tan^{-1}\left(\frac{a_n}{b_n}\right) = 0$

The n^{th} harmonic component can be mathematically expressed as

$$b_n = \frac{4V_{dc}}{n\pi}\sin\left(\frac{n\pi}{2}\right)\sin\left(\frac{n\pi}{3}\right) \tag{3.15}$$

The harmonic analysis of the line voltage waveform gives the n^{th} harmonic as, $n = 1,5,7,11,13,17,\cdots$ or, $n = 6k \pm 1$ for $k = 1,2,3,4,\cdots$

From (3.14) and (3.15) we get the final line voltage i.e.

$$V_{ab} = \sum_{n=1,5,7,\cdots}^{\infty} \frac{4V_{dc}}{n\pi}\sin\left(\frac{n\pi}{2}\right)\sin\left(\frac{n\pi}{3}\right)\sin(n\omega t)$$

$$= \sum_{n=1,5,7,\cdots}^{\infty} \frac{4V_{dc}}{n\pi}\cos\left(\frac{n\pi}{6}\right)\sin(n\omega t) \tag{3.16}$$

The rms value of the n^{th} harmonic component is given by

$$V_{ab}(rms) = \sum_{n=1,5,7,\cdots}^{\infty} \frac{4V_{dc}}{\sqrt{2}n\pi}\sin\left(\frac{n\pi}{2}\right)\sin\left(\frac{n\pi}{3}\right)\sin(n\omega t)$$

$$= \sum_{n=1,5,7,\cdots}^{\infty} \frac{4V_{dc}}{\sqrt{2}n\pi}\cos\left(\frac{n\pi}{6}\right)\sin(n\omega t) \tag{3.17}$$

The rms value of the fundamental can be obtained by substituting n=1,

$$V_{ab}(rms) = \sum_{n=1,5,7,\cdots}^{\infty} \frac{4V_{dc}}{\sqrt{2}\pi}\sin\left(\frac{\pi}{2}\right)\sin\left(\frac{\pi}{3}\right)\sin(n\omega t) = 0.7796968012V_{dc} = 77.909V_{dc}\%$$

From equation (3.17) we can calculate the magnitude of harmonics for 180-deg conduction with line voltage, which is shown in Table 3.3. In Figure 3.7 (a) and (b) shows the harmonic spectra and line voltage waveform.

Table 3.3 Generated harmonics for line voltage with 180-degree conduction from (3.17) with

Harmonic Order	1	5	7	11	13	17	19	23	25
Harmonic Magnitude (%)	77.969	-15.59	-11.14	5.997	-4.586	-4.103	3.39	3.1188	-2.688
Harmonic Order	29	31	35	37	41	43	47	49	53
Harmonic Magnitude (%)	-2.515	2.227	2.107	-1.901	-1.813	1.6589	1.5912	-1.471	-1.417
Harmonic Order	55	59	61	65	67	71	73	77	79
Harmonic Magnitude (%)	1.3215	1.278	-1.199	-1.17	1.0982	1.0681	-1.012	-0.987	0.9394

The order of harmonics and their amplitudes is shown in Table 3.6. From Table we can observe that the triple-n harmonics (3, 9, 12, 15, …) are zero. Here $k = 1,5,7,11,13,\cdots, or. k = 6n \pm 1,\ for n = 1,2,3,4,\cdots,$. The harmonic line voltage equation foe 180-deg is as (18)

$$V_{n(line)} = 0.77967 V_{dc}\left[\frac{1}{1}\sin(1\omega t) - \frac{1}{5}\sin(5\omega t) - \frac{1}{7}\sin(7\omega t) + \frac{1}{11}\sin(11\omega t) + \frac{1}{13}\sin(13\omega t)\cdots\right] \quad (3.18)$$

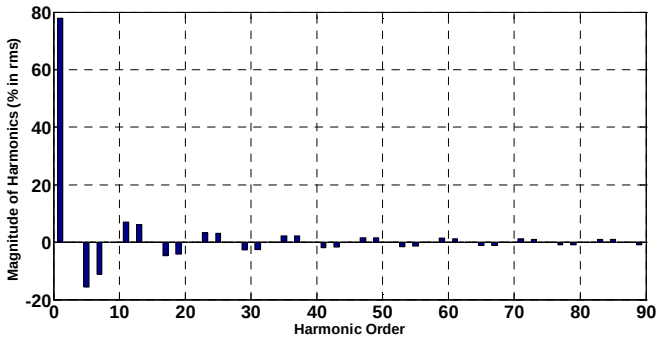

Figure 3.7 (a) The harmonic spectrum for line voltage with 180-degree conduction mode

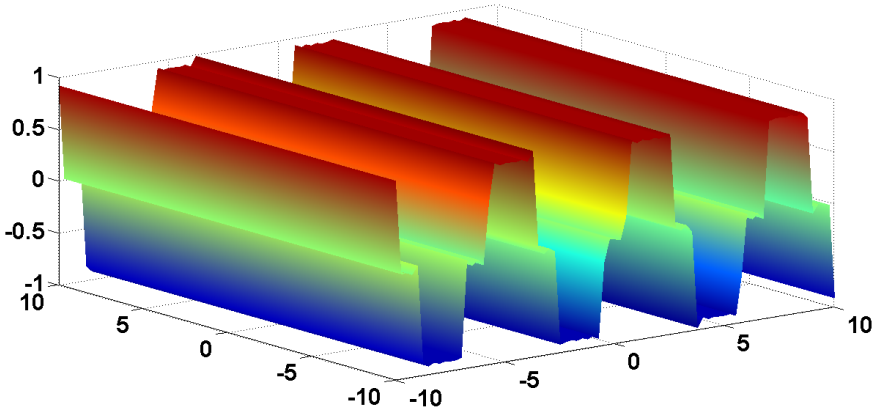

Figure 3.7 (b) The harmonic voltage spectrum for V_{ab} line voltages.

3.6.2 For 120° mode of operation

3.6.2.1 Existing Quasi sine wave 120-degree switching

In this type of control mode, each transistor conducts for 120° conduction mode. The gate triggering signals are control the phase and line voltages. At a time two load terminals are connected in dc supply and at that time third terminals remains open and the conduction period for each switch is 120°. For 120° mode of operation the instantaneous phase voltage are respectively V_{an}, V_{bn} and V_{cn} as in equation (3.19).

$$V_{aN} = \sum_{n=1,3,5,\cdots}^{\infty} \frac{2V_{dc}}{n\pi}\sin(n\pi/3)\sin n(\omega t + \pi/6)$$

$$V_{bN} = \sum_{n=1,3,5,\cdots}^{\infty} \frac{2V_{dc}}{n\pi}\sin(n\pi/3)\sin n(\omega t - \pi/2) \quad (3.19)$$

$$V_{cN} = \sum_{n=1,3,5,\cdots}^{\infty} \frac{2V_{dc}}{n\pi}\sin(n\pi/3)\sin n(\omega t - 7\pi/6)$$

On the other hand the line voltage a-to-b is $V_{ab} = \sqrt{3}V_{an}$ and the phase advance is 30°. For Y-connected load the line-to-line voltages as in equation (3.20)

$$V_{ab} = \sum_{n=1,3,5,\cdots}^{\infty} \frac{2\sqrt{3}V_{dc}}{n\pi} \sin\left(n\pi/3\right) \sin n\left(\omega t + \pi/3\right)$$

$$V_{bc} = \sum_{n=1,3,5,\cdots}^{\infty} \frac{2\sqrt{3}V_{dc}}{n\pi} \sin\left(n\pi/3\right) \sin n\left(\omega t - \pi/3\right) \quad (3.20)$$

$$V_{ca} = \sum_{n=1,3,5,\cdots}^{\infty} \frac{2\sqrt{3}V_{dc}}{n\pi} \sin\left(n\pi/3\right) \sin n\left(\omega t - \pi\right)$$

A three-phase six-step Quasi-sine waveforms of 120° switch conduction phase voltage is shown in Figure 3.8.

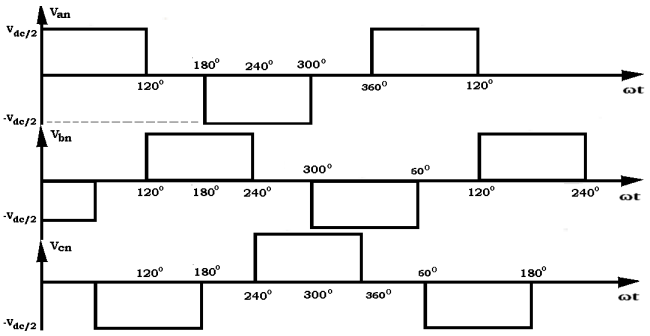

Figure 3.8 A three-phase six-step Quasi-sine waveforms of 120° switch conduction phase voltage applied.

The instantaneous phase voltage for 120° conduction mode V_{an}, V_{bn} and V_{cn} can be expressed in a Fourier series,

$$V_{an,bn,cn} = \frac{a_0}{2} + \sum_{n=1}^{\infty} \left(a_n \cos\left(n\omega t\right) + b_n \sin\left(n\omega t\right)\right)$$

The phase voltage waveform of a 3-phase bridge inverter is a quasi-square wave. The wave form has quarter-wave symmetry, due to the quarter-wave symmetry, we get

$a_0 = 0$ for all n, and $a_n = 0$, for all even n (3.21)

The phase voltage equation (3.21) becomes

$$V_{an} = \sum_{n=1}^{\infty} b_n \sin\left(n\omega t\right)$$

And the harmonics coefficient b_n can be expressed as

$$b_n = \frac{1}{\pi}\left[\int_0^{2\pi/3} \frac{V_{dc}}{2} \sin\left(n\omega t\right) d\left(\omega t\right) - \int_{\pi}^{5\pi/3} \frac{V_{dc}}{2} \sin\left(n\omega t\right) d\left(\omega t\right)\right] \text{ for all odd } 'n' \quad (3.22)$$

Or, $$b_n = \frac{V_{dc}}{2n\pi}\left[1 - \cos\left(\frac{2n\pi}{3}\right) - \cos\left(n\pi\right) + \cos\left(\frac{5n\pi}{3}\right)\right] \quad (3.23)$$

Now, the phase angle $\phi_n = \tan^{-1}\left(\frac{a_n}{b_n}\right) = 0$

From equation we can observed that the triple-n harmonics (3, 9, 12, 15 …) are zero. Here, $k = 1,5,7,11,13,\cdots, or. k = 6n \pm 1,\ for, n = 1,2,3,4,\cdots$

The general Fourier-series expansion is as

$$V_{n(phase)} = fun.V_{dc}\left[\frac{1}{1}\sin(1\omega t) - \frac{1}{5}\sin(5\omega t) + \frac{1}{7}\sin(7\omega t) - \frac{1}{11}\sin(11\omega t) + \frac{1}{13}\sin(13\omega t) - \cdots\right] \quad (3.24)$$

A three-phase six-step Quasi-sine waveforms of 120° switch conduction phase and line voltage as shown in Figure 3.9 and starting point 30° .

The phase voltage equation becomes

The instantaneous phase voltage (120° conduction mode) V_{an} , V_{bn} and V_{cn} are can be expressed in a Fourier series,

$$V_{an} = \frac{a_0}{2} + \sum_{n=1}^{\infty}\left(a_n \cos(n\omega t) + b_n \sin(n\omega t)\right)$$

The phase voltage waveform of a 3-phase bridge inverter is a quasi-square wave. The wave form has a quarter-wave symmetry, Due to the quarter-wave symmetry along the $\omega t - axis$, both a_0 and a_n are zero. Along y-axis at $\omega t - axis$, we can write the phase voltage waveform of a 3-phase bridge inverter is a quasi-square wave. The wave form has quarter-wave symmetry, due to the quarter-wave symmetry, we get

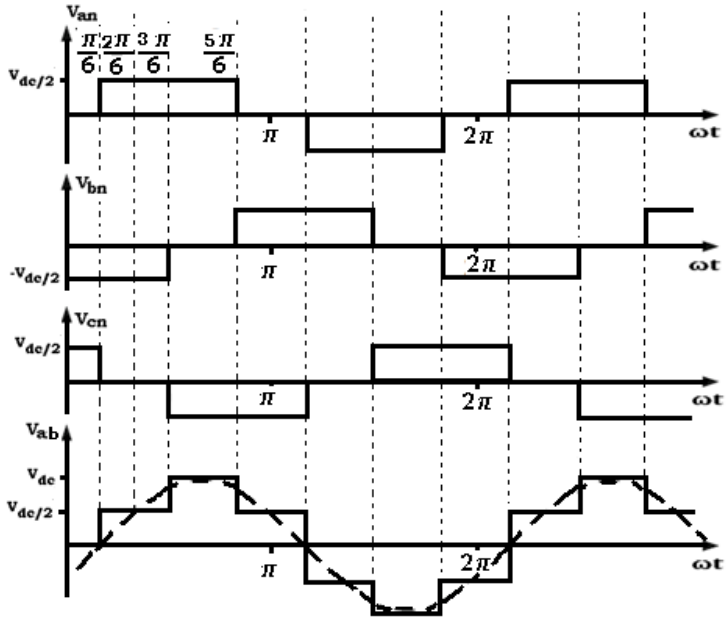

Figure 3.9 Three-phase six-step Quasi-sine waveforms of 120° switch conduction phase voltage.

$a_0 = 0$ for all n , and $a_n = 0$, for all even n

$$V_{an} = \sum_{n=1}^{\infty} b_n \sin(n\omega t)$$

And the harmonics coefficient b_n can be expressed as

$$b_n = \frac{4}{\pi}\int_0^{\pi/2} \frac{V_{dc}}{2}\sin(n\omega t)\, d(\omega t) \text{ for all odd } 'n'$$

$$= \frac{2V_{dc}}{n\pi}\left[\cos(n\omega t)\right]_{\pi/2}^{\pi/6}$$

Or, $b_n = \frac{2V_{dc}}{n\pi}\left[\cos\left(\frac{n\pi}{6}\right) - \cos\left(\frac{n\pi}{2}\right)\right]$

$$= \frac{2V_{dc}}{n\pi}\sin\left(\frac{n\pi}{2}\right)\sin\left(\frac{n\pi}{3}\right), here, \sin\left(\frac{n\pi}{2}\right) = \cos\left(\frac{n\pi}{6}\right) \quad (3.25)$$

Now, the phase angle $\phi_n = \tan^{-1}\left(\frac{a_n}{b_n}\right) = 0$

The overall phase voltage for 120-degree conduction and 30-degree phase shift is as (3.26)

$$V_{an} = \sum_{n=1}^{\infty}\frac{2V_{dc}}{n\pi}\sin\left(\frac{n\pi}{2}\right)\sin\left(\frac{n\pi}{3}\right)\sin(n\omega t) \quad (3.26)$$

From equation we can observed that the tripplen harmonics (3,9,12,15,…) are zero. Here, $k = 1,5,7,11,13,\cdots, or. k = 6n \pm 1,\ for, n = 1,2,3,4,\cdots$

The rms value of the fundamental can be obtained by substituting n=1,

$$V_{1(phase)} = \frac{2V_{dc}}{\sqrt{2}\pi}\sin\left(\frac{\pi}{2}\right)\sin\left(\frac{\pi}{3}\right) = 38.98484006V_{dc}\%$$

The Fourier-series is

$$V_{n(phase)} = 0.3898V_{dc}\left[\frac{1}{1}\sin(1\omega t) - \frac{1}{5}\sin(5\omega t) - \frac{1}{7}\sin(7\omega t) + \frac{1}{11}\sin(11\omega t) + \frac{1}{13}\sin(13\omega t) + \cdots\right]$$

From equation (3.25) the harmonic magnitude is as shown in Table 3.4 and the harmonic spectrum as shown in Figure 3.10.

Table 3.4 Generated harmonics for phase voltage with 120-degree conduction from (3.25) with

Harmonic Order	1	5	7	11	13	17	19	23	25
Harmonic Magnitude (%)	55.1329	-11.027	-7.876	5.0121	4.241	-3.2431	-2.9017	2.3971	2.2053
Harmonic Order	29	31	35	37	41	43	47	49	53
Harmonic Magnitude (%)	-1.9011	-1.7785	1.5752	1.4901	-1.3447	-1.2822	1.173	1.1252	-1.0402
Harmonic Order	55	59	61	65	67	71	73	77	79
Harmonic Magnitude (%)	-1.0024	0.9345	0.9038	-0.848	-0.8229	0.7765	0.7552	-0.716	-0.6979

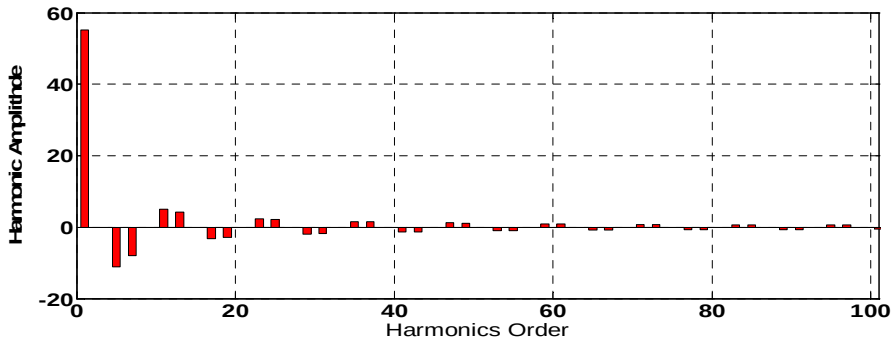

Figure 3.10 The harmonic spectrum for phase voltage with 120-degree conduction mode

From Figure 3.9 the line voltage waveform of a 3-phase bridge inverter is a quasi sine wave. The wave form has quarter-wave symmetry, due to the quarter-wave symmetry, we gat

$a_0 = 0$ for all n, and $a_n = 0$, for all even n

The line voltage equation (3.3) becomes

$$V_{ab} = \sum_{n=1}^{\infty} b_n \sin(n\omega t)$$

And the harmonics coefficient b_n can be expressed as

$$b_n = \frac{4}{\pi}\int_0^{\pi/2} e(\omega t)\sin(n\omega t)\,d(\omega t) \text{ for all odd } 'n'$$

$$\text{or, } b_n = \frac{4}{\pi}\left[\int_0^{\pi/3}\frac{V_{dc}}{3}\sin(n\omega t)\,d(\omega t) + \int_{\pi/3}^{\pi/2} V_{dc}\sin(n\omega t)\,d(\omega t)\right]$$

$$= \frac{4V_{dc}}{2n\pi}\left[\left[\cos(n\omega t)\right]_{\pi/3}^{0} + 2\left[\cos(n\omega t)\right]_{\pi/2}^{\pi/3}\right]$$

$$= \frac{4V_{dc}}{2n\pi}\left[1-\cos\left(\frac{n\pi}{3}\right)+2\cos\left(\frac{n\pi}{3}\right)-2\cos\left(\frac{n\pi}{2}\right)\right]$$

but, $\cos\left(\frac{n\pi}{2}\right) = 0$, for all odd n,

The n^{th} harmonic component can be mathematically expressed as

$$b_n = \frac{2V_{dc}}{n\pi}\left[1+\cos\left(\frac{n\pi}{3}\right)\right] \tag{3.27}$$

And the phase angle $\phi_n = \tan^{-1}\left(\frac{a_n}{b_n}\right) = 0$

The harmonic analysis of the line voltage waveform gives the n^{th} harmonic as, $n = 1,5,7,11,13,17,\cdots$

or, $n = 6k \pm 1$ for $k = 1,2,3,4,\cdots$

From (3.27) we get the final phase voltage i.e.

$$V_{ab} = \sum_{n=1}^{\infty}\frac{2V_{dc}}{n\pi}\left[1+\cos\left(\frac{n\pi}{3}\right)\right]\sin(n\omega t)$$

The rms value of the nth harmonic component is given by

$$V_{ab(rms)} = \sum_{n=1}^{\infty}\frac{\sqrt{2}V_{dc}}{n\pi}\left[1+\cos\left(\frac{n\pi}{3}\right)\right]$$

The Fourier-series is given by

$$V_{ab(line)} = fundamental.V_{dc}\left[\frac{1}{1}\sin(1\omega t)+\frac{1}{5}\sin(5\omega t)+\frac{1}{7}\sin(7\omega t)+\frac{1}{11}\sin(11\omega t)+\frac{1}{13}\sin(13\omega t)+\cdots\right]$$

From equation (3.27) the calculated harmonics is observed as Table 3.5 and from Table we can observe that the triple-n harmonics (3, 9, 12, 15,…) are zero at that time the harmonic spectrum for 120-degree line voltage is shown in Figure 3.11.

Table 3.5 Generated harmonics for 120-degree conduction from (3.27)

Harmonic Order	1	5	7	11	13	17	19	23	25
Harmonic Magnitude (%)	67.5237	13.5047	6.1385	5.1941	3.972	3.5539	2.9358	2.3971	2.7009
Harmonic Order	29	31	35	37	41	43	47	49	53
Harmonic Magnitude (%)	2.3284	2.1782	1.9292	1.825	1.6469	1.5703	1.378	1.274	1.2277
Harmonic Order	55	59	61	65	67	71	73	77	79
Harmonic Magnitude (%)	1.1445	1.1069	1.0388	1.0078	0.951	0.8769	0.8547	0.8135	0.7944

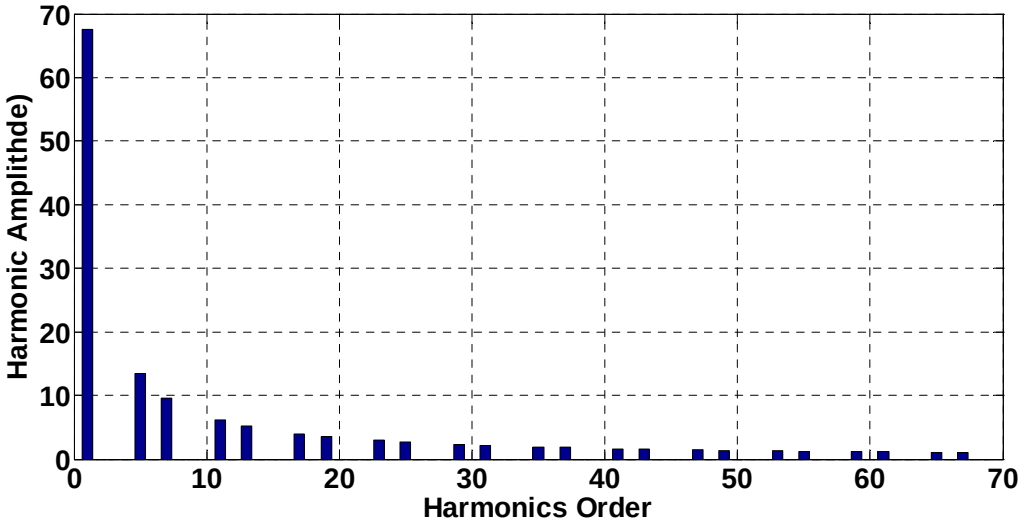

Figure 3.11 The harmonic spectrum for line voltage with 120-degree conduction

3.6.2.2 Proposed 120-degree SHE-PWM switching Scheme

A three-phase six-step Quasi-sine waveforms of 120° switch conduction phase voltage switching pattern with five switching angles and starting point 30° as shown in Figure 3.12.

The phase voltage waveform of a 3-phase bridge inverter is a quasi-square wave. The wave form has quarter-wave symmetry,

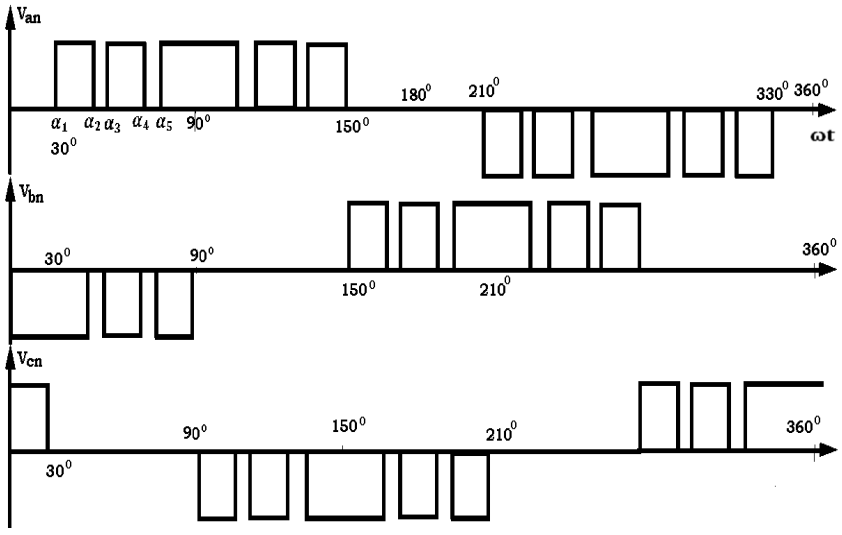

Figure 3.12 A three-phase six-step Quasi-sine waveforms of 120° switch conduction phase voltage switching pattern with five switching angles and starting point 30°.

$a_0 = 0$ for all n, and $a_n = 0$, for all even $'n'$

$$b_n = \frac{1}{\pi}\int_0^{2\pi} V_{an}\sin(n\omega t)\,d(\omega t)$$

$$b_n = \frac{4}{\pi}\int_0^{\pi/2} V_{an}\sin(n\omega t)\,d(\omega t)$$

$$= \frac{4}{\pi}\left[\int_{\alpha_1}^{\alpha_2} V_{an}\sin(n\omega t)\,d(\omega t) + \int_{\alpha_3}^{\alpha_4} V_{an}\sin(n\omega t)\,d(\omega t) + \int_{\alpha_5}^{\pi/2} V_{an}\sin(n\omega t)\,d(\omega t)\right]$$

$$= \frac{4}{\pi}\left[\int_{\alpha_1}^{\alpha_2} \frac{V_{dc}}{2}\sin(n\omega t)\,d(\omega t) + \int_{\alpha_3}^{\alpha_4} \frac{V_{dc}}{2}\sin(n\omega t)\,d(\omega t) + \int_{\alpha_5}^{\pi/2} \frac{V_{dc}}{2}\sin(n\omega t)\,d(\omega t)\right]$$

$$= \frac{4V_{dc}}{2n\pi}\left[(-1)\cos(n\omega t)\Big|_{\alpha_1}^{\alpha_2} + (-1)\cos(n\omega t)\Big|_{\alpha_3}^{\alpha_4} + (-1)\cos(n\omega t)\Big|_{\alpha_5}^{\pi/2}\right]$$

$$= \frac{2V_{dc}}{n\pi}\left[\cos n\alpha_1 - \cos n\alpha_2 + \cos n\alpha_3 - \cos n\alpha_4 + \cos n\alpha_5 - \cos n\pi/2\right]$$

$$= \frac{2V_{dc}}{n\pi}\left[\cos n\alpha_1 - \cos n\alpha_2 + \cos n\alpha_3 - \cos n\alpha_4 + \cos n\alpha_5\right]$$

$$\cos n\pi/2 = 0,\ for, n = 1,5,7,11,\cdots upto(6n \pm 1)$$

The expression for b_n can be written as,

$$b_n = -\left(\frac{2V_{dc}}{n\pi}\right)\sum_{k=1}^{m}(-1)^k\cos(n\alpha_k)$$

Or, the phase voltage is

$$V_{an} = -\left(\frac{2V_{dc}}{n\pi}\right)\left[\sum_{k=1}^{m}(-1)^k\cos(n\alpha_k)\right]\sin(n\omega t) \qquad (3.28)$$

Put $k = 1,5,7,11,13,\cdots$

$$b_1 = \frac{2V_{dc}}{\pi}\left[\cos n\alpha_1 - \cos n\alpha_2 + \cos n\alpha_3 - \cos n\alpha_4 + \cos n\alpha_5\right]$$

$$b_5 = \frac{2V_{dc}}{5\pi}\left[\cos n\alpha_1 - \cos n\alpha_2 + \cos n\alpha_3 - \cos n\alpha_4 + \cos n\alpha_5\right]$$

$$b_7 = \frac{2V_{dc}}{7\pi}\left[\cos n\alpha_1 - \cos n\alpha_2 + \cos n\alpha_3 - \cos n\alpha_4 + \cos n\alpha_5\right]$$

For 5-switching, the mathematical statement of these circumstances is then (3.29)

$$\begin{cases} \cos\alpha_1 - \cos\alpha_2 + \cos\alpha_3 - \cos\alpha_4 + \cos\alpha_5 = \mathrm{M} \\ \cos 5\alpha_1 - \cos 5\alpha_2 + \cos 5\alpha_3 - \cos 5\alpha_4 + \cos 5\alpha_5 = 0 \\ \cos 7\alpha_1 - \cos 7\alpha_2 + \cos 7\alpha_3 - \cos 7\alpha_4 + \cos 7\alpha_5 = 0 \\ \cos 11\alpha_1 - \cos 11\alpha_2 + \cos 11\alpha_3 - \cos 11\alpha_4 + \cos 11\alpha_5 = 0 \\ \cos 13\alpha_1 - \cos 13\alpha_2 + \cos 13\alpha_3 - \cos 13\alpha_4 + \cos 13\alpha_5 = 0 \end{cases} \quad (3.29)$$

The $5^{th}, 7^{th}, 11^{th}$ and 13^{th} order of harmonics would be eliminated if $b_5 = b_7 = b_{11} = b_{13} = 0$ and the higher order harmonic would be suppressed by proper choice of switching angle. In

3.6.2 .3 For 60° MODULATION

A three-phase six-step Quasi-sine waveforms of 120° switch conduction MODIFIED phase voltage is shown in Figure 3.13. The phase voltage waveform of a 3-phase bridge inverter is a quasi-square wave. The wave form has quarter-wave symmetry, and

$$a_0 = 0 \text{ for all } n, \text{ and } a_n = 0, \text{ for all even } 'n'$$

$$b_n = \frac{1}{\pi}\int_0^{2\pi} V_{an}\sin(n\omega t)\,d(\omega t)$$

$$b_n = \frac{4}{\pi}\int_0^{\pi/2} V_{an}\sin(n\omega t)\,d(\omega t)$$

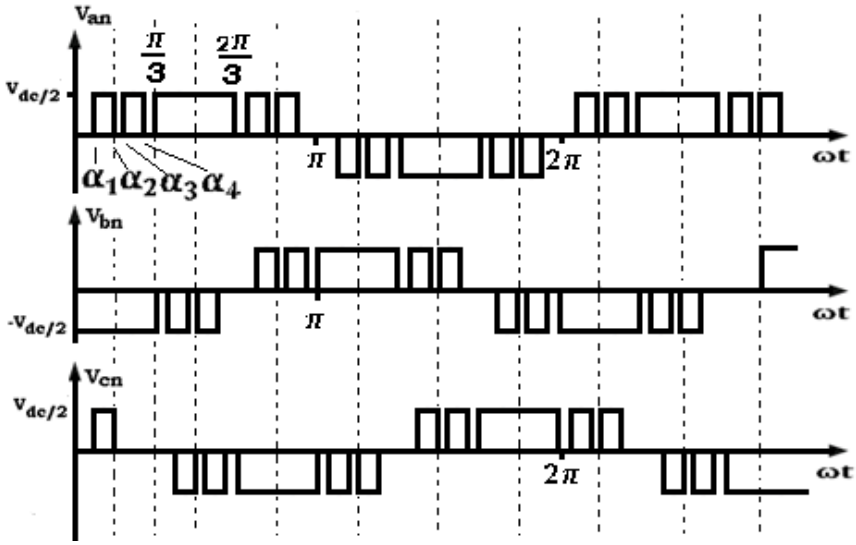

Figure 3.13 A three-phase six-step Quasi-sine waveforms of 120° switch conduction MODIFIED phase voltage switching pattern.

$$= \frac{4}{\pi}\left[\int_{\alpha_1}^{\alpha_2} V_{an}\sin(n\omega t)\,d(\omega t) + \int_{\alpha_3}^{\alpha_4} V_{an}\sin(n\omega t)\,d(\omega t) + \int_{\alpha_5}^{\alpha_6} V_{an}\sin(n\omega t)\,d(\omega t) + \int_{\pi/3}^{\pi/2} V_{an}\sin(n\omega t)\,d(\omega t)\right]$$

$$= \frac{4}{\pi}\left[\int_{\alpha_1}^{\alpha_2} \frac{V_{dc}}{2}\sin(n\omega t)\,d(\omega t) + \int_{\alpha_3}^{\alpha_4} \frac{V_{dc}}{2}\sin(n\omega t)\,d(\omega t) + \int_{\alpha_5}^{\alpha_6} \frac{V_{dc}}{2}\sin(n\omega t)\,d(\omega t) + \int_{\pi/3}^{\pi/2} \frac{V_{dc}}{2}\sin(n\omega t)\,d(\omega t)\right]$$

$$= \frac{4V_{dc}}{2n\pi}\left[(-1)\cos(n\omega t)\Big|_{\alpha_1}^{\alpha_2} + (-1)\cos(n\omega t)\Big|_{\alpha_3}^{\alpha_4} + (-1)\cos(n\omega t)\Big|_{\alpha_5}^{\alpha_6} + (-1)\cos(n\omega t)\Big|_{\pi/2}^{\pi/2}\right]$$

$$= \frac{2V_{dc}}{n\pi}\left[\cos n\alpha_1 - \cos n\alpha_2 + \cos n\alpha_3 - \cos n\alpha_4 + \cos n\alpha_5 - \cos n\alpha_6 + \cos n\,\pi/3 - \cos n\,\pi/2\right]$$

$$\cos n\,\pi/2 = 0,\ for, n = 1,5,7,11,\cdots upto\left(6n \pm 1\right)$$

$$= \frac{2V_{dc}}{n\pi}\left[\frac{1}{2} + \cos n\alpha_1 - \cos n\alpha_2 + \cos n\alpha_3 - \cos n\alpha_4 + \cos n\alpha_5 - \cos n\alpha_6\right]$$

The expression for b_n can be written as (3.30),

$$b_n = \left(\frac{2V_{dc}}{n\pi}\right)\left[\sum_{k=1}^{m}\frac{1}{2} - (-1)^k \cos\left(n\alpha_k\right)\right] \tag{3.30}$$

Put $k = 1,5,7,11,13,\cdots$

$$b_1 = \frac{2V_{dc}}{\pi}\left[\frac{1}{2} + \cos n\alpha_1 - \cos n\alpha_2 + \cos n\alpha_3 - \cos n\alpha_4 + \cos n\alpha_5 - \cos n\alpha_6\right]$$

$$b_5 = \frac{2V_{dc}}{5\pi}\left[\frac{1}{2} + \cos n\alpha_1 - \cos n\alpha_2 + \cos n\alpha_3 - \cos n\alpha_4 + \cos n\alpha_5 - \cos n\alpha_6\right]$$

$$b_7 = \frac{2V_{dc}}{7\pi}\left[\frac{1}{2} + \cos n\alpha_1 - \cos n\alpha_2 + \cos n\alpha_3 - \cos n\alpha_4 + \cos n\alpha_5 - \cos n\alpha_6\right]$$

For 5-switching, the mathematical statement of these circumstances is then (3.31)

$$\begin{cases} \frac{1}{2} + \cos\alpha_1 - \cos\alpha_2 + \cos\alpha_3 - \cos\alpha_4 + \cos\alpha_5 - \cos n\alpha_6 = \mathrm{M} \\ \frac{1}{2} + \cos 5\alpha_1 - \cos 5\alpha_2 + \cos 5\alpha_3 - \cos 5\alpha_4 + \cos 5\alpha_5 - \cos n\alpha_6 = 0 \\ \frac{1}{2} + \cos 7\alpha_1 - \cos 7\alpha_2 + \cos 7\alpha_3 - \cos 7\alpha_4 + \cos 7\alpha_5 - \cos n\alpha_6 = 0 \\ \frac{1}{2} + \cos 11\alpha_1 - \cos 11\alpha_2 + \cos 11\alpha_3 - \cos 11\alpha_4 + \cos 11\alpha_5 - \cos n\alpha_6 = 0 \\ \frac{1}{2} + \cos 13\alpha_1 - \cos 13\alpha_2 + \cos 13\alpha_3 - \cos 13\alpha_4 + \cos 13\alpha_5 - \cos n\alpha_6 = 0 \end{cases} \tag{3.31}$$

The $5^{th}, 7^{th}, 11^{th}$ and 13^{th} order of harmonics would be eliminated if $b_5 = b_7 = b_{11} = b_{13} = 0$ and the higher order harmonic would be suppressed by proper choice of switching angles.

For three switching the voltage waveforms is shown in Figure 3.14

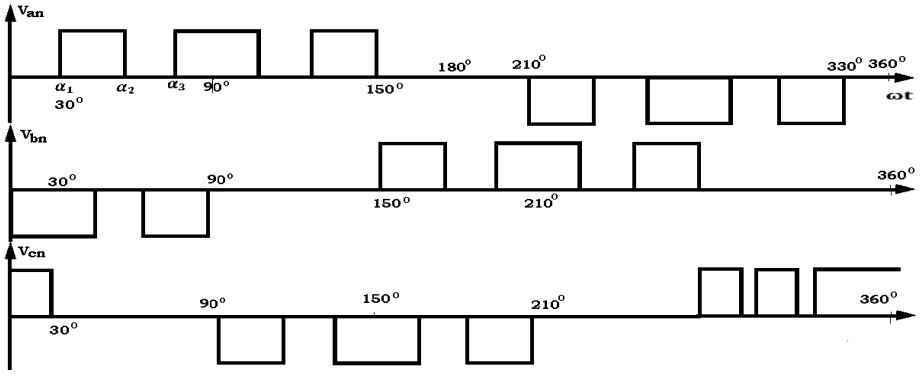

Figure 3.14 Three-phase six-step Quasi-sine waveforms of 120° switch conduction phase voltage switching pattern with three switching angles and starting point 30°.

For 3-switching the nonlinear equation is (3.32)

$$\begin{cases} \cos\alpha_1 - \cos\alpha_2 + \cos\alpha_3 = \mathrm{M} \\ \cos 5\alpha_1 - \cos 5\alpha_2 + \cos 5\alpha_3 = 0 \\ \cos 7\alpha_1 - \cos 7\alpha_2 + \cos 7\alpha_{35} = 0 \end{cases} \quad (3.32)$$

The $n^{th} and 7^{th}$ harmonics would be eliminated if $b_5 = b_7 = 0$ .These equations can be solved iteratively and calculate the switching angles $\alpha_1, \alpha_2 and \alpha_3$.

3.7 Proposed Scheme for Rotor Harmonics Elimination Technique

The proposed technique the normal six-step quasi sine wave is modified with extra switchings per quarter cycle. The number of switching can be more to eliminate wider range of harmonics. This can increase switching losses and can lead to derated operation of the inverter. Thus, the main aim is to reduce as many nos. of harmonics as possible with lesser number of switching for efficient inverter operation. In this chapter, a heuristic search based method of BBO is used to minimize the maximum number of harmonics with lower no. of switching. This can also reduce the overall THD in the stator side voltage of DFIG at any operating speed. In the proposed technique, the selected lower order harmonics are eliminated and the rest higher orders are minimized through BBO technique by optimizing the chosen objective function $F(\alpha)$ defined by (34). The switching angles are computed off-line and stored in processor memory for on line application.

3. 7.1 Proposed Harmonic Elimination Principle using BBO Algorithm

In the proposed method, the harmonic elimination problem is converted to optimization problem and the switching angles are found out offline to contribute minimum voltage THD. BBO technique is chosen as it is simple and has not yet been explored extensively to solve the problem of converter switching. Moreover, unlike the other meta-heuristic techniques, BBO does not require unreasonable amount of computational effort [85] and relatively faster convergence rate.

The objective function $F(\alpha)$ is formulated to satisfy the desired constraints as,

$$F(\alpha) = (b_1 - M)^2 + K_5(b_5 - \varepsilon_5)^2 \cdots + K_n(b_n - \varepsilon_n)^2 \quad (3.33)$$

Where b_1 is the fundamental amplitude, $K_5, \cdots, K_n$ are the penalties for individual harmonics which are set to high values so that the magnitudes of $b_5, b_7, b_{11}, \cdots, b_n$ are forced to follow the desired values. The constants $\varepsilon_5, \varepsilon_7, ..., \varepsilon_n$ are the permissible limits of individual harmonics which are chosen very close to zero for the selected lower order harmonics and to the desired value for other higher order of harmonics.

Mathematically, the problem can be formulated as,

Minimize $F(\alpha) = F(\alpha_1, \alpha_2, \alpha_3, \cdots, \alpha_m)$ (3.34)

Subject to: $0 < \alpha_1 < \alpha_2 < \alpha_3 < \cdots < \alpha_m < (\pi/2)$; (3.35)

To minimize $F(\alpha)$ BBO algorithm is used for the present technique. In this method, each search point of the population is composed of the switching angles per quarter cycle α_1 through α_m.To start the search procedure, the switching angles are randomly generated satisfying the conditions of (3.35) for the chosen number of population. Using these random values,

individual harmonics representing the fitness of the particular search point are computed. The best combination of angles among the population of the given search points up to present iteration are called the elite or best solution for the variables α_1 through α_m. New search points are generated from the current search points at each iteration and the information regarding the best solutions is found out by using the BBO.

The brief statement of algorithm in steps is,

i. Start the search procedure for the set of values switching angles α.

$$\alpha^0 = [\alpha_1^0, \alpha_2^0, \alpha_3^0, \alpha_4^0, \cdots; \alpha_m^0]^T \tag{3.36}$$

ii. Initialize the suitable BBO parameters, i.e., P_{mod} Habitat modification probability, K_{eep} Elitism parameter, I Maximum immigration rate, E Maximum emigration rate, dt Step size, m_{max} Maximum mutation rate, P_{mutate} Mutation probability, λ_{lower} Lower bound for immigration probability per generation, λ_{upper} Upper bound for immigration probability per generation, μ_{lower} Lower bound for emigration probability per generation, μ_{upper} Upper bound for emigration probability per generation, S_{max} Maximum species count,

iii. Set SIVs: Assume the switching angles α_m where $m = 1, 2, 3, \cdots, k$ and b_n, $n = 1, 5, 7, \cdots, N$

iv. Set: P_{size} Total population size, G_{max} Maximum number of generation, Num_{var} Number of variable, P_{count} Species count probability of each habitat.

v. Update α_m and V_{an} using equations (3.6) & (3.10).

vi. Is the condition of $0 < \alpha_1 < \ldots < \alpha_m < \pi/2$ satisfied? If yes then set the best value of $F(\alpha)$ satisfying $b_1 = M, b_5 \le \varepsilon_1, b_7 \le \varepsilon_2$ and $b_n \le \varepsilon_n$ otherwise go to next step.

vii. Determine fitness values of the objective using emigration and immigration rate and compute HSI i.e. α_m and b_n by using (3.37) [85]. The probability P_s that the habitat contains exactly S species at time $t + \Delta t$ can be expressed as,

$$P_s(t+\Delta t) = P_s(t)(1 - \lambda_s \Delta t - \mu_s \Delta t) + P_{s-1}\lambda_{s-1}\Delta t + P_{s+1}\mu_{s+1}\Delta t \tag{3.37}$$

Where λ_s and μ_s are the immigration and emigration rates.

viii. For each habitat, update the probability of its species count using (3.38) and compute each habitat suitability index (HSI). This is to indicate the best region for the biological species to survive. HSI is satisfies the suitability index variable (SIV) constraints [85].

$$\dot{P}_s = \begin{cases} -(\lambda_s + \mu_s)P_s + \mu_{s+1}P_{s+1} & S = 0 \\ -(\lambda_s + \mu_s)P_s + \lambda_{s-1}P_{s-1} + \mu_{s+1}P_{s+1} & 1 \le S \le S_{max} - 1 \\ -(\lambda_s + \mu_s)P_s + \lambda_{s-1}P_{s-1} & S = S_{max} \end{cases} \tag{3.38}$$

ix. The mutation rate m is inversely proportional to the solution probability and is given by,

$$m(S) = m_{\max}\left(\frac{1-\mathrm{P}_s}{\mathrm{P}_{\max}}\right) \tag{3.39}$$

Where $m_{\max}$ is the maximum mutation rate which is a user-defined parameter. This equation makes high habitat suitability index (HSI) solutions.HSI indicates the quality of the solution set. For the problem being considered, HSI is represented by the $F(\alpha)$ value generated by the solution set.

x. Apply migration and evaluate fitness.

xi. If desired fitness achieved then set the best value otherwise go to next step.

xii. Update the probability of each species count. Apply mutation and evaluate fitness.

a. Control the value of

$$F(\alpha^0) = F^0 \tag{3.40}$$

b. Linearize $F(\alpha) = 0$ about α^0.

$$F^0 + \left[\frac{\partial F}{\partial \alpha}\right]^0 d\alpha = 0 \tag{3.41}$$

Where

$$\left[\frac{\partial F}{\partial \alpha}\right]^0 = \begin{bmatrix} \frac{\partial F_1}{\partial \alpha_1} & \frac{\partial F_1}{\partial \alpha_2} & \cdots & \frac{\partial F_1}{\partial \alpha_m} \\ \frac{\partial F_2}{\partial \alpha_1} & \frac{\partial F_2}{\partial \alpha_2} & \cdots & \frac{\partial F_2}{\partial \alpha_m} \\ \vdots & \vdots & \vdots & \vdots \\ \frac{\partial F_m}{\partial \alpha_1} & \frac{\partial F_m}{\partial \alpha_2} & \cdots & \frac{\partial F_m}{\partial \alpha_m} \end{bmatrix} \tag{3.42}$$

Evaluate at α^0 and

$$d\alpha = [d\alpha_1, d\alpha_2, d\alpha_3, d\alpha_4, \cdots, d\alpha_m]^T$$

c. Solve eq-(3.41) for $d\alpha$.

d. Reiteration (updated) (a to d)

$$\alpha^{j+1} = \alpha^j + d\alpha^j \text{ or, } \alpha^1 = \alpha^0 + d\alpha^0 \tag{3.43}$$

e. The above process is repeated until the objective function $F(\alpha)$ reduces below the specified minimum value. When the function has converged, a solution will be achieved. In case of divergence from the initial guess, a new initial guess is to be made.

f. Determine the best HSI i.e. switching angles, magnitude of harmonics and THD. If the solution converged then set the best value otherwise go to step iii.

The process terminates if the changes in the fitness values between consecutive iterations are less than a given tolerance, or the fitness values do not change for a number of iterations, or the permissible number of iteration runs are completed. The

switching angles corresponding to minimum voltage THD for varying modulation index m_d are stored in the form of mixed model equations [46, 93] in the processor memory for online application. The elite values are updated after every iteration.

To justify the application of BBO algorithm for the given problem, the optimization was tried with the help of other search based algorithms e.g. GA, PSO, Gravitational Search algorithm (GSA), Cuckoo Search algorithm (CSA) and BBO to check the convergence of the objective function. A typical case of M=0.8 with elimination of 5th, 7th, 11th and 13thorder of harmonics is chosen for comparison. The comparative convergence plot is shown in Figure 3.15. Form Figure 3.15, it can be observed that convergence through BBO is much faster than other techniques. The BBO parameters considered during programming are, total population size=50, generation count limit=50, number of genes in each population member=5, mutation probability=0, habitat modification probability=1, initial mutation probability=0.005, elitism parameter=2, lower bound for immigration probability per gene=0.0, upper bound for immigration probability per gene=1, step size used for numerical integration of probabilities=1, max immigration rate for each island=1, max emigration rate, for each island=1.

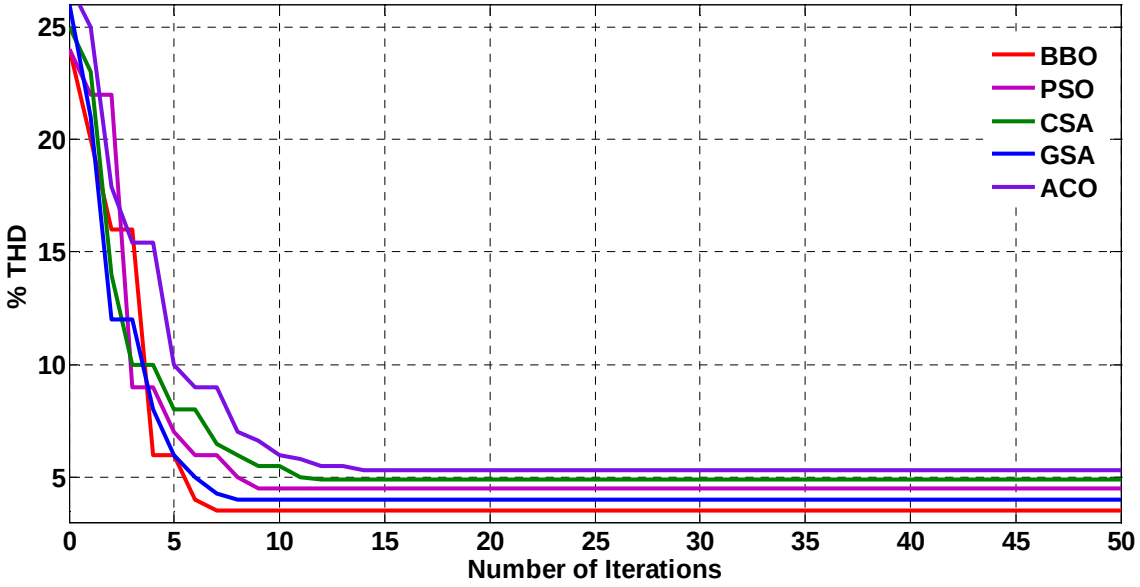

Figure 3.15.Variation of the objective function with GA, PSO, GSA, CSA and BBO method for M=0.8 with eliminating 5th, 7th, 11th and 13th, order harmonics.

3.8 Simulation and Experimental Results

The proposed scheme has been simulated in MATLAB 7.8/Simulink environment for both 120° and 180° switching mode of inverter. Both these modes are separately simulated and the results are shown separately.

3. 8.1 180° ***switching mode of operation*** The simulation results considering five switching per quarter cycle for the BBO-based SHEPWM inverter are shown in Figure 3.16(a). The objective function $F(\alpha)$of Eq. (3.14) is optimized to obtain switching angles. The $5^{th}, 7^{th}, 11^{th}$ and 13^{th} order of harmonics are set to zero. The fundamental voltage amplitude has been set as per the desired m_d . Figure 3.16(b) shows the plot of minimum weighted THD for output voltage taken up to 41st order of harmonics with varying m_d for 3, 4, 5, 6 and 7-switching angles per quarter cycle.

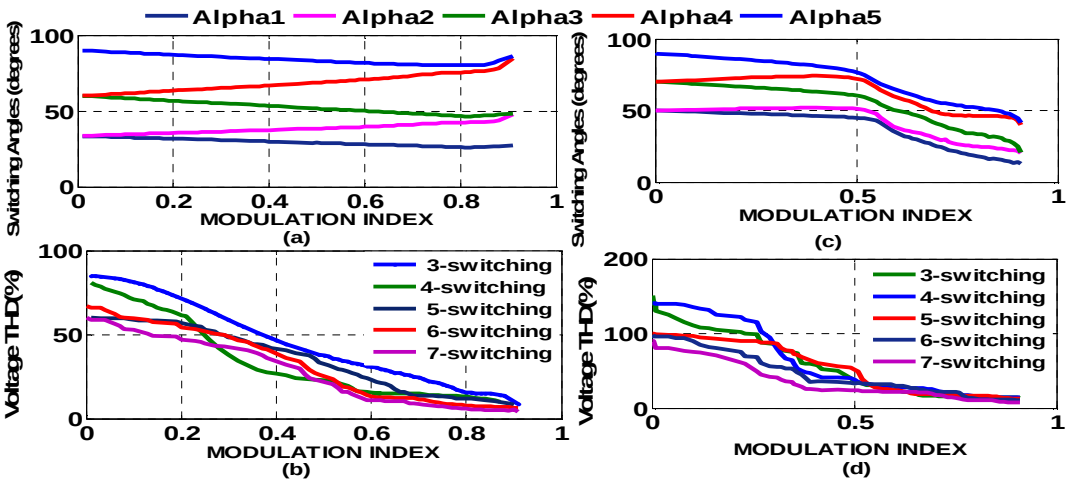

Figure 3.16 (a) Variations of switching angles against modulation index for180-degree conduction and 5-Switching (b) Minimum Voltage THD (%) Vs. Modulation Index with 180-degree conduction and different no. of switchings (c) Variations of switching angles against modulation index for120-degree conduction and 5-Switching (d) Minimum Voltage THD (%) Vs. Modulation Index for 120-degree conduction and different no. of switchings.

3. 8.2 120^0 switching mode of operation

The simulation results in this mode for the BBO-based SHE-PWM inverter considering 5-switching are shown in Figure 3.16(c). The plot of minimum weighted THD for output voltage taking up to 41st order of harmonics with varying m_d, for different switchings per quarter cycle is shown in Figure 3.16(d). In this method, the eliminated lower order harmonics for 3-switching are 5^{th} and 7^{th}, for 5-switching are $5^{th}, 7^{th}, 11^{th}$ and 13^{th} and for 7-switching are $5^{th}, 7^{th}, 11^{th}, 13^{th}, 17^{th}$ and 19^{th}.

3.9 System implementation

Table 3.6 Parameters of the experimental system

Micro grid Specification		Solar panel Specification		Proposed DFIG Specification			
				Stator Parameters		Rotor Parameters	
V_{grid}	415	Rated power	1.5 kW	V_s	415	V_r	110 V
f	50 Hz	Voltage	110	Δ-Connected		Y-Connected	
				f_s	50 Hz	R_r	1.5 Ω
Rated Capacity	7.5 kVA	Battery	500	P	3 KW	L_{lr}	12
				I_s	4:00 A	I_r	14 A
$5^{th}, 7^{th}$, … harmonic voltage	As per grid codes	Capacitance Specification	1000 µF, 400V	R_s	1.2 Ω	N_r	1450 rpm
				L_{ls}	12		
				L_m	320		

The experimental set up used for verification of the proposed scheme is shown in Figure 3.1. The stator of the DFIG is directly connected to grid. The rotor side of the DFIG is fed from an inverter supplied from a solar array or the grid side converter. An

optional battery is also connected in parallel with the solar array to store excess energy. The scheme is tested after connecting the stator to a micro-grid although the same is applicable for any type DFIG control modes e.g. grid connected or grid isolated mode. The specifications of the test micro-grid system, solar panel battery and the DFIG are shown in Table 3.6.

3.10 Experimental Results

The proposed method of harmonic elimination is initially verified through simulation for the scheme described in Figure 3.1. An IGBT based inverter operating in bi-directional mode is used for this purpose. The reference voltages V_a^*, V_b^* and V_c^* are generated from the P and Q controllers after comparing with the set value of P^* and Q^*. The modulation index m_d is calculated on-line based on these reference values of V_a^*, V_b^* and V_c^* as shown in Figure 3.1.

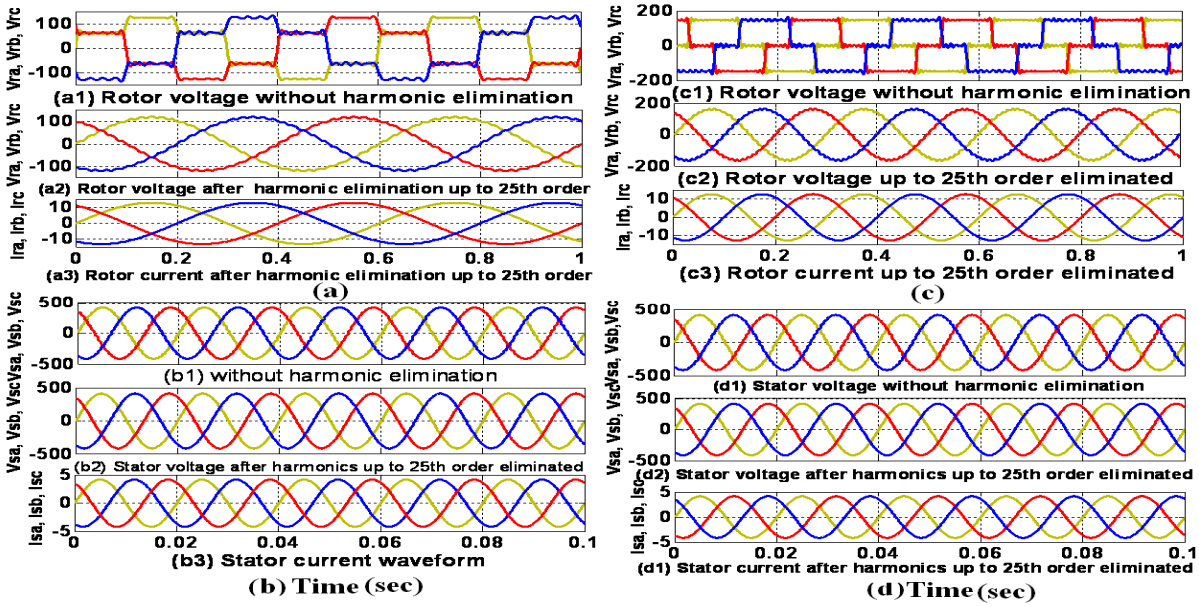

Figure 3. 17 DFIG phase a, b, c (a) rotor voltage and currents with quasi-sine rotor injection at 180-degree conduction mode at 1450 rpm **(b)** stator voltage and currents with quasi-sine rotor injection at 180-degree conduction mode at 1450 rpm **(c)** rotor voltage and currents with quasi-sine rotor injection at 120-degree conduction mode **(d)** stator voltage and current with quasi-sine rotor injection 120-degree conduction mode.

Then the SHE-PWM pulses are generated based on stored data in the processor memory to produce optimum voltage THD. The DFIG is run at a speed of 1450 rpm at rated load. The rotor side converter provides quasi-sine wave voltage waveform in 180^0 mode. The rotor and stator voltage waveforms for this operation are shown in Figures 3.17(a1) and 3,17 (b1) respectively. The modified rotor and stator voltages after the elimination of lower order harmonics up to 25^{th}in the rotor input are shown in Figures 3.17(a2) and 3.17(b2) respectively. The corresponding rotor and stator current waveforms are shown in Figures 3.17(a3) and 3.17.(b3). Then the proposed control strategy is also applied for 120^0 switching mode at the 1450 rpm speed of the generator. The obtained voltage and current waveforms are shown in Figures 3.17(c) and 3.17(d). The proposed scheme is experimentally verified for 180^0 mode for a speed variation between1450 rpm to 1550 rpm through synchronous speed of 1500 rpm at 75% full load after eliminating harmonics up to 25^{th} order from the rotor voltage. The corresponding experimental plots are shown in Figure 3.18(a) for speed and rotor current and Figure 3.18(b) for stator voltage. Then the same is verified for 120^0 mode for same speed variation at 75% full load after eliminating harmonics up to 25^{th} order from the rotor voltage. The corresponding experimental plots are shown in Figure 3.18(c) for speed and rotor current and Figure 3.18(d) for stator voltage. Then in Figure 3.19(a) the comparison of the speed and torque for the DFIG is shown both for the compensated and uncompensated system. The active and reactive power is also shown in Figure 3.19(b) at 1550 rpm near half load. Then the proposed method was compared with the existing conventional method of quasi sine wave for the rotor voltage at m_d=0.8. In

Figure 3.20(a) voltage harmonics for 180-deg conduction without harmonic eliminations are shown whereas in Figure 3.20(c) the same is shown after harmonic elimination. Similarly, Figures 3.20(b) and 3.20(d) represent voltage harmonic pattern before and after harmonic elimination for 120-deg mode. Then the proposed switching was compared with the conventional switching demonstrated in [84] for the injected rotor voltage THD and the result is shown in Figure 3.20(e) which also confirms the superiority of the proposed scheme.

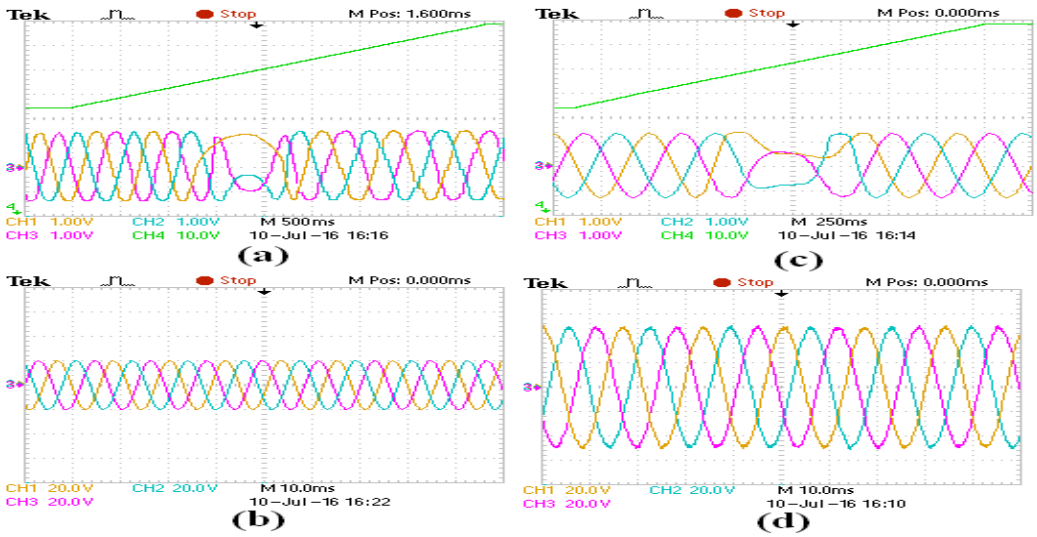

Figure 3.18. Experimental waveform for (a) rotor current with changing speed (Channel 1, 2 and 3: Y-axis: 10A/div., Channel 4: Y axis 30 rpm/div.) for 180-degree conduction mode (b) stator voltage (Channel 1, 2 and 3: Y-axis: 600V/div.) for 180-degree conduction mode (c) rotor current with changing speed (Channel 1, 2 and 3: Y-axis: 10A/div., Channel 4: Y axis 30 rpm/div.) for 120-degree conduction mode (d) stator voltage (Channel 1, 2 and 3: Y-axis: 250V/div.) for 120- degree conduction mode.

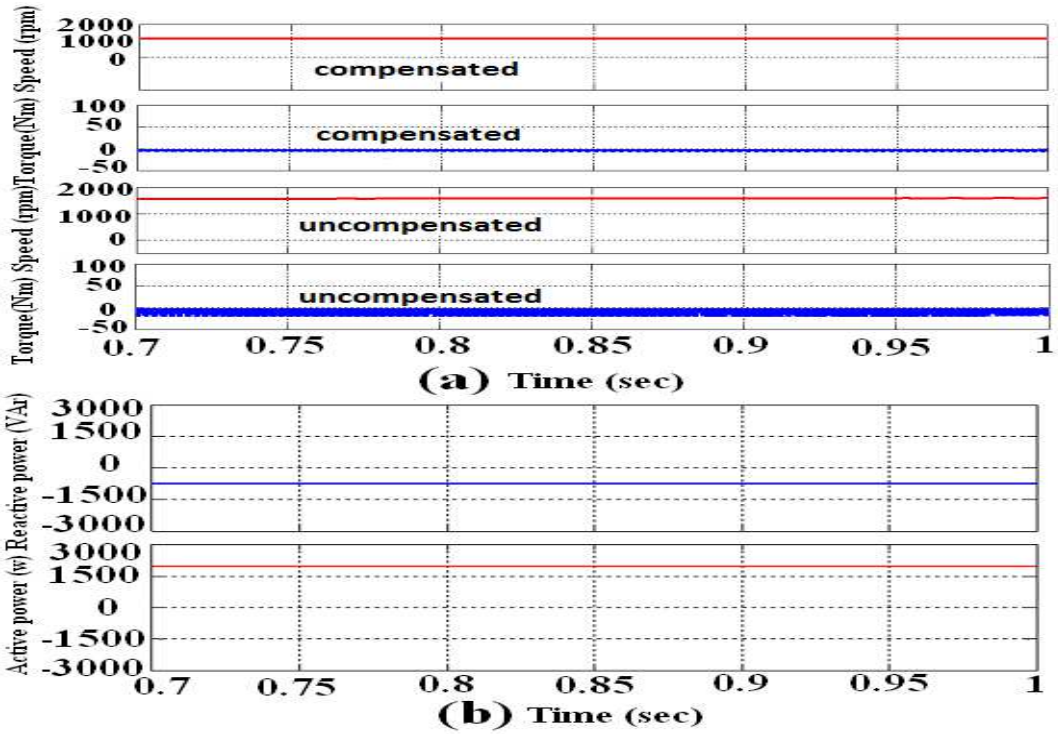

Figure 3.19. Variation of torque and power at half load, 1550 rpm (a) speed and torque of DFIG for compensated and uncompebnsated system (b)Reactive and active power for proposed technique.

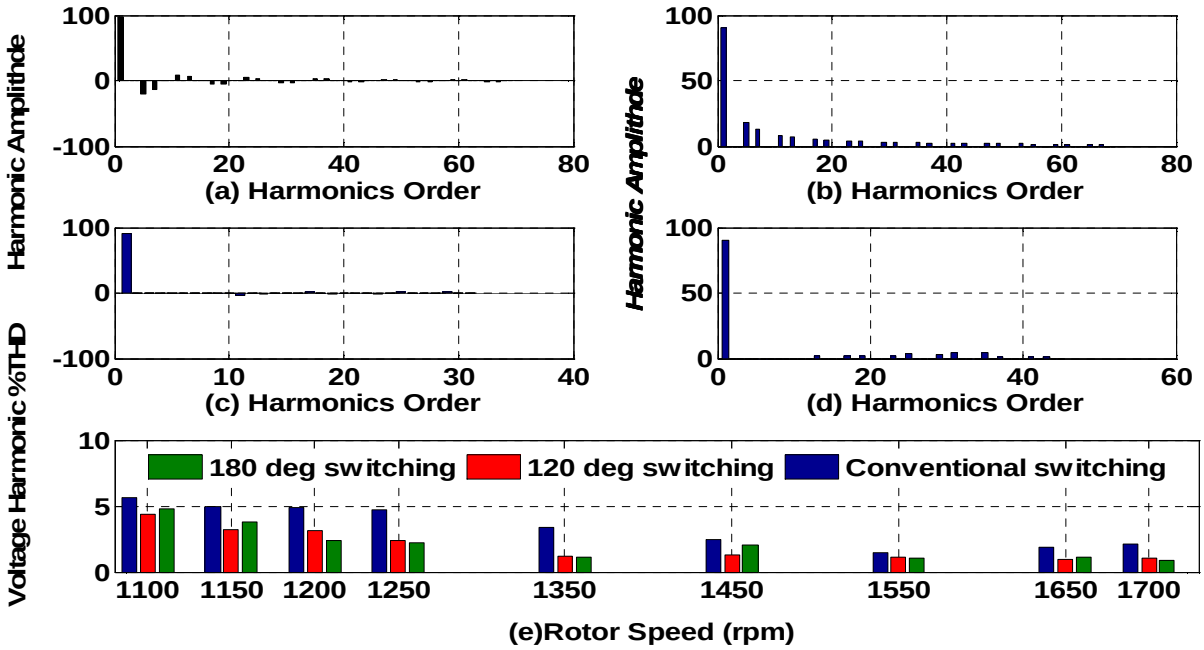

Figure 3.20 DFIG rotor voltage harmonics spectra (a)180-degree conduction mode without harmonic elimination (b) 120-degree conduction mode without harmonic elimination (c) 180-degree conduction mode with 5^{th} , 7^{th} , 11^{th} and 13^{th} harmonic elimination (d) 120-degree conduction mode with 5^{th} , 7^{th} , 11^{th} and 13^{th} harmonic elimination (e) %THD comparison with conventional and proposed system.

3.11 Sub-harmonic elimination

For the machine with *P* poles and rotor speed N_r rpm, the frequency of the rotor voltage to be injected can be given by $f_r = f_s - f_m$, where mechanical frequency $f_m = PN_r/120\,Hz$ and the slip is given by $s=(N_s-N_r)/N_s$. Thus the induced generated stator frequency due to rotor injected frequency is given by $\left|(6n\pm1)\,f_r \pm f_m\right|$. Therefore the generated stator sub harmonic order is $\left|(6n\pm1)\,f_r \pm f_m\right|/50$. For a rotor speed of 1434 rpm in a four-pole DFIG, the corresponding rotor mechanical frequency is 47.8 Hz and the rotor injection frequency is 2.2 Hz for 50 Hz stator frequency. Therefore, the 5^{th}harmonic rotor injected frequency at the rotor side is -11 Hz. The reflected stator frequency due to 5^{th} harmonic injected rotor voltage is 36.8 Hz. Hence the generated stator sub-harmonic order is 0.736. For same speed, the 7^{th} harmonic rotor injected frequency is 15.4 Hz. The stator frequency due to 7^{th} harmonic injected rotor voltage is 63.2 Hz. Hence the generated stator sub-harmonic order is 1.264. At the same time, the stator sub-harmonic orders generated by the rotor injected frequency of 11^{th} and 13^{th} harmonics are 0.472 and 1.528 respectively. For 120-deg conduction with $M = 0.9$ and switching angles of $\alpha_1 = 13.7765^\circ, \alpha_2 = 21.7013^\circ, \alpha_3 = 28.2888^\circ, \alpha_4 = 43.0082^\circ$ and $\alpha_5 = 44.8806^\circ$, the sub-harmonics 0.736, 1.264, 0.472 and 1.528 are eliminated. The orders of speed dependent sub-harmonics generated in stator are computed and listed in Tables 3.7 and 3.8. The sub-harmonic orders of the stator voltages for different rotor speed at 180-degree conduction mode are evaluated and given in Table 3.8.

Table 3.7 Sub-harmonic elimination for a constant speed with different M for 120-degree mode

Rotor Speed (rpm)	Rotor Harmonic Order	Stator Harmonic Order	M	Switching Angles (Degrees)	M	Switching Angles (Degrees)	M	Switching Angles (Degrees)
	1	1	0.7	25.2877	0.8	18.349	0.9	13.7765
	5	0.736	0	30.5946	0	24.9836	0	21.7013
1434	7	1.264	0	40.8175	0	33.8218	0	28.2888
	11	0.472	0	48.7581	0	46.4864	0	43.0082
	13	1.528	0	56.0092	0	52.0462	0	44.8806
	1	1	0.72	9.5935	0.86	15.6429	0.91	12.9566
	5	0.88	0	20.7615	0	23.367	0	20.3837
1470	7	1.12	0	34.7128	0	30.8979	0	26.7645
	11	0.76	0	66.1092	0	45.9741	0	39.7003
	13	1.24	0	75.4025	0	49.3134	0	41.4639
	1	1	0.69	7.0505	0.79	16.0547	0.89	10.2894
	5	1.08	0	13.7869	0	19.8486	0	16.2491
	7	0.92	0	18.6633	0	27.7591	0	23.1625
1520	11	1.16	0	63.9661	0	34.9498	0	32.3052
	13	0.84	0	71.5247	0	40.4393	0	35.7122
	17	1.24	0	78.5801	0	50.3456	0	69.701
	19	0.76	0	87.6307	0	54.4512	0	70.9183
	1	1	0.75	14.6222	0.85	13.2037	0.9	11.2431
	5	1.24	0	24.7237	0	17.6294	0	16.0995
	7	0.76	0	32.3633	0	24.9662	0	22.7053
1560	11	1.48	0	52.3221	0	33.5254	0	31.7772
	13	0.52	0	56.4046	0	37.8208	0	34.9508
	17	1.72	0	75.3325	0	50.1776	0	47.8883
	19	0.28	0	80.9581	0	52.6247	0	48.814

Table 3.8 Sub-harmonic elimination for a constant speed with different M for 180-degree mode

Rotor Speed (rpm)	Rotor Harmonic Order	Stator Harmonic Order	M	Switching Angles (Degrees)	M	Switching Angles (Degrees)	M	Switching Angles (Degrees)
	1	1	0.71	16.7618	0.75	17.5192	0.81	16.1865
	5	0.8	0	50.5877	0	49.3321	0	52.2769
1450	7	1.2	0	56.6270	0	54.9915	0	59.3863
	11	0.6	0	77.7156	0	79.9317	0	76.1276
	13	1.4	0	88.5657	0	88.5909	0	87.8062
	1	1	0.65	18.8951	0.75	7.6329	0.85	8.9988
	5	1.2	0	45.3321	0	13.7796	0	14.2152
	7	0.8	0	52.2947	0	18.9506	0	19.5773
1550	11	1.4	0	60.5199	0	65.0922	0	67.3986
	13	0.6	0	63.6014	0	70.7815	0	69.8578
	17	1.6	0	79.3839	0	79.8942	0	82.3730
	19	0.4	0	89.2259	0	88.5177	0	88.2181

3.12 Proposed on-line Control Scheme

As observed from Table 3.1, the rotor injected harmonics on stator side will depend mainly on the rotor speed. The rotor harmonics are injected due to RSC switching which can be either six-step or PWM. For six step switching, all the odd harmonics except the triple-n order will be present in the injected phase voltage waveform. On the other hand, the PWM switching can reduce the lower order harmonics depending on selected switching frequency. Too high a switching frequency can increase converter losses, which can affect the converter rating, life and efficiency. Thus usually six-step switching is preferred, which can have the disadvantage of harmonic injection to the stator side. In the proposed technique, a selective harmonic elimination and optimization based PWM switching is employed, which either eliminates or reduces the lower order harmonics and simultaneously optimizes the other higher order harmonics with lower minimum no of switching per quarter cycle. The no. of switching considered for the present problem depends on the rotor speed. The optimum switching angles are calculated off line as a function of m_d using BBO and stored in processor memory for on line application. The switching angles as function of m_d are shown in Figure 3.2(b) and Figure 3.2(d) for 180^0 and 120^0 modes which can be stored through mixed model equations [93]. When the rotor is operating in steady state at a fixed speed, the switching pattern will be decided by the angles already stored in the processor memory. With variation of wind speed, the generated harmonics pattern changes which can even result in generation of sub or fractional order harmonics as shown in Table-3.7 and Table- 3.8 for 120 and 180 degree switching modes. In these tables the computed switching angles are shown eliminating lower order rotor side harmonics which can generate stator side sub-harmonics at different speed and m_d. As an example, in Table-3.7 at 1434 rpm the five switching angles are shown at m_d=0.7 eliminating rotor side harmonics up to 13^{th} order which automatically eliminates stator side sub-harmonics as shown in the table. It can be observed from Table-3.1 that the presence of 17^{th} harmonics in the rotor voltage can only introduce fundamental frequency at 1500 rpm. A small deviation of speed to 1520 rpm will generate a fractional order

harmonic of 1.24 due to the presence of 17th harmonics at the rotor side at m_d=0.69as given in Table-3.7. The effect of other machine parameters for the rotor injected harmonics is negligible compared to RSC injected harmonics. Figure 3.21 shows generated stator side harmonics with rotor speed variation from 1200 rpm to 1800 rpm for RSC injected harmonics up to 19th order.

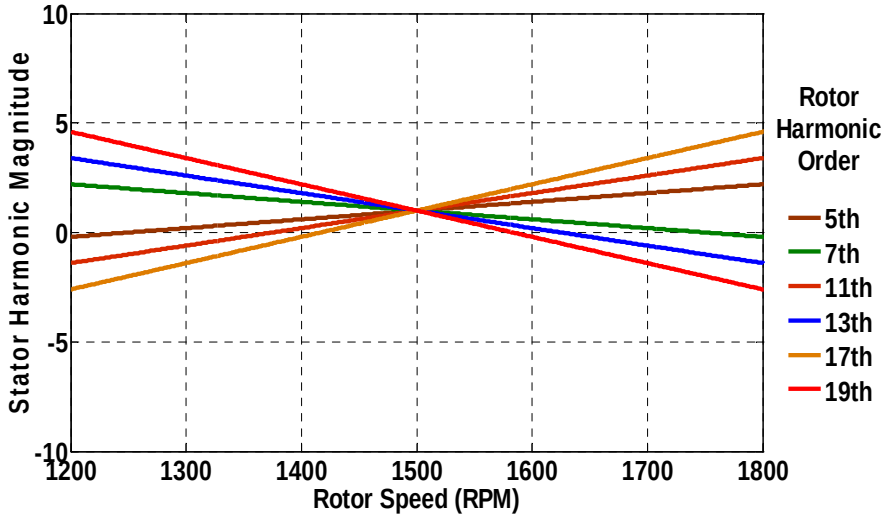

Figure 3.21 Developed Stator harmonics for RSC injected harmonics up to 19th order against speed variation from 1200 rpm to 1800 rpm.

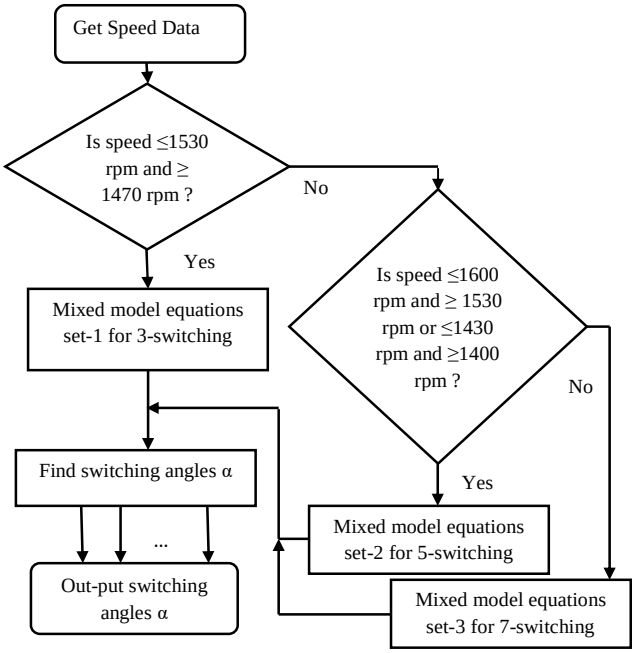

Figure 3.22 RSC control flowchart.

The rotor side higher orders harmonics are not considered as their magnitudes are comparatively less to have any significant effect on the stator voltage waveform. The speed range selected based on the slip variation of -20% to +20%, which conforms to most of the practical applications. It can be observed that in the speed range of 1470 to 1530 rpm all the generated stator side harmonics are in the vicinity of fundamental frequency where elimination of lower order rotor side harmonics is more essential as their magnitudes are higher. Thus, in this speed range three switching per quarter cycle for the RSC is adopted. While calculating the switching angles in this range through BBO, the objective function is adjusted in such a way which can eliminate harmonics up to 7th order and rest higher orders are minimized. In the next speed range of 1400 to 1470 rpm or of

1530 to 1600 rpm five switching per quarter cycle is adopted eliminating rotor side harmonics up to 13th and rest higher order is minimized. This is done as stator side harmonic orders are deviating more from the fundamental as shown in Figure 3.21, which can produce more prominent distortion of the stator voltage. Similarly, for the same reason for speed ranges below1400 rpm to 1200 rpm or above 1600 rpm to 1800 rpm seven switchings per quarter cycle are adopted eliminating RSC injected harmonics up to 19th order while minimizing the higher order. The same has been demonstrated through flowchart shown in Figure 3.22 which is programmed in the processor memory for online application.

The switching angles are separately calculated off line for all the 3, 5 and 7 switching methods and stored in the processor memory through mixed model equations [93] for on-line application. The plots for 5-switching angles with m_d for with 180 and 120 degree conduction mode is shown in Figure 3.16 (a) and (c) respectively. For 180 degree conduction mode the mixed model equations (3.44) and (3.45) following procedure of [93] are given by,

For, $0.1 \le m_d \le 0.8$ the switching angles are,

$$\alpha_1 = -5m_d + 34.1$$

$$\alpha_2 = 10.94m_d + 33.93$$

$$\alpha_3 = -16.5m_d + 60 \qquad (3.44)$$

$$\alpha_4 = 19.16m_d + 59.52$$

$$\alpha_5 = -13.2m_d + 89.7$$

Also $0.81 \le m_d \le 95$

$$\alpha_1 = 296.34m_d^2 - 488.05m_d + 231.48$$

$$\alpha_2 = 971.87m_d^2 - 1628.6m_d + 725.52$$

$$\alpha_3 = 56.16m_d^2 - 117.44m_d + 12.1 \qquad (3.45)$$

$$\alpha_4 = 1705m_d^2 - 2857.2m_d + 1272.8$$

$$\alpha_5 = 779.8m_d^2 - 1284.3m_d + 609.2$$

Similar equations can be generated for 3 or 7 switching methods and stored in processor memory. The modulation index m_d will be decided by the RSC controller to provide the desired magnitude of injected voltage where as the speed is taken from speed sensor. During speed transition for change of number of switching angles a hysteresis of 5 rpm is considered for the present experiment to avoid any fluctuation in the stator voltage. The overall control is decided through the flowchart demonstrated in Figure 3.22 during on-line application. The simulated harmonic spectra of stator voltage at different speeds are shown in Figure 3.23 before and after the application of proposed method, which shows clear improvement after application of the proposed method. The corresponding experimental harmonic spectra are shown in Fig. 3.24 indicating improvement by the proposed method which conforms to the simulation results. In these spectra the speeds chosen are 1520 rpm, 1580 rpm and 1350 rpm for 3, 5 and 7 switchings respectively.

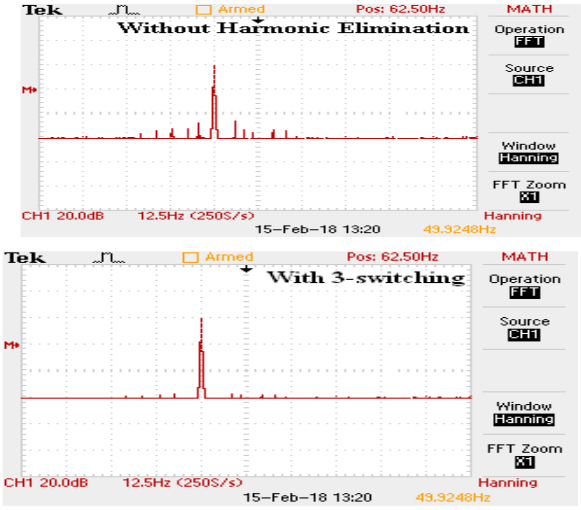

(a)

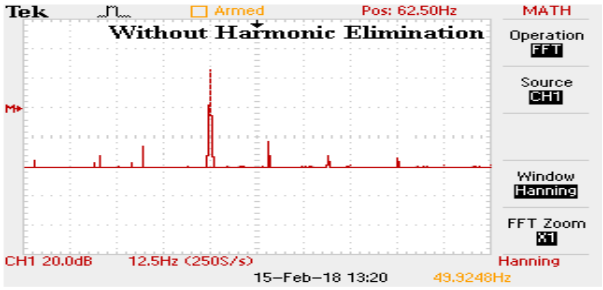

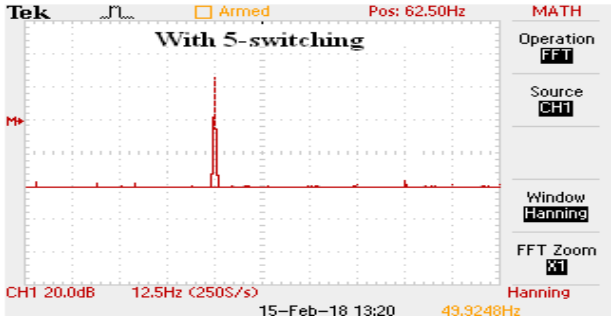

(b)

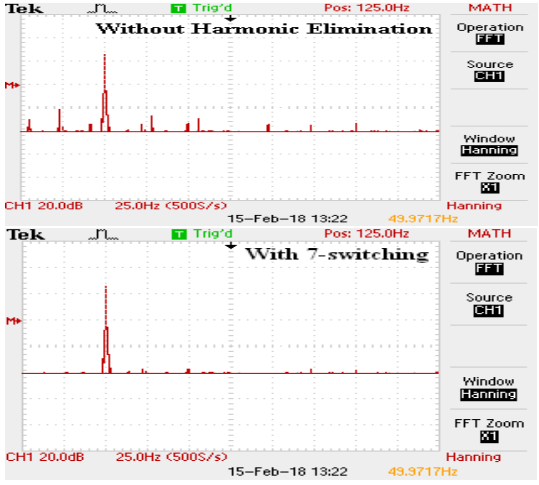

(c)

Figure 3. 23 Experimental output for DFIG stator side harmonic spectra before and after proposed switchings (a) at 1520 rpm (b) at 1580 rpm (c) at 1350rpm.

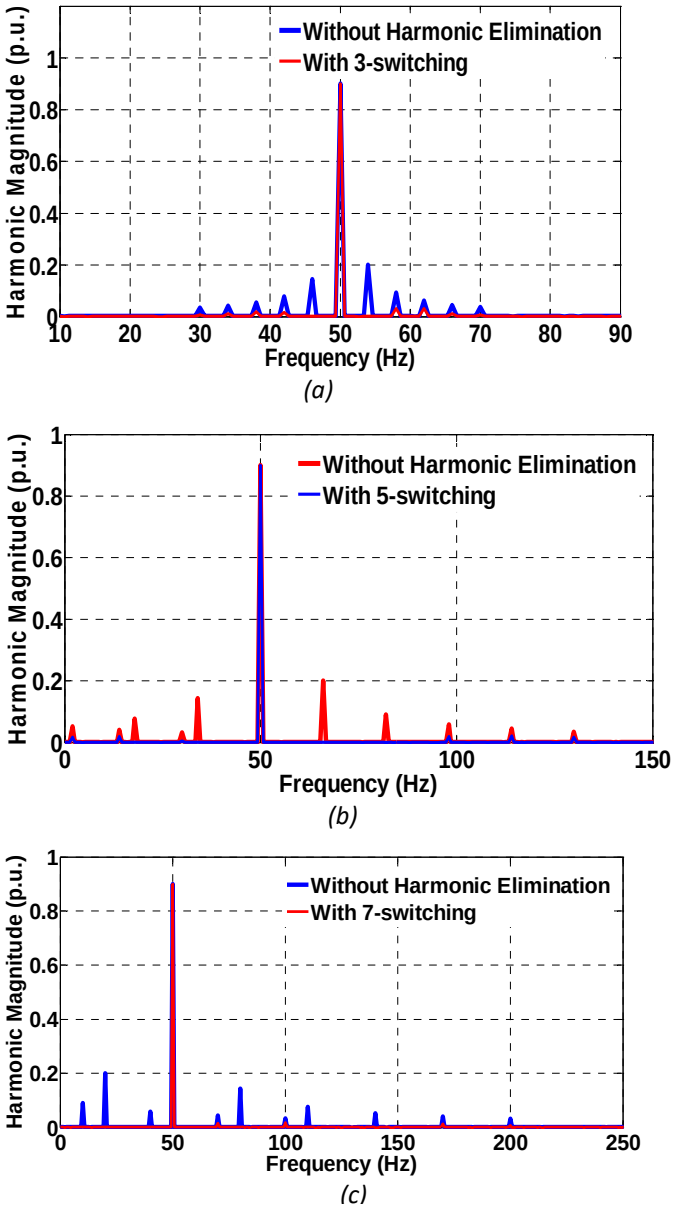

Figure 3.24 DFIG stator side harmonic spectra with and without harmonic elimination for (a) 5^{th} and 7^{th} harmonic elimination at 1520 rpm (b) 5^{th}, 7^{th}, 11^{th} and 13^{th} harmonic elimination at 1580 rpm (c) 5^{th}, 7^{th}, 11^{th}, 13^{th}, 17^{th} and 19^{th} harmonic elimination at 1350rpm.

3.13 Conclusion

An optimized switching strategy for the rotor side converter (RSC) for a DFIG is proposed in this chapter. This can eliminate undesired stator harmonics injected from RSC which can deteriorate its power quality. The selected lower order harmonics of the RSC generated voltage are removed and rest higher orders are minimized by BBO-based SHE technique. In the proposed algorithm, a modified RSC switching technique is adopted based on rotor speed with variation of number of switching angles per quarter cycle. The switching angles contributing minimum voltage THD at different modulation indices and speeds are computed by the BBO algorithm and stored in a processor memory in the form of mixed model equations for online application. Thus, the overall voltage THD in the stator voltage can be minimized. The proposed scheme can be efficiently employed for online control of any number of DFIGs connected with grid system or in grid isolation mode of operation.

Chapter 4

Proposed Combined Performance of DFIG, DVR, STATCOM and UPQC with common DG systems

Chapter 4

4.1 Chapter Overview

This chapter investigates the combined operation and performance of the doubly fed induction generator (DFIG) and powerful custom power devices such as dynamic voltage restorer (DVR), static compensator (STATCOM) and unified powr quality conditionar (UPQC) with common distributed generation (DG) systems. Improved multilevel inverter based topologies for DVR, STATCOM and UPQC operations using DFIG and PV are proposed in this chapter. The proposed technique can efficiently mitigate the power quality problems e.g. voltage sag, swell, flicker, reactive power, voltage interruption, unbalance neutral current, voltage and current harmonics etc. in the distribution system. The proposed DG connected three phase multilevel converter for photo voltaic (PV) system reduces filtering requirements, increases redundancy and enables transformerless interface with grid. Biogeography-Based Optimization (BBO) technique is applied for calculating the exact switching angles for the inverter at each modulation index considering low total harmonic distrotion (THD) for the output voltage. The performance of the UPQC mode is compared with both DVR and STATCOM models. For the proposed topology, the simulation studies with MATLAB are presented which show that the proposed DFIG and PV based UPQC performs significantly better than the DG-DVR and DG-STATCOM combinations

4.2 Importance of DG, DFIG, STATCOM, DVR, UPQC, SHEPWM [94-100]

Interconnection and grid integration of distributed generation (DG) based sources has become a widely addressed research topic in the past two decades. Doubly fed induction generator (DFIG) in wind generation scheme and the solar PV based sources are the two most commonly used DGs. Various control strategies for operation and performance of DFIG systems have been well studied in literature [32, 44, 45, 76, 88, 101-103]. The harmonic analysis of DFIG has been covered in [45, 88, 101] for wind energy conversion system. In [102, 103], hybrid model of a DFIG is thoroughly studied. Grid harmonics is minimized using optimized coordinated approach in [71,104] with six–step switching while maintaining stipulated quality of power as recommended in IEEE 519 standard range. In [105], multilevel inverter using particle swarm optimization technique is described. Space vector pulse width modulation technique has been utilized in [106] for the multilevel voltage source inverter with photovoltaic system. Flying capacitor multilevel converter control is proposed in [62, 107] and five level neutral-point clamped inverter is introduced in [108]. Transformer-less series sag compensation with a cascade multilevel inverter is also proposed in [109]. Five level neutral-point clamped inverter is introduced in [110] for dynamic voltage restorer to mitigate the voltage sag. The short circuit in the grid, inrush currents when large machines are switched on the high power and voltage quality problems in the power distribution systems are addressed in [111]. Power quality problems such as sags, swells, flickers, notch, spike, harmonics, transients and reduction of three phase voltage unbalance are studied in the various works regarding static VAr compensators (SVCs) [98, 99,112], static synchronous compensators (STATCOMs) [94, 113], unified power quality conditioner [96, 97, 114, 115, 116] (UPQCs), and custom power

devices based on energy storage systems, e.g., dynamic voltage restorers (DVRs) [117, 118, 119, 120]. All these literatures are concentrated on isolated operations in any of the modes e.g., DVR, UPQC, STACOM etc. Moreover, introduction of renewable sources are not widely used for such compensators.

This chapter develops a framework for employing a PV-wind hybrid distributed generation system for DVR, STATCOM or UPQC [94-100] operation using multilevel converter with optimized switching. The selected harmonic elimination pulse width modulation (SHE-PWM) based multilevel inverter (MLI) switching scheme optimizes the overall injected voltage and current THD in such a way that line harmonics present in the supply also gets reduced. The proposed scheme can inject active power from the hybrid sources while reactive power injection can take place in either of DVR, STATCOM or UPQC operation. The conventional UPQC mode of operation usually does not compensate the voltage interruption alone without energy storage element in the dc-link. But the proposed DG-DFIG-UPQC scheme compensates the voltage interruption in the source with the help of the common shared DC bus between the DFIG rotor side and PV interconnection. In the present approach, Biogeography-Based Optimization (BBO) [52, 87, 121] based SHE-PWM optimization algorithm technique is used to calculate switching angles for the line infacing inverters. Various simulations using MATLAB/Simulink and the corresponding experimental results confirm that the proposed DG-UPQC scheme using hybrid generation performs significantly better than the DG-DVR and DG-STATCOM.

4.3 Proposed System Configuration

The block diagram of the proposed system considering only wind and PV based hybrid generation and DVR sharing common DC bus is shown in Figure 4. 1. In Figure 4. 1, the DFIG and the PV panels with DC-DC converter are connected in parallel with transformer less DVR interface to Micro-grid. The DVR can reduce the unbalance in load side voltage, sag, swell, flicker, spike, reactive power unbalance etc. A multilevel inverter is used as the DVR interface to reduce the harmonic content of the output voltage. The stators of the DFIGs are directly connected to 50 Hz micro grid. The DFIG is mechanically coupled with a wind turbine because most of the supply is of mechanical power. A battery is provided between the two converters to store the extra energy from the PV panel when the rotor side power demand is less than PV panel output. The same can also act as a dc source in the absence of sun light to inject the power to the rotor during sub-synchronous operation or store the power coming from the DFIG rotor at super-synchronous speed. Inverters feeding the rotors of the DFIGs, handle high current. Thus the devices will have high current stress both during switching and continuous conduction. Since the conduction current cannot be minimized as it is decided by load, the switching losses should be reduced. The Figure 4.2 shows the DVR system is same as Figure 4.1 except that the interface is made with the help of series transformer. The schemes in Figure 4.1 and 10.2 are limited to only DVR operation besides active power injection from wind and PV sources. The proposed schemes shown in Figure 4.3 and Figure 4.4 are for improved operation in UPQC mode with reduced injected harmonics. The scheme in Figure 4.3 illustrates proposed transformer-less connection while Figure 4.4 shows transformer connected PV-UPQC respectively. The SHE-PWM based multilevel inverters are used for interface with grid in both the cases. The transformer less scheme has some important features like lower cost, lower size,

free from saturation, neutral current or inrush current related problems etc. On the other hand, the inverter voltage has to be higher and the output voltage THD can be higher compared to scheme with transformer for same number of switchings. The Micro-grid and the DFIG specifications used for the proposed scheme are given in Table 4.1.

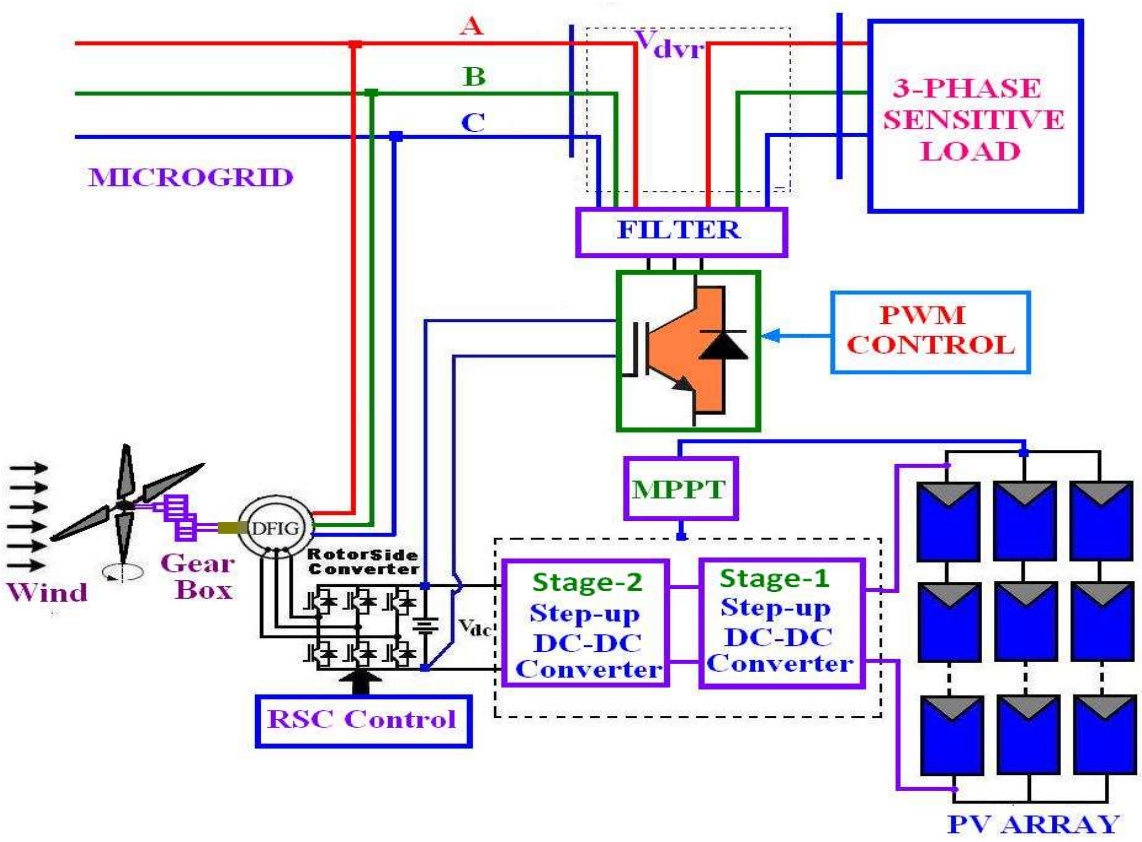

Figure 4. 1 Proposed transformer less DVR system with PV

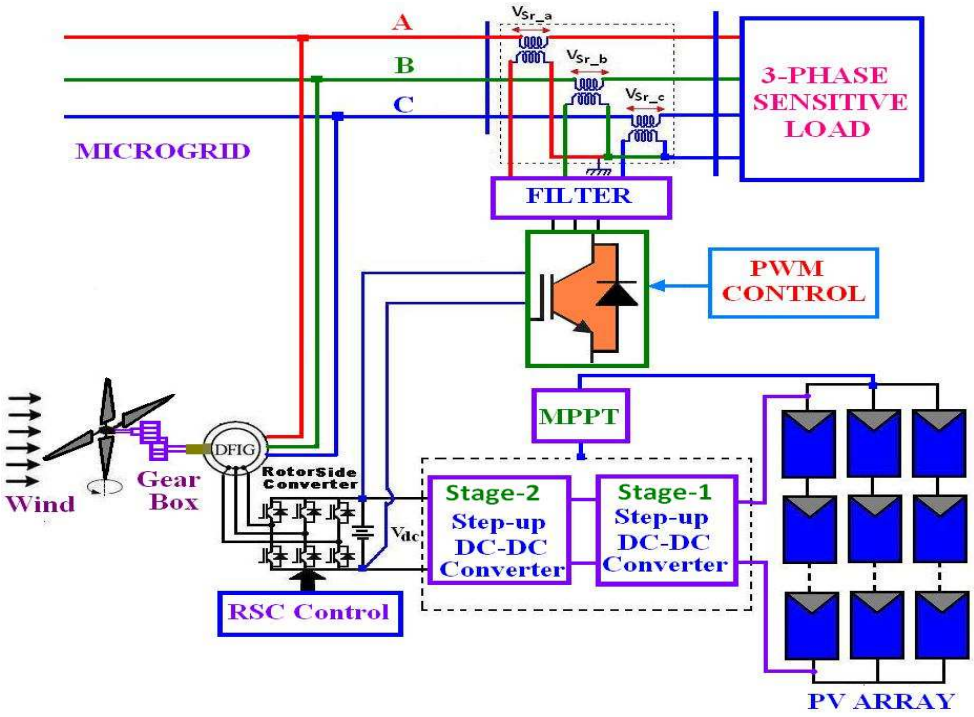

Figure 4. 2 Proposed transformer connected DVR system with PV

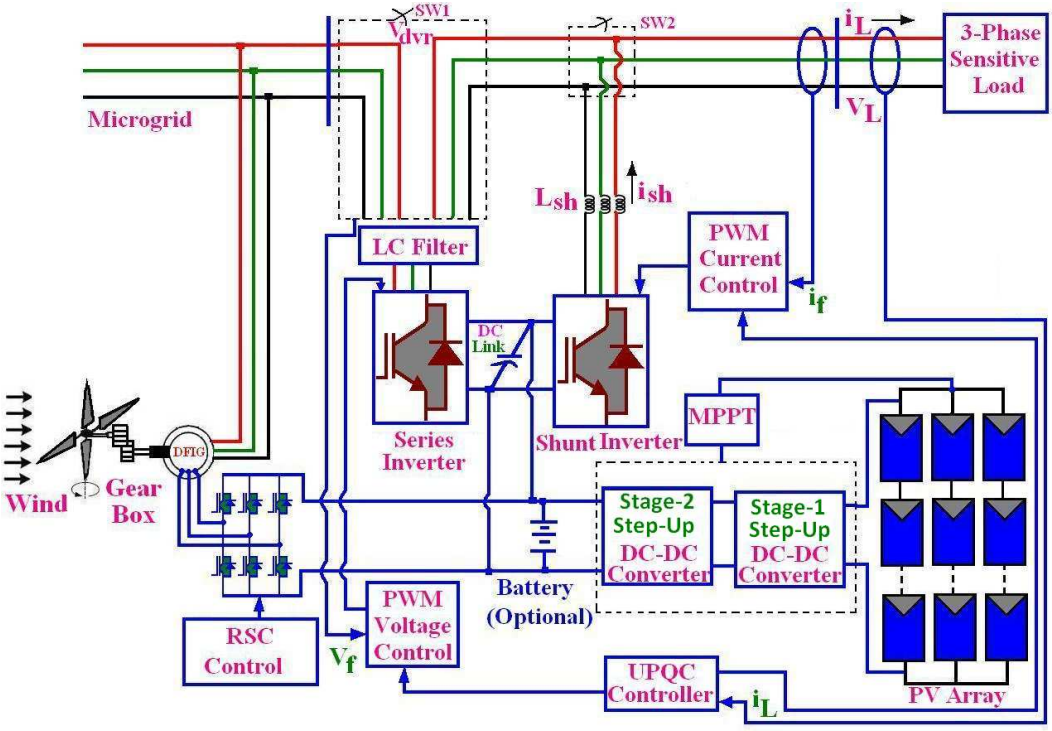

Figure 4.3 Proposed transformer less UPQC system with PV

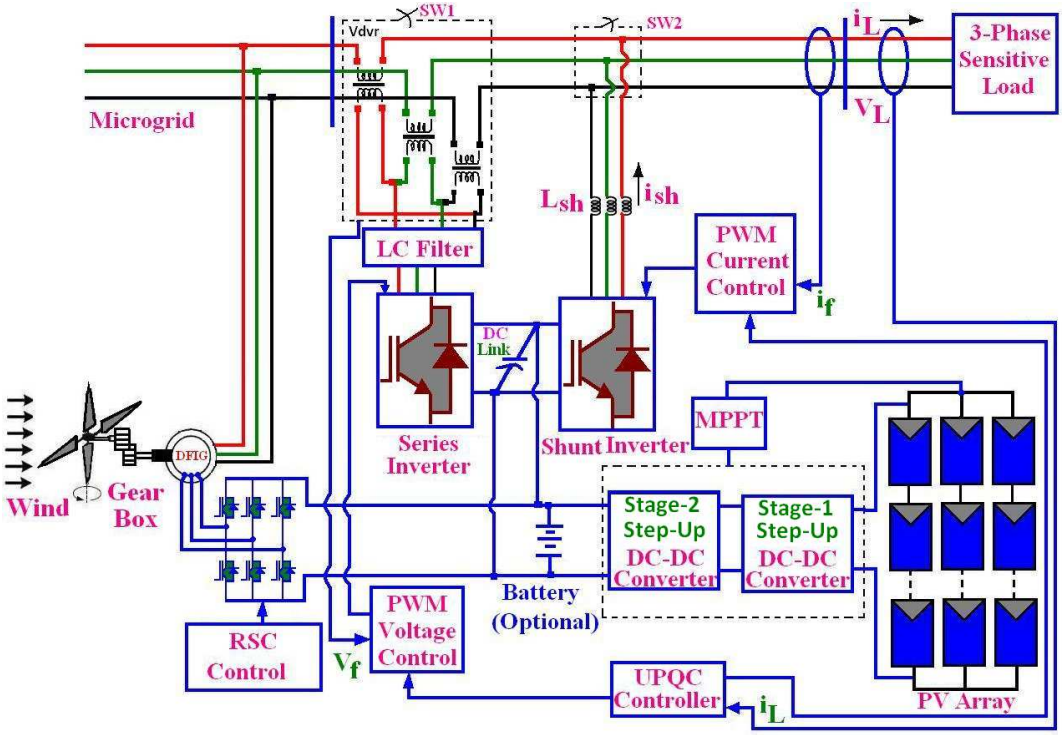

Figure 4.4 Proposed transformer connected UPQC (DVR+STATCOM) system with PV

Table 4.1 Parameters of the experimental system

Micro grid Specification		DFIG Specification			
		Stator Parameters		Rotor Parameters	
Vgrid	415 V	V_s	415 V	V_r	110 V
f_s	50 Hz	Δ-Connected		Y-Connected	
Rated Capacity	5 kVA	f_s	50 Hz	R_r	1.7 Ω
		P	2.2 KW	L_{lr}	11 mH
5^{th}, 7^{th}	As per	I_s	5 A	I_r	14 A
11^{th}, …	grid	R_s	1.6 Ω	N_r	1450 rpm
harmonic	codes	L_{ls}	12 mH	Battery	1000 AH
voltage		L_m	295 mH		

4.4 Existing and Proposed Switching Strategies

The DFIG rotor voltage supplied from inverter is usually a quasi-sine wave to reduce switching losses in the semiconductor devices. Similar is the case for DVR, STATCOM and UPQC inverters. The quasi-sine voltage

waveforms generated by these inverters can introduce various odd harmonics of the orders of $6k \pm 1$, $k = 1, 2, 3, \cdots$ to the grid. Elimination of such harmonics through PWM needs higher switching frequencies which can increase inverter losses and reduce system efficiency. In the proposed method, a modified BBO based SHEPWM technique is introduced to substantially reduce the injected harmonics.

4.4.1 Space Vector Pulse Width Modulation (SVPWM) Switching Control Strategies

For improved dc bus utilization and with lower output voltage THD, the SVPWM multilevel converter switching technique is most suitable. The space vector modulation is one of the advanced, computation intensive, flexible and real time modulation techniques. Using SVPWM switching technique determination of the switching instant of the switching vectors α, β planes the magnitude and angle of the rotating vector can be found by the mean of Clark's Transformation with respect to stationary reference frame. Figure 4.5 shows the representation of rotating vector in complex plane with typical space vector diagram for two-level inverter and Figure 4.6 shows the space vector diagram for three-level inverter.

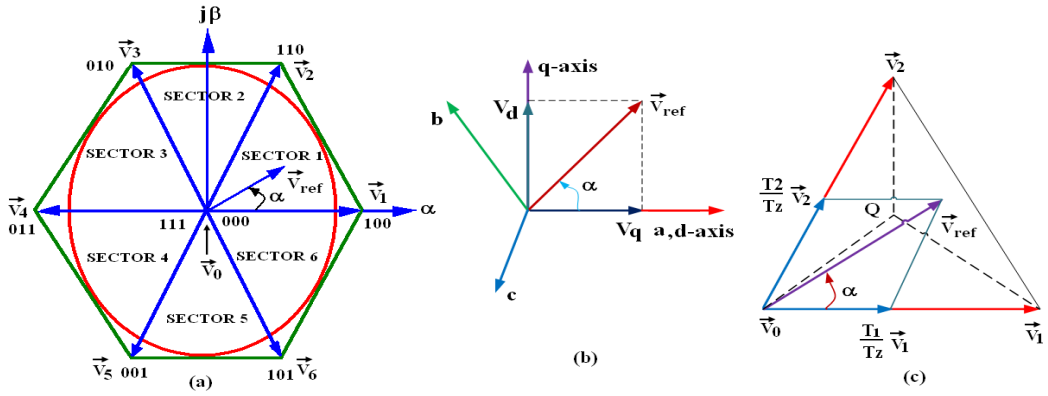

Figure 4.5 Space vector diagram for (a) two-level inverter (b) voltage space vector and its components (d, q) (c) reference vector as a combination of adjacent vectors at sector 1.

Considering Figure 4.5, the reference voltage can be written as

$$\vec{V}_{ref} = V_\alpha + jV_\beta = 2/3\left(V_a + aV_b + a^2V_c\right) \tag{4.1}$$

Where, $a = e^{j(2\pi/3)} = e^{j120^\circ}$

Thus, the magnitude of the reference vector is given by,

$$\left|\vec{V}_{ref}\right| = \sqrt{V_\alpha^2 + V_\beta^2}, \alpha = \tan^{-1}\left(V_\beta / V_\alpha\right) \tag{4.2}$$

Substitution of operator 'a' in equation (4.1) gives,

$$V_\alpha + jV_\beta = 2/3\left(V_a + e^{j(2\pi/3)}V_b + e^{-j(2\pi/3)}V_c\right)$$

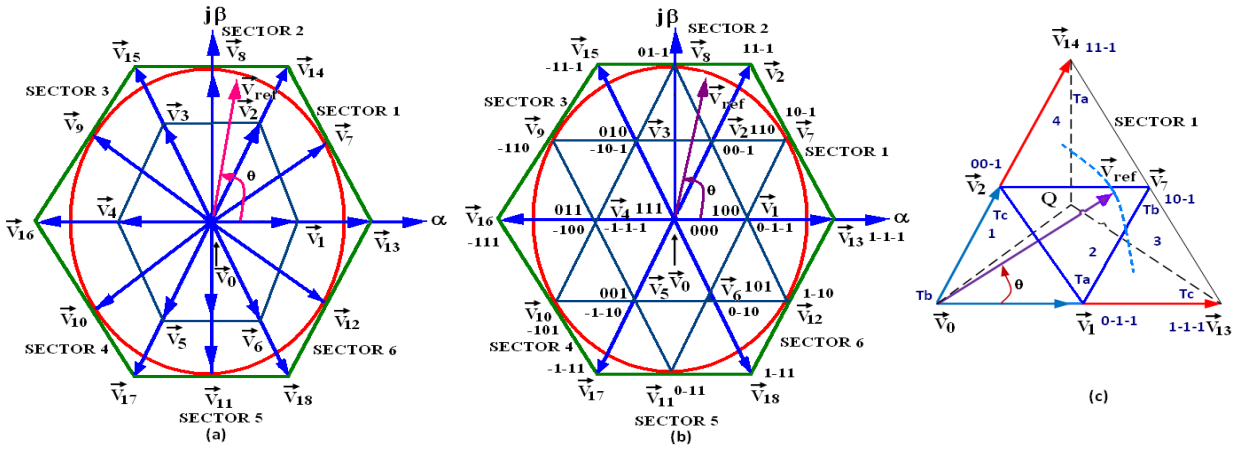

Figure 4.6 Space vector Positions for (a) three-level inverter (b) division of sectors and region for three-level inverter (c) voltage vector 1 and their times.

$$= 2/3\left(V_a + \cos(2\pi/3)V_b + \cos(2\pi/3)V_c\right) + j\,2/3\left(\sin(2\pi/3)V_b - \sin(2\pi/3)V_c\right) \tag{4.3}$$

Equating real and imaginary parts of equation (4.3),

$$V_\alpha = 2/3\left(V_a + \cos(2\pi/3)V_b + \cos(2\pi/3)V_c\right) \tag{4.4}$$

$$V_\beta = 2/3\left(0V_a + \sin(2\pi/3)V_b - \sin(2\pi/3)V_c\right) \tag{4.5}$$

Expressions (4.4) and (4.5) can be combined in matrix form as,

$$\begin{bmatrix} V_d \\ V_q \end{bmatrix} = \frac{2}{3}\begin{bmatrix} 1 & \cos(2\pi/3) & \cos(2\pi/3) \\ 0 & \sin(2\pi/3) & -\sin(2\pi/3) \end{bmatrix}\begin{bmatrix} V_a \\ V_b \\ V_c \end{bmatrix} \tag{4.6}$$

Figure 4.7 (a-c) shows that the simulation result of SVPWM for DCMLI for line voltage V_a, V_b and V_c respectively and Figure 4.7 (d- f) shows phase voltages V_{an}, V_{bn} and V_{cn} respectively. Figure 4.7 (g) shows the inverter output

phase voltages after filtering. Table 4.2 shows the comparison of % THD with SVPWM and SPWM considering different levels up to 35 for DCMLI, NPC and cascaded multilevel inverters.

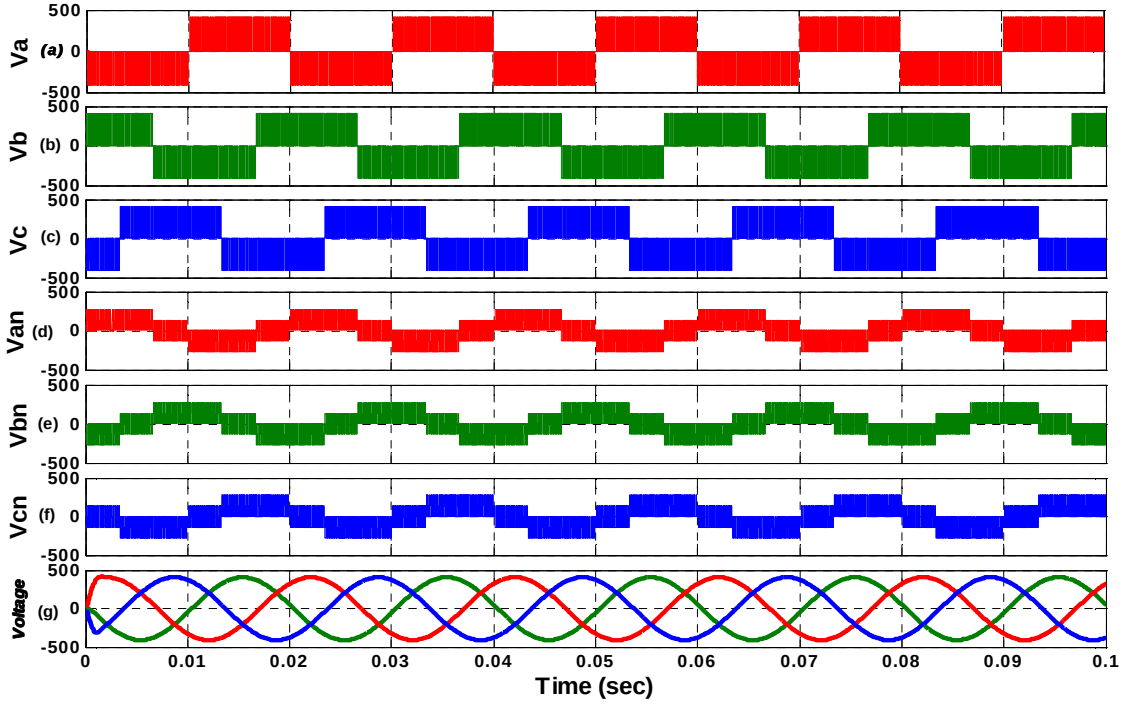

Figure 4.7 Simulated waveforms of DCMLI: (a)-(c) line voltages V_a, V_b and V_c ; (d)-(f)phase voltages V_{an}, V_{bn} and V_{cn} (g) phase voltages after filtering

Table 4.2 Comparison between % THD for SVPWM with SPWM.

No of	SVPWM (% THD)			SPWM (% THD)		
levels	DCMLI	NPC	Cascade	DCMLI	NPC	Cascade
2	15.264	16.2508	4.9861	17.432	16.876	7.435
7	4.6356	10.3778	2.6202	11.8453	13.682	5.549
9	3.2577	10.1405	2.7754	11.235	12.203	5.0453
11	3.002	10.0761	2.0955	11.0701	11.002	4.374
13	2.9557	8.8655	1.8804	10.214	10.549	4.113
15	2.813	8.7752	1.1123	8.045	9.326	3.541
17	2.4359	7.7785	1.0087	6.834	7.162	3.179
19	2.2826	5.0087	1.0243	5.457	6.349	3.0058
23	2.214	4.108	0.3034	4.348	5.23	2.738
25	2.1001	3.543	0.1423	3.678	4.473	2.548
29	1.322	2.8945	0.2046	2.564	4.12	1.3769
31	0.153	2.125	0.0072	2.743	3.032	1.417
35	0.093	2.0537	0.0050	1.973	2.23	1.001

4.4.2 Conventional Unipolar Programmed switching Case

For unwanted harmonic elimination the most versatile unipolar switching method is very essential and is shown in Figure 4.8 (a) and (b). From the output voltage the output voltage label is $+V_{dc}, -V_{dc}, and \ 0$ where the width of the pulse is adjustable. By using different computational iterative technique, the proper switching angles may be determined and this switching angle eliminate the lesser order harmonics and at the similar time the high magnitude harmonics can be controlled or suppressed. At low modulation indices this switching scheme is more advantages but for high modulation this is also applicable. For small periods of time in H-bridge inverter the switching method of unipolar allows for the preferred voltage to be achieved. Unipolar case produces a inferior harmonics and %THD than Bipolar. It is seen that the unipolar scheme provide a more expected approximation to a sinusoidal waveform compares to bipolar. For unipolar case the generation of EMI is very less.

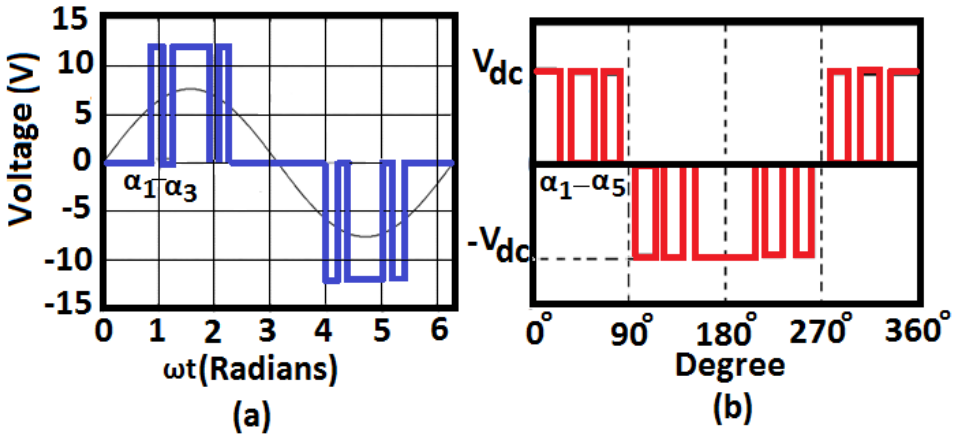

Figure 4.8 Selective harmonic PWM switching patterns for (a) three switching and (b) five switching angles.

The configuration of the unipolar voltage notch is shown in Figure 4.8 (b) the harmonic coefficient b_n is given by

$$b_n = \frac{4V_{dc}}{\pi}\left[\int_0^{\alpha_1}\sin(n\omega t)d(\omega t)+\int_{\alpha_2}^{\alpha_3}\sin(n\omega t)d(\omega t)+\int_{\alpha_3}^{\alpha_4}\sin(n\omega t)d(\omega t)+\int_{\alpha_4}^{\alpha_5}\sin(n\omega t)d(\omega t)+\int_{\alpha_5}^{\pi/2}\sin(n\omega t)d(\omega t)\right]$$

$$=\frac{4V_{dc}}{n\pi}\left[1-\cos(n\alpha_1)+\cos(n\alpha_2)-\cos(n\alpha_3)+\cos(n\alpha_4)-\cos(n\alpha_5)+\cdots\right] \quad (4.7)$$

Equation (3.7) can be extended to m notches per quarter wave as (4.8)

$$b_n = \frac{4V_{dc}}{n\pi}\left[1+\sum_{k=1}^{m}(-1)^k\cos(n\alpha_k)\right], \text{ for } n=1,3,5,\cdots \quad (4.8)$$

Where the switching angles are satisfied as, $\alpha_1 < \alpha_2 < \alpha_3 < \cdots < \alpha_k < \pi/2$

The harmonic voltage equation (4.9) gives the basic idea of the output,

$$V(\omega t) = \frac{4V_{dc}}{n\pi}\left[1+\sum_{k=1}^{m}(-1)^k\cos(n\alpha_k)\right]\sin(n\omega t) \quad (4.9)$$

From equation (4.8) we get the harmonic coefficient as (4.10),

$$b_1 = \frac{4V_{dc}}{\pi}\left[1-\cos(1\alpha_1)+\cos(1\alpha_2)-\cos(1\alpha_3)+\cos(1\alpha_4)-\cos(1\alpha_5)\right]$$

$$b_5 = \frac{4V_{dc}}{5\pi}\left[1-\cos(5\alpha_1)+\cos(5\alpha_2)-\cos(5\alpha_3)+\cos(5\alpha_4)-\cos(5\alpha_5)\right]$$

$$b_7 = \frac{4V_{dc}}{7\pi}\left[1-\cos(7\alpha_1)+\cos(7\alpha_2)-\cos(7\alpha_3)+\cos(7\alpha_4)-\cos(7\alpha_5)\right] \quad (4.10)$$

$$b_{11} = \frac{4V_{dc}}{11\pi}\left[1-\cos(11\alpha_1)+\cos(11\alpha_2)-\cos(11\alpha_3)+\cos(11\alpha_4)-\cos(11\alpha_5)\right]$$

$$b_{13} = \frac{4V_{dc}}{13\pi}\left[1-\cos(13\alpha_1)+\cos(13\alpha_2)-\cos(13\alpha_3)+\cos(13\alpha_4)-\cos(13\alpha_5)\right]$$

From equation (4.10) we get the equation (4.11)

$$1-\left[\cos(1\alpha_1)-\cos(1\alpha_2)+\cos(1\alpha_3)-\cos(1\alpha_4)+\cos(1\alpha_5)\right]=M$$

$$1-\left[\cos(5\alpha_1)-\cos(5\alpha_2)+\cos(5\alpha_3)-\cos(5\alpha_4)+\cos(5\alpha_5)\right]=0$$

$$1-\left[\cos(7\alpha_1)-\cos(7\alpha_2)+\cos(7\alpha_3)-\cos(7\alpha_4)+\cos(7\alpha_5)\right]=0 \quad (4.11)$$

$$1-\left[\cos(11\alpha_1)-\cos(11\alpha_2)+\cos(11\alpha_3)-\cos(11\alpha_4)+\cos(11\alpha_5)\right]=0$$

$$1-\left[\cos(13\alpha_1)-\cos(13\alpha_2)+\cos(13\alpha_3)-\cos(13\alpha_4)+\cos(13\alpha_5)\right]=0$$

The 5th, 7th, 11th and 13th harmonics would be eliminated if we select the proper switching angle in (4.12)

$$\cos(1\alpha_1)-\cos(1\alpha_2)+\cos(1\alpha_3)-\cos(1\alpha_4)+\cos(1\alpha_5)=M$$

$$\cos(5\alpha_1)-\cos(5\alpha_2)+\cos(5\alpha_3)-\cos(5\alpha_4)+\cos(5\alpha_5)=0$$

$$\cos(7\alpha_1)-\cos(7\alpha_2)+\cos(7\alpha_3)-\cos(7\alpha_4)+\cos(7\alpha_5)=0 \quad (4.12)$$

$$\cos(11\alpha_1)-\cos(11\alpha_2)+\cos(11\alpha_3)-\cos(11\alpha_4)+\cos(11\alpha_5)=0$$

$$\cos(13\alpha_1)-\cos(13\alpha_2)+\cos(13\alpha_3)-\cos(13\alpha_4)+\cos(13\alpha_5)=0$$

For any odd number harmonics, (4.9) can be reached out up-to k^{th} term, where m is the numeral factors with respect to changing points of variables regarding to inverter switching angles from α_1 through α_m in the primary quadrant. In selection of harmonic elimination, α_1 is taken as they require value for fundamental component and the other switching angle coefficients regarding to the harmonics elimination to be vanished are consider to zero or very small value. From (4.12) the number of switching angles are five where one switching angles determined the fundamental magnitude and rest of the switching angles eliminate the 5th, 7th,11th and 13th order unwanted harmonic and the higher order harmonics are suppress for low %THD.

For better harmonics optimization the modified unipolar switching with 60-degree modulation technique is very versatile and this configuration is illustrated in Figure 4.9. For 6-switching the harmonic coefficient can be expressed as (4.13),

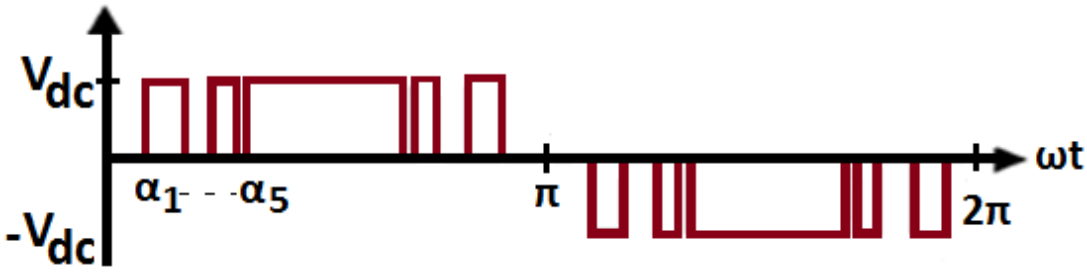

Figure 4.9 Selected harmonic PWM switching pattern with five switching angle.

$$b_n = \frac{4V_{dc}}{n\pi}[\int_{\alpha_1}^{\alpha_2} \sin(n\omega t)d(\omega t) + \int_{\alpha_3}^{\alpha_4} \sin(n\omega t)d(\omega t) + + \int_{\alpha_5}^{\alpha_6} \sin(n\omega t)d(\omega t) + \int_{\pi/3}^{\pi/2} \sin(n\omega t)d(\omega t)]$$

$$b_n = \frac{4V_{dc}}{n\pi}\left[\frac{1}{2} - \cos(n\alpha_1) + \cos(n\alpha_2) - \cos(n\alpha_3) + \cos(n\alpha_4) - \cos(n\alpha_5) + \cos(n\alpha_6) - \cdots\right] \quad (4.13)$$

The harmonic voltage equation is (4.14)

$$V(\omega t) = \frac{4V_{dc}}{\pi}\left[\frac{1}{2} - \sum_{k=1}^{m}(-1)^k \cos(n\alpha_k)\right]\sin(n\omega t) \quad (4.14)$$

The general harmonic coefficient is in (4.15)

$$b_n = \frac{4V_{dc}}{n\pi}\left[\frac{1}{2} - \sum_{k=1}^{m}(-1)^k \cos(n\alpha_k)\right] \quad (4.15)$$

For 5-switching the different harmonic coefficient are shown in equation (4.16)

$$b_1 = \frac{4V_{dc}}{\pi}\left[\frac{1}{2} - \cos(1\alpha_1) + \cos(1\alpha_2) - \cos(1\alpha_3) + \cos(1\alpha_4) - \cos(1\alpha_5)\right]$$

$$b_5 = \frac{4V_{dc}}{5\pi}\left[\frac{1}{2} - \cos(5\alpha_1) + \cos(5\alpha_2) - \cos(5\alpha_3) + \cos(5\alpha_4) - \cos(5\alpha_5)\right]$$

$$b_7 = \frac{4V_{dc}}{7\pi}\left[\frac{1}{2} - \cos(7\alpha_1) + \cos(7\alpha_2) - \cos(7\alpha_3) + \cos(7\alpha_4) - \cos(7\alpha_5)\right] \quad (4.16)$$

$$b_{11} = \frac{4V_{dc}}{11\pi}\left[\frac{1}{2} - \cos(11\alpha_1) + \cos(11\alpha_2) - \cos(11\alpha_3) + \cos(11\alpha_4) - \cos(11\alpha_5)\right]$$

$$b_{13} = \frac{4V_{dc}}{13\pi}\left[\frac{1}{2} - \cos(13\alpha_1) + \cos(13\alpha_2) - \cos(13\alpha_3) + \cos(13\alpha_4) - \cos(13\alpha_5)\right]$$

Further modification the harmonic equation is (4.17)

$$1/2-\left[\cos(1\alpha_1)-\cos(1\alpha_2)+\cos(1\alpha_3)-\cos(1\alpha_4)+\cos(1\alpha_5)\right]=M$$

$$1/2-\left[\cos(5\alpha_1)-\cos(5\alpha_2)+\cos(5\alpha_3)-\cos(5\alpha_4)+\cos(5\alpha_5)\right]=0$$

$$1/2-\left[\cos(7\alpha_1)-\cos(7\alpha_2)+\cos(7\alpha_3)-\cos(7\alpha_4)+\cos(7\alpha_5)\right]=0 \qquad (4.17)$$

$$1/2-\left[\cos(11\alpha_1)-\cos(11\alpha_2)+\cos(11\alpha_3)-\cos(11\alpha_4)+\cos(11\alpha_5)\right]=0$$

$$1/2-\left[\cos(13\alpha_1)-\cos(13\alpha_2)+\cos(13\alpha_3)-\cos(13\alpha_4)+\cos(13\alpha_5)\right]=0$$

For five switching, $b_5=b_7=b_{11}=b_{13}=0$, the 5th, 7th, 11th and 13th order harmonic are eliminated and fundamental are controlled where the condition of switching angles is $\alpha_1<\alpha_2<\alpha_3<\cdots<\alpha_k<\pi/2$.

4.4.3 For bipolar switching

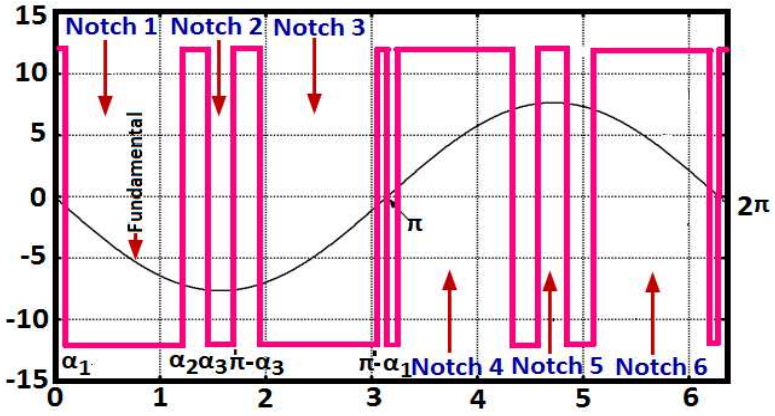

(a)

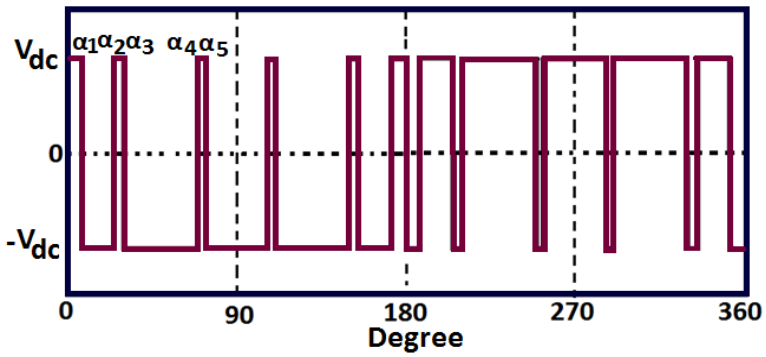

(b)

Figure 4.10 Bipolar Programmed PWM using for (a) three switching angles and (b) five switching angles.

Figure 4.10 (a) delineates the very common Bipolar switching setup with utilizing three numbers of switching angles and (b) for five number of switching angles. This switching technique gives the yield voltage is either $+V_{dc}$ or $-V_{dc}$. The amount of pulse notches sever per basic cycle is equivalent to double the quantity of switching angles. By using

harmonic minimization method the preferred lesser order selected harmonics are removed and the upper harmonics are suppressed.

Advantage:

- **i.** The switching strategy is extremely straightforward not entangled as some other switching plans**.**
- **ii.** Bipolar switching can utilize low modulation indices.
- **iii.** Another advantage is redundancy.
- iv. It can be utilized for higher modulation indices in addition to low modulation indices.

Disadvantages:

Bipolar Programmed PWM also has some disadvantages.

- i. Bipolar switching produces voltage changes equal to double and for a large V_{dc} can produce a considerable amount of EMI.
- ii. Bipolar PWM inherently increases the effective switching frequency.
- iii. Bipolar switching for low modulation indices produces high amount of harmonic content in the output. Sometimes for certain modulation indices the Total Harmonic Distortion (THD) may be more than 100%.

A generalized bipolar waveform with k number of switching and having quarter-wave symmetry is periodic. In the line-to-line voltage of the inverter output, the triplen i.e. 3rd, 9th, 15th and 18th harmonics are cancelled and the amplitude of the nth harmonic b_n, given in the following Fourier series expression, is expressed only with the first quadrant switching angles $\alpha_1, \alpha_2, \cdots, \alpha_m$:

The Fourier series of output voltage can be expressed as

$$v_0 = \sum_{n=1,3,5,\cdots}^{\infty} b_n \sin(n\omega t) \tag{4.18}$$

Where

$$b_n = \frac{4V_{dc}}{\pi}\left[\int_0^{\alpha_1} \sin(n\omega t)d(\omega t) - \int_{\alpha_1}^{\alpha_2} \sin(n\omega t)d(\omega t) + \int_{\alpha_3}^{\alpha_4} \sin(n\omega t)d(\omega t) - \int_{\alpha_4}^{\alpha_5} \sin(n\omega t)d(\omega t) + \int_{\alpha_5}^{\pi/2} \sin(n\omega t)d(\omega t)\right] \tag{4.19}$$

Equation (4.19) can be extended to m switching per quarter-wave as

$$b_n = \frac{4V_{dc}}{\pi}\left[1 - 2\cos(n\alpha_1) + 2\cos(n\alpha_2) - 2\cos(n\alpha_3) + 2\cos(n\alpha_4) - 2\cos(n\alpha_5) + \cdots\right] \tag{4.20}$$

The general harmonic coefficient is expressed as equation (4.21)

$$b_n = \frac{4V_{dc}}{\pi}\left[1 + 2\sum_{k=1}^{m}(-1)^k \cos(n\alpha_k)\right] \tag{4.21}$$

Which is satisfied the condition as $\alpha_1 < \alpha_2 < \alpha_3 < \cdots < \alpha_k < \pi/2$.

For individual harmonic coefficient in bipolar case is (4.22)

$$b_1 = \frac{4V_{dc}}{\pi}\left[1 - 2\cos(1\alpha_1) + 2\cos(1\alpha_2) - 2\cos(1\alpha_3) + 2\cos(1\alpha_4) - 2\cos(1\alpha_5)\right]$$

$$b_5 = \frac{4V_{dc}}{5\pi}\left[1 - 2\cos(5\alpha_1) + 2\cos(5\alpha_2) - 2\cos(5\alpha_3) + 2\cos(5\alpha_4) - 2\cos(5\alpha_5)\right]$$

$$b_7 = \frac{4V_{dc}}{7\pi}\left[1 - 2\cos(7\alpha_1) + 2\cos(7\alpha_2) - 2\cos(7\alpha_3) + 2\cos(7\alpha_4) - 2\cos(7\alpha_5)\right] \quad (4.22)$$

$$b_{11} = \frac{4V_{dc}}{11\pi}\left[1 - 2\cos(11\alpha_1) + 2\cos(11\alpha_2) - 2\cos(11\alpha_3) + 2\cos(11\alpha_4) - 2\cos(11\alpha_5)\right]$$

$$b_{13} = \frac{4V_{dc}}{13\pi}\left[1 - 2\cos(13\alpha_1) + 2\cos(13\alpha_2) - 2\cos(13\alpha_3) + 2\cos(13\alpha_4) - 2\cos(13\alpha_5)\right]$$

The N nontriplen odd harmonics are eliminated with $N+1$ switching angles, obtained from the solution of the following system of equations (4.23).

$$1 - 2\left[\cos(1\alpha_1) - \cos(1\alpha_2) + \cos(1\alpha_3) - \cos(1\alpha_4) + \cos(1\alpha_5)\right] = M$$

$$1 - 2\left[\cos(5\alpha_1) - \cos(5\alpha_2) + \cos(5\alpha_3) - \cos(5\alpha_4) + \cos(5\alpha_5)\right] = 0$$

$$1 - 2\left[\cos(7\alpha_1) - \cos(7\alpha_2) + \cos(7\alpha_3) - \cos(7\alpha_4) + \cos(7\alpha_5)\right] = 0 \quad (4.23)$$

$$1 - 2\left[\cos(11\alpha_1) - \cos(11\alpha_2) + \cos(11\alpha_3) - \cos(11\alpha_4) + \cos(11\alpha_5)\right] = 0$$

$$1 - 2\left[\cos(13\alpha_1) - \cos(13\alpha_2) + \cos(13\alpha_3) - \cos(13\alpha_4) + \cos(13\alpha_5)\right] = 0$$

The 5th, 7th, 11th and 13th harmonics would be eliminated if $b_5 = b_7 = b_{11} = b_{13} = 0$ for proper choice of switching angles. The Fourier series expansion of the voltage wave form is as (4.24)

$$V(\omega t) = \frac{4V_{dc}}{n\pi}\left[1 + 2\sum_{k=1}^{m}(-1)^k \cos(n\alpha_k)\right]\sin(n\omega t) \quad (4.24)$$

4.4.4 PWM switching for Virtual Stage [25, 26, 27]

This switching scheme is a mix between unipolar and the multilevel fundamental switching scheme. The switching "on" and "off" strategy is illustrated in Figure 4.11 (a) per fundamental cycle. For MLI switching scheme each and every one of the dc supplies are generally involved within one fundamental cycle. Figure 4.11 shows two dc sources and the corresponding four switching angles are used. The pattern of virtual switching stage is illustrated in Figure 4.11 (b), where the number of dc supplies is three and four numbers of required switching angles. The fourth control switching angle forces the third H-bridge to supply a zero output voltage.

Advantage:

i. The switching pattern is very simple.

ii. Contain low harmonics and lower THD.

iii. This type of PWM is substitute to Bipolar PWM switching and with Unipolar switching PWM.

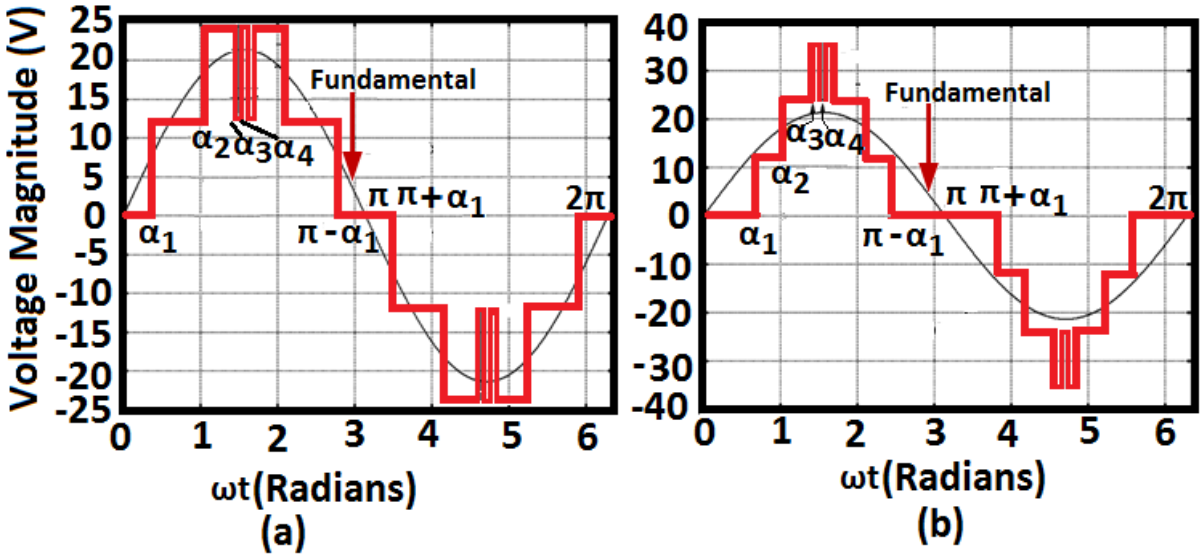

Figure 4.11 Virtual Stage PWM using (a) two dc sources (b) three dc sources.

4.4.5 Proposed harmonic elimination technique for multilevel inverter

The concept of Biogeography-Based optimization algortthm based multilevel voltage source inverters and their modulation topologies are described in this chapter. By applying this concept, appropriate switching angles can be calculated, specific harmonics can be eliminated and controlled, and the output voltage THD can be reduced. A wye-configured m-level cascaded-inverter is illustrated in Figure 4.12.

Figure 4.13 shows the multilevel output-voltage waveform of phase-a for the inverter. Fourier Co-efficient of waveform for V_{an} in Figure4.13 can be obtained as,

$a_0 = 0$ for all n, and $a_n = 0$, for all even n and,

$$b_n = (4V_{dc}/n\pi)\left[\sum_{k=1}^{m}\cos(n\alpha_k)\right] \quad (4.25)$$

Where, k is the number of switching angles per quarter cycle.

Therefore, considering for five switching per quarter cycle forming 11-level inverter, the phase voltage V_{an} can be written as,

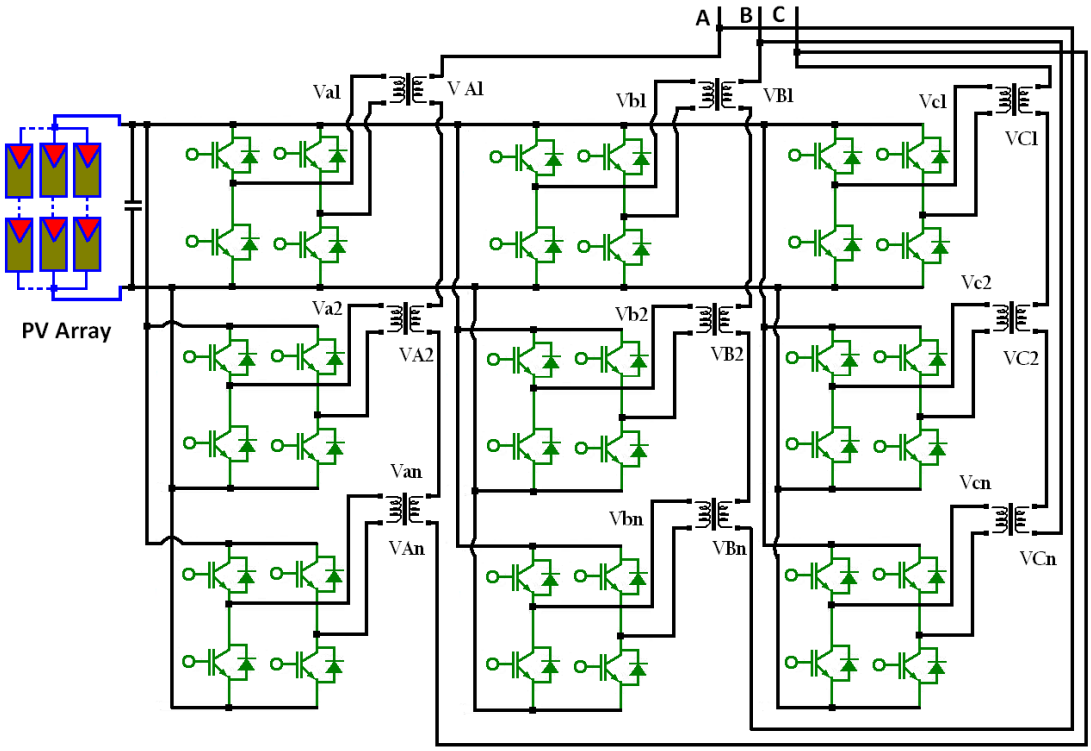

Figure 4.12 A general configuration of three-phase Wye-connected cascaded-multilevel inverter

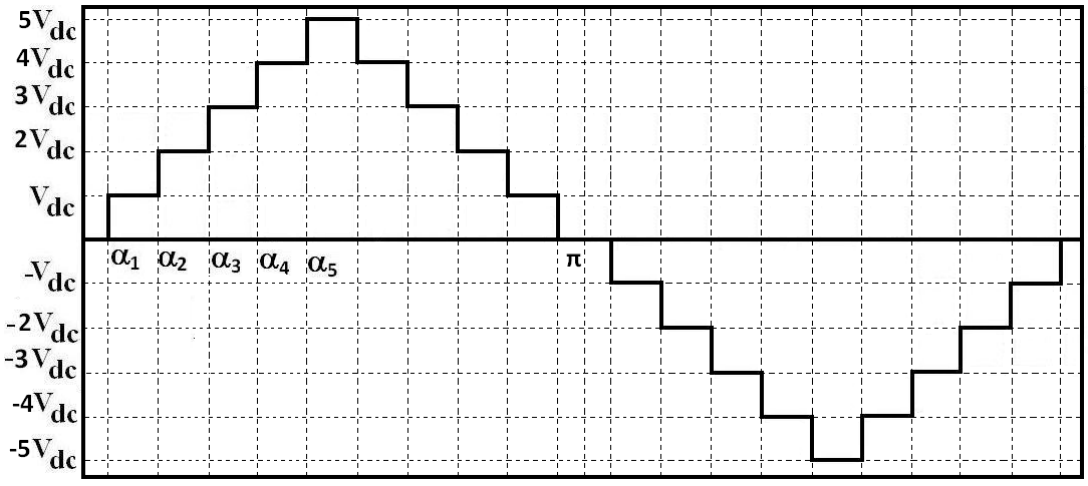

Figure 4.13 Output voltage waveform of cascaded-multilevel inverter

$$V_{an}(\omega t)=\sum_{n=1,5,7,\ldots}^{\infty}\frac{4V_{dc}}{n\pi}\left\{\cos(n\alpha_1)+\cos(n\alpha_2)+\cos(n\alpha_3)+\cos(n\alpha_4)+\cos(n\alpha_5)\right\}\sin(\omega t) \qquad (4.26)$$

Thus the co-efficient of fundamental and other odd harmonics in phase voltage can be obtained from expression (4.26) and a set of equations can be formed to determine the switching angles with selected harmonics eliminated as,

$$\begin{cases} \cos\alpha_1 + \cos\alpha_2 + \cos\alpha_3 + \cos\alpha_4 + \cos\alpha_5 = \mathrm{M} \\ \cos 5\alpha_1 + \cos 5\alpha_2 + \cos 5\alpha_3 + \cos 5\alpha_4 + \cos 5\alpha_5 = 0 \\ \cos 7\alpha_1 + \cos 7\alpha_2 + \cos 7\alpha_3 + \cos 7\alpha_4 + \cos 7\alpha_5 = 0 \\ \cos 11\alpha_1 + \cos 11\alpha_2 + \cos 11\alpha_3 + \cos 11\alpha_4 + \cos 11\alpha_5 = 0 \\ \cos 13\alpha_1 + \cos 13\alpha_2 + \cos 13\alpha_3 + \cos 13\alpha_4 + \cos 13\alpha_5 = 0 \end{cases} \quad (4.27)$$

It can be observed from equation (4.27) that the $5^{th}, 7^{th}, 11^{th}$ and 13^{th} harmonics can be eliminated with a desired value of fundamental. By solving (4.27), the switching angles $\alpha_1, \alpha_2, \alpha_3, \cdots, \alpha_5$ can be computed.

A wide range of harmonic elimination requires more number of switching per quarter-cycle, which can increase switching losses due to higher switching frequency. This imposes a limit on the inverter rating. Thus, efforts should be made to reduce as many number of harmonics as possible with lesser number of switching for lower inverter losses. Conventional SHE-PWM techniques involve elimination of unwanted order harmonics and control of the amplitude of the fundamental component with more number of switchings per cycle. In the present technique, the lower order harmonics are individually eliminated in each DFIG, DVR, STATCOM and UPQC inverter switching while the higher orders are minimized. This requires use of a suitable heuristic optimization technique for practical implementation. In the present work BBO is applied to find the optimum switching angles of the converters. The reasons for obtaining the solution using BBO are the followings:

iv. BBO technique has not yet been explored extensively to solve the problem of converter switching.

v. BBO does not require unreasonable amount of computational effort [121].

vi. Application of BBO is rather straight forward, requires less tuning of its parameters.

The %voltage THD, which can be expressed as,

$$\%THD = \left[\frac{1}{V_{a1}^2} \sum_{n=5}^{\infty} \left(V_{an}\right)^2 \right]^{1/2} \times 100 \text{ , where } n = 6k \pm 1 \text{ for} \left(k = 1, 2, 3, 4, ...\right) \quad (4.28)$$

The objective function $F(\alpha)$ is formulated to satisfy the desired constraints as,

$$F(\alpha) = K_1 \left(V_{a1} - M\right)^2 + K_5 \left(V_{a5} - \varepsilon_5\right)^2 + K_7 \left(V_{a7} - \varepsilon_7\right)^2 + \cdots\cdots + K_n \left(V_{an} - \varepsilon_n\right)^2 \quad (4.29)$$

Subjected to, $0 < \alpha_1 < \alpha_2 < \alpha_3 < ... < \alpha_m < (\pi/2)$ (4.30)

Where V_{a1} is the fundamental amplitude, $K_1, K_5, \cdots, K_n$ are the penalties for the fundamental and individual harmonics which are set to high values so that the magnitudes of $V_{a5}, V_{a7}, V_{a11}, \cdots, V_{an}$ are forced to follow the desired values. The constants $\varepsilon_5, \varepsilon_7, \cdots, \varepsilon_n$ are the permissible limits of individual harmonics which are chosen very close to zero for the selected lower order harmonics. For the present case, the lower order 5^{th}, 7^{th}..13^{th} harmonic

constants $\varepsilon_5, \varepsilon_7, \varepsilon_{11}, \varepsilon_{13}$ are set to 0.0001. For the higher order harmonics from 17^{th},..,31^{st} the constants $\varepsilon_{17}, \cdots, \varepsilon_{31}$ are set as per grid code IEEE519:1992 [104]. On the other hand, the penalties are selected in such a way that the most prioritized component have the greater penalty. For the given problem the values chosen are: K_1=200, K_5=K_7=K_{11}=K_{13}=150, K_{17}=K_{19}=100, K_{23}=K_{25}=80, K_{29}=K_{31}=50. The fundamental value of the output is to be maintained under top priority and hence its given penalty is the highest. In a similar manner the targeted lower order harmonics are given higher penalties as they are intended to be eliminated. On the other hand, the higher order harmonics are given lower penalties as their targeted values are higher. A wrong or random selection these penalties can affect convergence and sometimes might not optimize the objective function as per the given goal. In the present problem, each search point of the population is composed of the switching angles per quarter cycle i.e., from α_1 to α_m. To start the search procedure, the switching angles are randomly generated satisfying the conditions of equation (4.30) for the chosen number of population. Using these random values, individual harmonics are computed which represents the fitness of the search point. The best combination of angles among the population of search points up to present iteration is called the elite or best solution for the variables α_1 to α_m. At each iteration, new search points are generated from the current search points and the information regarding the best solution is found out by using BBO. Considering the probability P_s that the habitat contains exactly S species the change in P_s from time t to time $t+\Delta t$ can be written as,

$$\mathrm{P}_s\left(t+\Delta t\right)=\mathrm{P}_s\left(t\right)\left(1-\lambda_s\Delta t-\mu_s\Delta t\right)+\mathrm{P}_{s-1}\lambda_{s-1}\Delta t+\mathrm{P}_{s+1}\mu_{s+1}\Delta t \tag{4.31}$$

Where λ_s and μ_s are the immigration and emigration rates with S species in the habitat. Assuming that Δt is small enough so that $\Delta t \to 0$ the equation (4.14) can be obtained. For each habitat, the probability of its species count using equation (4.32) is updated and each habitat suitability index (HSI) is computed which satisfies the suitability index variable (SIV) constraints.

$$\dot{\mathrm{P}}_s=\begin{cases}-\left(\lambda_s+\mu_s\right)\mathrm{P}_s+\mu_{s+1}\mathrm{P}_{s+1} & S=0\\ -\left(\lambda_s+\mu_s\right)\mathrm{P}_s+\lambda_{s-1}\mathrm{P}_{s-1}+\mu_{s+1}\mathrm{P}_{s+1} & 1\le S\le S_{\max}-1\\ -\left(\lambda_s+\mu_s\right)\mathrm{P}_s+\lambda_{s-1}\mathrm{P}_{s-1} & S=S_{\max}\end{cases} \tag{4.32}$$

The $\dot{\mathrm{P}}_s$ described by (4.32) for $S=0,\cdots,n$ can be rewritten as a single matrix equation given by,

$$\dot{\mathrm{P}}=\mathrm{AP} \tag{4.33}$$

For the straight line curves shown in [121],

$$\mu_k=\frac{\mathrm{E}k}{n} \text{ and } \lambda_k=\mathrm{I}\left(1-\frac{k}{n}\right) \tag{4.34}$$

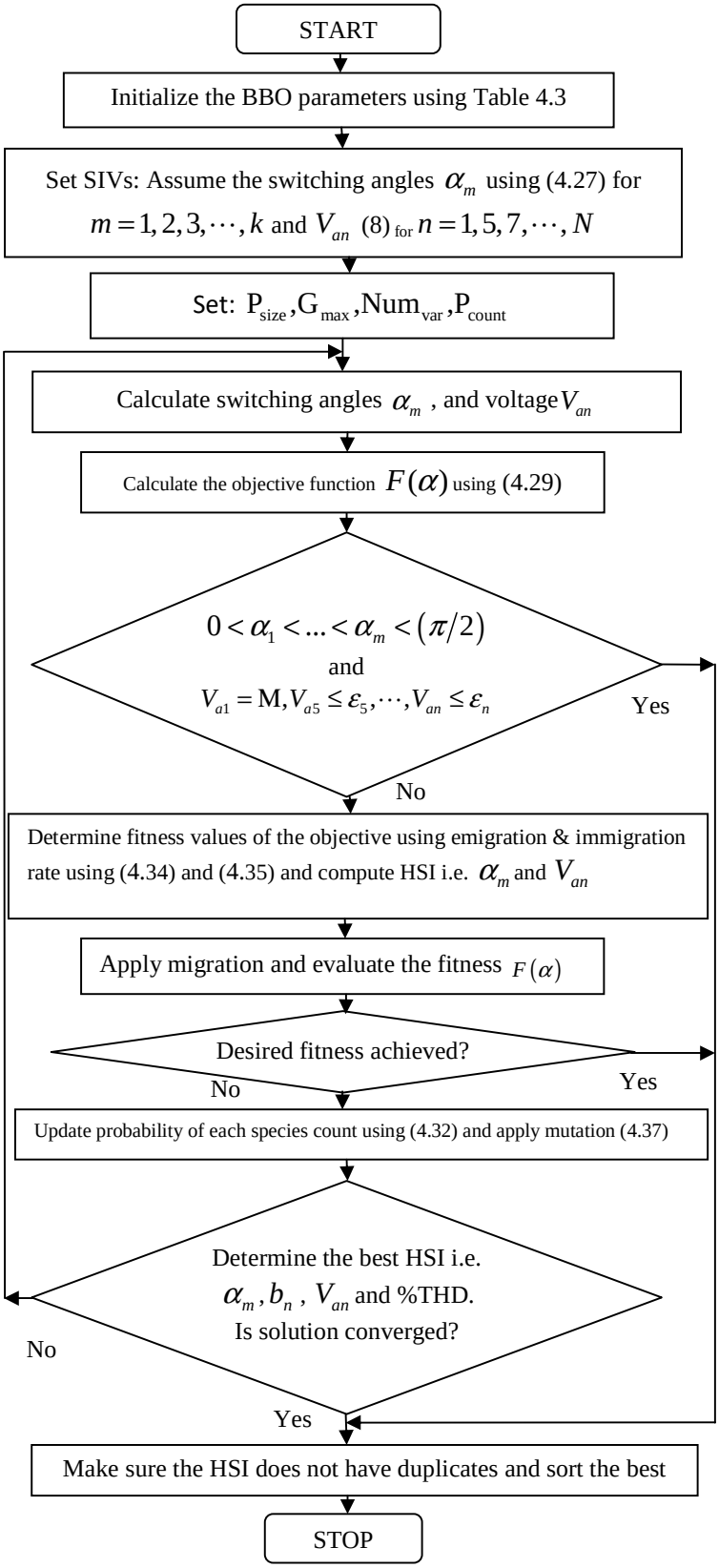

Figure 4. 14 Flowchart of the BBO algorithm**.**

Where, μ_k and λ_k are emigration and immigration rates and k be the number of species. The maximum possible immigration rate to the habitat is I and the maximum emigration rate is E. For the special case where E=I, equation (4.34) can be modified as,

$$\lambda_k + \mu_k = \mathrm{E} \tag{4.35}$$

The steady state value for the probability of the number of each species is given by,

$$\mathrm{P}(\infty) = \frac{V}{\sum_{i=1}^{n+1} V_i} \tag{4.36}$$

Where, V is the eigen vector.

The mutation rate m is inversely proportional to the solution probability is given by,

$$m(S) = m_{\max}\left(\frac{1-\mathrm{P}_s}{\mathrm{P}_{\max}}\right) \tag{4.37}$$

Where $m_{\max}$ (maximum mutation rate) is a user-defined parameter. This equation makes high habitat suitability index (HSI) solutions. The computation algorithm is described through the flowchart given by Figure 4.14.

4.5 Comparative study of different soft-computing techniques

Though the problem described in this chapter can be solved by any search based soft computing techniques e.g. Genetic Algorithms (GA), Particle Swarm Optimization (PSO), Gravitational Search algorithm (GSA) and Cuckoo Search algorithm (CSA), the authors have chosen Biogeography-Based Optimization (BBO) for its simplicity and other advantages already stated in the previous section.

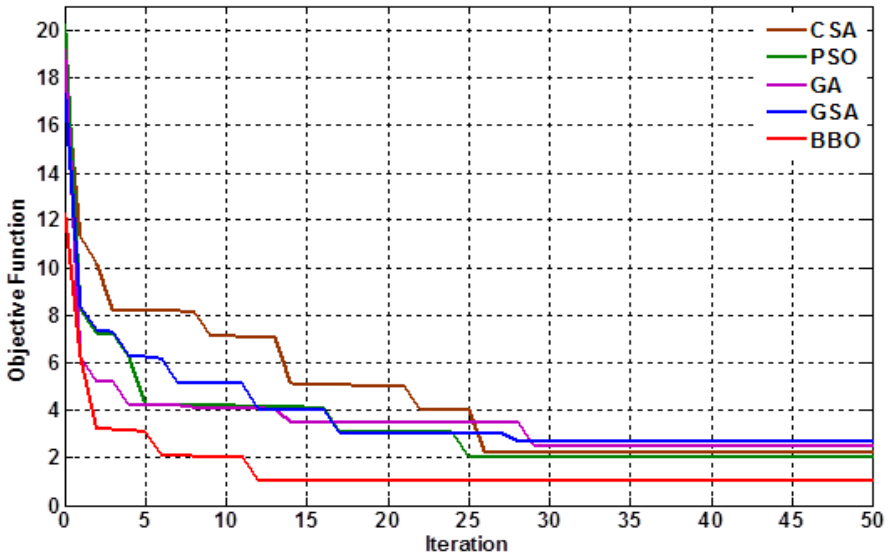

Figure 4.15 Value of the objective function with GA, PSO, GSA, CSA and BBO method for M=0.85 with eliminating 5th, 7th, 11th and 13th, order harmonics.

For justification a comparative study of convergence of the objective function is shown in Figure4.15. A typical case of M=0.85 with elimination of 5^{th}, 7^{th}, 11^{th} and 13^{th}order of harmonics is considered. The parameters taken for different optimization algorithms are given in Table 4.3. Form Figure4.15, it can be observed that convergence through BBO is much faster than other optimization techniques.

Table 4.3 Different parameters for BBO, GSA, PSO, GA and CSA method of computation

BBO		**GSA**	
Total population size (P_{size})	50	Number of agents	50
Generation count limit (G_{max})	50	Maximum iterations	50
Number of genes in each population member (Num_{var})	5	Elitist Check	1 or 0
Mutation probability	0	Index of the test function	1
Habitat modification probability	1	Rpower	1
Initial mutation probability	0.005	Minimum flag	1
Elitism parameter	2	Convergence Iteration	28
Lower bound for immigration probability per gene	0	CPU time (sec)	0.5998
Upper bound for immigration probability per gene	1	%THD	2.9432
Step size used for numerical integration of probabilities	1		
		GA	
Maximum immigration rate for each island	1	Total population size	50
Maximum emigration rate, for each island	1	Generation count limit	50
Convergence Iteration	12	Crossover type single point	1
CPU time (sec)	0.3984	Crossover probability	1
%THD	1.2804	Initial mutation probability	0.01
PSO		Elitism parameter	2
Elitism parameter	2	Convergence Iteration	29
Size of particle swarm neighborhood	0	CPU time (sec)	0.5332
Inertial constant	0.3	%THD	2.2213
Cognitive constant	1	**CSA**	
Social constant for swarm interaction	1	Number of iteration	50
Social constant for neighborhood interaction	1	Discovery rate of alien eggs	0.25
Personal best of each particle	Population	Tolerance	1.00E-05
Neighborhood best of each particle	Population	Lower bounds & Upper bounds	conditionally
global best	Population	Convergence Iteration	26
Convergence Iteration	25	CPU time (sec)	0.4992
CPU time (sec)	0.4821	%THD	2.0943
%THD	2.0122		

4.6 Effect of variation of free parameters with BBO

The effect of variation of free parameters of BBO on switching angles calculation is also studied in the present work. It has been observed that the population size has the most influence on computation of the switching angles. The other parameters like elitism parameters, mutation and migration has negligible impact on the accuracy of the

computed angles. The calculated switching angles along with voltage THD in % are shown in Table 4.4 considering different number of populations. From Table 4.4 it is clear that if the population size is too small or too large the optimization performance will suffer. The considered population sizes in Table 4.4 are 25, 35, 40 and 50 respectively. It can be observed that the fundamental harmonic magnitude are not satisfied as well as 5^{th}, 7^{th}, 11^{th}, and 13^{th} harmonic magnitude are not satisfied for smaller population sizes of 25, 35 and 40. But when the population size is 50, the targeted results are accurately obtained. If the population size is very high above 50 the SIV and the HSI are satisfied but BBO slows down taking larger time to converge. The comparative output phase voltage harmonic spectra with population sizes of 25, 35, 40 and 50 are shown In Figure4.16.

Table 4.4 Computed switching angles, THD and individual harmonic magnitude for BBO with different population size.

Phase voltage harmonics order	Voltage harmonics magnitude when population size is 50	Voltage harmonics magnitude when population size is 25	Voltage harmonics magnitude when population size is 35	Voltage harmonics magnitude when population size is 40	switching angles, %THD, best and mean of Generation	Switching angles when population size is 50	Switching angles when population size is 25	Switching angles when population size is 35	Switching angles when population size is 40
V_1	0.83	0.8185	0.8294	0.829	α_1	6.3667	5.8246	6.1172	6.2964
V_5	0	0.004	0.0017	0.0005	α_2	15.0521	16.499	15.670	15.2199
V_7	0	0.3267	0.1355	0.0162	α_3	23.5422	23.436	23.503	23.5328
V_{11}	0	0.3714	0.1541	0.0212	α_4	37.2328	36.449	36.909	37.1463
V_{13}	0	0.2176	0.0904	0.0141	α_5	58.1614	59.322	58.645	58.2913
V_{17}	0.0177	0.0717	0.0411	0.0241	%THD	3.3703	4.4796	3.8293	3.3813
V_{19}	0.102	0.1332	0.1246	0.1167	Best	*3.3703*	4.4796	3.8293	*3.3813*
V_{23}	0.0395	0.0534	0.0784	0.0936	Mean	*3.3703*	4.4997	3.8293	*3.3823*
V_{25}	0.0168	0.0599	0.0379	0.0293	Elitism parameter	2	2	2	2
V_{29}	0.0209	0.0176	0.0233	0.0267	CPU time	0.3974	0.3845	0.388	0.3878
V_{31}	0.0217	0.0217	0.0329	0.0393	Convergence rate	>95%	86%<	86%<	86%<

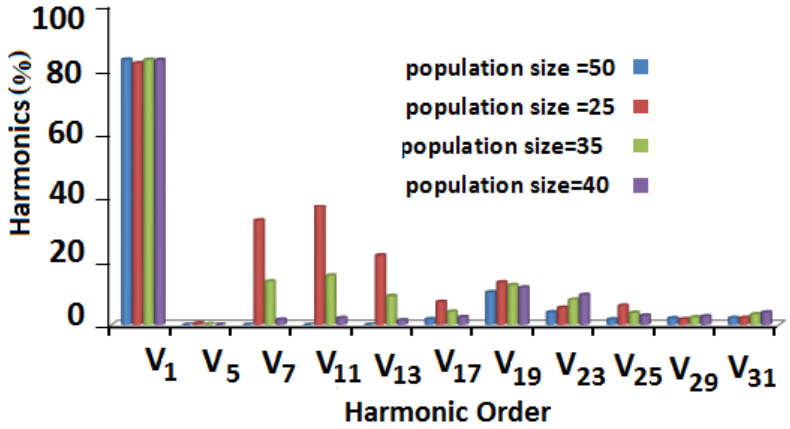

Figure 4.16 Phase voltage harmonic magnitudes for population sizes of 25, 35, 40 and 50.

4.7 Simulation Results for Proposed and Conventional Inverter

Table 4.5 Comparison between % THD for different switching mode when 5^{th}, 7^{th}, 11^{th} and 13^{th} order harmonic eliminated using SHE-BBO optimization technique.

Switching	M	Alpha-1	Alpha-2	Alpha-3	Alpha-4	Alpha-5	% THD
Conventional Unipolar	0.7	25.2877	30.5946	40.8175	48.7581	56.0092	12.4707
	7.5	21.2183	26.9395	36.526	46.8175	53.8419	11.4113
	0.8	18.349	24.9836	33.8218	46.4864	52.0462	10.4206
	0.85	16.0714	23.6406	31.4069	46.1609	49.8861	8.3428
	0.87	15.2132	23.0699	30.3625	45.6847	48.6365	8.2881
	0.9	13.7765	21.7013	28.2888	43.0082	44.8806	8.2881
Conventional Bipolar	0.74	11.3045	15.2224	68.2668	72.2672	87.2139	17.3421
	0.78	10.973	15.1741	68.7919	71.9327	87.6046	13.2356
	0.82	10.6494	15.1398	69.3874	71.6679	87.9947	12.1132
	0.9	9.6869	15.3716	47.1674	47.7364	88.7871	9.2134
	0.91	9.8689	15.4125	45.313	45.6816	88.8972	8.8473
Proposed Multilevel	0.7	8.2387	28.6566	41.305	53.4399	73.3851	6.6748
	0.75	12.7916	21.0151	35.8177	56.5999	61.3167	4.95
	0.8	6.5698	18.9402	27.1833	45.1358	62.2425	3.4308
	0.84	6.3667	15.0521	23.5422	37.2328	58.1614	2.6703
Conventional 120-degree	0.7	25.2877	30.5946	40.8175	48.7581	56.0092	12.5774
	0.75	21.2183	26.9395	36.526	46.8175	53.8419	11.2914
	0.8	18.349	24.9836	33.8218	46.4864	52.0462	10.8888
	0.9	13.7765	21.7013	28.2888	43.0082	44.8806	9.0502
	0.91	12.9566	20.3837	26.7645	39.7003	41.4639	7.8506
Conventional 180-degree	0.6	44.68	52.1617	59.9016	80.2784	85.1307	13.1091
	0.65	16.0737	51.2779	58.1904	75.4281	88.8788	11.7142
	0.7	16.623	50.7743	56.9453	77.2835	88.6002	10.8258
	0.75	17.5192	49.3321	54.9915	79.9317	88.5909	8.0902
	0.77	18.1717	48.1399	53.8236	81.8184	88.8762	7.986
	0.78	18.694	47.2179	53.0702	83.5487	89.327	6.1159

The switching angles corresponding to minimum voltage THD for varying modulation index are stored as look-up table in the memory of the DSP for online application. The elite values are updated after every iteration. The process is repeated until the convergence is obtained. The process terminates if the changes in the fitness values between consecutive iterations are less than a given tolerance, or the fitness values do not change for a number of iterations, or the permissible number of iteration runs are completed. Table 4.5 shows that comparison between % THD for

proposed and conventional different switching mode when 5^{th}, 7^{th}, 11^{th} and 13^{th} order harmonic eliminated using SHE-PWM-BBO optimization technique. The optimum switching angles are calculated off line as a function of modulation index using BBO and stored in microcontroller memory for on line application. The total simulation controls the power quality.

In Figure 4.17 the variation of switching angles with modulation index and the corresponding voltage THD are shown for the proposed multilevel inverter. In Figures. 4.18 to 4.21 the variation of switching angles with modulation index and the corresponding voltage THD are shown for the conventional inverter with 180^0 conduction, 120^0 conduction, unipolar and bipolar mode for comparative study.

For elimination of N no of harmonics, $(N+1)$ switching angles are required. The angles can be obtained after solving he modified expression (9). The selected lower order harmonics for 3-switching are 5^{th} and 7^{th}, for 4-switching are $5^{th}, 7^{th}$ and 11^{th}, for 5-switching are $5^{th}, 7^{th}, 11^{th}$ and 13^{th}, for 6-switching are $5^{th}, 7^{th}, 11^{th}, 13^{th}$ and 17^{th} and for 7-switching are $5^{th}, 7^{th}, 11^{th}, 13^{th}, 17^{th}$ and 19^{th} order respectively. All these harmonics are eliminated by optimizing the switching angle through minimization of the objective function $F(\alpha)$.

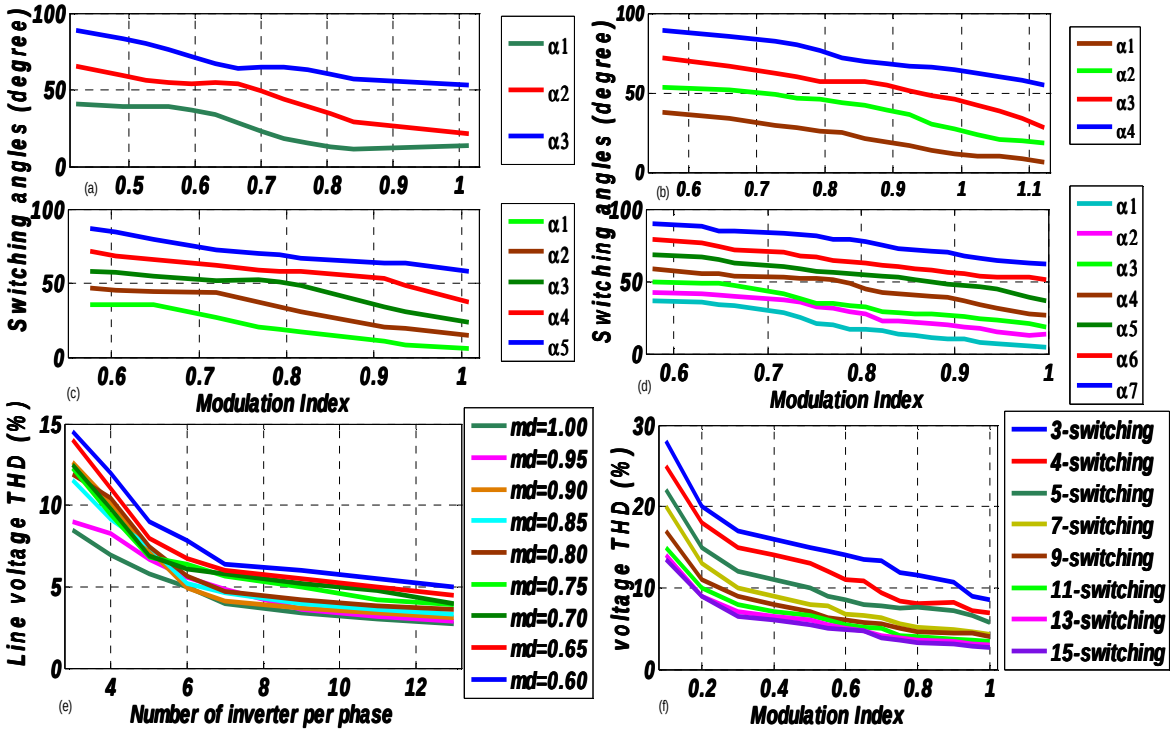

Figure 4.17 Modulation index vs. switching angles : (a) for 7-level cascaded inverter (b) for 9-level cascaded inverter(c) for 11-level cascaded inverter (d) for 15-level cascaded inverter (e) The line voltage THD with constant modulation index as function of the number of inverters per phase. (f) Voltage THD vs. modulation index for level inverter.

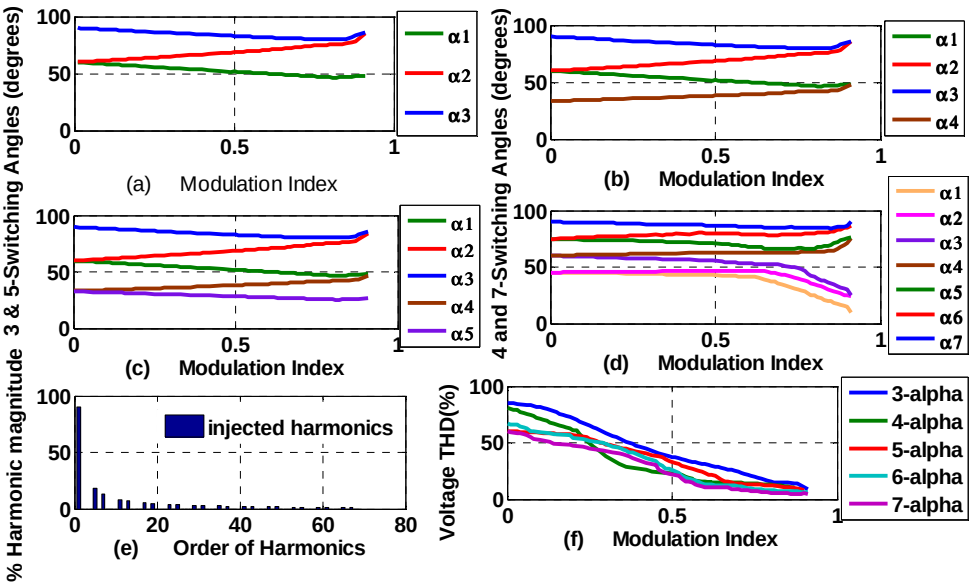

Figure 4.18 Modulation index vs. switching angles for 180 degree conduction mode (a) for 3-switching (b) for 4-switching (c) for 5-switching (d) for 7-switching (e) Harmonic pattern without switching (f) Voltage THD vs. modulation index with different no. of switching angles.

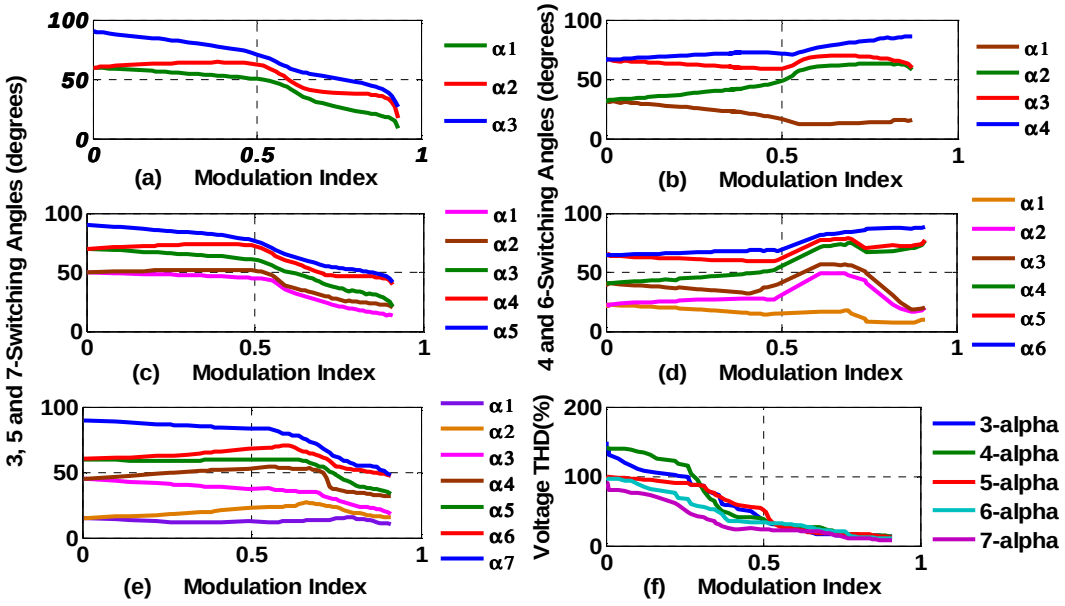

Figure 4.19 Modulation index vs. switching angles for 120 degree (a) for 3-switching (b) for 4-switching (c) for 5-switching (d) for 6-switching (e) for 7-switching and (f) Voltage THD vs. modulation index with different no. of switching angles.

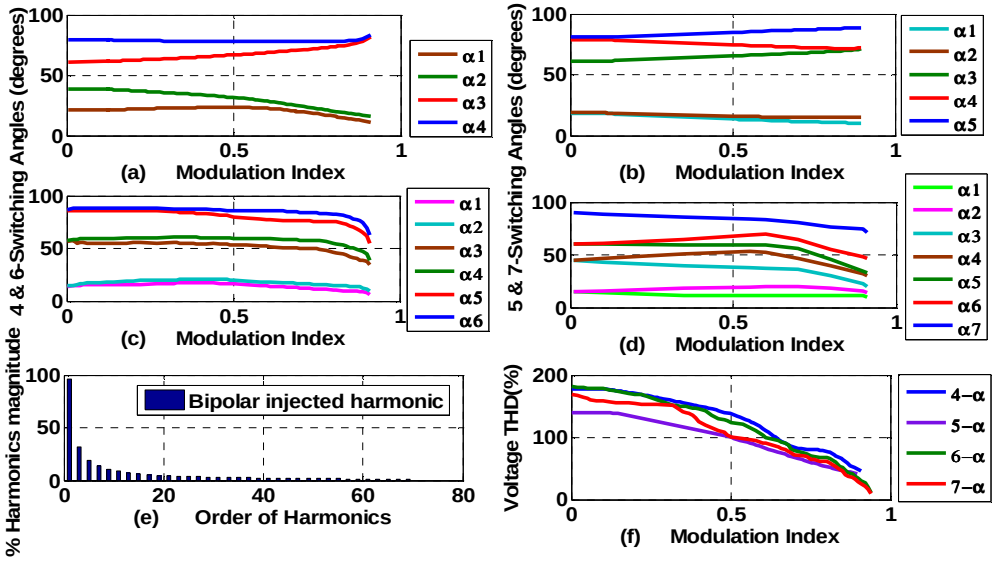

Figure 4.20 Modulation index vs. switching angles for bipolar switching mode (a) for 4-switching (b) for 5-switching (c) for 6-switching (d) for 7-switching (e) Harmonic pattern without switching (f) Voltage THD vs. modulation index.

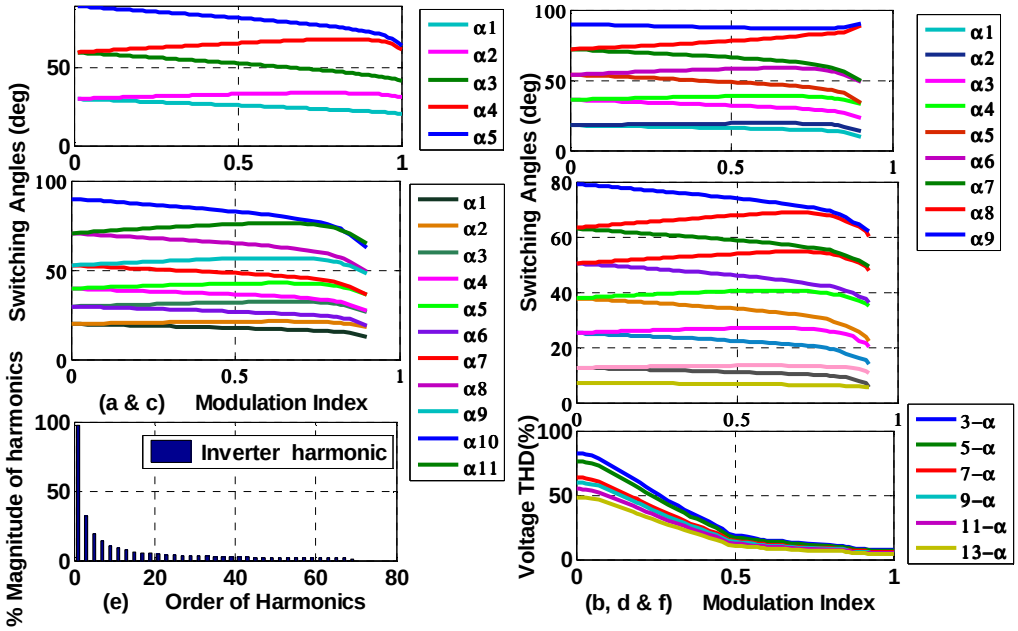

Figure 4.21 Modulation index vs. switching angles for unipolar switching mode (a) for 3-switching (b) for 9-switching (c) for 11-switching (d) for 12-switching (e) Harmonic pattern without switching (f) Voltage THD vs. modulation index with different no. of switching angles.

4.8 Matlab Simulation for PV based DC-DC Converter

The most attractive features of cascade multilevel inverters with separate dc source are as follows like they can operate low switching frequency, they draw very low input current distortion, they generate smaller common-mode

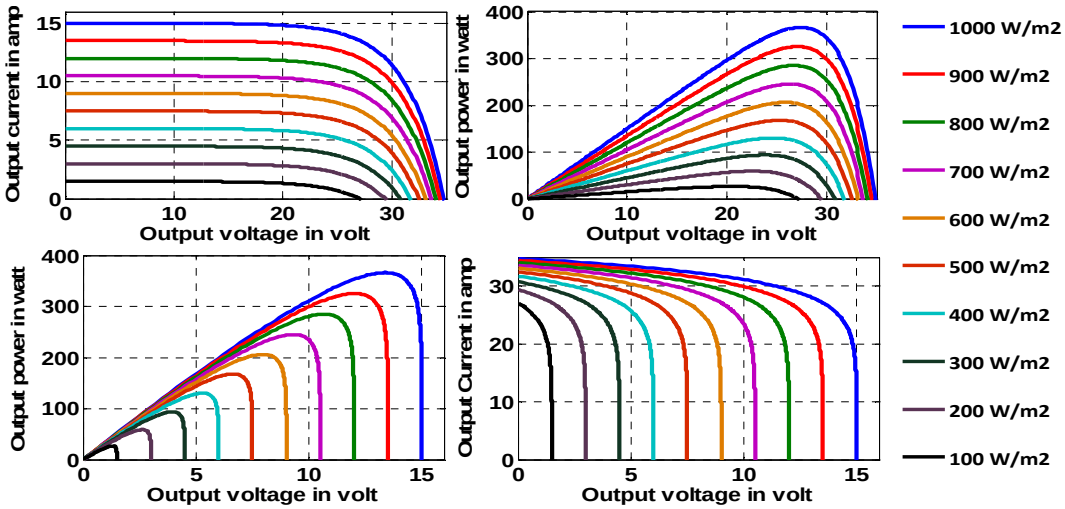

Figure 4.22 Simulation results of (a) I-V characteristics for parallel connection of PV cell (b) P-V characteristics for parallel connection of PV cell (c) P-V characteristics for series connected PV (d) I-V characteristics for series connected PV.

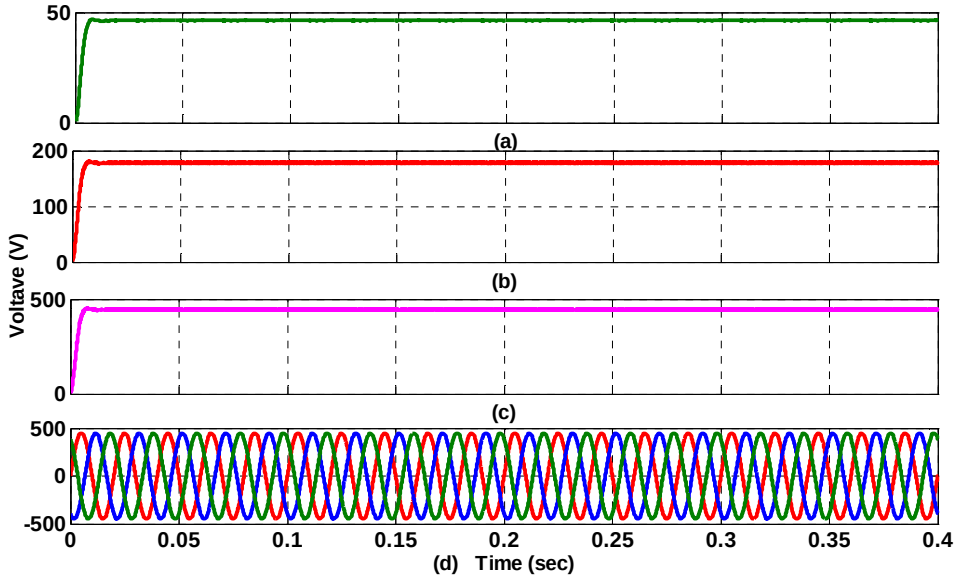

Figure 4.23 The output voltage for (a) PV cell (b) Step-up boost voltage, Stage-1 (c) Step-up boost voltage, stage-2 (d) Filtered output grid voltage.

voltage, circuit layout has more flexible, no extra clamping diodes or balancing capacitor, the output voltage levels can be easily adjusted. However, in the proposed scheme, a single dc source is used and the outputs for the different levels are added with isolation transformers. The schematic diagram for the proposed scheme is shown in Figure 4.12. The multilevel inverters can be easily used in FACTS, DG etc. but the power is not shared equally or it creates new problems such as sub-harmonics. Also for the proposed configuration, unequal power sharing among the different inverters for different levels can occur and as a result, the maximum power point operation for the PV or wind energy system would not be achieved. Therefore, MPPT algorithms are not applicable for the proposed multilevel inverter. On the other hand, for the conventional PWM inverters e.g. unipolar, bipolar etc., MPPT tracking can be easily applicable. In this chapter several PWM switching strategies have been developed for comparative studies. Figure 4.22 shows simulation results of MPPT and different other characteristics for PV inverter operating in 120-deg mode. Figure 4.23 shows the output voltage for PV cell and different other stages of DC to DC converter feeding the proposed multilevel inverter.

4.9 Simulation Results for DVR, STATCOM and UPQC with Filter

Table 4.6 Simulation parameters for the scheme in Figure 4.(1-4).

Description	Parameter	Symbols	Value
PV module specification	No of solar cell	N_{solar}	63 (7x9)
	Nominal voltage	V_{nom}	2x12 V
	Maximum power	$P_{\max}$	219 W
	Voltage at $P_{\max}$	V_{mp}	35.24 V
	Current at $P_{\max}$	I_{mp}	8.37 A
Injection Transformer 1:1	Power	P_{inj}	100 VA
	Voltage rating	V_P/V_S	230/230 V
	Resistance	R_P/R_S	0.0000261 ohm
	Inductance	X_P/X_S	0.0003 ohm
	Magnetizing	X_m	0.00004 ohm
DVR	DC voltage of DVR	V_{dc}	240-260 V
	DC link capacitance	C_{dc}	29 μF
UPQC	Filter inductance	L_f	217µH
	Filter capacitance	C_f	139 µH
	Switching	f_{sw}	4.0 kHz
Parameters of the grid voltage	Nominal voltage	V_s	220-240 V
	frequency	f_s	50 Hz
	Leakage impedance	Z	0.039 pu

The

performance of the SVPWM switching technique of the PV connected DVR, STATCOM and UPQC system is implemented by considering different cases of voltage disturbances such as balance and unbalanced deep voltage sage, voltage swells, voltage flicker, voltage spike, harmonics and voltage variation for long duration. The proposed controller for PV based FACTS compensator establishes the proper voltage quality level that is required by the sensitive load for both normal and transient operation with appropriate active and reactive power control. From the simulation results by using MATLAB/Simulink for multilevel PV based FACTS inverter with and without transformer it is observed that the number of levels reach infinity, the output THD approaches zero, i.e., the switching loss problem is overcome. The simulation and experimental parameters are shown in Table 4.6.

4.9.1 Simulation Results for DVR, STATCOM and UPQC with Filter

For this simulation, the considered DFIG speed is 1550 rpm with 50 Hz frequency and the DVR is turned-on at t=0.15 sec due to the occurrence of a balanced three phase fault due to which a voltage sag results since t=0.25 sec. The system was connected to a nonlinear rectifier type load. Figure 4.24 shows the response of the DVR and other voltage and currents respectively. Similar fault for unbalances condition has also been simulated and the corresponding waveforms are shown in Figure 4.25. In Figure 4.26, the different responses of three phase balanced fault occurring from t=0.15 sec to t=0.25 sec under UPQC mode of operation is shown.

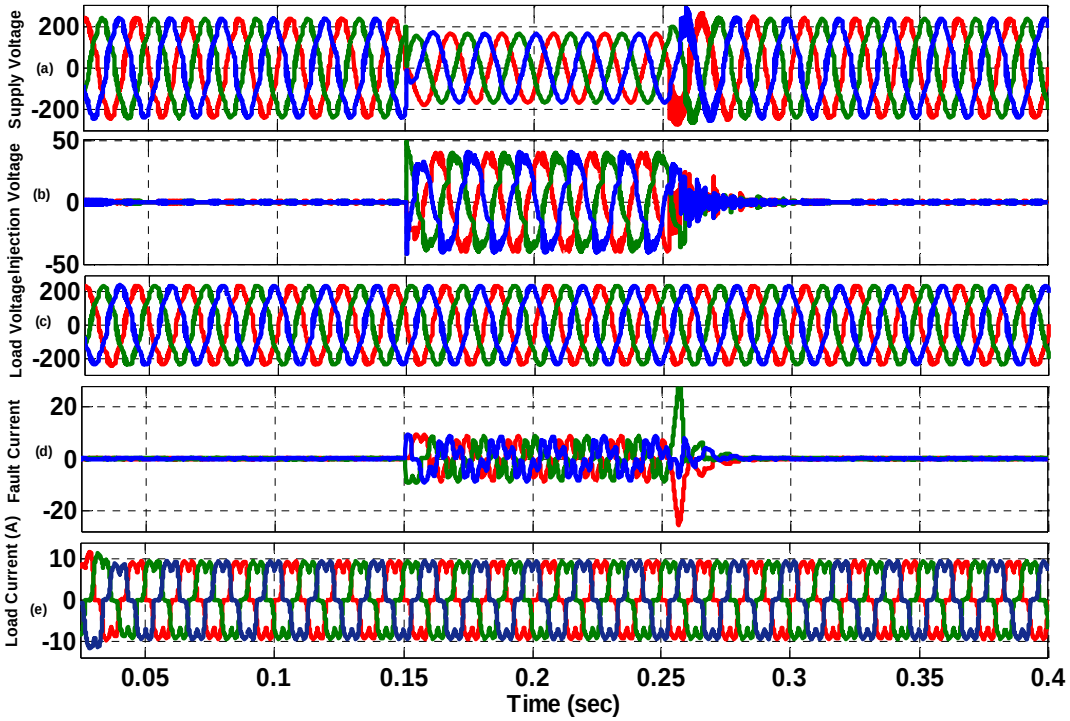

Figure 4.24 Simulated response of DVR for nonlinear (RL) load and voltage sag resulting from balanced three phase fault (a) three phase balanced fault voltage (b) DVR injected voltage (c) three phase load voltage (d) fault current (e) load current.

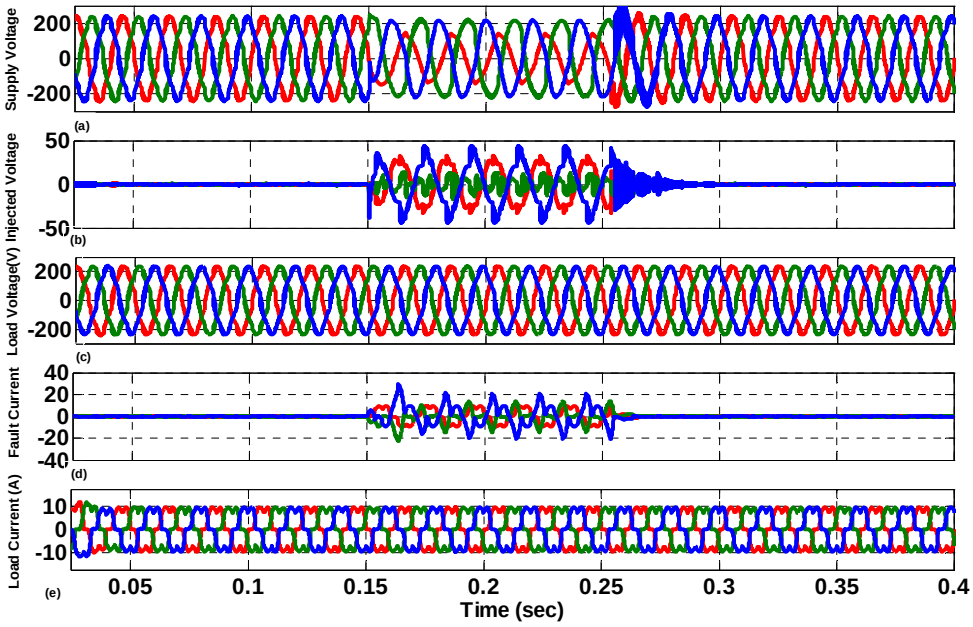

Figure 4.25 Response of DVR with voltage sag for nonlinear (RL) load with phase a, b and ground fault (a) three phase unbalanced fault voltage (b) DVR injection voltage (c) Three phase load voltage (V) (d) three phase fault current (e) three phase load current.

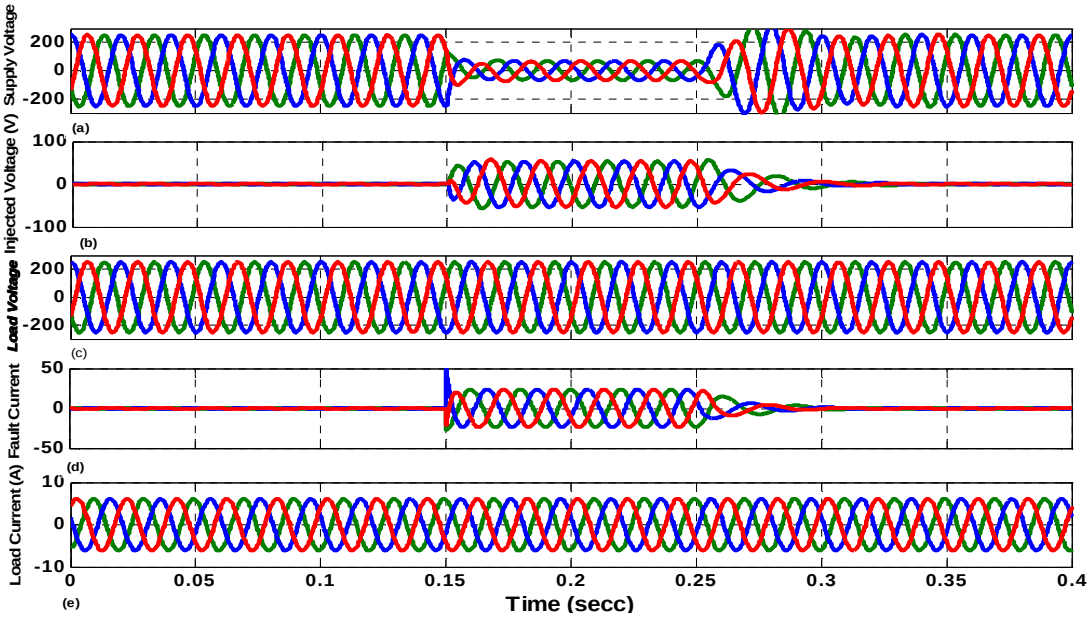

Figure 4.26 Response of UPQC with voltage sag for linear load with balanced three phase fault (a) three phase balanced fault voltage (b) UPQC injection voltage (c) three phase load voltage (d) three phase fault current (e) three phase load current.

4.9.2 Performance Comparison of the proposed DFIG-PV system under UPQC, DVR and STATCOM modes

The present chapter highlights the operation and performance of a PV based power quality compensating equipment operating under UPQC mode supplying nonlinear and voltage sensitive loads. The proposed scheme can provide some common benefits such as power flow control in the distribution system, loading capability enhancement of micro-grid, system security improvement, voltage sag, swell, flicker and spike mitigation. It is observed that the performance of the proposed dual voltage control UPQC compared to that of already available custom power compensators is better. Using dual voltage control loop the UPQC reduces more numbers of injected harmonics to the supply and thereby improving the power quality supplied to nonlinear and voltage sensitive loads. Using shunt connected multilevel converter the UPQC provides the additional VAR requirement by the load

Table 4.7 Harmonic contents of the inverter source voltage with filter and DVR

Harmonic order	DCMLI (five level inverter)			DCMLI (five level inverter)			DCMLI (five level inverter)		
	Before compensation (%)			SVPWM+LC compensation (%)			SVPWM+LC+DVR compensation (%)		
	Phase-A	Phase-B	Phase-C	Phase-A	Phase-B	Phase-C	Phase-A	Phase-B	Phase-C
5	0.08	0.07	0.08	0.05	0.05	0.05	0.03	0.03	0.02
7	0.02	0.05	0.04	0.03	0.03	0.03	0.01	0.002	0.02
11	0.03	0.03	0.01	0.02	0.02	0.02	0.002	0.01	0.001
13	0.03	0.02	0.03	0.02	0.02	0.02	0.001	0.01	0.002
17	0.02	0.02	0.02	0.01	0.01	0.02	0.01	0.001	0
19	0.01	0.02	0.02	0	0.02	0.01	0	0.001	0.01
23	0.02	0.01	0.02	0.02	0	0	0	0	0.01
25	0.02	0.02	0.01	0.01	0.01	0.01	0.001	0.001	0.001
29	0.01	0.01	0.02	0.02	0.01	0.01	0.001	0.002	0.001
31	0.02	0.01	0.03	0	0.02	0.01	0	0.001	0.01
35	0.02	0.02	0.01	0.01	0.01	0.01	0.001	0	0
37	0.03	0.03	0.01	0.01	0	0.01	0.001	0	0
41	0.02	0.03	0.01	0.01	0.01	0.01	0	0.001	0.001
43	0.02	0.02	0.01	0	0.01	0.01	0.001	0.001	0.001
47	0.02	0.01	0.03	0.01	0	0	0	0	0
53	0.01	0.01	0.01	0.01	0.01	0.01	0	0	0
%THD	11.501	11.421	11.471	7.549	7.549	7.416	3.331	3.3376	3.330

Therefore, the additional power factor correction equipment is not necessary. Due to the presence of supply voltage sag, UPQC always maintains load end voltage at the rated value. No real power is consumed by the series connected multilevel compensator. In steady state also the series compensator shares the VAR load along with the shunt compensator, so that the VA rating of shunt compensator is reduced. In Table 4.7 and 4.8, the comparison is shown for different harmonic orders and %THD with only diode clamp multilevel inverter (DCMLI) without PWM,

DCMLI with SVPWM and LC filter, DCMLI with SVPWM and LC filter and DVR operative, DCMLI with SVPWM along with LC filter and STATCOM operative, DCMLI with SVPWM along with LC filter and UPQC operative with and without transformer. The system is loaded with unbalanced nonlinear load in all the cases. It can be observed that the performance in UPQC mode can reduce the individual harmonic magnitudes with reduction in %THD of the injected voltage compared to the other modes.

Table 4.8 Harmonic contents of the inverter source voltage with filter, STATCOM and UPQC with and without transformer.

Harmonic Order	DCMLI (five level inverter) SVPWM+LC+STATCOM Compensation (%)			DCMLI (five level inverter) SVPWM+LC+UPQC (Transformer less) compensation (%)			DCMLI (five level inverter) SVPWM+LC+UPQC (With transformer) compensation (%)		
	Phase-A	Phase-B	Phase-C	Phase-A	Phase-B	Phase-C	Phase-A	Phase-B	Phase-C
5	0.03	0.03	0.03	0.02	0.02	0.02	0.01	0.01	0.01
7	0.01	0.01	0.002	0.003	0.002	0.0012	0.001	0.001	0.002
11	0.002	0.002	0.001	0.002	0.002	0.002	0.001	0.001	0
13	0	0	0.002	0.002	0.002	0.001	0.001	0.001	0.001
17	0.01	0.01	0	0.001	0.001	0.001	0	0	0
19	0.002	0.002	0.002	0	0.003	0	0.002	0.002	0.001
23	0.001	0.001	0.002	0	0	0.001	0	0	0.001
25	0	0	0	0.001	0.002	0.001	0	0	0
29	0.001	0.001	0.01	0.001	0.001	0.001	0.001	0.001	0.001
31	0	0	0	0	0	0	0	0	0
35	0.003	0.003	0.001	0	0	0	0	0	0
37	0.001	0.001	0.002	0	0.002	0.001	0.001	0.001	0
41	0	0	0.001	0.001	0	0	0	0	0
43	0.002	0.002	0	0.001	0	0	0	0	0
47	0	0	0	0	0	0	0	0	0
53	0	0	0.01	0	0.001	0.001	0.001	0.001	0.001
%THD	3.3526	3.3526	3.3511	2.0542	2.0784	2.0308	1.0488	1.0488	1.0440

In Table 4.9, a comparison of % THD for different modes of operation is shown with non-linear load connected to the system. The load side uncompensated phase voltage THDs are 17.76%, 17.64%, 19.85% and the current THDs are 21.36%, 21.53%, 21.87% respectively. It can be observed from Table 4.9 that, after compensation with the different switching techniques, the load side %THD is significantly improved. The improvement is more UPQC mode of operation. On the other hand, Table 4.10 shows the comparison of % THD for different modes of DVR, STATCOM and UPQC for the source side considering the same nonlinear load. The uncompensated source side voltage THDs are 7.37%, 7.96%, 8.73% and current THDs are 9.23%, 9.21%, 9.08% respectively. From Table 4.10,

it can also be shown that the proposed system can improve the source voltage and current THD to a much lower value compared to the other existing schemes.

Table 4.9 Comparison of % THD at load side for different operating modes after compensation with existing and proposed methodology.

(a) DVR mode of operation							
	Phase	Bipolar	Unipolar	120-deg	180-deg	Proposed MLI	DCMLI
MI=0.85	V_{la}	4.21	4.11	3.79	1.86	0.217	0.428
	V_{lb}	4.21	3.98	3.76	1.86	0.195	0.428
	V_{lc}	3.96	3.87	3.41	1.07	0.265	0.386
	I_{la}	5.29	3.43	3.76	2.03	0.628	0.925
	I_{lb}	5.16	4.18	4.13	2.03	0.597	0.899
	I_{lc}	5.31	4.01	3.87	1.98	0.518	0.897
(b) STATCOM mode of operation							
	Phase	Bipolar	Unipolar	120-deg	180-deg	multilevel	DCMLI
MI=0.85	V_{la}	4.35	4.01	3.41	1.87	0.497	0.768
	V_{lb}	4.26	4.03	3.36	1.91	0.476	0.675
	V_{lc}	4.01	3.89	2.98	1.91	0.413	0.675
	I_{la}	2.73	1.98	1.78	1.39	0.554	0.589
	I_{lb}	3.12	1.98	1.86	1.38	0.627	0.711
	I_{lc}	3.91	1.37	1.86	1.38	0.532	0.711
(c) UPQC mode of operation							
	Phase	Bipolar	Unipolar	120-deg	180-deg	multilevel	DCMLI
MI=0.85	V_{la}	4.35	3.13	2.58	1.21	0.067	0.325
	V_{lb}	4.26	3.21	2.31	1.31	0.032	0.325
	V_{lc}	4.01	3.21	2.17	0.98	0.073	0.287
	I_{la}	2.11	1.21	1.36	1.21	0.521	0.896
	I_{lb}	2.79	1.93	1.41	1.43	0.428	0.751
	I_{lc}	2.63	1.68	1.41	1.43	0.179	0.772

Table 4.10 Comparison of % THD at source side for different operating modes after compensation with existing and proposed methodology.

(a) DVR mode of operation							
	Phase	Bipolar	Unipolar	120-deg	180-deg	Proposed MLI	DCMLI
MI=0.85	V_{sa}	3.02	2.97	2.01	1.08	0.327	0.397
	V_{sb}	4.21	2.97	2.01	1.13	0.203	0.397
	V_{sc}	3.15	1.83	1.98	1.13	0.203	3.79
	I_{sa}	4.23	2.88	2.78	1.89	0.512	0.794
	I_{sb}	4.15	2.93	2.68	1.09	0.311	0.748
	I_{sc}	3.97	2.93	2.32	1.09	0.311	0.748
(b) STATCOM mode of operation							
	Phase	Bipolar	Unipolar	120-deg	180-deg	multilevel	DCMLI
MI=0.85	V_{sa}	3.77	2.16	2.32	1.17	0.389	0.482
	V_{sb}	4.39	2.38	2.31	1.15	0.283	0.474
	V_{sc}	3.52	2.17	2.41	1.15	0.283	0.474
	I_{sa}	3.63	2.72	1.54	1.02	0.592	0.658
	I_{sb}	4.61	2.72	1.56	1.01	0.373	0.687
	I_{sc}	3.63	2.71	1.56	1.01	0.382	0.687
(c) UPQC mode of operation							
	Phase	Bipolar	Unipolar	120-deg	180-deg	multilevel	DCMLI
MI=0.85	V_{sa}	2.87	2.01	1.68	1.01	0.139	0.247
	V_{sb}	3.21	2.01	1.68	1.13	0.082	0.231
	V_{sc}	3.21	2.07	2.02	1.13	0.082	0.231
	I_{sa}	2.97	2.01	1.23	0.96	0.452	0.523
	I_{sb}	2.97	2.01	1.23	0.93	0.309	0.517
	I_{sc}	2.03	1.98	1.05	0.93	0.109	0.517

4.10 Experimental Result and Discussion

The proposed scheme is experimentally verified for 180-deg and 120-deg mode for a speed variation between1460 rpm to 1560 rpm through synchronous speed of 1500 rpm at 75% full load after eliminating harmonics up to 25^{th} order from the rotor voltage. The corresponding experimental plots are shown in Figure 4.27 (a) for stator current with changing speed for 120-degree conduction mode. In Figure 4.27 (b) the experimental waveform for stator voltage for 180-degree conduction mode is shown. Figure 4.27 (c) and (d) shows the experimental waveforms for rotor current with changing speed for 180-degree conduction mode and for stator voltage for 120-degree conduction mode.

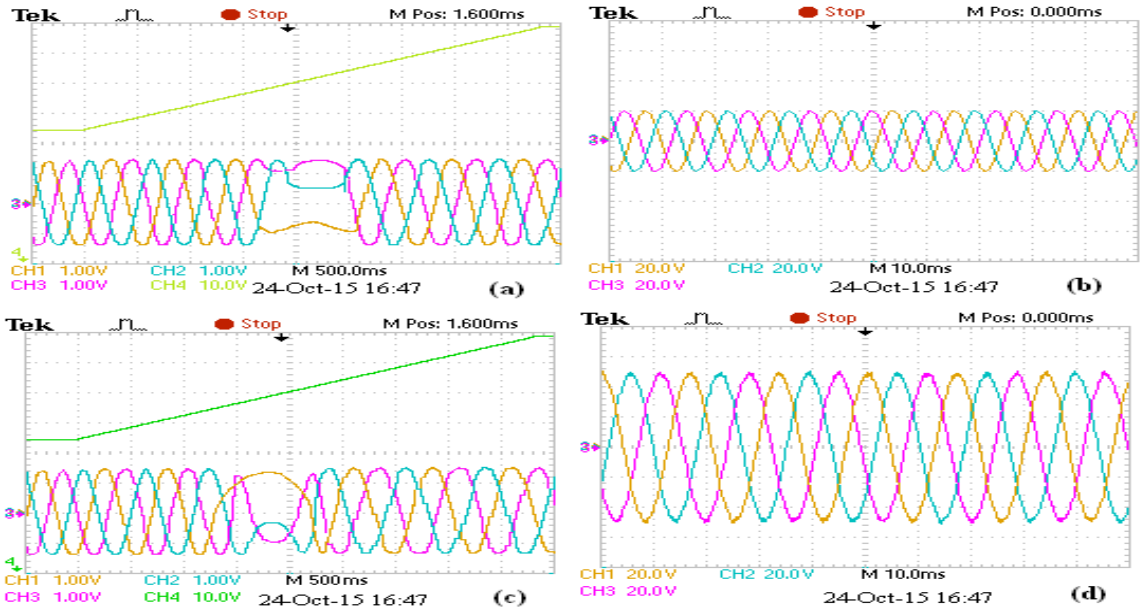

Figure 4.27 Experimental output waveforms of DFIG (a) rotor current with changing speed (Channel 1, 2 and 3: Y-axis: 10A/div., Channel 4: Y axis 30 rpm/div.) for 120-degree conduction mode. (b) Stator voltage (Channel 1, 2 and 3: Y-axis: 600V/div.) for 180-degree conduction mode. (c) Rotor current with changing speed (Channel 1, 2 and 3: Y-axis: 10A/div., Channel 4: Y axis 30 rpm/div.) for 180-degree conduction mode. (d) Stator voltage (Channel 1, 2 and 3: Y-axis: 250V/div.) for 120-degree conduction mode.

4.11 Conclusion

This chapter investigates the new model of PV-wind based hybrid DG system suitable for DVR, STATCOM and UPQC modes of operation. The proposed technique is capable to compensate networks faults, injected harmonics and load harmonics, reactive power in distribution power systems. The DVR has the boundary on capability of injection of active power i.e., either zero or minimum active power mode. The harmonics of the output voltage are eliminated by ML-SHE-PWM switching technique and corresponding THD is also low. The injected harmonics for the proposed system is significantly reduced using BBO based optimized switching. The BBO technique is used to eliminate or reduce more number of harmonics with less number of switching for improved inverter efficiency. A comparison of BBO based computation of switching angles for this problem with other existing soft computing techniques has also been made for justification of usage of BBO. The quality of the load voltage during the operation of DVR, STATCOM, UPQC and this THD also can fulfill IEEE 519 std. range. Different simulation study cases are verified to evaluate the potential application of the proposed control approach with various advantages. Various experimental results are also shown to justify the proposed concept.

Chapter 5

Proposed Photovoltaic (PV) based Dynamic Voltage Restorer (PV-DVR)

Chapter 5

5.1 Chapter Overview

In this chapter, a photovoltaic (PV) based Dynamic Voltage Restorer (PV-DVR) is described which can mitigate voltage sags, swells, flickers and harmonics for low or medium voltage residential micro-grid system. The existing DVR system usually compensates the grid abnormalities without considering the injected harmonics or the device losses which can oversize the system. The proposed PV-DVR system consists of a selected harmonic elimination and moderation PWM (SHEAM-PWM) based multilevel inverter system fed from PV module, step-up DC–DC boost converter and a series injection transformer. The multilevel inverter is chosen to reduce device voltage stress while optimizing number of switching to reduce switching losses. The proposed configuration can reduce overall voltage THD to a considerable amount and achieve high dynamic performance. Biogeography-Based Optimization (BBO) -based SHEAM-PWM technique is employed for switching optimization purpose. The optimum switching angles are computed off line to eliminate the lower order harmonics and the switching angles are stored in microcontroller processor memory using mixed model equations for on line application. The proposed method is simulated considering a practical system and the results indicate that the voltage harmonics are highly reduced by the proposed technique.

5.2 Introduction

In the modern civilization, the consumption of fossil fuel is increasing continuously with the abruptly increase in power demand. Consequently, the energy crisis and environmental pollution problems are becoming a grave concern. As an aftermath, the renewable energy sources are drawing a great attention as the substitute of fossil fuel based habitual electric power system. Studies on varying nature of wind, integration of large wind generating system in to electric power grid have been covered in [122]. The technological improvement on grid integration with solar PV system has been studied in [123]. Analysis of the mathematical properties and physical nature related to the hydro-power generation optimization problem has been implemented in [124]. Optimization of the performance of a biomass steam gasification system with integrated solar assisted steam production and electricity generation by a micro gas turbine has been studied in [125]. Usage of various types of bio-fuels as sources of energy is shown in [126]. For discontinuous operation of solar power plant, the low temperature geothermal water is introduced in [127] to overcome the problem.

Besides the linear load, the use of non-linear load is also increasing day-by-day which demands stricter power quality. The improved and reliable power quality problem includes minimization of THD, voltage sag, swell, flicker and reduction of three phase voltage unbalance [128] etc. There are a number of power quality improvement devices reported in open literature, such as, renewable energy based distributed generation (DG) systems (e.g., wind turbine farms(WTFs), photovoltaic panels (PVPs), bio-fuel engines, biogas based engines, cogeneration, etc.), energy storage systems (e.g. batteries, capacitors, super capacitors, flywheels, electromagnetic storage, proton exchange membrane fuel cell (PEMFC) etc.), superconducting magnetic energy (SMES) systems (e.g., voltage source inverter SMES (VSISMES), current source inverter SMES (CSISMES), etc.), high voltage direct current (HVDC) systems

pertaining to the offshore wind farms, flexible alternating current transmission system (FACTS) devices based on energy storage elements (e.g., static var compensators (SVCs), static synchronous compensators (STATCOMs), unified power flow controllers [129] (UPFCs), etc.), and custom power devices based on energy storage systems (e.g., dynamic voltage restorers (DVRs), active power filters (APFs), etc.)

Among these FACTS devices, DVR [130] is an effective custom power device, being one of the key components of distributed generation systems (DGSs) connected to micro-grids (MGs). This DVR is a series connected and energy storage based device. DVR can mitigate voltage sag, swells, flickers and compensate voltage harmonics along with limit on transient voltages and fault currents.

PWM scheme is required to control the three phase inverter, connected to PV. The THD ratios are obtained at proper values according to international standards and grid codes. SHEAM-PWM technique with optimized harmonic elimination for low switching frequency is very suitable for a proposed inverter circuit. The SHEAM-PWM method reduce the values of specific harmonics to meet the grid codes, instead of making them zero, which limit the harmonics amounts in the grids. It can eliminate the specific harmonic components. The elimination of specific harmonics from a given output voltage waveform generated by voltage source inverter using PWM has been reported in [34, 73, 131]. SHE-PWM [35, 74, 132] offers a tight control of the harmonic spectrum of a given voltage waveform, generated by a power electronic converter along with a low number of switching transition. These methods can theoretically provide the highest quality output among all the PWM methods. The SHE problem becomes complex with the increase in number of harmonics to be eliminated.

Multilevel inverters [133] are gaining more importance for their usage in high-power medium voltage applications due to their superior performance compared to two-level inverters, e.g. lower common-mode voltage, draw input current with very low distortion, lower harmonics in output voltage or reduced voltage stress on the power switches. SHE-PWM technique along with the multilevel topology generates less harmonic distortion in the output voltages waveform without using any filter circuit and considering low number of switching to reduce switching losses. However, in high frequency PWM like in phase disposition sinusoidal pulse width modulation (SPWM), the THD depends on carrier frequency [134], which can increase inverter losses.

The use of a custom power device DVR, or a voltage sag/swell compensator, is one of the most effective solutions to “restoring” the quality of voltage at its load-side terminals when the quality of voltage at its source-side terminals is disturbed. This chapter develops a framework for optimization of switching for a PV based DVR, connected to micro-grid. PV based DVR connected inverter switching schemes is anticipated to diminish the overall voltage THD. Since the inverters connected to the grid system are subjected to handle bulk amount of power, so, a lesser number of switching per cycle is advantageous for satisfactory operation and reduced switching losses (lower switching frequency means lower switching loss i.e., higher efficiency is achieved). The BBO-based [52, 87, 121, 135] SHE-PWM technique can be applied to low and high switching of the inverters. In the present approach, for the inverters connected to the PV-DVR, a SHEAM-PWM based algorithm is used to compute the switching angles leading to elimination of selected lower order harmonics for grid harmonic and also mitigate the voltage sags, swells

and flicker. In the present approach, the SHEAM-PWM algorithm optimizes the harmonics to contribute the minimum THD at all modulation indices. As the number of levels reach infinity, the output THD approaches zero. That can overcome the switching loss problem, as well as Electromagnetic Interference problem. In [136, 137] the hybrid BBO/MADS algorithms for selective harmonics elimination employing BBO algorithm have been presented. The study on inverters with multifunctional ability connected to grid for various purposes has also been carried out in [138-140].

In this chapter, PV based DVR with cascaded multilevel configuration is proposed to provide an effective solution to the grid abnormalities e.g. voltage sags, swells, flicker etc. Since the DVR is fed from an isolated PV source, the DVR controller will not be directly affected by grid disturbances. This constitutes one of the foremost advantages of the projected scheme. Moreover, as a multilevel inverter is used in the proposed scheme, the number of switchings is reduced compared to the two level inverters used in the existing schemes, while maintaining low harmonic injection. An optimized SHEAM-PWM technique is used to reduce harmonic injection for the proposed scheme. This can reduce switching losses considerably to provide better converter efficiency. The utility of the proposed method has been verified through simulation with low and medium voltage three phase DVR prototypes under various grid conditions including distorted supply voltage, nonlinear load, placement of capacitors near a DVR and an induction motor load for justification.

5.3 Proposed micro-grid configuration with DVR

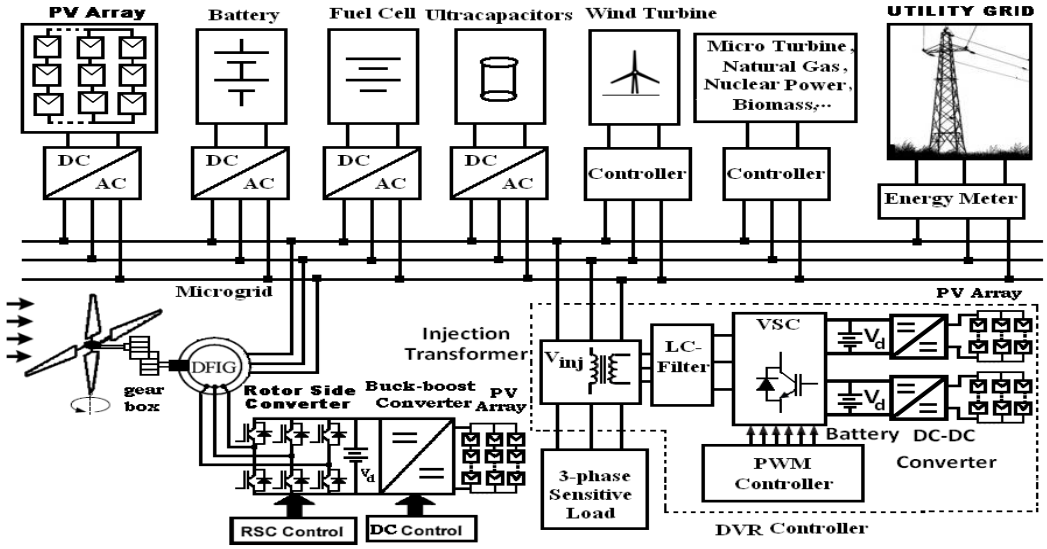

Figure 5.1 Schematic diagram of a proposed micro grid system.

Figure 5.1 shows the configuration of the proposed micro-grid consisting of PV based DVR system connected to a critical load terminal. During disturbance in a network DVR injects an appropriate voltage to recover the voltage at the load and exchanges active and reactive power with the surrounding system. As per the IEEE 519-1992 and IEEE 1159-1195 standards, a typical allowable duration of voltage sag and voltage swell is mentioned to be 10 ms to 1 min [141].

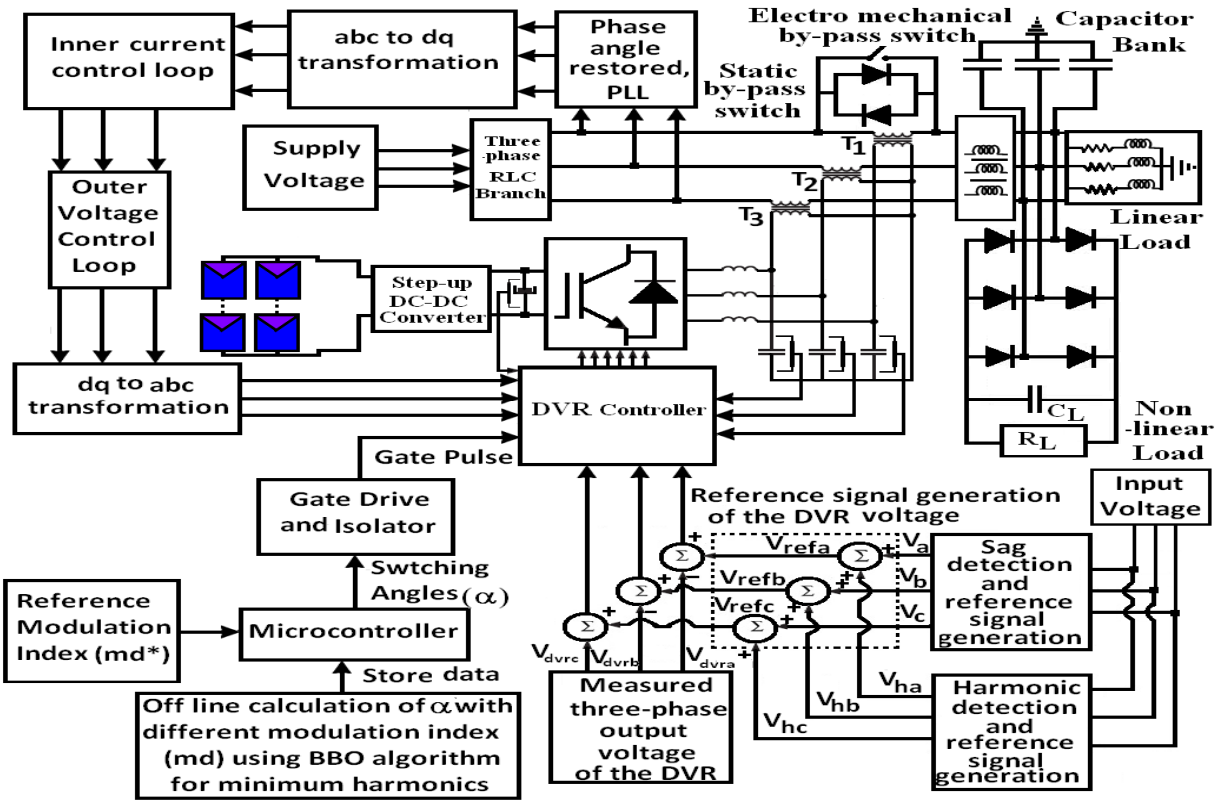

Figure 5.2 Schematic diagram of a simulation circuit of PV-DVR system.

The schematic diagram of proposed PV-DVR simulation circuit is illustrated in Figure 5.2. The proposed system consists of a PV array, multi-level equal and unequal voltage source converter (VSC), step-up DC-DC converter, battery, energy storage device (ESD), PWM inverter, series injection transformer, an inverter output filter etc. The PV panel output is connected to the micro-grid through dc to dc converter in series with a three-phase bridge inverter. A battery V_d is connected between the two converters to store the extra energy from the PV panel when the grid side power demand is less than PV panel output. This also can act as a dc source in the absence of solar irradiation and injects power to the micro-grid. The grid connected inverters handles high current. Thus the devices will have high current stress both during switching and continuous conduction modes. Since the conduction current cannot be minimized, as these dependents on load, the switching losses should be reduced. Thus in the proposed scheme the number of switching is optimized to have optimum switching and the harmonics are also reduced below a considerable level.

The harmonics injected from the DVR inverters to the distribution system can potentially affect critical loads. In the multilevel inverter based DVR; the number of output voltage levels generally depends on the voltage sag depth. Also the multilevel inverters operate with high modulation indices regardless of the voltage sag depth. The LC filter installed between the VSC and injection transformer, reduces harmonic in the output of DVR. The filter voltage is injected into distribution system via series injecting transformer. The required phase angle of the utility supply is obtained through Phase Locked Loop (PLL) as shown in Figure5.2. In multilevel inverter, the harmonic quality of

voltage is directly related to the number of voltage levels considered, which is improved with number of voltage levels. The proposed control strategy for the DVR circuit improves the voltage sag/ swells conditions while reducing the harmonics from the output voltage waveform.

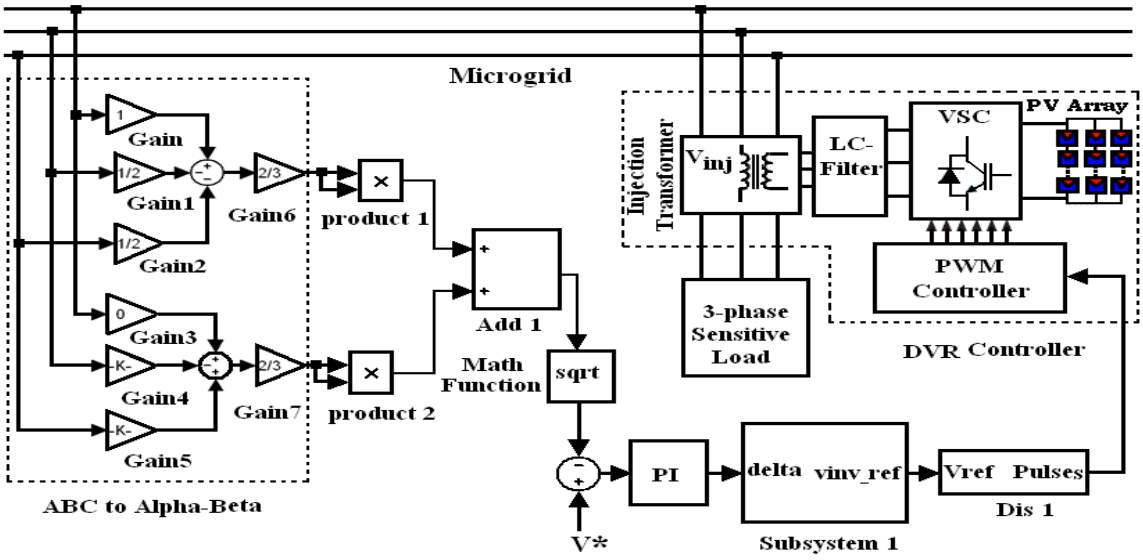

Figure 5.3 Schematic diagram of a PV-DVR with reactive power control circuit.

Table 5.1 Filter parameters for % THD calculation (for five level inverter)

Description	Parameter	Symbols	Value	Without filter %THD	With filter %THD
LC Filter	Filter inductance	L_f	35 mH		0.09
	Filter capacitance	C_f	21 μF		
2nd order LP filter	Cut of frequency	f_c	200	5.108	0.131
	damping factor	d	0.707		
Three phase Harmonic filter	frequency	f_n	50 Hz		0.46
	quality factor	Q	16		

The LC filter capacitor is connected in the line side to obtain relatively faster dynamic response, while eliminating the voltage notches or spikes at the beginning and ending of voltage sags and improving the load voltage THD. The filter capacitor is inserted in the converter side to filter the high-frequency switching harmonics locally. The filter and simulation parameters are shown in Table 5.1 and Table 5.2 respectively. The schematic diagram of a PV-DVR with reactive power control circuit is shown in Figure 5.3. This control circuit controls the reactive power at normal

and transient conditions. From Table 5.1, it is found that; %THD in case of LC filter is 0.09%, which is smaller than that of other filters mentioned above.

Table 5.2 Simulation parameters for the scheme in Figure 5.1.

Description	Parameter	Symbols	Value
PV module specification	No of solar cell	N_{solar}	54 (6x9)
	Nominal voltage	V_{nom}	12 V
	Maximum power	$P_{\max}$	200 W
	Voltage at $P_{\max}$	V_{mp}	29.22 V
	Current at $P_{\max}$	I_{mp}	5.36 A
Step-up DC-DC converter	Inductance	L_m	13 μH
		L_k	0.27 μH
	Switching frequency	f_{s2}	120 kHz
	Capacitance	C_1	315.1 μF /100 V
	Output DC voltage	V_0	230 V
Injection Transformer 1:1	Power	P_{inj}	100 VA
	Voltage rating	V_P/V_S	230/230 V
	Resistance	R_P/R_S	0.0000001 ohm
	Inductance	X_P/X_S	0.0005 ohm
	Magnetizing	X_m	0.00005 ohm
DVR	DC voltage of DVR	V_{dc}	260 V
	DC link capacitance	C_{dc}	25 μF
Three phase PLL	Regulator gain	K_p	180
		K_i	3200
		K_d	1
Parameters of the grid voltage	Nominal voltage	V_s	240 V
	frequency	f_s	50 Hz
	Leakage impedance	Z	0.035 pu

5.4 Existing and Proposed Switching Strategies:

The PV-DVR voltage waveform fed from inverter is generally a quasi-sine wave, which in turn, reduces switching losses in the semiconductor devices. The inverters can be switched under SHEAM-PWM mode of operation to eliminate some of the significant harmonics from the PV-DVR voltage waveform.

5.4.1 Multilevel operation

The concept of BBO-based multilevel voltage source inverters and their modulation topologies are described in this chapter. By applying this concept, appropriate switching angles can be calculated, specific harmonics can be eliminated, and the output voltage THD can be improved. A wye-configured m-level cascaded-inverter is illustrated in Figure 5.4 which used for the proposed system. The proposed system the dc sources of the multilevel inverter are all equal to one another or not equal to one another.

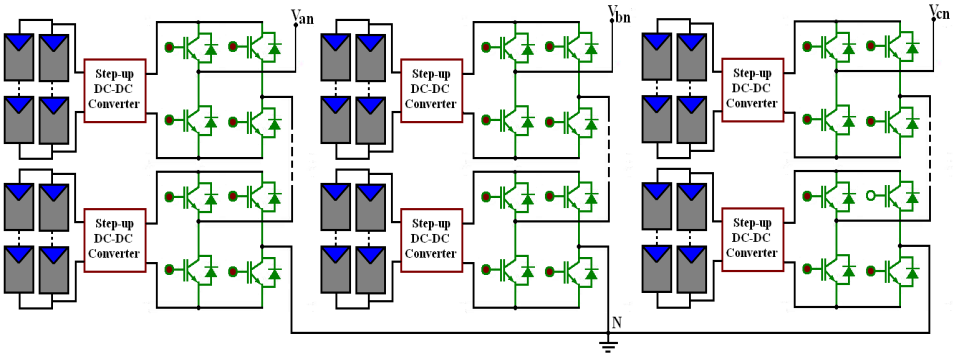

Figure 5.4 A general three-phase Wye-configuration of cascaded-multilevel inverter

For cascade multilevel inverter the phase voltage waveform is shown in Figure 5.5, where the level is m=6 including 0 level. From this phase voltage we finding the switching angles to eliminate the specific harmonics per half phase per leg is

$$V_{an} = V_{a1} + V_{a2} + V_{a3} + V_{a4} + \cdots + V_{am-1}$$

Due to the quarter-wave symmetry both the Fourier coefficient a_0 and a_n are zero and we get the harmonic coefficient as

$$b_n = \frac{4V_{dc}}{\pi}\left[\int_{\alpha_1}^{\pi/2} \sin(n\omega t)d(\omega t) + \int_{\alpha_2}^{\pi/2} \sin(n\omega t)d(\omega t) + \cdots + \int_{\alpha_{m-1}}^{\pi/2} \sin(n\omega t)d(\omega t)\right]$$

And finally the b_n coefficient is in equation

Figure 5.5 shows the multilevel output-voltage waveform of phase-a for the proposed inverter. Waveform for V_{an} is known as an odd-quarter wave symmetric. The phase voltage waveform of a 3-phase multilevel bridge inverter is a quasi-square wave. Due to the quarter-wave symmetry,

$a_0 = 0$ and $a_n = 0$ for all n, and $b_n = 0$ for all even n

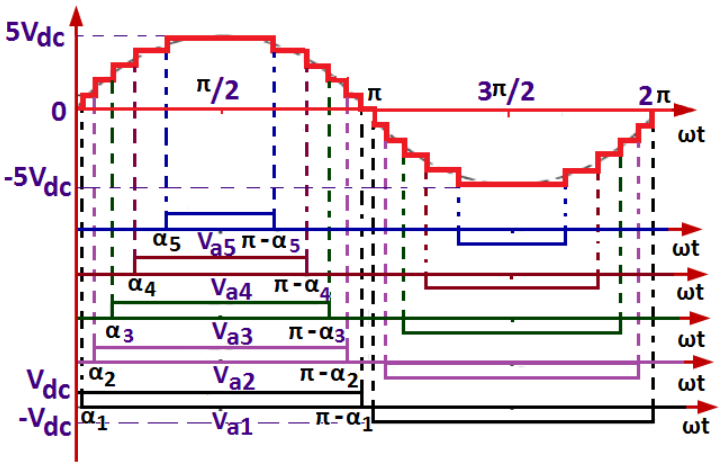

Figure 5.5 The output phase voltage waveform for 5 separate dc source and 11-level cascade multilevel inverter.

Thus for all odd n,

$$b_n = \frac{4V_{dc}}{n\pi}\left[\sum_{i=1}^{m-1}\cos(n\alpha_i)\right] \tag{5.1}$$

For $n = 6k \pm 1$, and $k = 0,1,2,3,\cdots$, the harmonic coefficient are in the form as

$$b_1 = \frac{4V_{dc}}{\pi}\left[\cos(1\alpha_1)+\cos(1\alpha_2)+\cos(1\alpha_3)+\cos(1\alpha_4)+\cos(1\alpha_5)\right]$$

$$b_5 = \frac{4V_{dc}}{5\pi}\left[\cos(5\alpha_1)+\cos(5\alpha_2)+\cos(5\alpha_3)+\cos(5\alpha_4)+\cos(5\alpha_5)\right]$$

$$b_7 = \frac{4V_{dc}}{7\pi}\left[\cos(7\alpha_1)+\cos(7\alpha_2)+\cos(7\alpha_3)+\cos(7\alpha_4)+\cos(7\alpha_5)\right]$$

$$b_{11} = \frac{4V_{dc}}{11\pi}\left[\cos(11\alpha_1)+\cos(11\alpha_2)+\cos(11\alpha_3)+\cos(11\alpha_4)+\cos(11\alpha_5)\right]$$

$$b_{13} = \frac{4V_{dc}}{11\pi}\left[\cos(13\alpha_1)+\cos(13\alpha_2)+\cos(13\alpha_3)+\cos(13\alpha_4)+\cos(13\alpha_5)\right]$$

For MLI the instantaneous phase voltage of only one phase V_{an} is as in equation (5.2)

$$V_{an}(\omega t) = \frac{4V_{dc}}{n\pi}\left[\sum_{i=1}^{m-1}\cos(n\alpha_i)\right]\sin(n\omega t)$$

The instantaneous phase voltage V_{an} can be written as

$$V_{an}(\omega t) = \sum_{n=1,5,7,\cdots}^{\infty}\frac{4V_{dc}}{n\pi}\left\{\cos(n\alpha_1)+\cos(n\alpha_2)+\cos(n\alpha_3)+\cos(n\alpha_4)+\cos(n\alpha_5)\right\}\sin(\omega t) \tag{5.2}$$

If the carrier phase voltage and peak output voltage $V_{an(peak)}$ is equal than $V_{cr(peak)} = (m-1)V_{dc}$.

Thus, the modulation index for MLI becomes

$$M = \frac{V_{cr(peak)}}{V_{an(peak)}}$$

$$= \frac{V_{cr(peak)}}{(m-1)V_{dc}}$$

If the ML switching angles $\alpha_1, \alpha_2, \alpha_3, \alpha_4, \cdots, \alpha_{m-1}$ calculate by some iterative method and with the condition is $\alpha_1 < \alpha_2 < \alpha_3 < \cdots < \alpha_k < \pi/2$ the lower order harmonics are eliminated and the higher order harmonics are suppressed the total harmonic distortion of the phase voltage is minimized. For five switching the 5th, 7th, 11th and 13th order harmonics are eliminated and the peak fundamental phase voltage can be set maximum value by controlling the switching angles with respect to modulation index.

For 11-levels multilevel converters, the mathematical statement of these circumstances can be expressed as,

$$\begin{aligned}
&\cos(1\alpha_1) + \cos(1\alpha_2) + \cos(1\alpha_3) + \cos(1\alpha_4) + \cos(1\alpha_5) = (m-1)M \\
&\cos(5\alpha_1) + \cos(5\alpha_2) + \cos(5\alpha_3) + \cos(5\alpha_4) + \cos(5\alpha_5) = 0 \\
&\cos(7\alpha_1) + \cos(7\alpha_2) + \cos(7\alpha_3) + \cos(7\alpha_4) + \cos(7\alpha_5) = 0 \\
&\cos(11\alpha_1) + \cos(11\alpha_2) + \cos(11\alpha_3) + \cos(11\alpha_4) + \cos(11\alpha_5) = 0 \\
&\cos(13\alpha_1) + \cos(13\alpha_2) + \cos(13\alpha_3) + \cos(13\alpha_4) + \cos(13\alpha_5) = 0
\end{aligned} \tag{5.3}$$

In equation 5.3, the $5^{th}, 7^{th}, 11^{th}$ and 13^{th} harmonics would be eliminated if harmonic amplitude $b_5 = b_7 = b_{11} = b_{13} = 0$. Equation 5.3 can be solved to obtain the appropriate switching angles $\alpha_1, \alpha_2, \alpha_3, \cdots, \alpha_\kappa$ eliminating the desired harmonics.

For modulation index M =0.8 the fundamental nonlinear transcendental equations can be solved by iterative method to calculate the switching angles or % of THD with controlling the fundamental.

$$\cos(1\alpha_1) + \cos(1\alpha_2) + \cos(1\alpha_3) + \cos(1\alpha_4) + \cos(1\alpha_5) = (m-1)M$$

$$\cos(1\alpha_1) + \cos(1\alpha_2) + \cos(1\alpha_3) + \cos(1\alpha_4) + \cos(1\alpha_5) = 5 \times 0.8 = 4$$

5.4.2 Proposed Harmonic Elimination Principle Using BBO Algorithm

A typical output voltage $V(t)$ of an inverter can be represented as,

$$V(t) = \sum_{n=1}^{\infty} \left(a_n \cos n\alpha_n + b_n \sin n\alpha_n \right) \tag{5.4}$$

Due to quarter wave symmetry of inverter output voltage wave-form, $a_n = 0$ and b_n can be evaluated through equation (5.3) with the specified order of harmonics eliminated.

Since the aim is to eliminated the targeted lower order and minimize the other higher order harmonics for minimum voltage THD, the objective function for determination of the proper switching angles is considered as,

$$f(\alpha) = (b_1 - M)^2 + k_5(b_5 - \varepsilon_5)^2 + k_7(b_7 - \varepsilon_7)^2 + \ldots + k_n(b_n - \varepsilon_n)^2 \quad (5.5)$$

Subjected to $0 < \alpha_1 < \alpha_2 < \alpha_3 < \cdots < \alpha_m < (\pi/2)$; (5.6)

The term b_n in equation (5.5) can be obtained from equation (5.1) and the optimization to be realized subject to the consideration of the switching angle in (5.6). The term ε_n in (5.5) is the desired magnitude of the respective harmonics and k_n is the weightage function for elimination of these harmonics. For the harmonics to be eliminated, ε_n are considered to be low or zero and k_n are set to higher values compared to the other harmonics.

From (5.1), the %THD of the multilevel inverter output voltage can be expressed as,

$$\%THD = \left[\frac{1}{b_1^2} \sum_{n=5}^{\infty} (b_n)^2 \right]^{1/2} \times 100 \quad (5.7)$$

Where $n = 6k \pm 1$ for $(k = 1, 2, 3, 4, \cdots)$

In the proposed technique, Biogeography-Based Optimization technique is used which is comparatively recent and relatively easier to apply. The main reasons for using BBO for this problem are:

vii. BBO is a relatively recent, and has not yet been extensively explored to solve the problem of converter switching.

viii. BBO does not require unreasonable amount of computational effort [135], unlike the other metaheuristic techniques.

To start the search procedure, the switching angles are randomly generated satisfying the conditions of equation (5.6) for the chosen number of population of a potential solution. Using these random values, individual harmonics are computed which represents the best fitness of the search point. The best combination of switching angles among the population of search points up to present iteration is called the elite or best solution for the variables α_1 through α_m. At each iteration the best individual new search points are generated from the current search points and the information regarding the best solutions is found out from objective function by using the BBO algorithm.

The scheme of nonlinear equations in m variables to be optimized can be represented as

$$f_j(\alpha_1, \alpha_2, \alpha_3, \alpha_4, \cdots, \alpha_m) = 0, \quad j = 1, 2, 3, \cdots, m \quad (5.8)$$

These m equations are obtained for the problem by equating equation (5.1) to zero for any harmonics desired to be eliminated for different modulation index. BBO representation of the problem is shown in Figure 5.6.

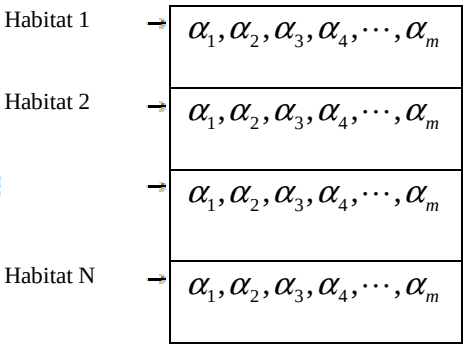

Figure 5.6. BBO representation of the problem**.**

Collection of one set of best switching angles, $\alpha_1, \alpha_2, \alpha_3, \cdots, \alpha_m$ form a solution set of the problem. This solution set is termed as a 'habitat' in BBO. N is nothing but the number of the set of habitat of the population based optimization algorithms. In BBO algorithm it is called the eco-system.

Habitat Suitability Index (HSI) indicates the quality of the solution set. For the problem being considered, HSI is represented by the total harmonic distortion (THD) value generated by the solution set.

Equation (5.8) is written in vector notation as

$$f(\alpha) = 0 \tag{5.9}$$

Where, $f = [f_1, f_2, f_3, f_4, \cdots, f_m]^T$, an $m \times 1$ matrix

$\alpha = [\alpha_1, \alpha_2, \alpha_3, \alpha_4, \cdots, \alpha_m]^T$, an $m \times 1$ matrix

Equation (5.9) can be solved by using a BBO technique, where the nonlinear equations give an approximate solution. The steps involved in computing a solution are as follows.

The switching angle matrix can be represented as

$$\alpha^j = [\alpha_1^j, \alpha_2^j, \alpha_3^j, \alpha_4^j, \cdots, \alpha_m^j]^T \tag{5.10}$$

The elite values are updated after every iteration. The process is repeated until the convergence is obtained. The process terminates if the changes in the fitness values between consecutive iterations are less than a given tolerance, or the fitness values do not change for a number of iterations, or the permissible number of iteration runs are completed. A flowchart of the BBO algorithm used for optimization of switching angle $\alpha_1, \alpha_2, \alpha_3, \alpha_4, \cdots, \alpha_m$ to obtained minimum voltage THD is shown in Figure 5.7. The calculated switching angles, %THD and generated signal are imported to the simulated PV-based DVR circuit. BBO based optimization technique is applied for generation of pulses.

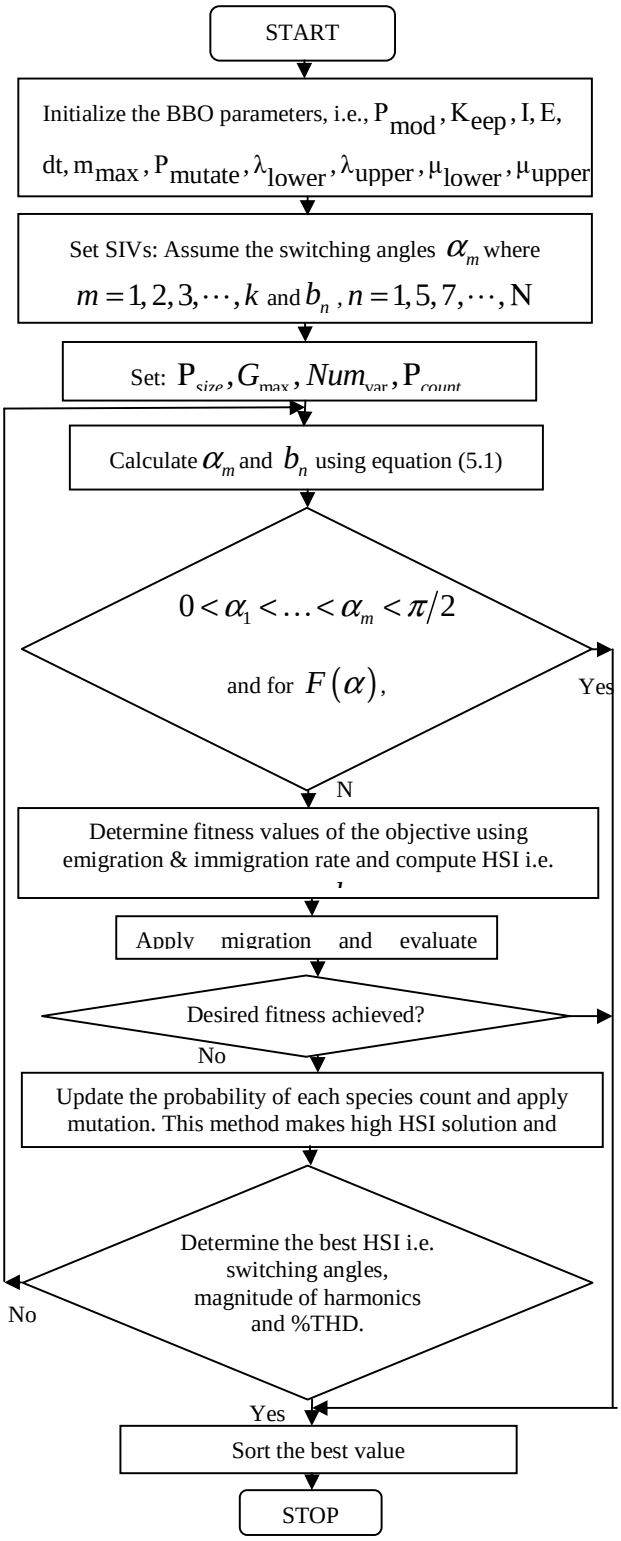

Figure 5.7 Flowchart of the proposed BBO algorithm.

Figures. 5.8 and 5.9 show simulation results of PWM voltage for five-level and nine-level inverter respectively. The THD levels of three phases for seven, eleven, and fifteen are compared in Tables 5.3 and 5.4. The harmonic content decreases as the number of levels increases and filtering requirements are reduced. Another advantage of multilevel cascaded-inverter is circuit layout flexibility because each level has the same structure, and there are no extra clamping diodes or voltage balancing capacitor. These converters offer a low output voltage THD, a high efficiency and required power factor.

Cascaded multilevel inverter is used in the proposed scheme as this can reduce the physical size of the compensator and improve its performance during micro-grid contingencies. The results of Table 5.3 are coming by using the diode clamped multilevel inverter (DCMLI) with the help of SPWM and SVPWM respectively for three, seven and eleven-level respectively. From Table 5.4, it is found that the minimum %THD for three, five and seven switching of proposed inverter scheme are 5.0087, 2.6356 and 1.2804 respectively which are smaller compare to the % THD found in Table 5.3. From the comparative study of Tables 5.3 and 5.4, it is seen that in the proposed scheme the reduction in % THD is increased with the increase in switching level and it is a necessary criterion for PV-DVR system. The procedural steps for interfacing of Matlab simulation and BBO algorithm are shown in flowchart of Figure 5.10.

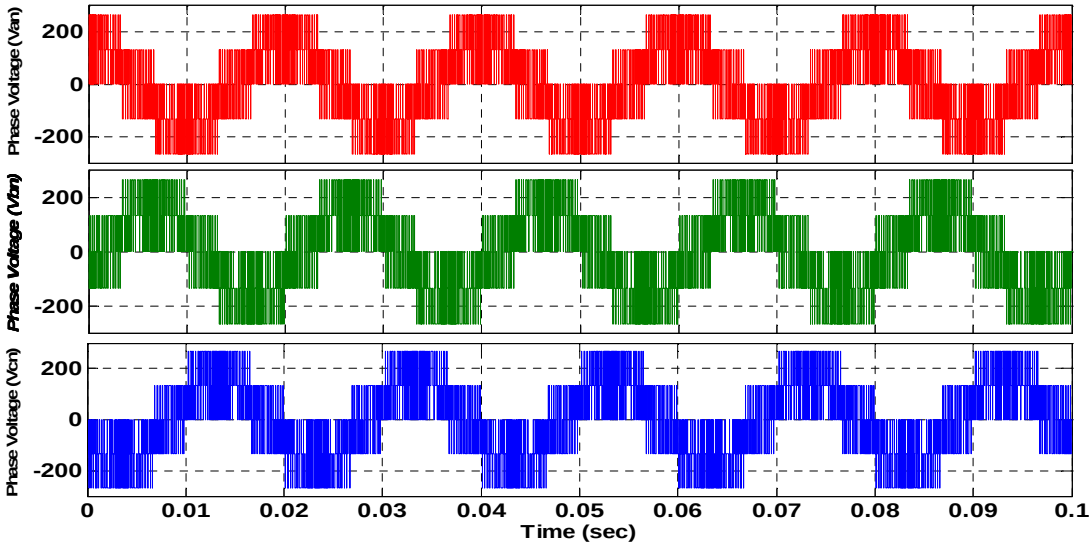

Figure 5.8 Simulation result of PWM phases voltage V_{an}, V_{bn} and V_{cn} for five-level inverter.

The different optimization techniques e.g. Genetic Algorithms (GA), Particle Swarm Optimization (PSO), Gravitational Search algorithm (GSA), Cuckoo Search algorithm (CSA) and Biogeography-Based Optimization (BBO) are used to compare the results obtained from BBO based technique for switching angle calculation. The comparative result is shown in Table 5.5 which shows that the optimized %THD achieved by BBO technique with minimum nos. of iteration. In addition, Figure 5.11 shows the convergence of the objective function with CSA, PSO, GA, GSA and BBO method for M=5.3 after eliminating 5^{th}, 7^{th}, 11^{th}, 13^{th}, 17^{th} and 19^{th} order of harmonics. It has been observed that BBO based technique converges faster than the other methods. In the present chapter the

objective function considered is given by the expression (5), which can minimize the overall voltage THD while any other equivalent objective function can also be considered [142] providing almost equivalent result. The computation of the switching angles were carried out with various search based existing techniques e.g. GA, PSO, GSA, CSA, BBO for comparison purpose with same initial conditions and the results are shown in Table-5.5. However, for changed initial values for optimization, the results or the in no. of iterations for convergence as shown in Table-5.5 may be different [142].

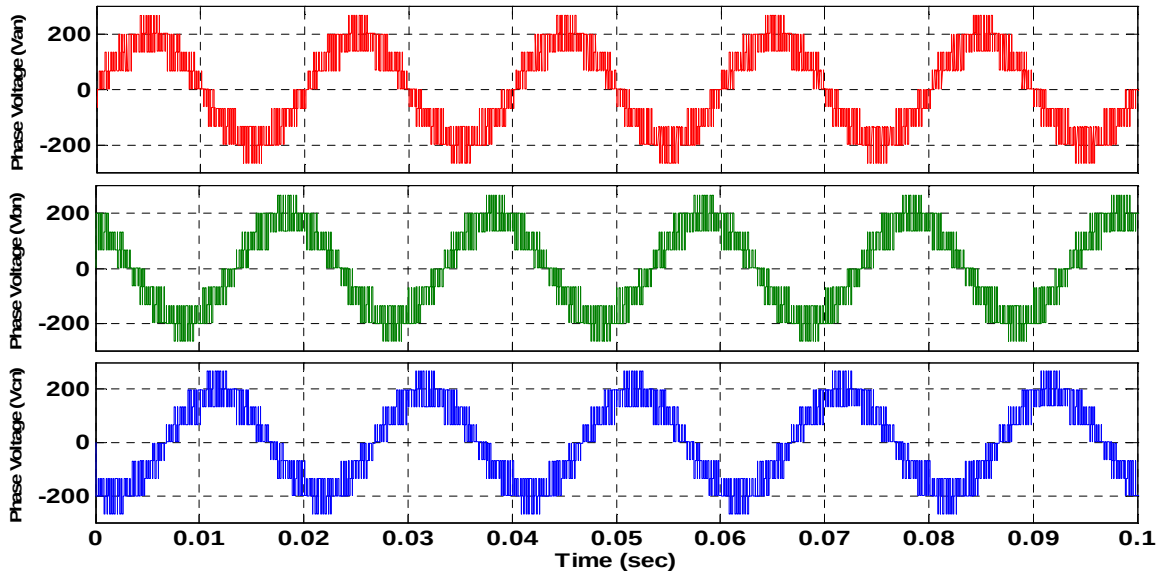

Figure 5.9 Simulation result of PWM phases voltage V_{an}, V_{bn} and V_{cn} for nine-level inverter.

Table 5.3 %THD Comparison and Comparisons of three multilevel inverters

No of levels	SPWM (%)	SVPWM (%)	Converter Type	Diode Clamp	Flying Capacitors	Cascade Inverter
3	39.38	16.1	Main switching devices	$(m-1)\times 2$	$(m-1)\times 2$	$(m-1)\times 2$
7	35.27	9.08	Main diodes	$(m-1)\times 2$	$(m-1)\times 2$	$(m-1)\times 2$
11	13.11	5.68	Clamping diodes	$(m-1)\times(m-2)$	0	0
			DC bus capacitors	$(m-1)$	$(m-1)$	$(m-1)/2$
			Balancing capacitors	0	$(m-1)\times(m-2)/2$	0

Table 5.4 Switching angles and %THD calculation for different level multilevel inverter.

M	α_1	α_2	α_3	$\%THD$	Harmonics
1.2	40.5406	65.1268	88.8859	15.2508	
1.4	39.4402	58.9832	83.545	10.9005	
1.5	39.4251	56.2501	80.0973	10.3778	
1.6	39.0177	54.3353	76.1131	10.1405	5th and 7th harmonics are zero
1.7	37.1788	53.9445	71.6586	10.0761	
1.8	33.4978	54.759	67.103	8.8655	
1.9	28.4109	54.0656	64.3048	8.7752	
2	22.9092	49.5308	64.5427	7.7785	
2.3	12.459	34.1158	60.2878	5.0087	
2.4	11.5042	28.7169	57.106	5.108	

M	α_1	α_2	α_3	α_4	α_5	$\%THD$	Harmonics
2.4	35.3174	46.565	58.0801	71.5606	87.0496	4.0264	
2.52	35.6044	45.2589	57.0617	68.75	84.4413	4.3503	
2.7	35.2511	44.2019	55.1368	65.7425	79.3958	2.6356	5th, 7th, 11th and 13th harmonics
3	26.6415	43.9304	51.5339	62.3994	72.5045	2.6577	are zero
3.2	20.7765	37.3286	52.4303	58.4782	70.2871	5.8002	
3.3	18.4493	33.9904	50.8389	57.8658	68.97	2.7557	
3.4	16.8703	30.5365	48.5645	57.9358	67.1025	3.3813	
3.8	10.7581	20.7282	33.9312	52.8877	63.3064	3.2359	
4.2	6.3667	15.0521	23.5422	37.2328	58.1614	2.8826	

M	α_1	α_2	α_3	α_4	α_5	α_6	α_7	$\%THD$	harmonics
4.8	15.3171	23.2117	34.1057	48.5344	55.4639	61.2871	67.7316	3.9861	
4.9	13.507	22.0118	31.5508	45.2477	57.0556	58.4742	67.8134	2.1322	5th, 7th,
5	6.2742	20.525	29.4755	41.623	49.2509	59.9149	72.7022	2.6202	11th, 13th
5.1	7.3985	20.141	26.9154	39.6328	50.2542	58.4442	69.8217	2.7754	17th and
5.2	9.9708	18.4653	25.4845	36.7237	51.3631	58.6651	65.2958	2.0955	19th
5.3	5.7727	17.4273	23.8973	34.2905	47.0717	56.0442	68.2306	1.2804	harmonics
5.6	7.2191	13.0716	20.8466	27.7533	39.1321	54.5322	62.716	1.5123	are zero
5.7	4.695	13.6967	18.3465	26.9029	36.186	51.0207	62.954	1.4787	

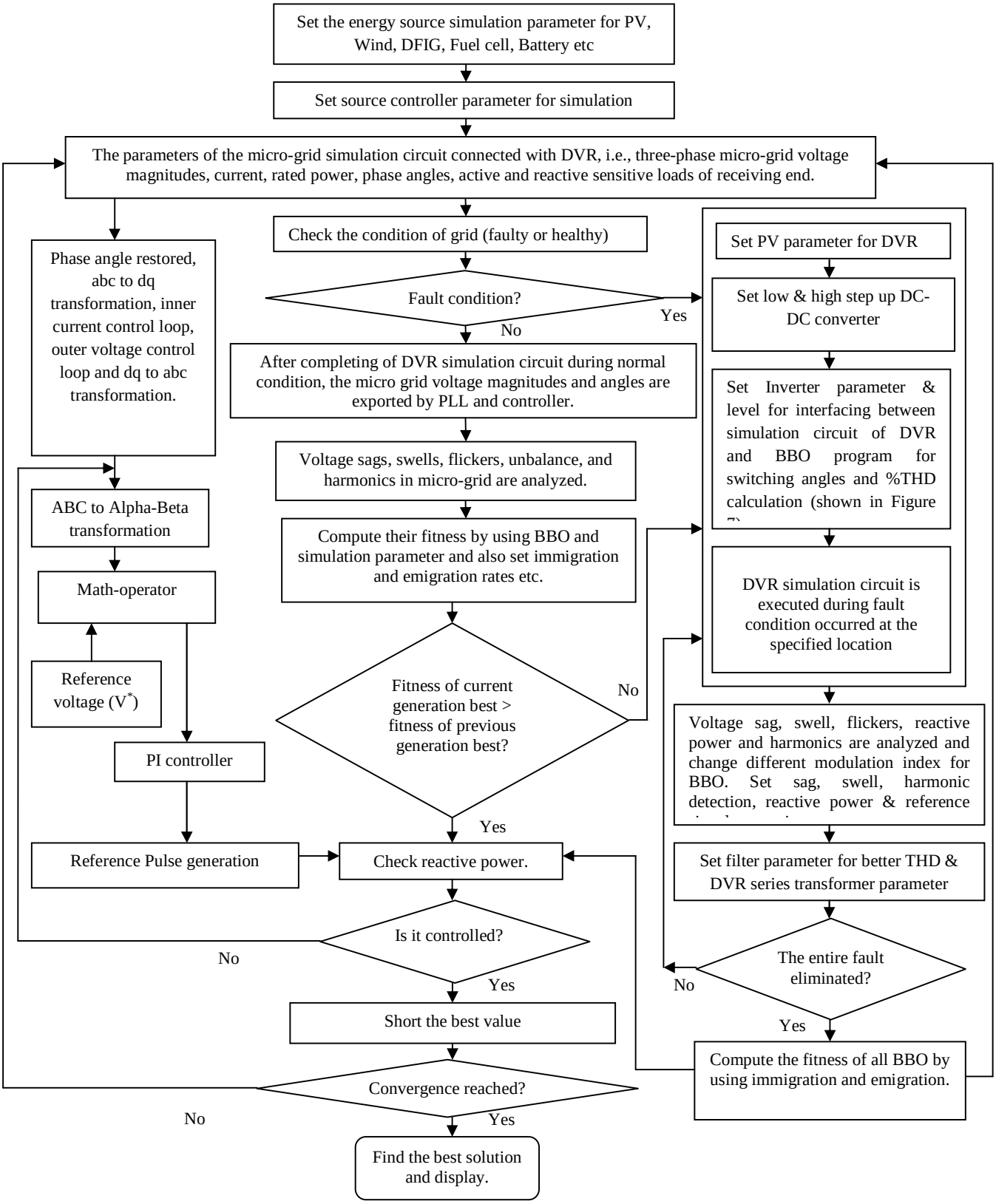

Figure 5.10 Flow chart of DVR implementation by BBO algorithm.

Table 5.5 Optimization results for the Different Population- Based Optimization technique

	GA	PSO	GSA	CSA	BBO
Iteration	29	25	28	26	12
CPU time	0.5332	0.4821	0.5998	0.4992	0.3984
%THD	2.2213	2.0122	2.9432	2.0943	1.2804

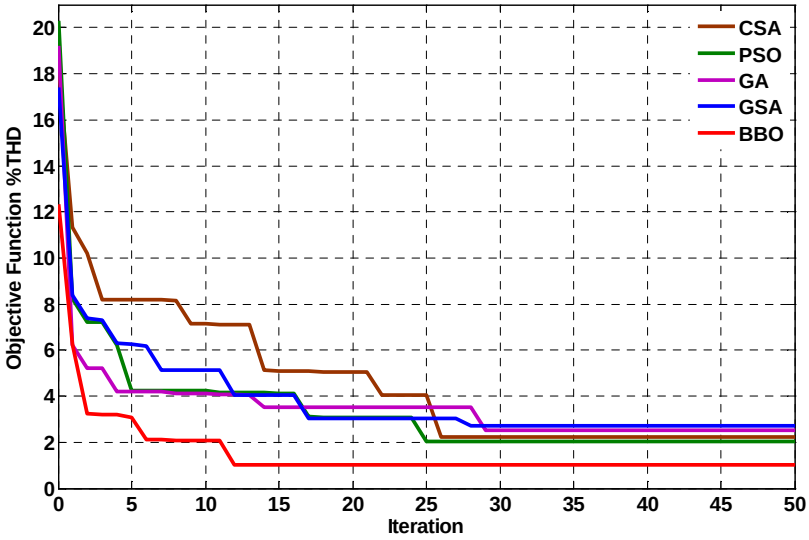

Figure 5.11 Value of the objective function with CSA, PSO, GA, GSA and BBO method for M=5.3 with eliminating 5^{th}, 7^{th}, 11^{th}, 13^{th}, 17^{th} and 19^{th} order harmonics.

5.4.3. Proposed multilevel inverter with varying DC sources

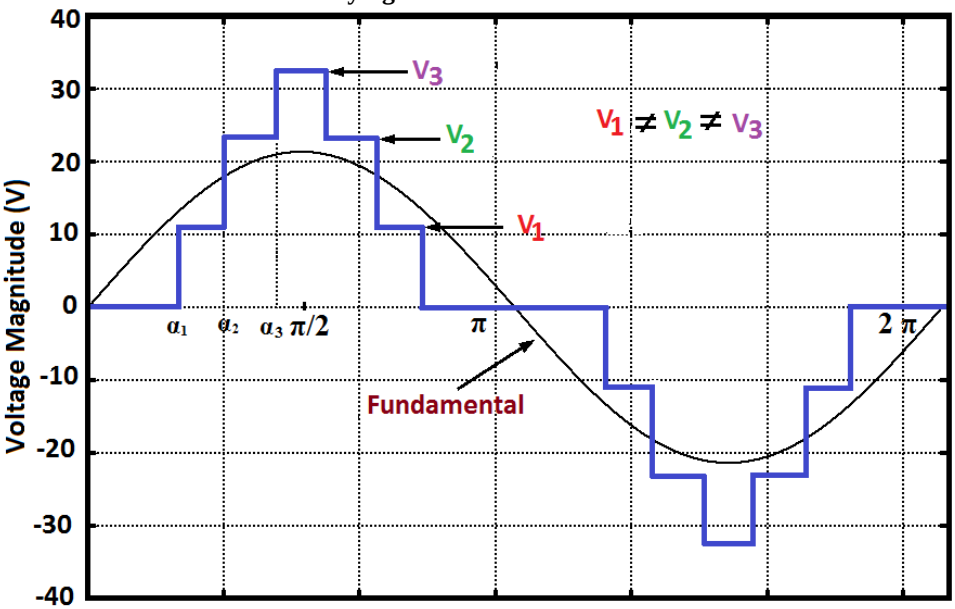

Figure 5.12 Three switching for multilevel inverter using unequal dc sources.

The multilevel switching scheme using three unequal dc sources is shown in Figure 5.12. When the voltage level of PV based dc sources are not equal, the BBO algorithm can also be used to calculate the switching angles to eliminate the lower order harmonics while the higher order harmonics are suppressed after maintaining the fundamental.

For 3-switching multilevel converters, the mathematical statement in this case can be expressed as,

$$\begin{cases} V_1 \cos\alpha_1 + V_2 \cos\alpha_2 + V_3 \cos\alpha_3 = \mathrm{M} \\ V_1 \cos 5\alpha_1 + V_2 \cos 5\alpha_2 + V_3 \cos 5\alpha_3 = 0 \\ V_1 \cos 7\alpha_1 + V_2 \cos 7\alpha_2 + V_3 \cos 7\alpha_3 = 0 \end{cases} \quad (5.11)$$

In general for ML switching scheme the dc sources were all equal to one another but for varying dc sources the sources are not equal to one another. For unequal dc sources it is quite difficult (different charging/discharging rates) to accomplish the different power electronics application. This type of switching configuration can solve harmonic problem and power quality issues by proper selection of switching angles.

Table 7.6 shows the switching angles when the voltages of the three dc sources are different, i.e., 8.4, 13.2 V, 14.4 V or 10.8 V, 13.2 and 12 V.

Table 5.6 Switching angles and %THD calculation for different level multilevel inverter with varying dc sources

M	α1	α2	α3	%THD	V1	V2	V3				
1.2	34.4225	58.7065	87.5542	15.7255							
1.3	35.8946	55.652	84.6306	15.4948							
1.4	21.1878	52.2246	86.4887	14.2438	8.4	13.2	14.4				
1.7	35.6421	48.7557	70.2281	7.688							
2.3	10.3025	27.8255	57.8552	7.5469							
1.4	37.8365	58.0283	83.8713	11.1478				5th and 7th harmonic are eliminated			
1.7	16.3021	47.5621	84.6111	10.6267	11.9	12.1	12				
2.3	10.7353	33.0537	60.4109	6.425							
1.3	39.1317	62.93	87.7835	12.5591							
1.4	38.6098	60.131	84.8302	10.0829							
2.2	14.0729	39.633	64.2577	8.9743	11.82	13.2	10.98				
2.3	11.4921	35.0734	61.6431	5.9124							
M	α1	α2	α3	α4	α5	%THD	V1	V2	V3	V4	V5
2.6	35.4295	48.7902	57.4544	72.544	87.3213	5.1642					
2.9	23.91	45.3243	55.9942	66.4945	89.1131	5.1553	14.4	13.2	10.8	15.6	6
3.1	25.3572	45.6921	52.5298	64.9827	72.5455	4.444					
3.4	17.5211	34.8717	52.411	60.1971	71.5664	4.0359	5th,7th , 11th and 13th harmonic are eliminated				
3.5	15.8513	31.7136	49.6713	59.9574	69.3186	4.0266					
3.6	10.2854	21.8471	36.5686	58.6716	89.9995	3.3552					
3.7	10.892	26.4957	40.7793	57.3584	71.9803	3.2928					

In equation 11, the 5^{th} and 7^{th} harmonics would be eliminated if harmonic amplitude $b_5 = b_7 = 0$. Equation 5.11 can be solved to obtain the appropriate switching angles $\alpha_1, \alpha_2, \alpha_3, \cdots, \alpha_\kappa$ eliminating the desired harmonics which

is incorporated in Table 5.6. However, the unequal DC sources can pose power sharing problems for the different sources and would require further modification in the switching scheme which can add another dimension to the problem.

5.5 DVR operating states

In the proposed system the DVR must be able to detect voltage sag, swells, flicker and harmonics especially at sensitive load points by injecting an appropriate voltage through an injection transformer. For nonlinear loads such as thyristor-controlled rectifiers pre-sag compensation method is used to compensate load voltage during fault to pre fault condition. Figure 5.13 (a) shows the vector diagrams of the pre-sag compensation. When a fault occurs in other lines, supply voltage Vs drops and the DVR injects a series voltage, V_{DVR} through the injection transformer which can be represents as:

$$V_{DVR} = V_L - V_S \tag{5.12}$$

In-phase compensation technique is used to compensate the voltage drop across a load by injecting a voltage through a series injection transformer in-phase with the source voltage. The vector diagram is shown in Figure 5.13 (b). The supply voltage $\left(V_{presag}\right)$ and the load voltage are equal with zero phase angles. The sag/swell events are compensated by injecting DVR compensating voltage V_{inj} in-phase with the supply voltage to restore the voltage at nominal value. Thus the injected voltage of a DVR $\left(V_{inj}\right)$ can be expressed as

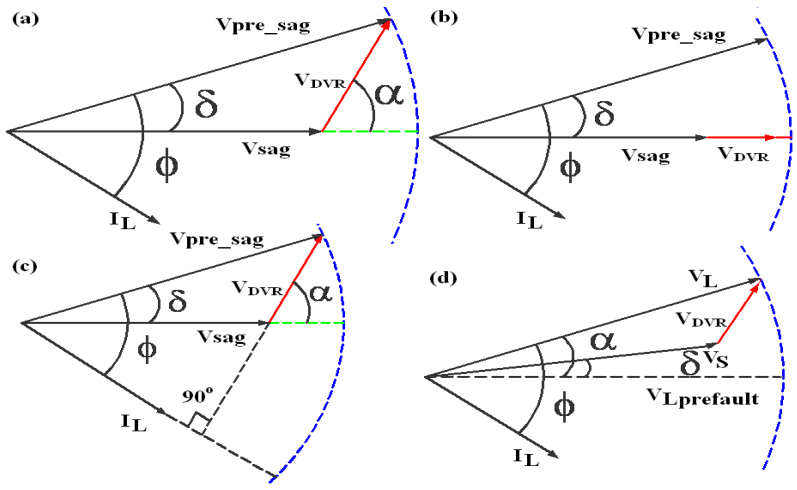

Figure 5.13 Vector diagram of (a) Pre-sag compensation (b) In-phase voltage compensation method (c) Minimal energy technique and (d) Vector diagram of phase advance method.

$$\left|V_{inj}\right| = \left|V_{presag}\right| - \left|V_{sag}\right| \tag{5.13}$$

The steady state injected active power is given by,

$$P_{DVR} = 3(V_L - V_S) I \cos\phi \tag{5.14}$$

Figure 5.13 (c) shows the phasor diagram for the minimal energy control strategy. The relation between δ, α can be written as:

$$\alpha = \frac{\pi}{2} - \phi + \delta \tag{5.15}$$

The angle δ can be obtained as:

$$\delta = \phi - \cos^{-1}\left(\frac{V_L \cos\phi}{V_S}\right) \tag{5.16}$$

The phase advance method shown in Figure 5.13 (d) is realized by moving the phase angle of Vs from pre-fault angle to any angle of advance α. The injected power, output power and DVR power can be expressed as,

$$P_{in} = \sum_i V_{Si} I \cos\left(\phi - \alpha + \delta_j\right) \tag{5.17}$$

$$P_{out} = \sum_i V_L I \cos(\phi) = 3V_L I \cos(\phi) \tag{5.18}$$

$$P_{DVR} = P_{out} - P_{in} \tag{5.19}$$

$$= 3V_L I \cos(\phi) - \sum_i V_{Si} I \cos\left(\phi - \alpha + \delta_j\right) \tag{5.20}$$

Where I means each phase like a, b and c and V_{Si} and δ_j are the magnitude of supply voltage and phase angle jump during fault. During severe deep sag, the optimum α, that makes P_{DVR} to be minimized, can be calculated by solving $dV_{DVR}/d\alpha = 0$.

5.6 Simulation Results for Inverter:

The simulation results with three, four, five and seven switchings per quarter cycle with varying modulation index (m_d) for the BBO-based SHEAM-PWM inverter are shown in Figures. 5.14 (a), (b) ,(c) and (d) respectively. The plot of the line voltage THD with constant modulation index as a function of the number of inverters per phase and Voltage THD vs. modulation index for different multi-level inverters are shown in Figure 5.14 (e) and (f) respectively. From Figure 5.14 (f), it is shown that as the switching level increases, the % THD decreases with the change in Modulation index.

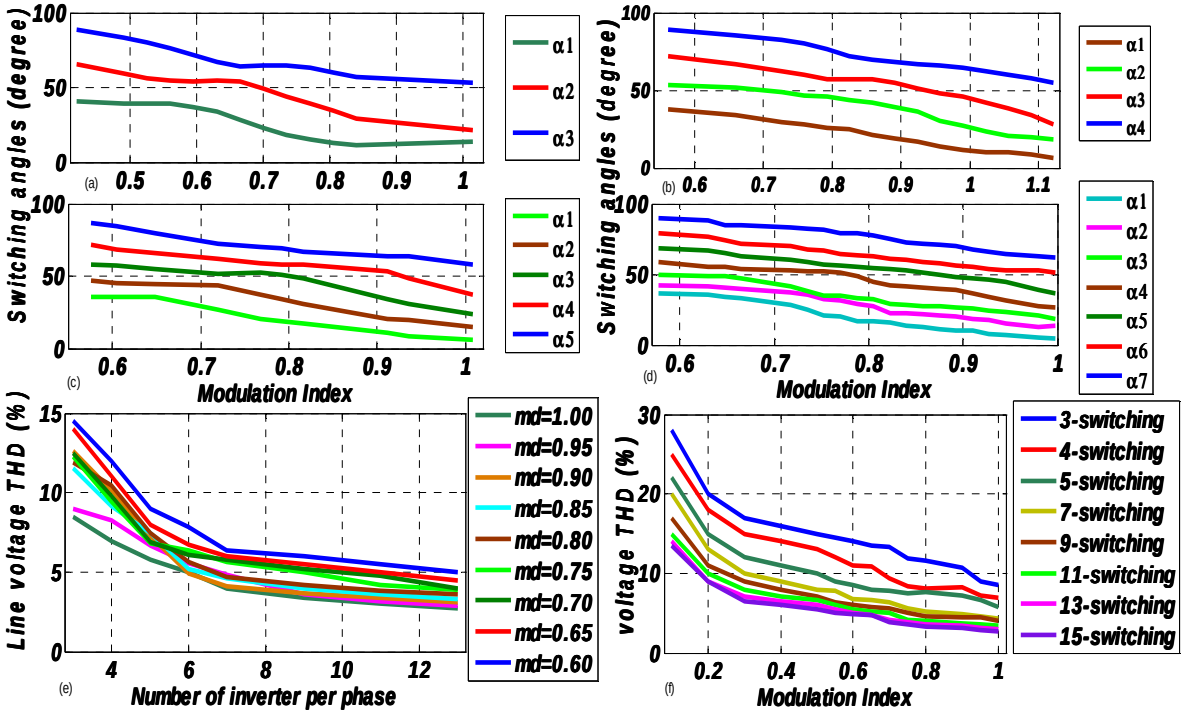

Figure 5.14 The output results (a) modulation index vs. switching angles for 7-level cascaded inverter (b) modulation index vs. switching angles for 9-level cascaded inverter(c) modulation index vs. switching angles for 11-level cascaded inverter (d) modulation index vs. switching angles for 15-level cascaded inverter (e) The line voltage THD with constant modulation index as function of the number of inverters per phase. (f) Voltage THD vs. modulation index.

5.7 Simulation Results for DVR and filter:

The performance of the proposed PV connected DVR system is tested by considering different cases of voltage disturbances such as balanced and unbalanced deep voltage sags, voltage swells, voltage flicker, and long duration voltage variation. A simple PV-DVR distribution system, shown in Figure 5.1, is implemented in the Matlab/Simulink package to assess the dynamic performance of the proposed compensation technique. In MATLAB Simulink, the DVR is simulated to be in operation only when the supply voltage differs from its nominal value or when the PV array generates excessive power or equal power to the load demand. It reduces the energy consumption from the utility grid. The simulation load parameters of the system study are shown in Table 5.7.

Table 5.7 Load Parameters for simulation.

Description	Parameter	Symbol	Value
Non-linear load	AC inductor	L	1.19 mH
	Rating	P_L	5 kW
	DC capacitor	C_{Ln}	2000 μF
	Resistance	R_{Ln}	21 ohm
Linear load	Load resistance	R_L	0.2 or 1 ohm
	Load inductance	L_L	0.002 H
	Load frequency	f	50 Hz
Capacitive Load	Capacitive reactive power	Q_C	1800000
Induction motor load parameters	Rated voltage	V_{rat}	240 V
	frequency	f	50 Hz
	Rated output power	P_{rat}	3 kW
	Power factor	pf	0.83
	Nominal speed	N_S	1430 rpm
	No. of poles	P	4

5.7.1 Resistive load with balanced and unbalanced voltage sag mitigation

The DVR is turned on at t=0.15 s, with a source voltage of 230 volt. At t=0.15 s, a three phase fault has occurred at the supply side which causes a voltage sag between t=0.15 s to t=0.25 s. Figure 5.15 shows the waveforms of the supply side voltage and the injected voltage by the DVR, and the resistive load side voltages. It can be seen from Figure 5.15 that the proposed control strategy is able to drive the DVR to inject the appropriate three phase voltage component with acceptable phase to remove the supply voltage anomalies due to the three phase fault. It quickly injects necessary voltage components to smoothen the load voltage upon detecting voltage sag and also minimize the harmonics. Figure 5.16 shows the response of DVR with vector control for unbalanced voltage sag and linear load. It quickly injects the required unbalanced necessary voltage components to smoothen the load voltage and keeps it at nominal value. Figure 5.17 illustrates the response of DVR with vector control for balanced voltage sag and linear (R-L-C) load.

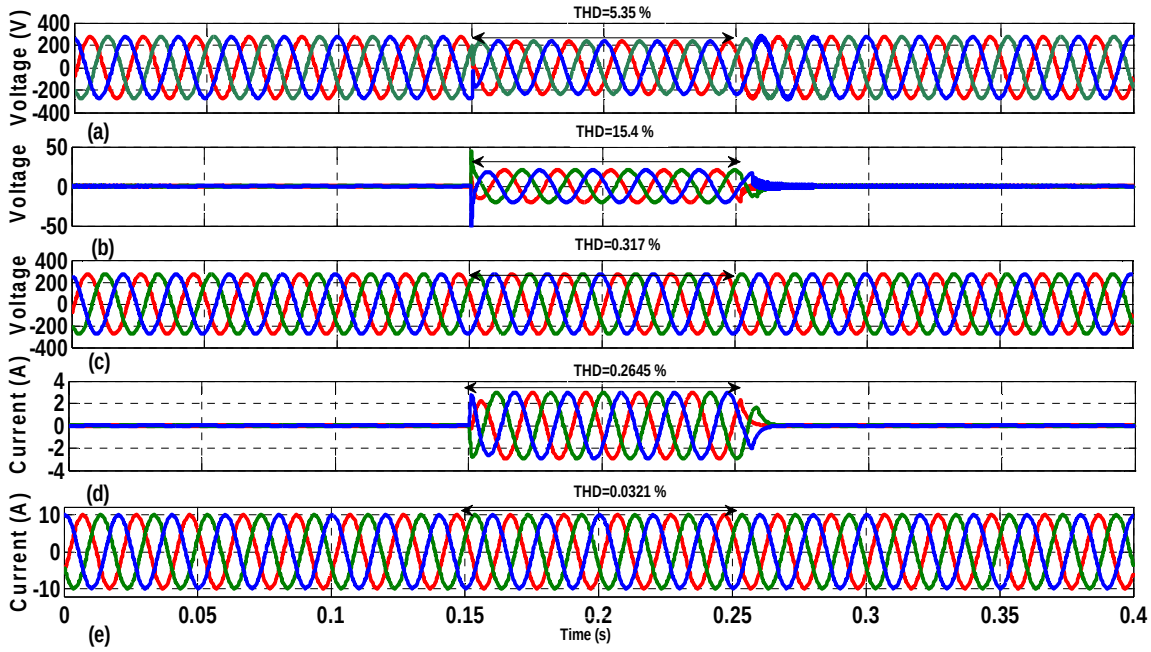

Figure 5.15 Response of DVR with vector control for balanced voltage sag and linear (R-L) load (a) Three phase source side sag voltage (b) Injected DVR voltage (c) Three phase load voltage (d) Extra fault current (e) Three phase load current.

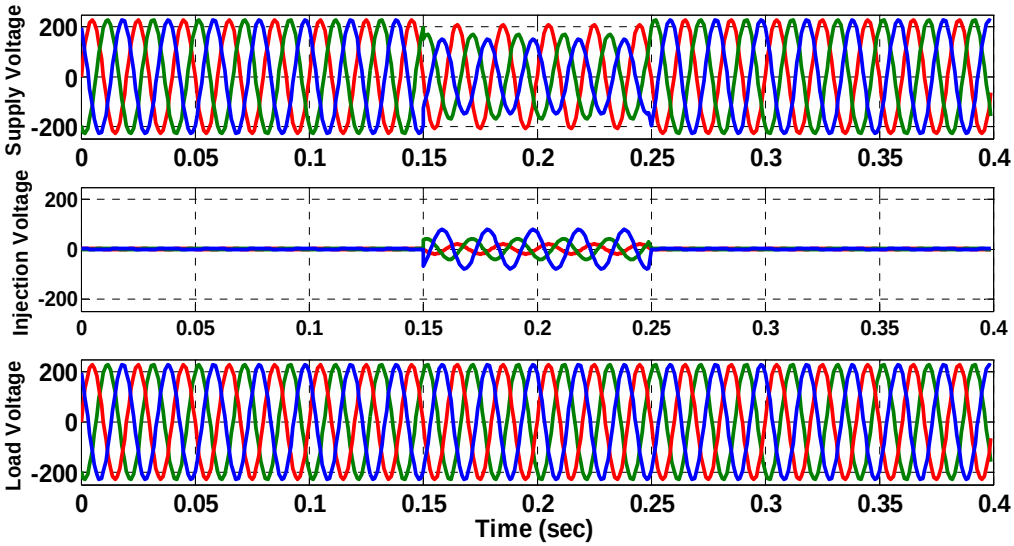

Figure 5.16 Response of DVR with vector control for unbalanced (double line fault) voltage sag and linear load.

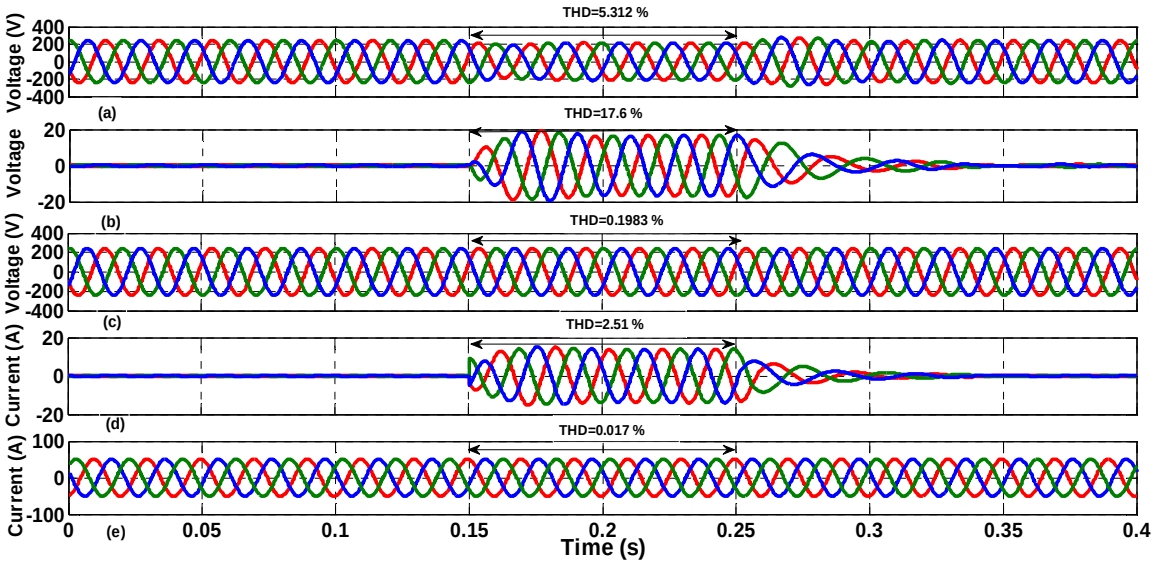

Figure 5.17 Response of DVR with vector control for balanced voltage sag and linear (R-L-C) load (a) Three phase source side sag voltage (b) Injected DVR voltage (c) Three phase load voltage (d) Extra fault current (e) Three phase load current.

5. 7.2 Balanced and unbalanced voltage swells mitigation

In order to see the performance of proposed DVR control for voltage swells, a balanced voltage swell was simulated by connecting three phase capacitor banks in the system. Figure 5.18 shows the three phase waveforms of the supply side voltages, the injected voltage by the proposed PV- DVR, and the load side voltages.

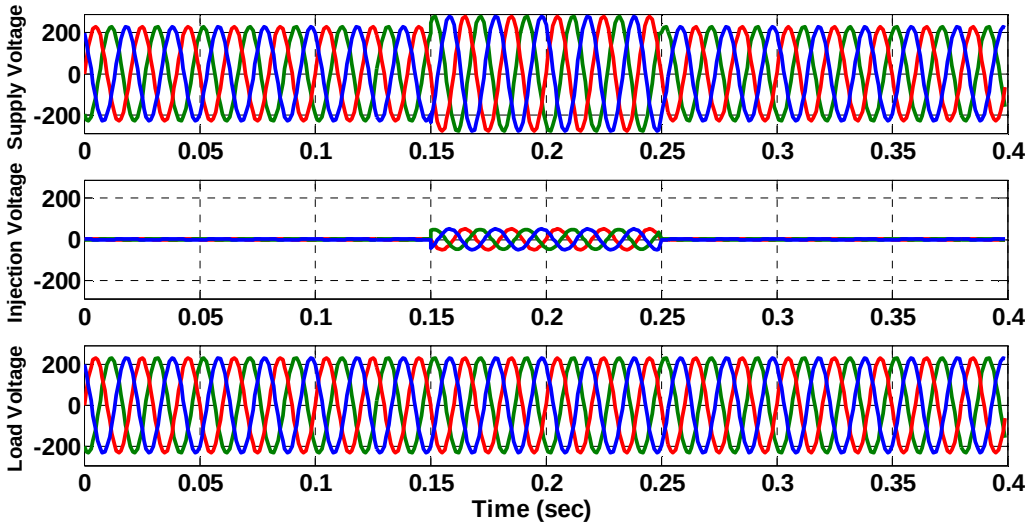

Figure 5.18 Response of DVR with vector control for balanced voltage swells.

It can be seen from the Figs. 5.18 and 5.19; that the proposed control strategy is able to drive the DVR to inject the negative appropriate three phase voltage components with correct phase to remove the supply voltage anomalies due to the three phase fault. It quickly injects negative appropriate three phase necessary voltage components to smoothen the load voltage upon detecting voltage swell.

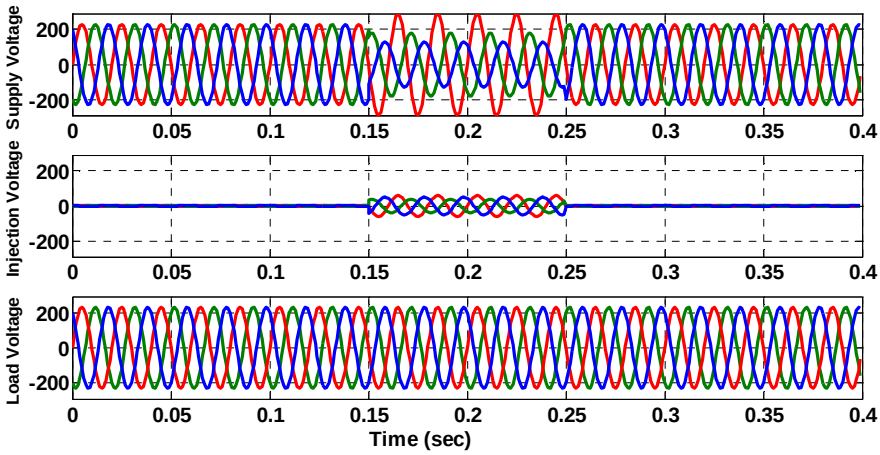

Figure 5.19 Response of DVR with vector control for unbalanced voltage swells.

Figure 5.19 shows the DVR control for unbalanced voltage sag and swell created by single line to ground fault in the system. It can be seen from the Figure5.19 that the proposed control strategy is able to drive the DVR to inject the appropriate unbalanced voltage components for correcting the load voltage and keep the three phase voltages at nominal values.

5. 7.3 Balanced and unbalanced voltage sags and swells mitigation for nonlinear load.

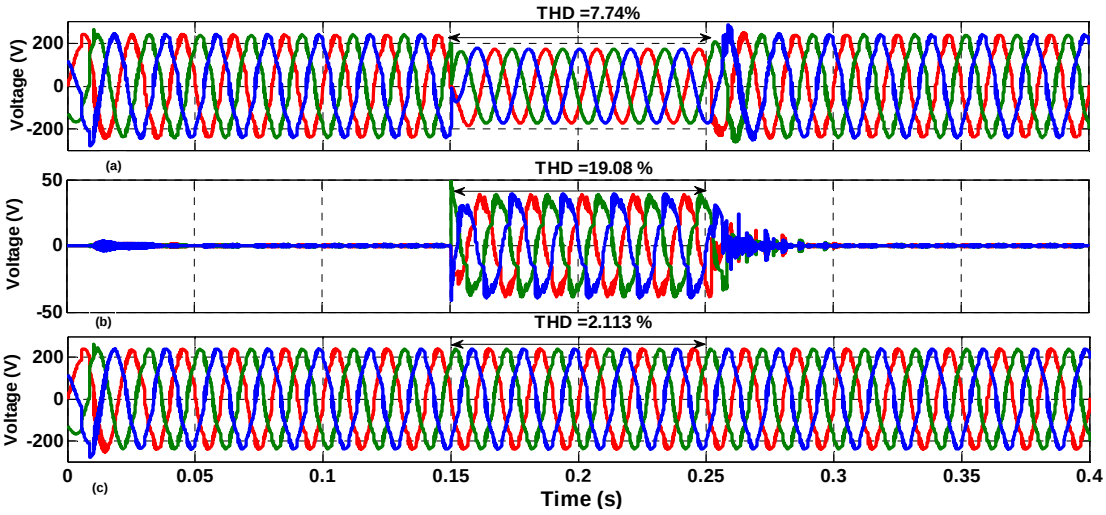

Figure 5.20 Response of DVR with vector control voltage sags for nonlinear load.

For non-linear electric load in an electric distributed power system are a result of harmonic voltage and currents. Harmonic frequencies in the distributed power grid are a frequent cause of power quality problems and the reduction of harmonics is considered desirable. In Figure5.20, the three phase diode rectifier at 230 V and 5 kW was used as a load. Figure5.20 shows the supply side voltages, the injected voltage by the DVR, and the nonlinear load side voltages.

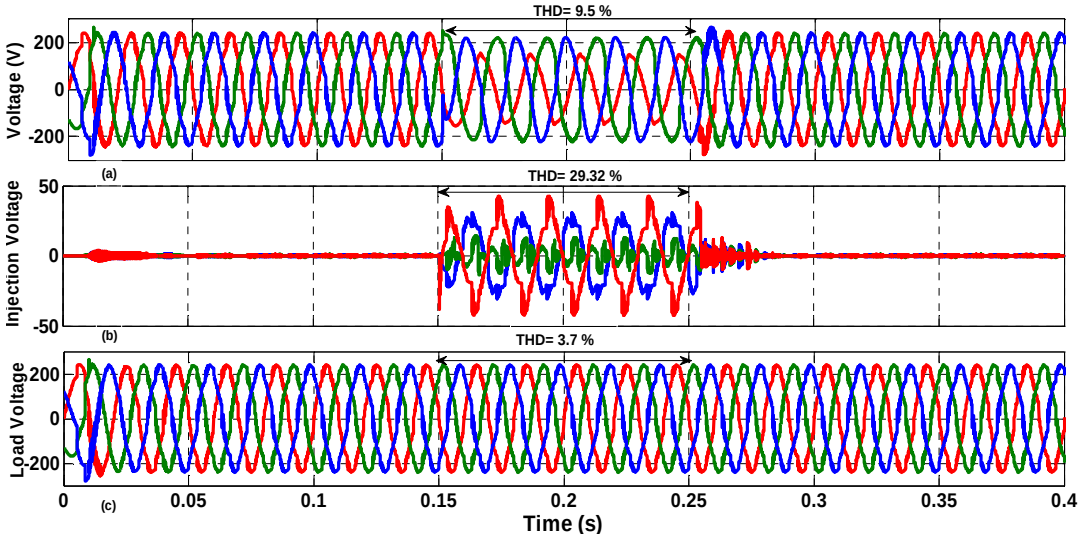

Figure 5.21 Response of DVR with vector control voltage sag for nonlinear (RL) load with phase a, b and ground fault (a) three phase unbalanced fault (b) DVR injection voltage (c) Three phase load voltage (V).

The performance of the DVR under unbalance voltage sags conditions is also investigated through a nonlinear load. Unbalance three phase voltage sag occur when one of the phase drops down near about 31% compared to the other phases as shown in Figure 5.21. DVR quickly detect the voltage sag, swell, flicker, spikes and compensate the load voltage. The immediate action taken by the DVR is to protect the sensitive loads from the unbalanced voltage sages and the connected load returns to its nominal value.

5. 7.4 Placement of capacitors near a DVR

The shunt capacitor banks are switched simultaneously both on the load and the supply side of the DVR. The shunt capacitors are connected as power factor correction devices to a load that requires a high power quality. Switch on of the shunt capacitors perform power factor correction and at the same time transient over voltages can occur on the load side. In Figure 5.22, capacitor bank is installed on the load side to improve the load power factor. The effect of resonance phenomenon that causes transient over voltages during capacitor switching and the subsequence transient responses when the DVR is energized. In this case, response of DVR with vector control voltage sag-swell when capacitor banks are placed on load side also illustrates the waveform of the current through the DVR. The capacitor effects are present in DVR injected voltage waveform and the current waveform.

In Figure 5.23, the load voltage waveform and the current through the DVR are obtained when the capacitor banks are placed on the supply side of the system. The load current is distorted and appears to have transient overshoots when the DVR is switched on and off. The shunt capacitors reduce line current of the system, it improves voltage level of the load, it improves power factor, it reduces the system losses, and it reduces capital investment per mega watt of the load. All the above mentioned benefits, that the effect of capacitor reduces reactive current flowing through the whole system.

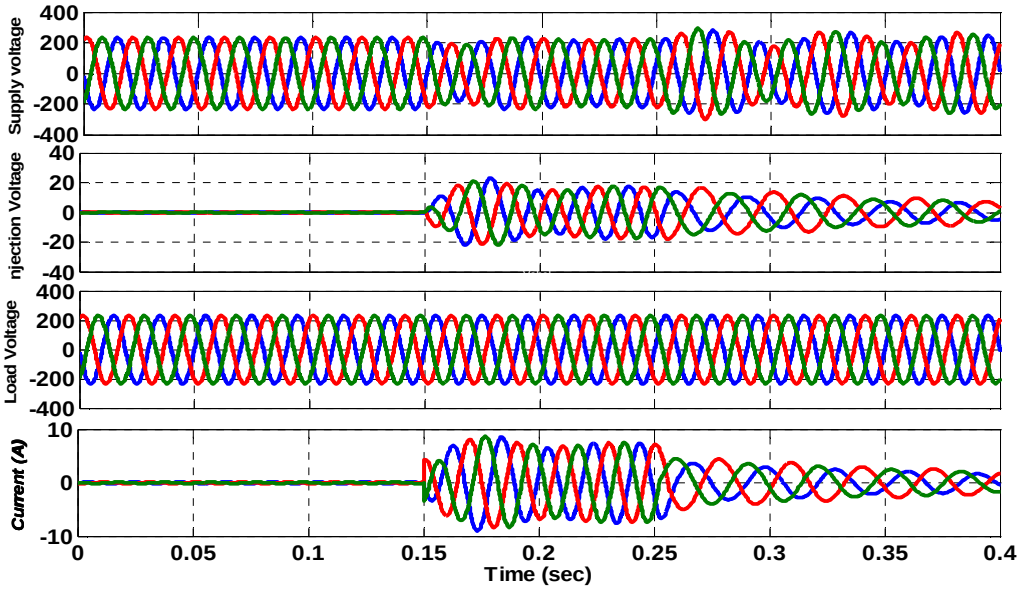

Figure 5.22 Response of DVR with vector control voltage sag when capacitor banks are placed on load side and sag swell related current.

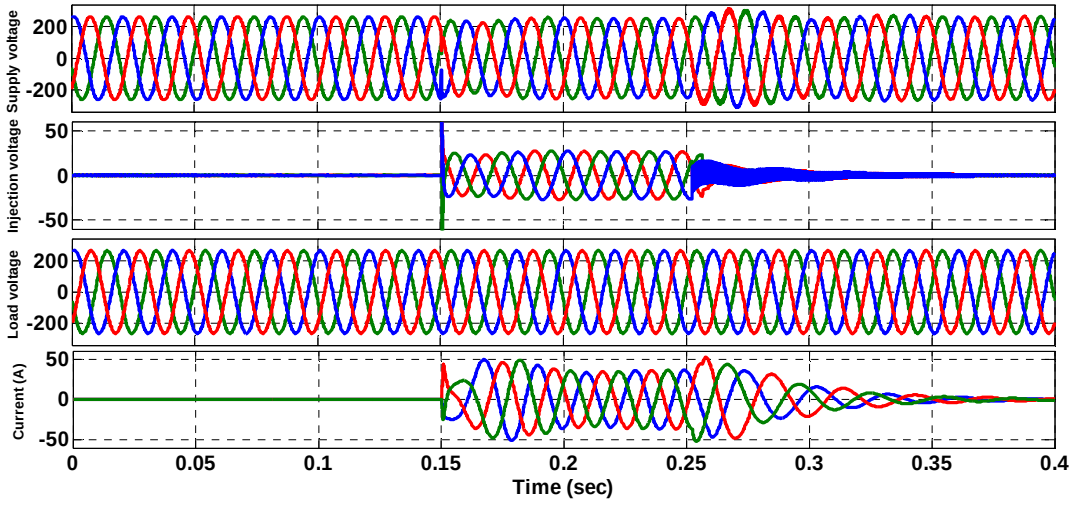

Figure 5.23 Response of DVR with vector control voltage when capacitor banks are placed on supply side and sag swell related current.

5.7.5 Voltage Flicker suppression

Flicker is defined in the European standard EN 50160. Flicker is the impression of unsteadiness of visual sensation included by a light stimulus whose luminance or spectral distribution fluctuates with time. In this case, the system is subjected to an unbalanced voltage flicker. Figure 5.24 shows the response of DVR with vector control during three phase voltage flickers.

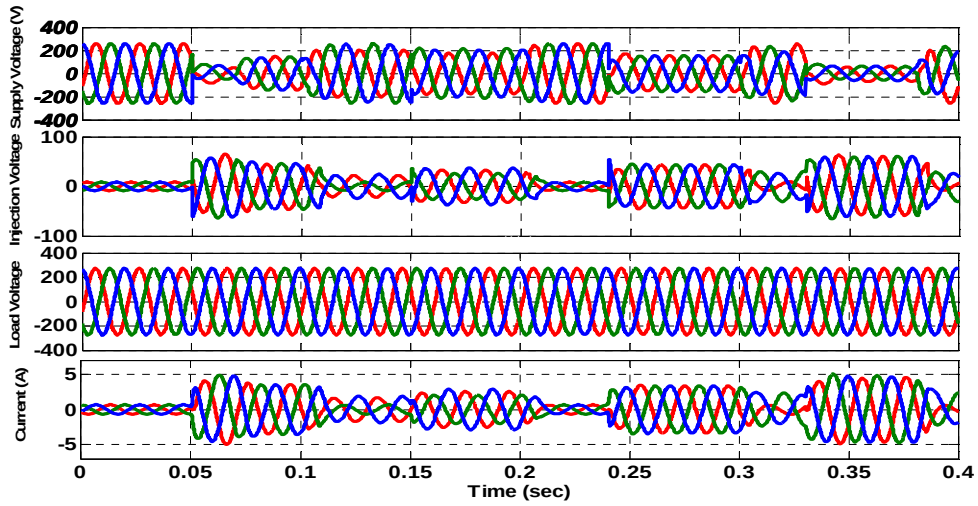

Figure 5.24 Response of DVR with vector control during three phase voltage flicker (i) the source-side voltage for voltage sag and swell (ii) the injected voltage (iii) the load-side voltage response (iv) Extra fault current.

5.7.6 Induction Motor Load

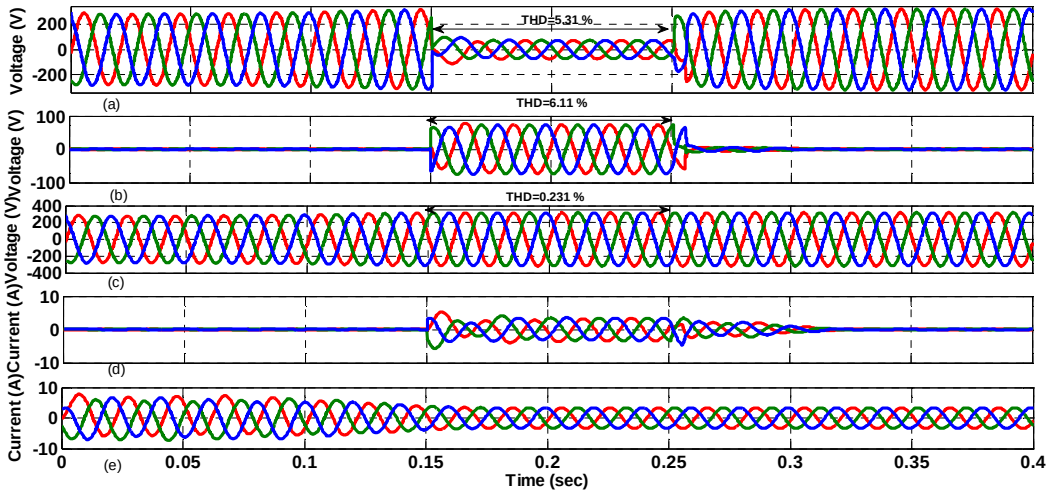

Figure 8.25 Response of DVR with vector control for balanced voltage sag and Induction Motor load (a) Three phase source side sag voltage (b) Injected DVR voltage (c) Three phase load voltage (d) Extra fault current (e) Three phase load current.

In this case, the verification is done with induction motor load connected in load side terminal and the parameters of the induction motor are listed in Table 5.7. The grid voltage sag, DVR injected voltages and the load current is shown in Figure 5.25. It can be observed that the DVR inject the required compensating voltage immediately after grid voltage sag, swell and flickers is detected; to maintain load voltages at desired level also mitigate of any anomalies in the series voltage injection. At that time obtained PV output voltage and current, step-up DC-DC converter output voltage and current, output power (Watt) and dc out-put voltage are shown in Figure 5.26. Figure 5.27 shows the performance of the DVR for instantaneous active and reactive power output for different condition.

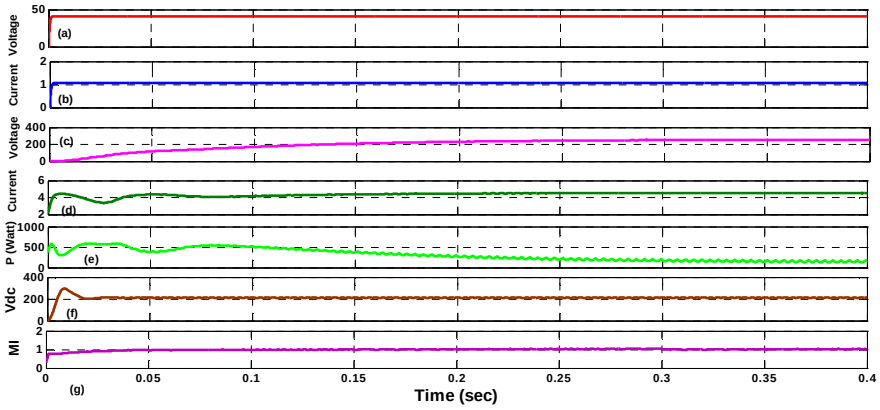

Figure 5.26 Response of DVR with vector control for balanced voltage sag and Induction Motor load (a) PV output voltage (b) PV output current (c) Output voltage of the high step-up DC-DC converter (d) Output current of the high step-up DC-DC converter (e) Simulation result of output power (Watt) (f) V_{dc} out-put voltage (g) Modulation index output.

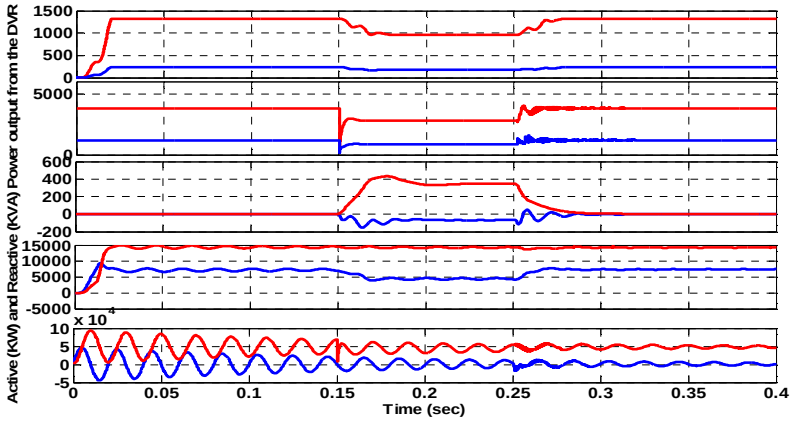

Figure 5.27 Performance of the DVR for (a) resistive load with unbalanced voltage sag active and reactive power output from the DVR (b) capacitive load with unbalanced voltage sag active and reactive power output from the DVR (c) resistive load with balanced voltage sag active and reactive power output from the DVR (d) non-linear load with unbalanced voltage sag active and reactive power output from the DVR (e) Induction motor load with unbalanced voltage sag active and reactive power output from the DVR.

5.8 Results comparison of the state of the art with proposed control method

The proposed PV-DVR efficiently eliminates the voltage sags, swells, flickers and harmonics as compared to existing schemes in [128, 143, 144] during different fault conditions with BBO-based optimized control technique. It decreases the THD level to 0.413% for Single Line Ground fault, 0.324% in Double Line Ground fault and 0.321% in 3-phase fault circumstance. The performance comparison of different fault conditions as observed from Table 8 shows that the BBO based optimized technique gives better harmonic compensation compared to other existing techniques. It is also observed from Table 8 that the compensation during grid voltage distortion for the proposed technique is better compared to [144].The outcome THD level fulfills the standard range of IEEE 519-1992.

Table 5.8 Comparison of harmonic compensation with different controllers and grid voltage distortion

Comparison of harmonic compensation with different controllers						Compensation during grid voltage distortion		
60% voltage sag	[143]	FL [128]	GA-with PI[128]	[143]	Proposed		THD (%)[144]	Proposed THD (%)
SLG fault	2.10%	0.6	0.87	0.52	0.513	Load voltage	4.54	2.13
DLG fault		0.49	0.75	0.41	0.394	Load current	16.66	7.34
3- phase to ground fault	0.80%	0.38	0.58	0.37	0.361	Grid voltage	35.15	11.73

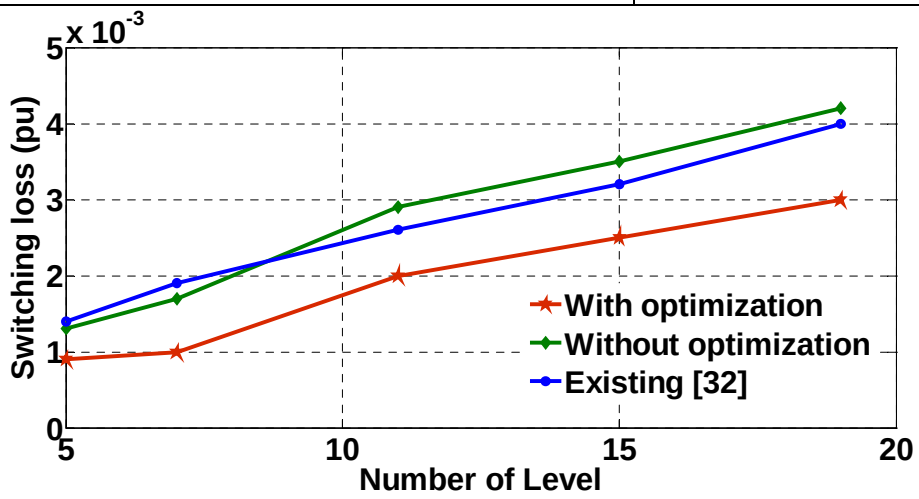

Figgure 5.28 (a) Switching losses Vs No. of levels for proposed, existing and unoptimized techniques

The switching, conduction and total losses for the proposed optimized technique, existing technique [145] and unoptimized techniques are calculated for MLI with different levels following the standard procedure shown in [145, 146]. The same are presented in graphical forms in Figure 5.28 (a), (b) and (c) respectively, which shows

improvement on switching and total losses through the proposed BBO based optimization. The proposed algorithm optimizes the switching angles so that the undesired lower order harmonics are eliminated while the other higher order harmonics are controlled from the output voltage without any additional switching. The inverters without optimized switching require additional switching for same output voltage THD, which can increase the switching losses while the conduction losses almost remain the same. This is the main advantage of the proposed scheme. The plots of THD with modulation index considering additional switching, unoptimized switching and for the proposed optimized switching are shown in Figure 5. 28(d), which shows improvement with the proposed scheme.

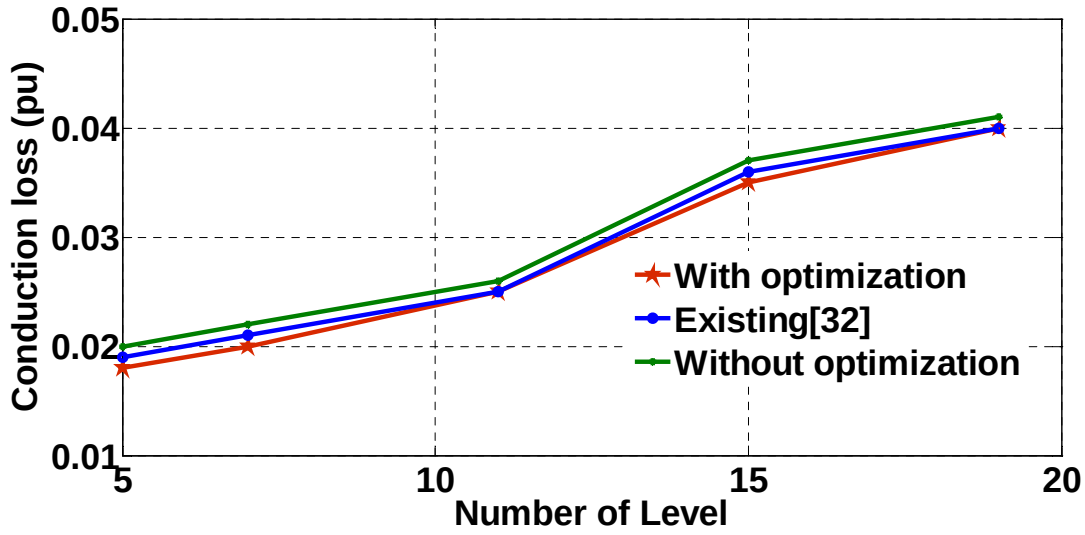

Figure 5. 28 (b) Conduction losses Vs No. of levels for proposed, existing and unoptimized techniques

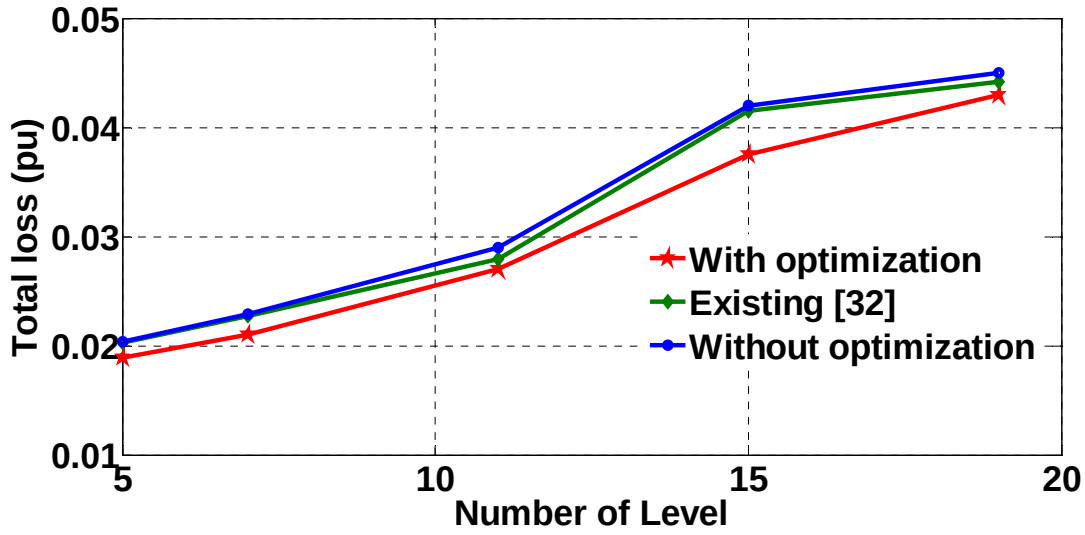

Figure 5. 28 (c) Total losses Vs No. of levels for proposed, existing and unoptimized techniques

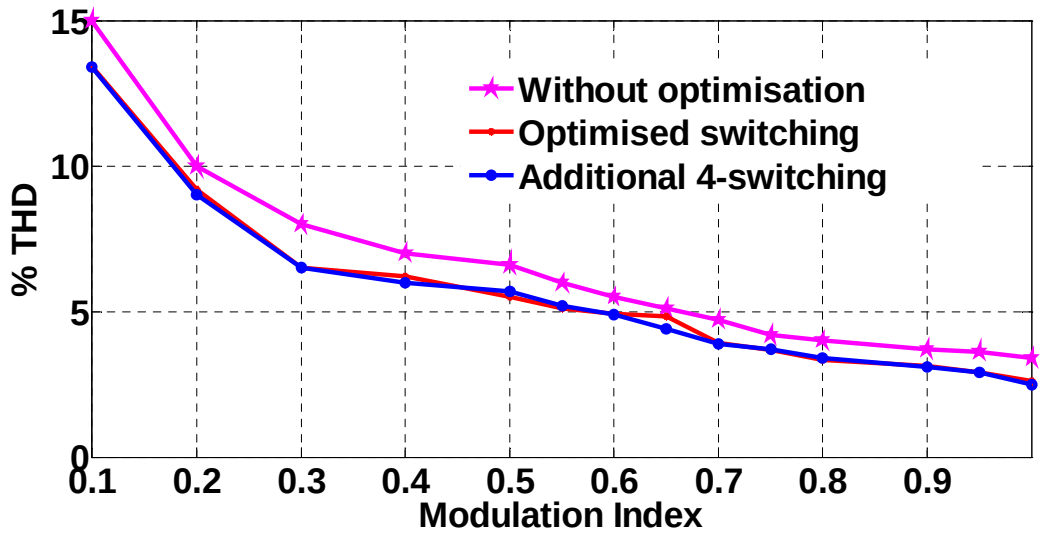

Figure 5.28 (d) Modulation index with % THD

5.9 Conclusion

This chapter investigates the new model of PV-DVR system with the presented control method. The proposed technique is capable to compensate networks faults and mitigate their effects on sensitive loads in distribution power systems. DVR has the boundary on capability of injection of active power i.e., either zero or minimum active power mode. The simulation results shows that the capability of PV-DVR in mitigating the voltage variation. The selected lower order harmonics of the output voltage are eliminated by BBO-based SHEAM-PWM switching technique and THD is also calculated to evaluate the quality of the load voltage during the operation of DVR and this THD fulfill IEEE 519 std. range. The switching angles contributing minimum voltage THD at different modulation indices are computed by the BBO algorithm and stored in a DSP as look-up table for online application. From the simulation results, it is obvious that the generated voltage spectrum is very much improved with increases in the level of the inverter and proposed system also decreases the overall voltage THD in the micro-grid, decreases the system loss, improving dc link voltage, increases the execution speed, solves commutation loss, electromagnetic interference, harmonics and high frequency switching problems. Different simulation study cases are verified to evaluate the potential application of the proposed control approach with superior advantage. A rapid response and precise compensation with optimum energy of the proposed control system are revealed in the simulation results considering practical load and system model.

Chapter 6

Proposed Three phase Micro-grid System of PV-wind- PEM - FCS with HCBLMI - based combined DVR, STATCOM and UPQC topology

Chapter 6

6.1 Chapter overview

This chapter describes an improved FACTS based custom power controller with Dynamic Voltage Restorer (DVR), Static Compensator (STATCOM) and Unified Power Quality Conditioner (UPQC) topology. The proposed controller can proficiently moderate the power quality problems like; sag, swell, flicker, reactive and active power compensation, voltage disturbances with harmonic problems to make sure power quality in the distribution system. The proposed configuration utilizes the DGs e.g. PV, wind and proton exchange membrane fuel cell stack (PEMFCS) connected to the micro grid for realilazisation of DVR, STATCOM and UPQC operation with reduced filtering requirements. Space Vector Pulse Width Modulation (SVPWM) based hybrid cascade bottom leg multilevel inverter (HCBLMI) has been used for this purpose. The proposed topology has been simulated using MATLAB/Simulink and it is shown that the UPQC performs significantly better than the DVR and PSTATCOM for improvement of different power quality issues.

6.2 Introduction

The global concerns about the environment, global warming and power safety have enabled the development of renewable and sustainable distributed energy resources to the power network for secured level of stability and flexibility in deregulated distributed power systems. The environmental friendly pollution free green power like solar [147, 148, 149] and wind [150] energy has acknowledged the most awareness because those appear to be some of the better solutions to ecological or most expected problems. Use of nonlinear sensitive loads, switching and non-switching loads and different process industries with specific manufacturing process are discussed in the literature [151,152]. Power superiority problems such as sags, swells, flickers, notch, spike, harmonics, transients and reduction of three-phase voltage unbalance are also addressed in the open literature [153].There are a number of power quality improvement devices reported in the existing literature including static VAr compensators (SVC) [154], static synchronous compensators (STATCOM) [155], unified power flow controllers (UPFC) [156], etc. The custom power devices based on energy storage systems e.g., dynamic voltage restorers (DVRs) are also explored in [157,158,159,160]. The DVR is a series connected (with and without transformer) energy storage based device which can mitigate voltage sag, swells, flickers and compensate voltage harmonics along with limit on transient voltages and fault currents. The power electronics based control of UPQC optimizes the voltage and current related issues in the power system while enabling simultaneous operation with shunt and series active power filters. The series part of the UPQC is known as DVR and shunt path is known as STATCOM. The series connected path injects the compensating voltages generated by the multilevel voltage source inverter (VSI) [161,162,163] to mitigate voltage unbalance and harmonics and controls the reactive power. Multilevel VSI converters such as multilevel flying capacitor converters [161], diode-clamp converters [162], cascade multilevel inverter [163] and three-phase neutral point clamped (NPC) converters [164,165] are able to synthesize voltage and current waveform. Pulse width modulations (PWM) based different techniques are also used to control the inverter have been discussed [166]. The

SVPWM technique directly uses the control variable for determining each switching vector for optimization of switching patterns [167].

In this chapter, a hybrid cascade bottom leg multilevel inverter (HCBMLI) is used along with combined PV-wind-PEMFCS based sources forming a micro grid system to address different power quality issues. The proposed HCBMLI can operate as DVR, STATCOM or UPQC for power quality improvement. SVPWM based switching scheme is adopted for the proposed inverter for control of overall voltage and current THD. The proposed scheme is operated under different modes and the performances are compared. In the present study, it is shown that the UPQC mode performs significantly must better than the DVR and STATCOM mode of operation.

6.3 Proposed Micro-grid Configuration

Figure 6.1 illustrates the proposed micro-grid structural scheme. The micro-grid is powered by distributed generators, distributed energy storage system, PEMFCS, renewable resources like PV, wind etc. When the micro-grid connects to the network at a point of common coupling that keeps voltage at the similar level as the central grid. The green and carbon free distributed generating resources are associated to the linear load as well as sensitive loads through contemporary power electronics converter to supply more consistent and stricter excellence power to the distributed loads. Usage of power electronic interface converters and nonlinear sensitive loads results in harmonics generation, which leads to different electrical power quality issues. The power quality disturbance is the most common severe for the industrial and domestic consumer which requirements vital attention for its compensation. With and without Transformer connected FACTS devices detect the disturbing power quality and mitigate it are in both low, medium and high power distributed system.

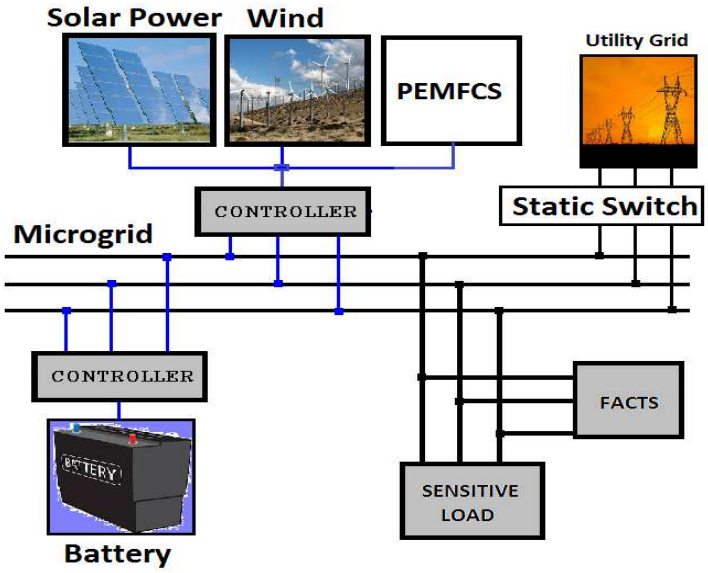

Figure 6.1 Schematic diagram of the Proposed configuration of the Micro-grid.

The detailed diagram for the proposed transformer less HCBMLI is illustrated in Figure 6.2 which can operate either in DVR, STATCOM or UPQC mode. The DC side of the inverters are DC-DC converters in two stages, one for low step up and the other for high step up [168, 169] converters. The inverters switching angles are controlled by space vector pulse width modulation switching technique (SVPWM). For low and medium voltage grid unbalance, the proposed transformer less configuration can work as DVR while operating the switches sw_1 in on and sw_2 in off position. The proposed configuration of DVR can be used in medium voltage network with low switching frequency with lower harmonics magnitude and lower switching losses.

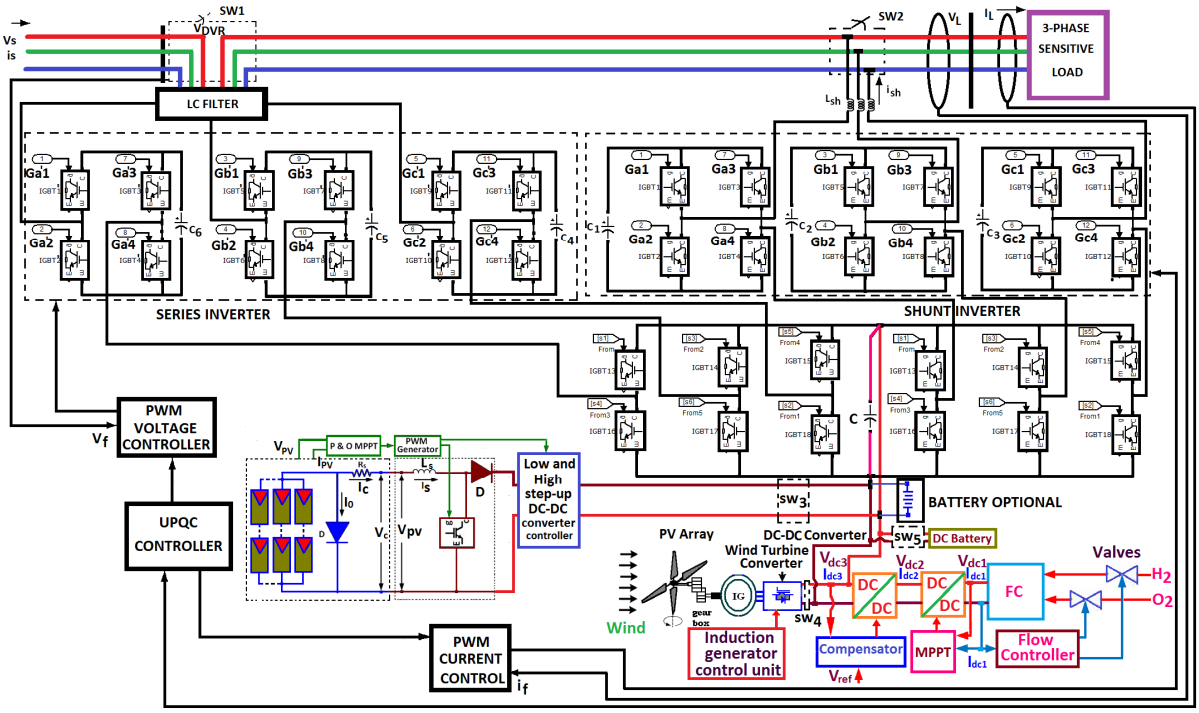

Figure 6.2 The configuration of the proposed transformerless DVR, STATCOM and UPQC

When sw_1 is off and sw_2 is on, the proposed model can be operated as a STATCOM which is a shunt connected FACTS device that can work in current control and voltage control modes. Shunt connected STATCOM provides voltage regulation on the power system and compensate dynamic reactive power support through the application of power electronic devices. The main component of the STATCOM is multilevel converter, which maintains the constant value of DC-link voltage into a three-phase set of balanced output voltages with the desired amplitude, frequency and phase. An AC filter is further connected across the inverter to bypass the harmonics generated by inverter switching. Shunt connected PV-wind-PEMFCS based multi level VSI provides adequate current regulator bandwidth, to achieve high efficiency, the THD of the source current is reduced to less than 5%, which complies with IEEE610000-3 and IEEE 519 harmonic standards and has faster transient response. When sw_1 and sw_2 are both operate the model is operate as a UPQC mode which consists of two VSCs that are connected to common DC

energy storage element and this DC-link is connected through a PV panel, wind power or both (emerging as alternate sources of electricity), PEMFCS, low and high step up DC-DC converter, and a battery. One of the converter is associated in shunt with a distribution grid, while the other one is attached in series with the same grid. The shunt inverter UPQC [170,171] is limited in current control mode. The main advantage presented by VSI topology over CSI includes lighter in weight, cheaper, blocking diodes is not needed, capability of multilevel operation with lower switching frequency, and extra flexible overall control.

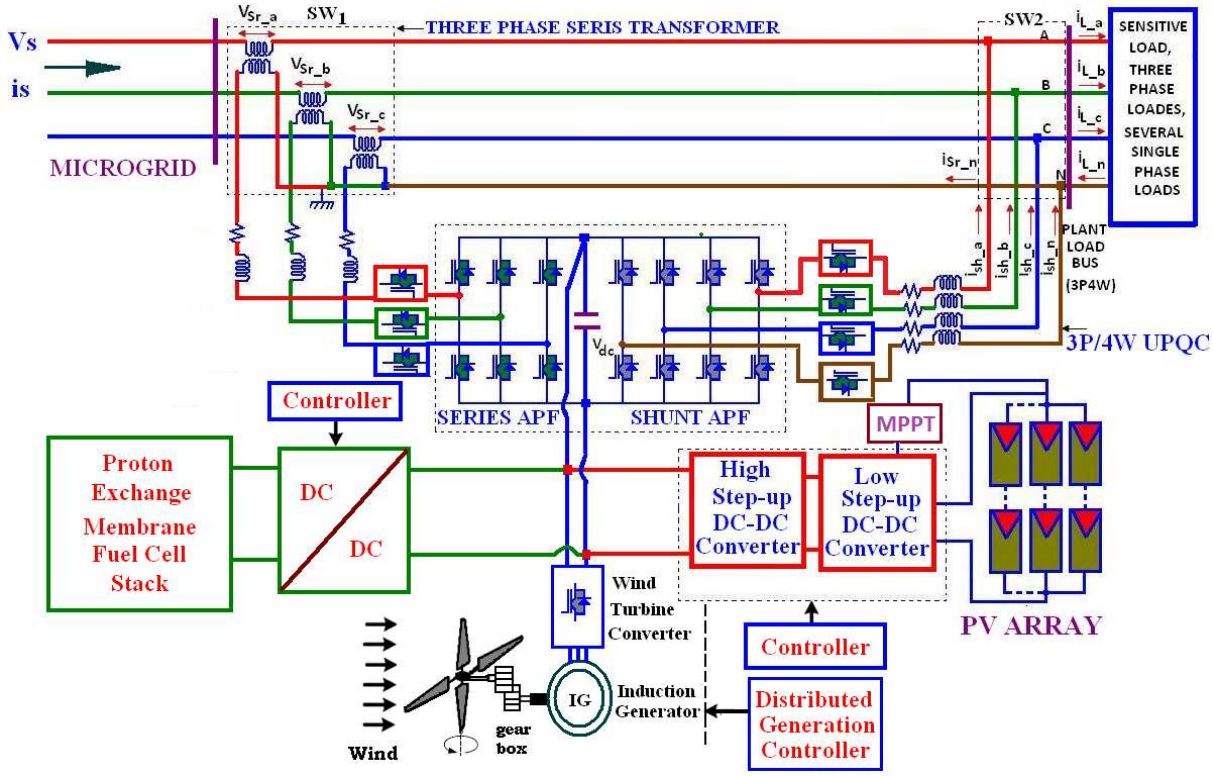

Figure 6.3 The new configuration of the proposed series connected transformer based PV-wind- fuel-cell –UPQC

A transformer connected typical configuration of PV-wind-PEMFCS based UPQC compensated distribution system is shown in Figure 6.3. The proposed UPQC monitors the peak supply voltage, and the d- and q-axis component of the supply voltage. As discussed in this chapter, the main purpose of the proposed UPQC is to regulate the sensitive load bus voltage through the series VSC and the shunt VSC controls the reactive power besides eliminating the unbalance and unwanted harmonics from the bus voltage. The multilevel current controlled VSI controls the voltage and reactive power level without the use of bulky transformers. When the voltage dip is high the transformer based UPQC is more suitable. A battery can be coupled for additional benefit to the PV-wind-PEMFCS generated bus, such that the excess DG generated power can be stored as a backup and compensate the voltage interruption. When the UPQC model is 3-phase-3-wire system, it is required to consider current unbalanced apart from reactive and harmonics current. The 3-phase-4-wire system shown in Figure 6.3 requires an additional loop for excessive neutral current compensation. PEMFCS [172] are used for prospective information for applications of micro-grid to their

better-quality efficiency, small amount of emissions and straight production of electricity. Figure 6.4 shows the simulation configuration of PV-PEMFCS-MPPT control unit; where in Figure 6.5 the hybrid cascade bottom leg PV-wind-PEMFCS multilevel inverter gate control unit is presented. Where the Figure 6.6 represents the PV, wind and converter simulation control unit and in Figure 6.7 represents the PV-wind-PEMFCS based DVR, STATCOM and UPQC control unit.

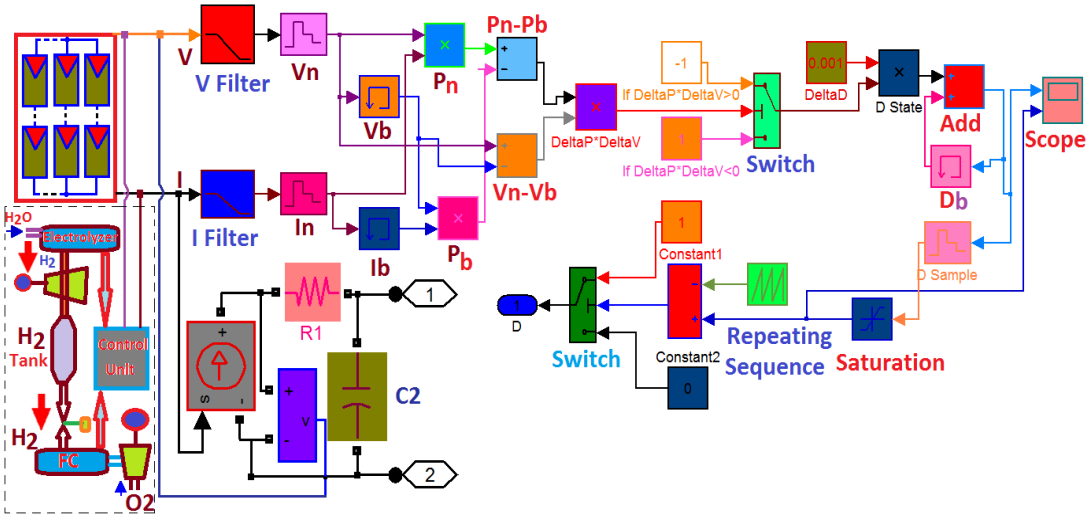

Figure 6.4 Simulation configuration of PV-PEMFCS-MPPT control unit

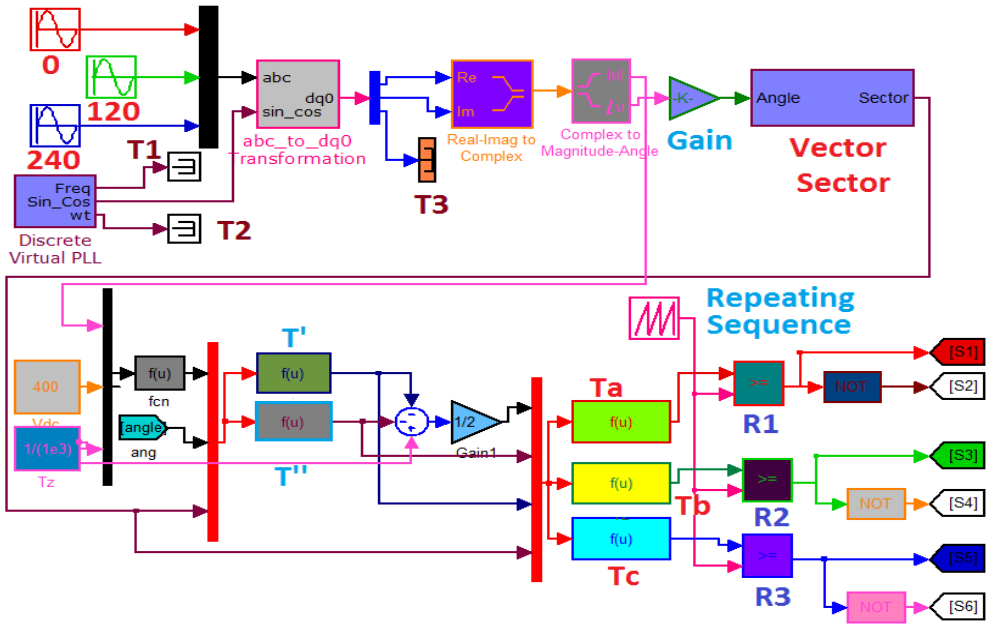

Figure 6.5 Hybrid cascade bottom leg PV-wind-PEMFCS multilevel inverter gate control unit

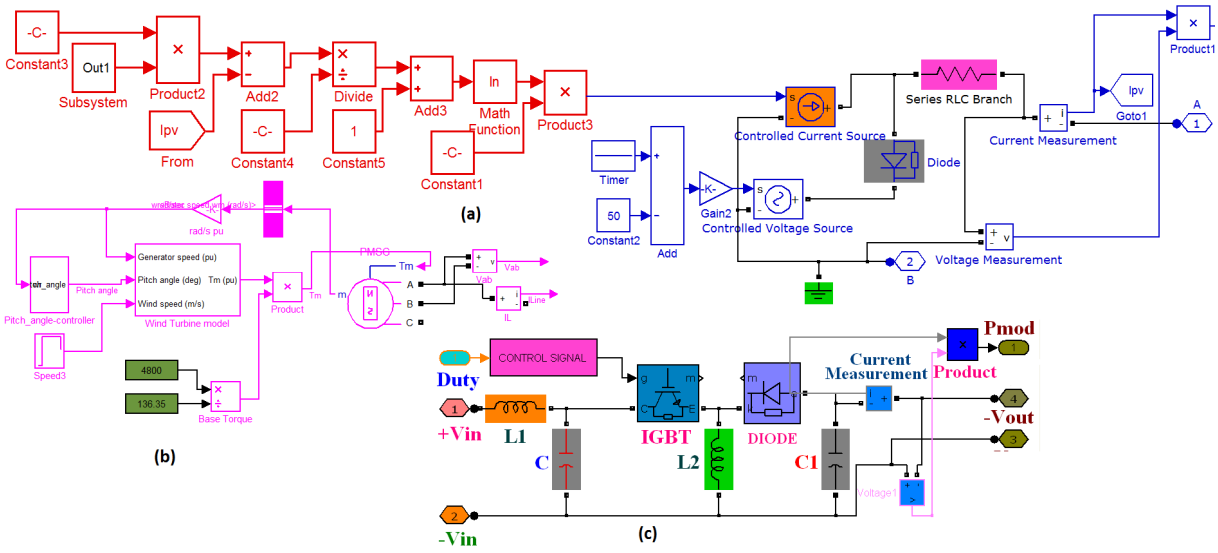

Figure 6.6 PV-wind-PEMFCS based converter simulation control unit

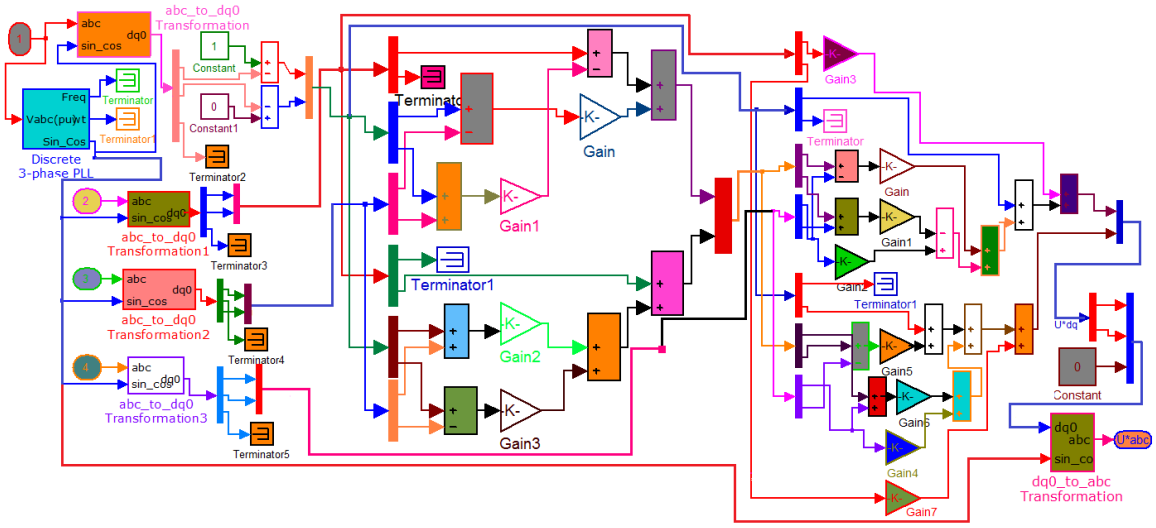

Figure 6.7 PV-wind-PEMFCS based DVR, STATCOM and UPQC control unit

6.4 Proposed DVR, STATCOM and UPQC Control System with SVPWM Algorithm

Inverters are multipurpose power electronic switching controls devices that convert DC electrical power to require AC electrical power and are key sources of harmonics. The flexible power electronics inverter output generated harmonic current is injected to the electrical utility circuit and extremely affecting the customers associated with the interrelated circuit. For better performance, a preferable filter is installed between the injection transformer and proposed VSC to diminish the harmonics from the output of FACTS (i.e., DVR, STATCOM, UPQC) and provide healthier power superiority of the output voltage. The inverter output necessary filter voltage is properly introduced

into the distribution system via with and without series injecting transformer. The PLL employed to regulate the electrical phase angle of the utility for synchronization of the grid. Within the multilevel structure converter, the superiority of voltage is straightforwardly interrelated to the number of voltage level and it improves as the number of voltage levels will increases i.e., low ripple and zero tracking to lofty quality of voltage waveform.

6.4.1 Proposed Multilevel Inverter Topology

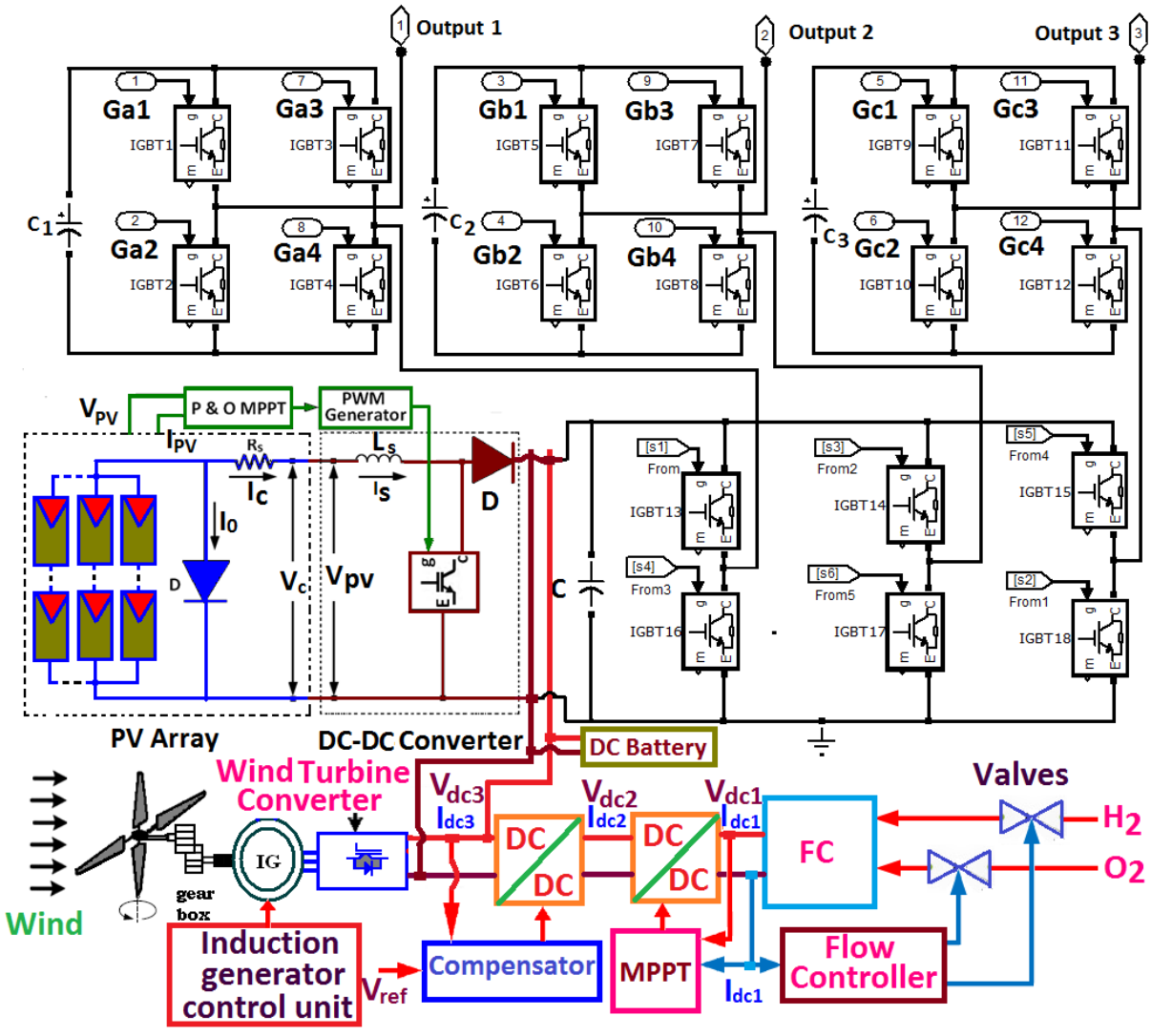

Figure 6.8 A general three-phase hybrid cascaded-multilevel inverter with PV-wind- PEMFCS

Fig 6.8 illustrates the proposed simulation block diagram of PV-wind-PEMFCS based mostly three-phase hybrid cascade bottom leg multilevel inverter. This type of construction of multilevel inverters is appropriate for the smallest amount of components and contains a standard modular layout. Also the multilevel FACTS (DVR,

STATCOM, UPQC) inverters are most straightforward, reduces the cost effecting filtering requirements, increases redundancy, and facilitate the transformer less FACTS operation which implies, low cost and size in a distribution system. To, achieve good quality of AC supply waveforms the construction of multilevel inverter is more appropriate. To, achieve high-quality of AC supply waveforms the multilevel converter is most excellent and appropriate. The assessment and comparison of diode clamped, flying capacitors and cascaded multilevel inverters are shown in Table 6.1.

Table 6.1 Comparisons of three multilevel inverters

Converter Type	Diode Clamp	Flying Capacitors	Cascade Inverter
Main switching devices	$(m-1)\times 2$	$(m-1)\times 2$	$(m-1)\times 2$
Main diodes	$(m-1)\times 2$	$(m-1)\times 2$	$(m-1)\times 2$
Clamping diodes	$(m-1)\times(m-2)$	0	0
DC bus capacitors	$(m-1)$	$(m-1)$	$(m-1)/2$
Balancing capacitors	0	$(m-1)\times(m-2)/2$	0

6.4.2 Proposed Space Vector Pulse Width Modulation Switching control strategies

For reduction of commutation losses, improvement of bus utilization and low order of harmonic THD, the SVPWM multilevel converter switching technique is most sophisticated. The space vector modulation is one of the advanced, computation intensive, flexible and real time modulation techniques. Using SVPWM switching technique determination of the switching instant of the switching vectors α-alpha, β-beta planes the magnitude and angle of the rotating vector can be found by the mean of Clark's Transformation with respect to stationary reference frame.

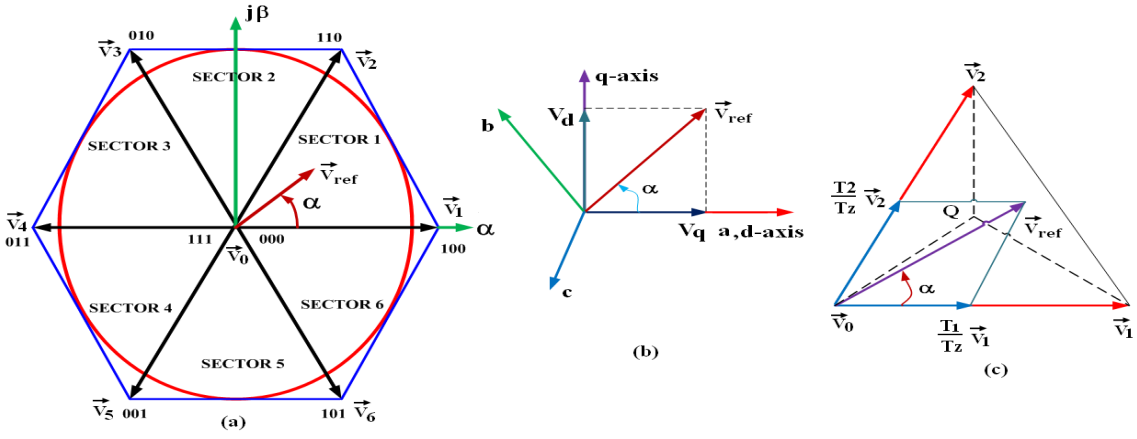

Figure 6.9 Space vector configurations for (a) two-level inverter (b) voltage space vector and its components (d, q) (c) reference vector as a combination of adjacent vectors at sector 1.

Figure 6.9 shows the representation of rotating vector in complex plane with typical space vector diagram for (a) two-level inverter (b) voltage space vector and its components (d-direct, q-quadrature) (c) reference vector as a combination of adjacent vectors at sector 1.

The reference voltage can be written as

$$\vec{V}_{reference} = V_{alpha} + jV_{beta} = 2/3\left(V_R + aV_Y + a^2V_B\right), \text{ where, } a = e^{j(2\pi/3)} = e^{j120^\circ} \tag{6.1}$$

$$\left|\vec{V}_{reference}\right| = \sqrt{V_{alpha}^2 + V_{beta}^2}, \alpha = \tan^{-1}\left(V_{beta}/V_{alpha}\right) \tag{6.2}$$

$$V_{alpha} + jV_{beta} = 2/3\left(V_R + e^{j(2\pi/3)}V_Y + e^{-j(2\pi/3)}V_B\right)$$

$$= 2/3\left(V_R + \cos\left(2\pi/3\right)V_Y + \cos\left(2\pi/3\right)V_B\right) + j\,2/3\left(\sin\left(2\pi/3\right)V_R - \sin\left(2\pi/3\right)V_Y\right) \tag{6.3}$$

Equating real and imaginary parts from equation (6.3):

$$V_{alpha} = 2/3\left(V_R + \cos\left(2\pi/3\right)V_Y + \cos\left(2\pi/3\right)V_B\right) \tag{6.4}$$

$$V_{beta} = 2/3\left(0V_R + \sin\left(2\pi/3\right)V_Y - \sin\left(2\pi/3\right)V_B\right) \tag{6.5}$$

The sinusoidal voltage can be treated as having a constant amplitude, constant frequency and transformed into a vector in the RYB reference frame to a stationary d-q coordinate frame.

$$\begin{bmatrix} V_{direct} \\ V_{quardrature} \end{bmatrix} = \frac{2}{3}\begin{bmatrix} 1 & \cos\left(2\pi/3\right) & \cos\left(2\pi/3\right) \\ 0 & \sin\left(2\pi/3\right) & -\sin\left(2\pi/3\right) \end{bmatrix}\begin{bmatrix} V_R \\ V_Y \\ V_B \end{bmatrix} \tag{6.6}$$

From vector diagram of Figure 6.9 (b), $\vec{V}_{reference}$ $V_{direct}, V_{quadrature}, \vec{V}_{refrence}$ and angle α are

$$V_{direct} = V_{Rn} - V_{Yn}.\cos(60) - V_{Bn}.\cos(60)$$

$$= V_{Rn} - (1/2).V_{Yn} - (1/2).V_{Bn} \tag{6.7}$$

$$V_{direct} = 0 - V_{Yn}.\cos(30) - V_{Bn}.\cos(30)$$

$$= 0.V_{Rn} - \left(\sqrt{3}/2\right).V_{Yn} - \left(\sqrt{3}/2\right).V_{Bn} \tag{6.8}$$

$$\begin{bmatrix} V_{direct} \\ V_{quadrature} \end{bmatrix} = \frac{2}{3}\begin{bmatrix} 1 & -1/2 & -1/2 \\ 0 & \sqrt{3}/2 & -\sqrt{3}/2 \end{bmatrix}\begin{bmatrix} V_R \\ V_Y \\ V_B \end{bmatrix} \tag{6.9}$$

$$\left|\vec{V}_{reference}\right| = \sqrt{V_{direct}^2 + V_{quadrature}^2}$$

$$\alpha = \tan^{-1}\left(V_{direct}/V_{quadrature}\right) = \omega_s t = 2\pi f_s t \tag{6.10}$$

Where, f_s is a fundamental frequency.

Considering that T_k is sufficiently small, the reference voltage $\vec{V}_{reference}$ could be constant during T_k. The time duration is

$$\vec{V}_{reference}T_k = \vec{V}_1\frac{T_1}{T_k} + \vec{V}_2\frac{T_2}{T_k} + \vec{V}_0\frac{T_0}{T_k}$$

$$\vec{V}_{reference} = \vec{V}_1 T_1 + \vec{V}_2 T_2 + \vec{V}_0 T_0, \text{ where } T_k = T_1 + T_2 + T_0 \tag{6.11}$$

T_1, T_2 and T_0 are the time for $\vec{V}_1$, $\vec{V}_2$ and $\vec{V}_0$ respectively. Therefore, the space vector can be written as follows:

$$\vec{V}_{reference} = \vec{V}_{reference}e^{i\theta}, \vec{V}_1 = (2/3)V_{direct}, \vec{V}_2 = (2/3)V_{direct}e^{j(\pi/3)}, \text{ and } \vec{V}_0 = 0 \tag{6.12}$$

$$T_k * \vec{V}_{reference} * \begin{bmatrix}\cos(\alpha)\\ \sin(\alpha)\end{bmatrix} = T_1 * \frac{2}{3} * V_{dc} * \begin{bmatrix}1\\ 0\end{bmatrix} + T_2 * \frac{2}{3} * V_{dc} * \begin{bmatrix}\cos(\pi/3)\\ \sin(\pi/3)\end{bmatrix} \tag{6.13}$$

The real part is, $T_k * \vec{V}_{reference} * \cos(\alpha) = T_1 * \frac{2}{3} * V_{dc} + T_2 * \frac{1}{3} * V_{dc}$ (6.14)

Imaginary part is, $T_k * \vec{V}_{reference} * \sin(\alpha) = T_2 * \frac{1}{\sqrt{3}} * V_{dc}$ (6.15)

By solving the above equations, T_1 and T_2 can be expressed as below:

$T_1 = T_k * a * \sin(\pi/3 - \alpha)$, $T_2 = T_k * a * \sin(\alpha)$ where $T_k = \frac{1}{f}$ for $0 \le \alpha \le 60^\circ$ and the modulation index is,

$m_d = \frac{\sqrt{3}V_{reference}}{V_{dc}}$.

Here T_1, T_2, T_0 represent the time widths for vectors V_1, V_2, V_0. T_0 is the period in a sampling period for null vectors should be filled. As each switching period T_k starts and ends with zero vectors i.e. there will be two zero vectors per T_k or four null vectors per T_k, duration of each null vector is $T_k/4$.

The space vector switching time duration at any sector is represented by equations (6.16) and (6.17).

$$T_1 = \frac{\sqrt{3}.T_k.\left|\vec{V}_{reference}\right|}{V_{dc}}\left(\sin\left(\frac{\pi}{3} - \alpha - \frac{n-1}{3}\pi\right)\right) = \frac{\sqrt{3}.T_k.\left|\vec{V}_{reference}\right|}{V_{dc}}\left(\sin\frac{n}{3}\pi.\cos\alpha - \cos\frac{n}{3}\pi.\sin\alpha\right) \tag{6.16}$$

$$T_2 = \frac{\sqrt{3}.T_k.\left|\vec{V}_{reference}\right|}{V_{dc}}\left(\sin\left(\alpha - \frac{n-1}{3}\pi\right)\right) = \frac{\sqrt{3}.T_k.\left|\vec{V}_{reference}\right|}{V_{dc}}\left(-\cos\alpha.\sin\frac{n-1}{3}\pi + \sin\alpha.\sin\frac{n-1}{3}\pi\right) \quad (6.17)$$

Where $n = 1$ through 6 and $T_k = T_1 + T_2 + T_0$ for $0 \le \alpha \le 60^\circ$

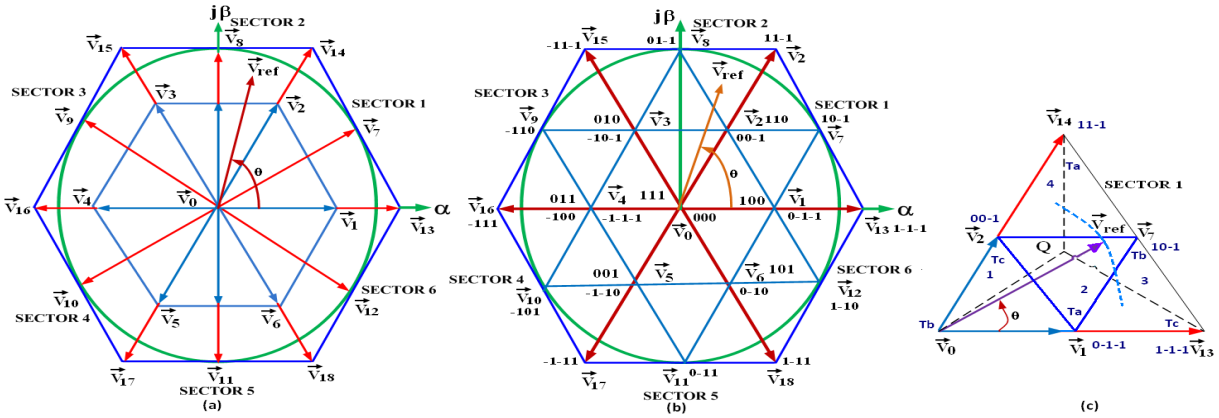

Figure 6.10 Space vector diagram for (a) three-level inverter (b) division of sectors and region for three-level inverter (c) voltage vector 1 and their times.

Figure 6.10 shows that the space vector diagrams for (a) three-level inverter (b) division of sectors and region for three-level inverter (c) voltage vector 1 and their times. If θ is between $0 \le \theta \le 60^\circ$ then $V_{reference}$ will be in sector 1, if θ is between $60^\circ \le \theta \le 120^\circ$ then V_{ref} will be in sector 2, if θ is between $120^\circ \le \theta \le 180^\circ$ then $V_{reference}$ will be in sector 3, if θ is between $180^\circ \le \theta \le 240^\circ$ then $V_{reference}$ will be in sector 4, if θ is between $240^\circ \le \theta \le 300^\circ$ then $V_{reference}$ will be in sector 4 and if θ is between $300^\circ \le \theta \le 360^\circ$ then $V_{reference}$ will be in sector 5.

The relationship between times and voltage is

$$V_1 T_a + V_7 T_b + V_2 T_c = V_{reference} T_s \quad (6.18)$$

$$T_a + T_b + T_c = T_s$$

From Figure 6.10 voltage vectors V_1, V_2 and V_7 can be observed as, $\vec{V}_1 = \frac{1}{3}V_{direct}$, $\vec{V}_2 = \frac{1}{3}V_{direct}e^{j(\pi/3)}$, $\vec{V}_7 = \frac{1}{3}V_{direct}e^{j(\pi/6)}$ and $\vec{V}_{reference} = V_{reference}e^{j\theta}$

$$\frac{1}{3}V_{direct}T_a + \frac{\sqrt{3}}{3}V_{direct}\left(\cos(\pi/6) + j\sin(\pi/6)\right)T_b + \frac{1}{3}V_{direct}\left(\cos(\pi/3) + j\sin(\pi/3)\right)T_c$$

$$= V_{reference}(\cos\theta + j\sin\theta)T_s$$

$$T_a + \frac{3}{2}T_b + \frac{1}{2}T_c = 3.\frac{V_{reference}}{V_d}.\cos\theta.T_s \tag{6.19}$$

$$\frac{3}{2}T_b + \frac{\sqrt{3}}{2}T_c = 3.\frac{V_{reference}}{V_d}.\sin\theta.T_s \tag{6.20}$$

Solving upper two equations for total time, $T_s = T_a + T_b + T_c$

$$T_a = T_s\left[1-2.m_d.\sin\theta\right], T_b = T_s\left[2.m_d.\sin\left(\frac{\pi}{3}+\theta\right)-1\right] \text{and} \, T_c = T_s\left[1-2.m_d.\sin\left(\frac{\pi}{3}+\theta\right)\right] \text{for}$$

$$0 \le \theta \le \pi/2 \tag{6.21}$$

The modulation index is, $m_d = \frac{V_{reference}}{V_{direct}}$.

6.5 SVPWM simulation output results

For the proposed system the simulations are performed by using Matlab/Simulink. The SVPWM technique controls the minimum harmonic distortion, position of reference vector according to fundamental frequency, reduction of switching losses, voltage sag, swell, flicker, unbalanced, active and reactive power, reduces the commutation losses and controls the inverter output voltage. Conjointly the construction of the multilevel SVM inverter can be developed for versatile applications, like as an active energetic power filter, static power unit VAR compensator, motor drive system (STATECOM), PV, fuel cells, battery etc. In this section, the merit and demerit of different multilevel inverters performance for FACTS control is examined.

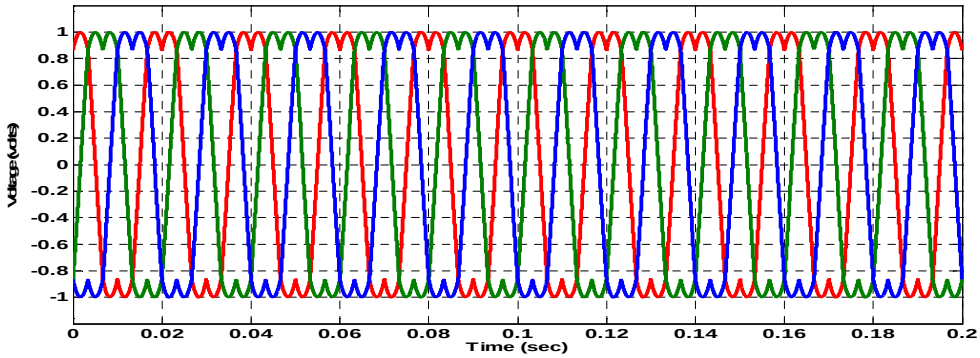

Figure 6.11 Switching instant of a SVPWM pulse waveform.

The switching instant of a space vector pulse width modulation pulse waveform is shown in Figure 6.11. Figures. 6.12 & 6.13 show the simulation result of cascade MLI for a three level and five level output voltage (V_{an}, V_{bn} and

V_{cn}). The THD measurement for the 5-level DCMLI is shown in Figure 6.13 where fundamental frequency is 50 Hz and the %THD is 4.62.

The THD measurement for the 5-level cascade multilevel inverter is shown in Figure 6.14 where fundamental frequency is 50 Hz and the %THD is 3.71.This proves that the proposed cascade multilevel inverter scheme can highly reduce the %THD than the others multilevel inverters. The THD values of the proposed cascade multilevel inverters are lower than that of the other multilevel inverter as shown in Table 6.2. So the proposed control techniques have good accuracy, flexibility, speed and each of implementation.

Table 6.2 Comparison between % THD for proposed system with SPWM.

No of	Proposed SVPWM (% THD)			SPWM (% THD)		
levels	DCMLI	NPC	Cascade	DCMLI	NPC	Cascade
2	5.264	15.2508	3.9861	12.432	15.876	7.435
5	4.62	10.9005	3.71	12.845	14.324	6.392
7	3.6356	10.3778	2.6202	11.8453	13.682	5.549
9	3.2577	10.1405	2.4754	11.235	12.203	5.0453
11	3.002	10.0761	2.0955	11.0701	11.002	4.374
13	2.9557	8.8655	1.8804	10.214	10.549	4.113
15	2.813	8.7752	1.1123	8.045	9.326	3.541
17	2.4359	7.7785	1.0087	6.834	7.162	3.179
19	2.2826	5.0087	1.0243	5.457	6.349	3.0058
23	2.214	4.108	0.3034	4.348	5.23	2.738
25	2.1001	3.543	0.1423	3.678	4.473	2.548
29	1.322	2.8945	0.2046	2.564	4.12	1.3769
31	0.153	2.125	0.0072	2.743	3.032	1.417
35	0.093	2.0537	0.0050	1.973	2.23	1.001

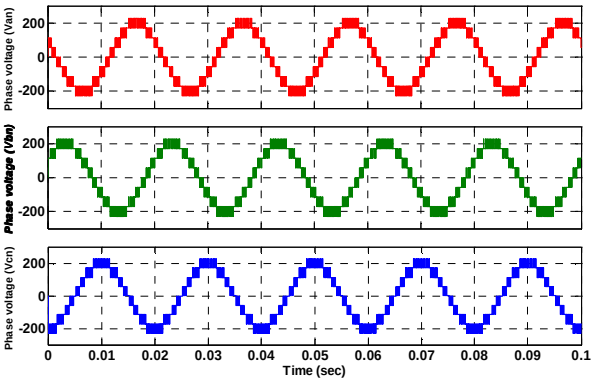

Figure 6.12 Simulation result of SVPWM for hybrid cascade MLI (Van, Vbn and Vcn) for a five level.

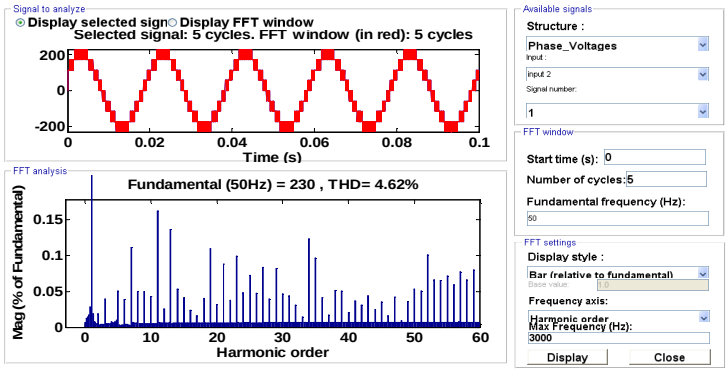

Figure 6.13 FFT output for 5-level diode clamp multilevel inverter

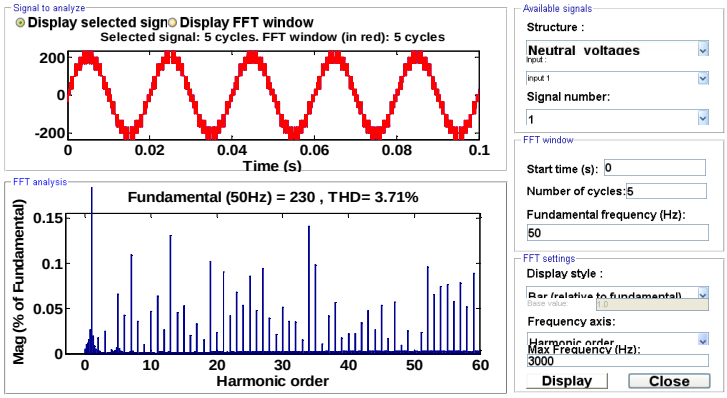

Figure 6.14 FFT output for 5-level cascade multilevel inverter

6.6 Simulation Results for DVR, STATCOM and UPQC with Filter

The performance of the proposed SVPWM switching technique of the PV-wind-PEMFCS connected DVR, STATCOM and UPQC system is implemented by considering different cases of voltage disturbances such as balanced and unbalanced deep voltage sag, voltage swells, voltage flicker, voltage spike, harmonics and long duration voltage variation. A simple PV-wind-PEMFCS-FACTS distribution system is shown in Figure 6.1.

The proposed controller PV-wind-PEMFCS based FACTS compensator establish the proper voltage quality level that is required by the sensitive load for both normal and transient operation with appropriate active and reactive power control. Simulation results using MATLAB/Simulink for multilevel PV-wind-PEMFCS based FACTS inverter with and without transformer shows that the number of levels reach infinity, the output THD approaches zero, i.e., the switching loss problem has been overcome. The simulation parameters are shown in Table 6.3.

Table 6.3 Simulation parameters for the scheme in Figure 6.1.

Description	Parameter	Symbols	Value
PV module specification	No of solar cell	N_{solar}	63 (7x9)
	Nominal voltage	V_{nom}	2x12 V
Step-up DC-DC converter	Inductance	L_m	57 μH
		L_k	0.271 μH
	Switching frequency	f_{s2}	120 kHz
	Capacitance	C_1	293 μF /100 V
	Output DC voltage	V_0	220-230 V
Injection Transformer 1:1	Power	P_{inj}	100 VA
	Voltage rating	V_P/V_S	230/230 V
	Resistance	R_P/R_S	0.0000261 ohm
	Inductance	X_P/X_S	0.0003 ohm
	Magnetizing	X_m	0.00004 ohm
DVR	DC voltage of DVR	V_{dc}	240-260 V
	DC link capacitance	C_{dc}	29 μF
UPQC	Filter inductance	L_f	217µH
	Filter capacitance	C_f	139 µH
	Switching	f_{sw}	4.0 kHz
Parameters of the grid voltage	Nominal voltage	V_s	220-240 V
	frequency	f_s	50 Hz
Parameters of Battery	Series & Parallel	V_{dc}	12V, 500 Ah

6.6.1 Proposed PV-wind- PEMFCS based DVR simulation results

The transformer-less PV-wind- PEMFCS hybrid DVR is based on a three-phase multilevel converter to dynamically inject a compensation voltage vector in series to protect sensitive loads from the electrical micro-grid voltage disturbance such as balanced and unbalanced voltage sag, swell, flicker and reduced voltage or current total harmonic distortion. Figure 6.15 shows the response of DVR with vector control voltage sag for nonlinear load with balanced three phase fault (a) three phase fault voltage, (b) DVR injection voltage, (c) Three phase load voltage (V), (d) three phase fault current, (e) three phase load current.

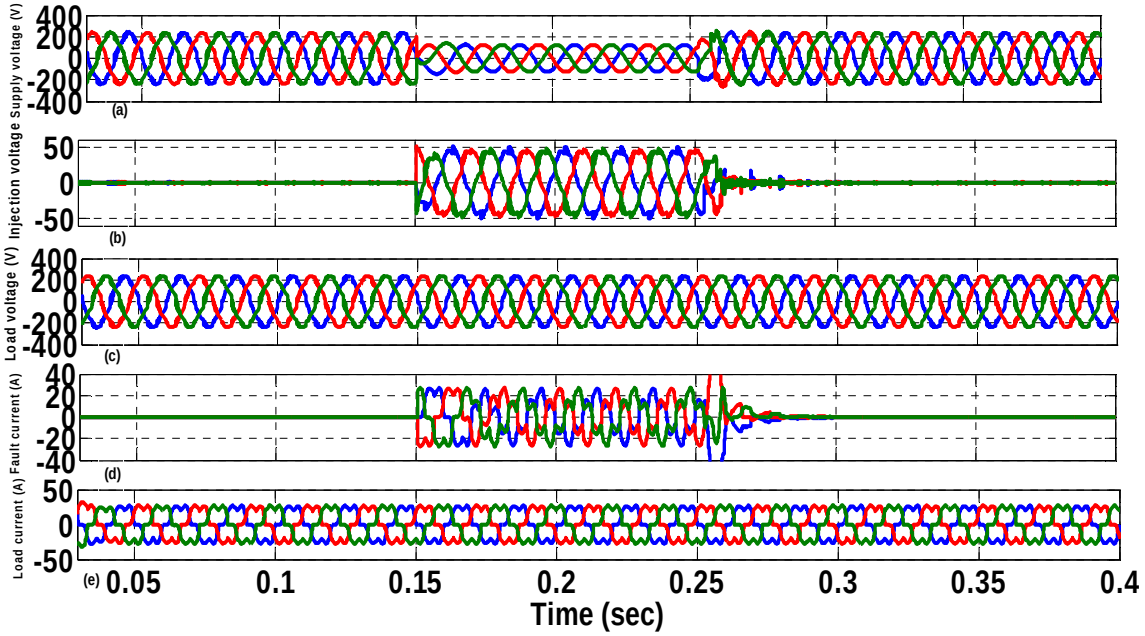

Figure 6.15 Response of DVR with vector control voltage sag for nonlinear load with balanced three phase fault (a) three phase unbalanced fault voltage (b) DVR injection voltage (c) three phase load voltage (V) (d) three phase fault current (e) three phase load current.

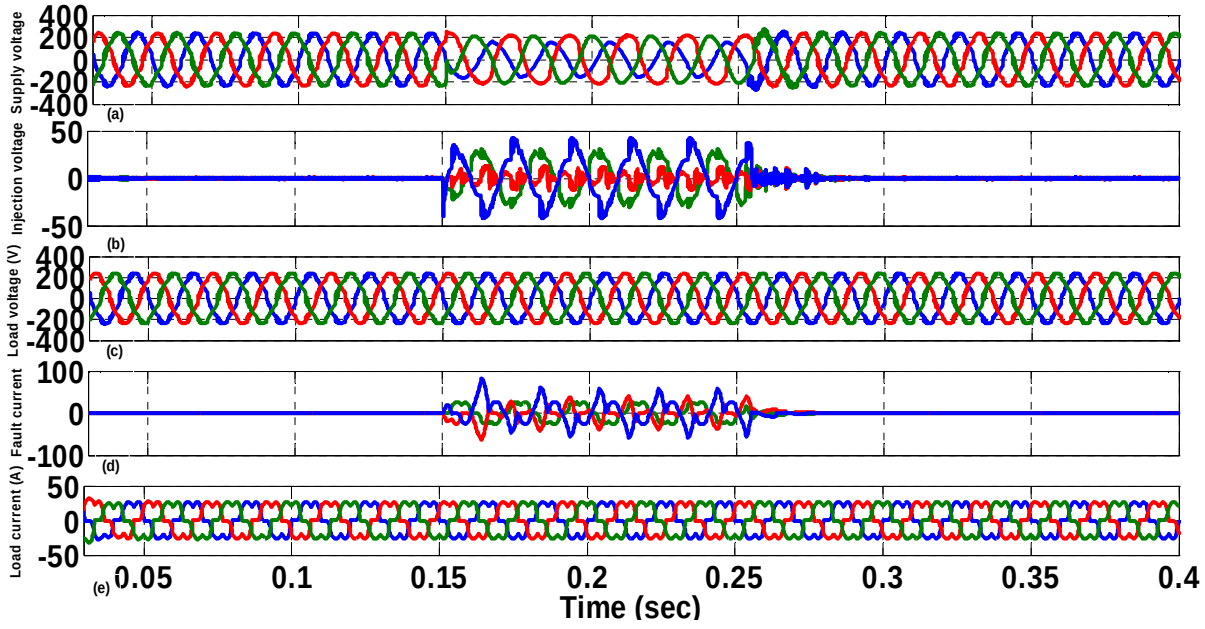

Figure 6.16 Response of DVR with vector control voltage sag for nonlinear (RL) load with phase a, b and ground fault (a) three phase unbalanced fault voltage (b) DVR injection voltage (c) Three phase load voltage (V) (d) three phase fault current (e) three phase load current.

Figure 6.16 shows response of DVR with vector control voltage sag for nonlinear (RL) load with phase a, b and ground fault (a) three phase unbalanced fault voltage, (b) DVR injection voltage, (c) Three phase load voltage (V), (d) three phase fault current, (e) three phase load current.

Figure 6.17 shows the performance of the DVR with vector control voltage sag for nonlinear (RL) load with three phases a, b, c and ground fault, active and reactive power output from the DVR. The PV-wind-PEMFCS based transformer-less DVR is turned on at t=0.15s and continue to t=0.25s. When the fault occurs the load voltage is distorted, it is obvious that the load side voltage is effectively regulated to its normal value and the power quality is maintained.

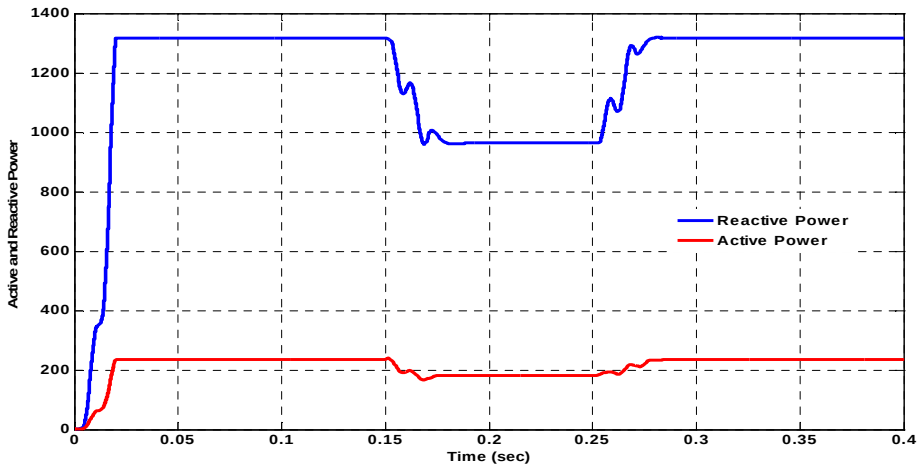

Figure 6.17 Performance of the DVR with vector control voltage sag for nonlinear (RL) load with three phase a, b, c and ground fault, active and reactive power output from the DVR.

6.6.2 Proposed PV-wind- PEMFCS based UPQC simulation results

The PV-wind-PEMFCS primarily based UPQC will operate with and while not electrical transformer operation. The operation and performance of the structure multilevel based PV-wind-PEMFCS UPQC is supposed to tightly regulate grid voltage of sensitive loads against voltage sag, swell, flicker, voltage unbalance, harmonics, negative sequence current, active and reactive power and the any other disturbance in the distribution electrical network. The UPQC is fed from a PV-wind- PEMFCS primarily based DC input within the proposed scheme and also the UPQC won't be directly affected from any grid disturbances. A common standard electrical capacitor is associated to a link of both series and shunt structure multilevel VSCs.

The projected UPQC mentioned during this chapter is meant to compensate the critical load bus voltage (i.e., balanced, sinusoidal, with pre-specified magnitude and phase angle) by series construction multilevel VSCs and the primary goal of the shunt constructed multilevel VSCs is regulate the mostly important real and reactive power to the capacitor and also eliminate the unbalance and harmonics. This twin voltage control operation procedure of the

multilevel based PV-wind-PEMFC-UPQC is controlled by SVPWM switching control loop, inner voltage regulation loop, inner current managing loop, transformation loop, phase angle management loop and filter control loop. Most of the system parameters are as exposed in Table 6.3. Figure 6.18 shows the response of PV-wind-PEMFC-UPQC with vector supervise voltage sag for sensitive nonlinear load with unbiased balanced three phase waveforms of the availability aspect of supply side voltages, the injected appropriate voltage by the UPQC (series PV-wind-DVR), the restored load side 3-phase voltage, 3-phase fault current and 3-phase load current.

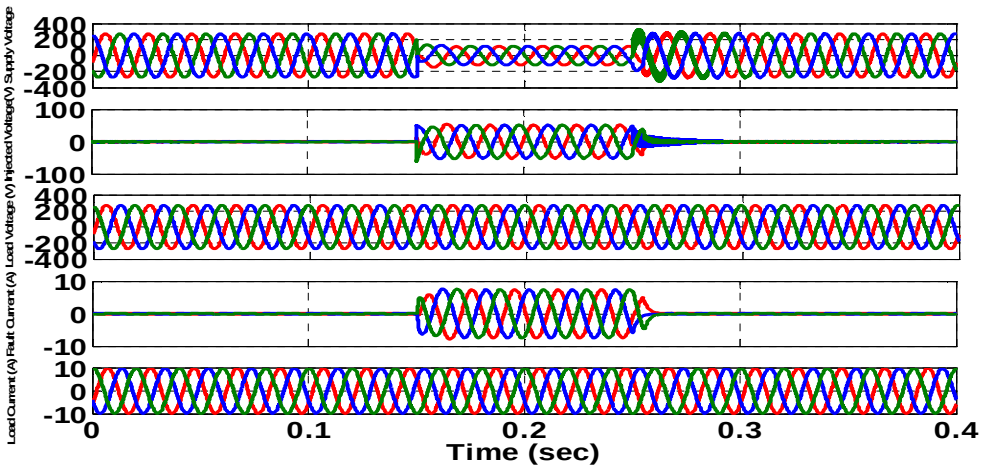

Figure 6.18 Response of UPQC with vector control voltage sag for nonlinear load with balanced three phase fault (a) three phase balanced fault voltage (b) UPQC injection voltage (c) Three phase load voltage (V) (d) three phase fault current (e) three phase load current.

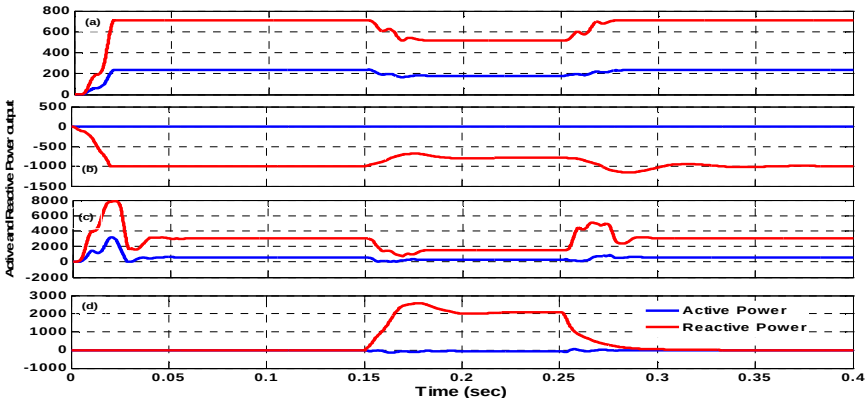

Figure 6.19 Performance of the UPQC for (a) resistive load with unbalanced voltage sag active and reactive (red) power output from the DVR (b) capacitive load with unbalanced voltage sag active and reactive power output from the DVR (c) resistive load with balanced voltage sag active and reactive power output from the DVR (d) non-linear load with unbalanced voltage sag active and reactive power output from the DVR (e) Induction motor load with unbalanced voltage sag active and reactive power output from the DVR

Figure 6.19demonstrates then presentation of the performance of the UPQC for (a) resistive load with unbalanced voltage sag dynamic and mostly important reactive power output from the UPQC, (b) capacitive load with unbalanced voltage sag active and reactive power output from the UPQC, (c) resistive load with balanced voltage sag active and reactive power output, (d) non-linear load with unbalanced voltage sag active and reactive power output from the PV-wind- PEMFC-UPQC, (e) Induction motor load with unbalanced voltage sag active and reactive power output from the UPQC. The proposed multilevel inverter based transformer less configuration of the PV-wind- PEMFC-UPQC overcomes transformer problems such as high cost, large size, losses, saturation, phase shift and inrush current. Also filter-less PV-wind- PEMFC-UPQC operation can be obtained at high number of inverter levels. For high voltage purpose we used transformer connected UPQC and this custom power compensator is employed to regulate the positive sequence component and to cancel the negative sequence component. The transformer connected PV-wind- PEMFC-UPQC output fault voltage waveform is shown in Figure 6.20, where voltage sag depth is (a) UPQC unbalanced fault with linear load (b) UPQC unbalanced fault with non-linear load (c) UPQC unbalanced fault with capacitor load (d) UPQC balanced fault with linear load.

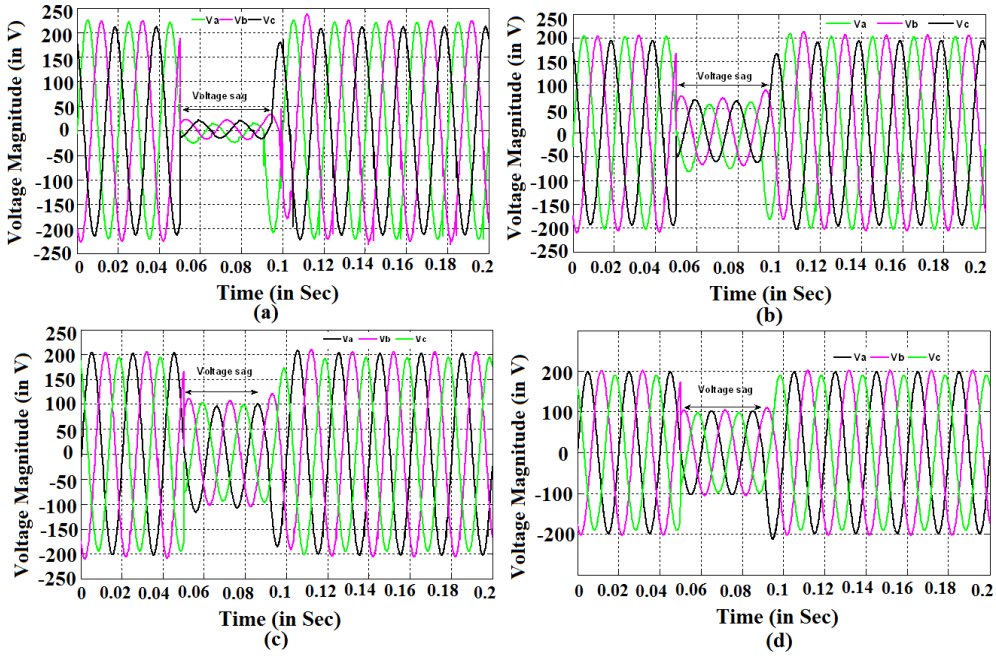

Figure 6.20 Voltage sag depth is (a) UPQC unbalanced fault with linear load (b) UPQC unbalanced fault with non-linear load (c) UPQC unbalanced fault with capacitor load (d) UPQC balanced fault with linear load.

6.6.3 Performance Comparison of the PV-wind- PEMFC-UPQC, PV-wind- PEMFC -DVR and STATCOM

A performance comparison is made for the proposed topology operating under DVR, STATCOM and UPQC modes. Tables 6.4, 6.5 and 6.6 demonstrate the comparison results obtained. The parameters observed are source and load

side voltage and current harmonics with the proposed control. The Table 6.4 and 6.5 shows the performance of the DVR and UPQC modes where the UPQC modes having lower harmonics in both the voltage and current waveforms. In Table-6.6, consists the level wise comparison for the source and load side voltage and currents. Here also it can be observed that the UPQC mode of operation results in lower harmonic generation compared to DVR or STATCOM modes.

Table 6.4 Source and load side voltage and current harmonic magnitude when DVR connected

Voltage and current unbalance harmonic (% of fundamental) when PV-wind-PEMEFC-DVR connected												
Harmonic	Source side voltage harmonic (%)			Source side current harmonic (%)			Load side voltage harmonic (%)			Load side current harmonic (%)		
order	V_{sa}	V_{sb}	V_{sc}	I_{sa}	I_{sb}	I_{sc}	V_{la}	V_{lb}	V_{ls}	I_{la}	I_{lb}	I_{lc}
5	1.03	2.32	0.58	0.48	0.52	0.82	2.52	1.89	2.15	2.53	3.18	1.32
7	0.58	1.2	0.47	0.03	0.58	0.91	1.93	1.54	2.62	1.73	1.85	1.91
11	0.47	0.48	0.01	0.01	0.33	0.63	0.93	0.02	1.02	1.12	0.57	0.93
13	0.28	0.49	0.53	0.47	0.02	0.21	1.02	1.38	1.11	0.05	0.06	0.34
17	0.13	0.12	0.06	0.07	0.04	0.05	0.78	1.03	0.09	0.79	0.94	0.84
19	0.04	0.65	0.52	0.21	0.27	0.03	0.24	0.59	0.74	1.01	0.41	0.69
23	0.27	0.45	0.48	0.16	0.06	0.01	0.03	0.36	0.43	1.25	0.11	0.36
25	0.02	0.01	0.13	0.31	0.11	0.08	0.46	0.65	0.24	0.94	0.42	0.12
29	0.01	0.04	0.01	0.08	0.21	0.11	0.91	0.02	0.53	0.06	0.23	0.01
31	0.11	0.73	0.21	0.03	0.07	0.02	0.03	0.51	0.08	0.19	0.01	0.03

Table 6.5 Source and load side voltage and current harmonic magnitude when UPQC connected

Voltage and current unbalance harmonic (% of fundamental) when PV-wind-PEMEFC-UPQC connected												
Harmonic	Source side voltage harmonic (%)			Source side current harmonic (%)			Load side voltage harmonic (%)			Load side current harmonic (%)		
order	V_{sa}	V_{sb}	V_{sc}	I_{sa}	I_{sb}	I_{sc}	V_{la}	V_{lb}	V_{ls}	I_{la}	I_{lb}	I_{lc}
5	0.06	0.82	0.14	0.38	0.43	0.52	1.32	0.69	1.04	1.32	1.04	1.71
7	0.83	0.72	0.43	0.11	0.38	0.04	1.22	0.47	1.07	1.03	0.03	0.79
11	0.13	0.21	0.02	0.02	0.05	0.25	0.23	0.122	0.05	0.67	0.47	0.24
13	0.08	0.23	0.24	0.01	0.12	0.04	0.74	0.06	0.32	0.01	0.01	0.11
17	0.11	0.11	0.01	0.02	0.03	0.01	0.41	0.003	0.11	0.03	0.11	0.31
19	0.01	0.05	0.49	0.04	0.41	0.1	0.01	0.09	0.51	0.53	0.35	0.14
23	0.13	0.29	0.12	0.13	0.01	0.02	0.02	0.32	0.28	0.59	0.2	0.12
25	0.01	0.03	0.11	0.11	0.09	0.02	0.17	0.31	0.04	0.44	0.17	0
29	0.02	0.01	0	0.02	0.06	0.03	0.11	0.01	0.08	0.02	0.01	0.01
31	0.05	0.03	0.01	0.01	0.04	0.01	0.02	0.11	0.02	0.11	0.03	0.02

Table 6.6 Source and load side %THD calculation when DVR, STATCOM and UPQC connected

hybrid cascade multilevel Inverter Level	Using DVR Compensator				Using STATCOM Compensator				Using UPQC Compensator			
	Source side %THD		Load side %THD		Source side %THD		Load side %THD		Source side %THD		Load side %THD	
	Voltage % THD	Current % THD	Voltage % THD	Current % THD	Voltage % THD	Current % THD	Voltage % THD	Current % THD	Voltage % THD	Current % THD	Voltage % THD	Current % THD
2	1.942	1.5496	2.974	3.547	1.954	1.201	3.172	2.73	1.4549	1.0057	2.44	1.959
3	1.326	1.264	2.034	3.286	1.867	0.9874	3.263	2	1.2325	0.9793	2.15	1.193
5	1.0321	0.9321	1.984	3.192	1.564	0.8487	2.154	1.95	1.0354	0.8362	1.96	1.452
7	0.9867	0.6403	1.436	2.879	0.993	0.6353	1.693	1.35	0.9621	0.4935	1.52	0.989
9	0.7326	0.5794	1.325	2.281	0.863	0.4752	1.538	1.22	0.5224	0.3142	1.32	0.897
11	0.4521	0.3867	1.176	1.984	0.563	0.3647	1.325	1.13	0.1243	0.3061	0.99	0.723
13	0.3653	0.1965	1.098	1.382	0.394	0.0926	1.193	1.04	0.0754	0.0873	0.95	0.574
15	0.2357	0.0984	0.984	1.047	0.391	0.0762	1.012	1	0.0521	0.0446	0.69	0.757
17	0.1843	0.0164	0.867	0.992	0.357	0.0099	0.984	0.83	0.4104	0.0098	0.62	0.562
19	0.0457	0.0096	0.738	0.946	0.084	0.0091	0.839	0.74	0.0343	0.0079	0.16	0.513
23	0.0243	0.0076	0.628	0.787	0.063	0.0006	0.767	0.63	0.0213	0.0061	0.08	0.418
25	0.0332	0.0084	0.394	0.531	0.009	0.0007	0.415	0.33	0.0043	0.0054	0.01	0.314

6.7 Conclusion

This chapter investigates new models of PV-wind- PEMFCS-DVR, PV-wind-PEMFCS-STATCOM and PV-wind-PEMFCS-UPQC system with the proposed control method. This innovative and potential method is capable to compensate network faults and mitigate their effects on sensitive loads in distribution power systems. DVR has the boundary limit for injection of active power. The simulation results indicate the capability of custom power device in mitigating the voltage variation and harmonic polluting loads. The harmonics of the output voltage is eliminated by SVPWM switching technique and THD is also calculated to evaluate the quality of the load voltage during the operation of DVR, STATCOM or UPQC which fulfills IEEE 519 std. range. From the simulation results, it is evident that the generated voltage spectrum is very much improved by increase in the level of the inverter. The proposed system also decreases the overall voltage THD in the micro-grid, decreases the total system loss, improves the dc link voltage, increases the effecting speed, and solves the loss of commutation, electromagnetic intervention; minimize the harmonics and optimized the high frequency switching problems. Different simulation case study is verified to evaluate the potential application of the proposed control approach with superior advantage. A rapid response and precise compensation with optimum energy of the proposed control system are also revealed in the simulation results.

Chapter 7

Conclusions and Future work

Chapter 7

7.1 Conclusion

The aim of this present thesis is to address power quality issues with different types of DGs having Inverter interface to MGs. The harmonic optimization and overall power quality issues has been dealt with by the use of renewable energy based PV and DFIG hybrid schemes operating under UPQC, DVR, STATCOM modes.

The most important aims of this present thesis are:

i. Control of power quality, harmonic optimization by different techniques.
ii. Usage of different soft computing techniques for generating switching pulses for DG based Inverters and different FACTS schemes with proposed configuration.

In **Chapter 2** a novel technique for diminution of voltage harmonics in a modern micro-grid consisting of DFIG as multiple DG resources is shown. The BBO-based SHE-PWM technique of DFIG rotor side inverters is employed for harmonic reduction. The chosen harmonics of the DFIG rotor output voltage e.g. 5^{th} and 7^{th} are removed by BBO-based SHE-PWM technique. The inverter switching angles are calculated by the BBO algorithm and stored as mixed model equation for on-line application. The higher order harmonics e.g. 11^{th}, 13^{th}, 17^{th}, and 19^{th} order are generated by other inverters in opposite phase while lessening their own lower order harmonics. Thus, the general voltage THD within the micro-grid is reduced. Thus the total switching losses of the inverters are lower compared to the situation when all the inverters are switched to eliminate both lower and higher order harmonics.

In **Chapter 3** an optimized switching strategy for the rotor side converter (RSC) for a DFIG is proposed. The undesired stator harmonics injected from RSC is eliminated, which can deteriorate the micro-grid power quality. The preferred lower order harmonics of the RSC generated voltage are removed and rest higher orders are minimized by BBO-based SHE technique. A rotor speed dependent modified RSC switching technique is developed with different switching angles per quarter cycle. The switching angles are computed through BBO algorithm and stored in a processor memory in the form of mixed model equations for online application. The proposed scheme can be used for online control of any number of DFIGs.

In **Chapter 4**, the model of PV-wind based hybrid DG system suitable for DVR, STATCOM and UPQC modes of operation has been developed. The proposed technique can compensate networks faults, reduce injected harmonics and act as reactive power compensator in distribution systems. The harmonics of the output voltage are eliminated by SHE-PWM switching technique with ML inverter using BBO based optimized switching. A comparison of BBO based computation of switching angles with other existing soft computing techniques has been prepared for justification. The load voltage quality for DVR, STATCOM, UPQC operation can fulfill IEEE 519 std. range. Various simulation and experimental results are shown to justify the proposed concept.

In **Chapter 5**, the PV-DVR system is investigated with the proposed control technique. The projected performance is able to compensate the system faults and moderate their effects on sensitive nonlinear loads in modern power systems. DVR controls the power flow, harmonics with THD and mitigate the voltage variation with high efficiency. The selected minimum order harmonics are completely eliminated by BBO-based SHEAM-PWM switching technique. The generated switching angles are stored in microcontroller memory for online application and contributing the least voltage THD at dissimilar modulation indices which is computed by the BBO algorithm. For the proposed model, the generated output voltage harmonic spectrum is better and the overall voltage THD is decreased.

Chapter 6 investigates new models of PV-wind- PEMFCS -DVR, PV-wind- PEMFCS -STATCOM and PV-wind-PEMFCS-UPQC system with the proposed control method. The projected technique is accomplished to balance the system faults and moderate their special effects on sensitive loads in grid, micro-grid and smart grid related power systems. By SVPWM switching, the voltage harmonics is optimized with minimum THD throughout the function of DVR, STATCOM and UPQC mode, fulfilling the IEEE 519 range. Different simulation case study is verified to evaluate the potential application of the future approach with higher advantage.

7.2 FUTURE WORK for MGs, PVs, DFIGs and FACTS

I. Application of high technology products like nano batteries, nano solar cells, nano super capacitors and nano fuel cells the MG storage capacities are increased and makes the MGs, simpler, smarter etc. In future for MGs operations the use of green and sustainable energy investigation more required.

II. For PV systems the partial shading problems are the major issues so primarily the targets to solve the problem and utilize the maximum purpose is to be investigated.

III. Power quality issues are the most significant factors in distribution and transmission networks. Some subjects for the future are very attractive in DFIG connected like effect of saturation of voltage unbalanced; the selection proper sizing of converter and DC link capacitor is another part of the future work, handling of high frequency switching for more accuracy in transient operation. Under and over voltage, over current, speed and frequency deviation protection should be established for developed for the DFIG for protection. DFIGs cost analysis is another most important factor for further research. In future the DFIG wind energy technology more usability for micro-grid power quality improvement is possible. It is further requirement that by controlling of DFIG the rotor injects electrical power into the grid and absorbing power from the grid system through converters at sub-synchronous speed and the active power with the reactive power balanced.

IV. Using the power electronics FACTS, inverter operation, PMU, smart meter, bidirectional effects, storage device and advances in automation the MG makes more popular like smart grid.

V. Further developing the FACTS device SVC, STATCOM, DVR, and UPQC can improve the active power, reactive power, voltage variation, harmonic polluting loads effects with high performance, low loss, cost effective. Further research it can be modified for simplicity, reliability, usability and controllability. The harmonic elimination also can be improved by improving the switching technology.

VI. In future Smart Grid normally improves and monitors the transmission and distribution system which is

- Controllable, observable and suitable for sensing.
- The proposed concept can be studied for smart grid application with already developed methods in power quality improvement algorithms.

Appendix

From, **Figure A.1-A.b.23** shows the simulation output results and which is investigate the different inverters output. **Table A.1-A. 13** Switching angles and %THD calculation for 180, 120-degree, bipolar and unipolar conduction mode with different Modulation index with 3, 4, 5, 6, 7-Switching angles (degrees). From, Figure A.24 –A.27 shows the hardware output results for FACTS and inverter respectively.

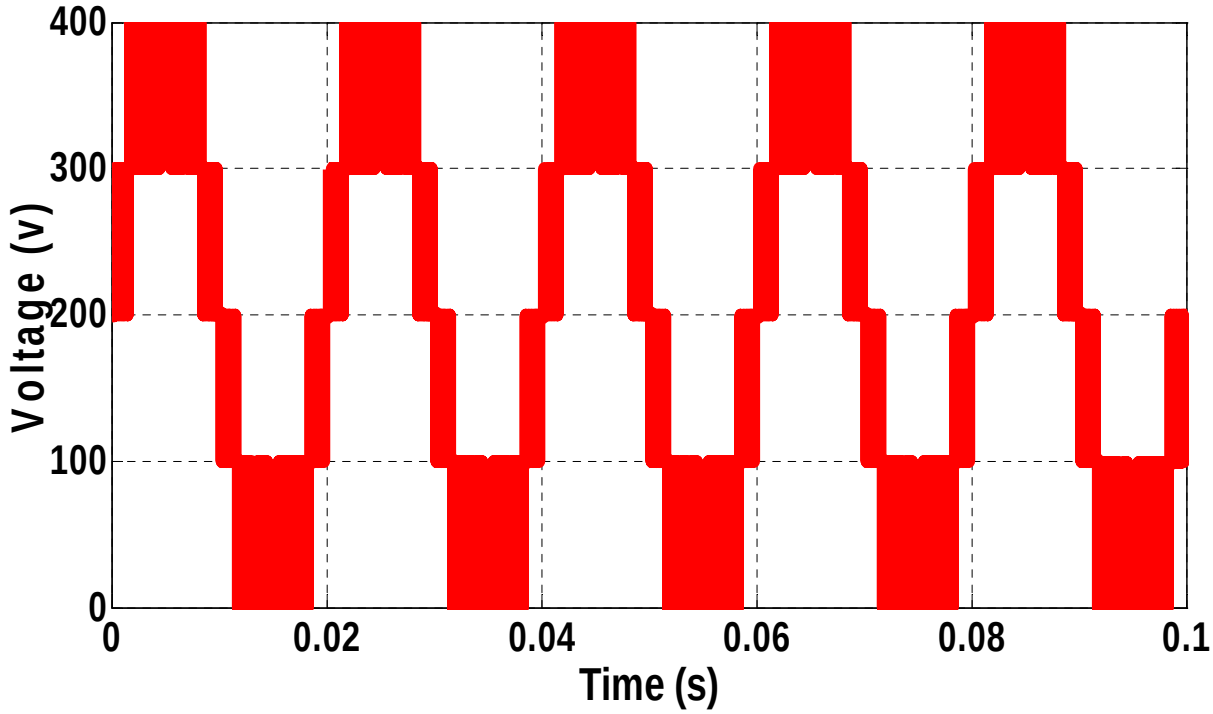

Figure A.1 Simulation result of single phase full bridge inverter.

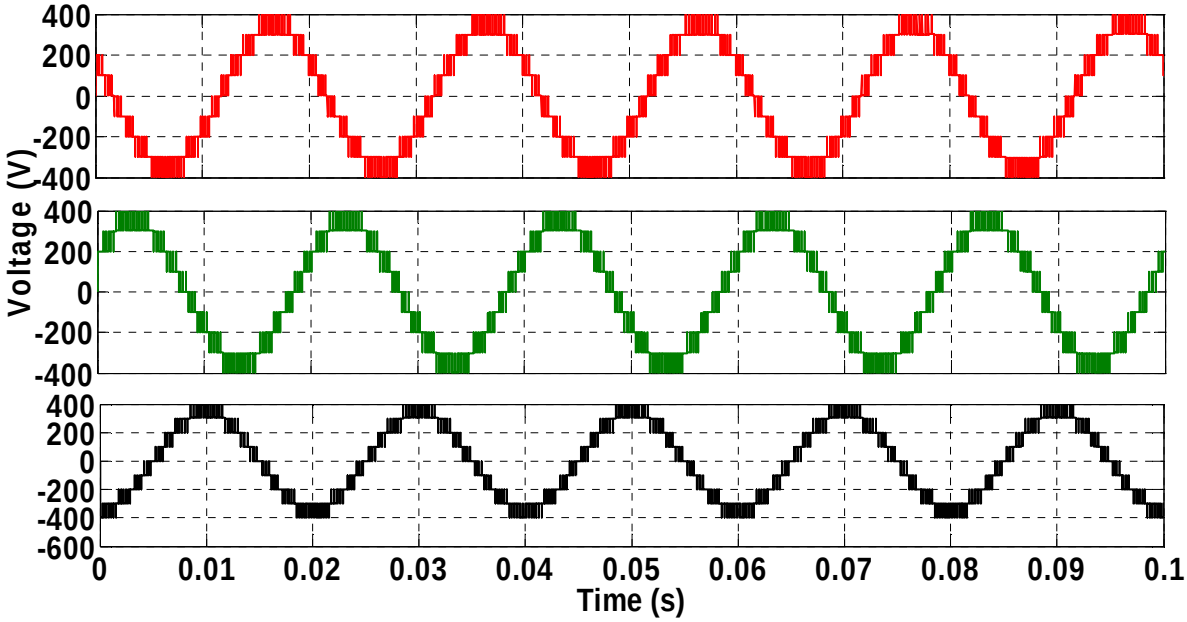

Figure A.2 Simulation result of three-phase nine-level DCMLI inverter.

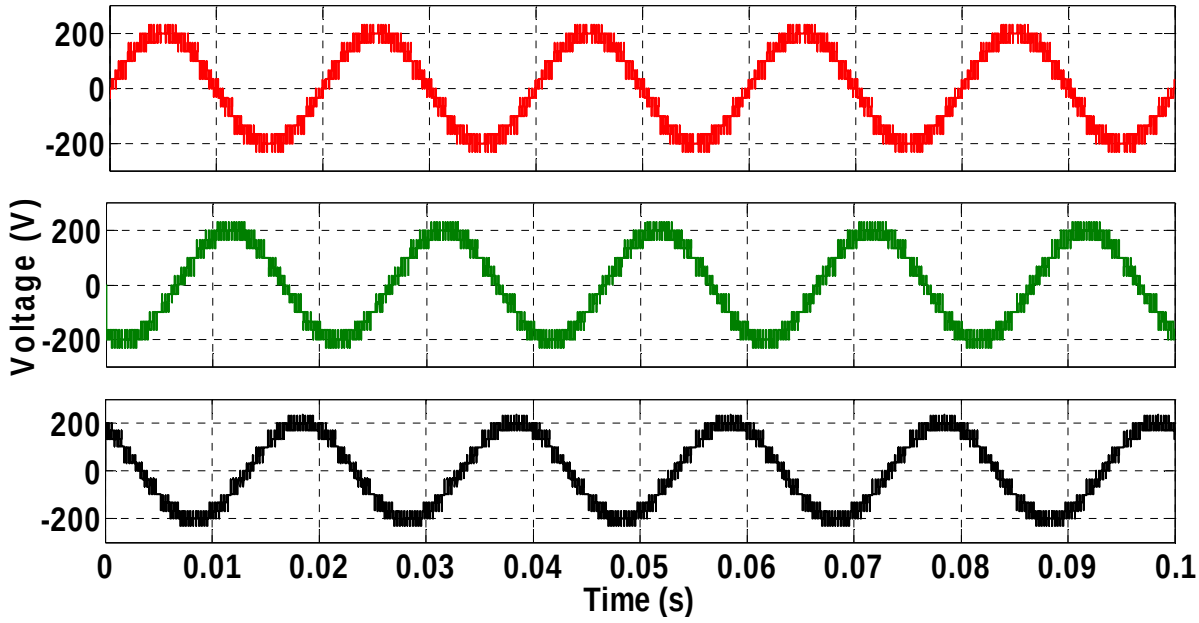

Figure A.3 Simulation result of three-phase nine-level NPCMLI inverter.

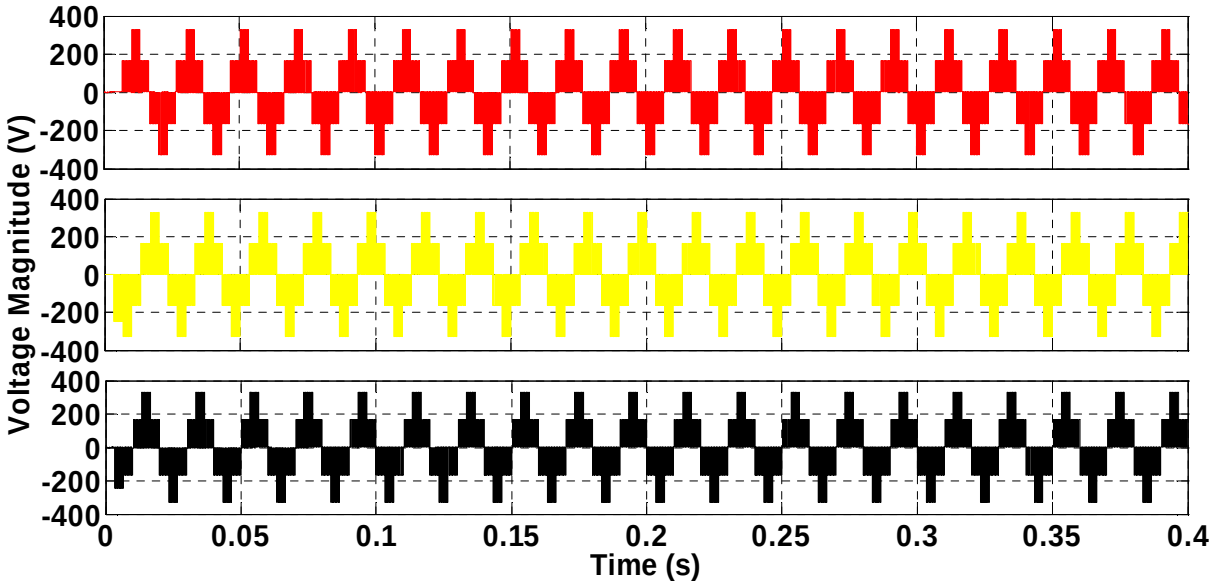

Figure A.4 Simulation result of three-phase five-level Cascaded H-bridges multilevel inverter.

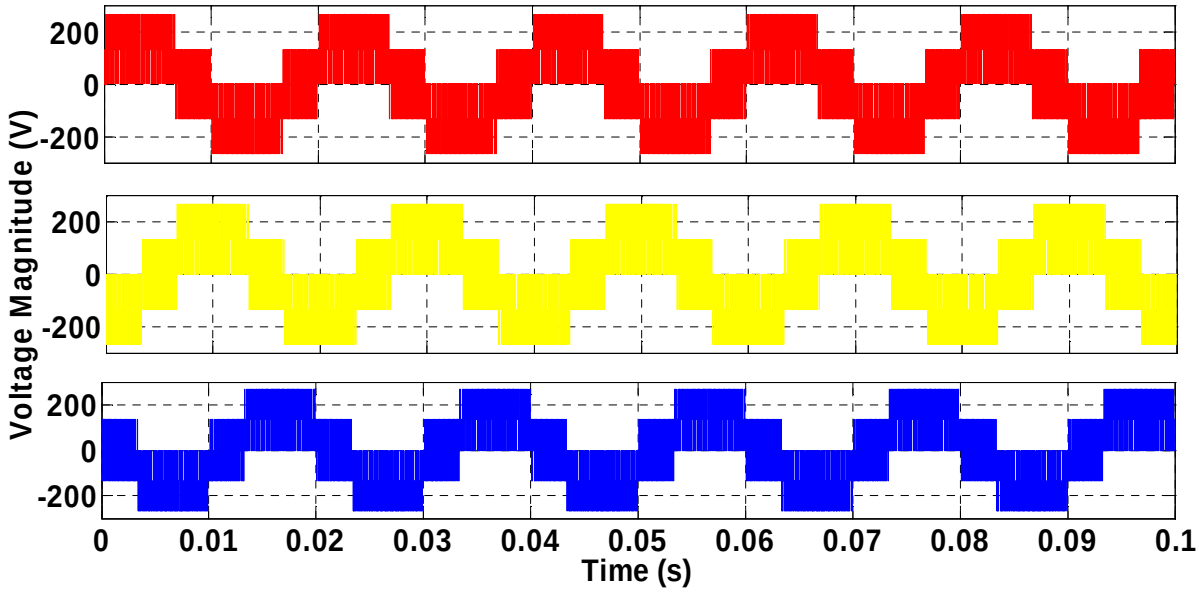

Figure A.5 Simulation result of three-phase Flying capacitors based Multi-level inverter.

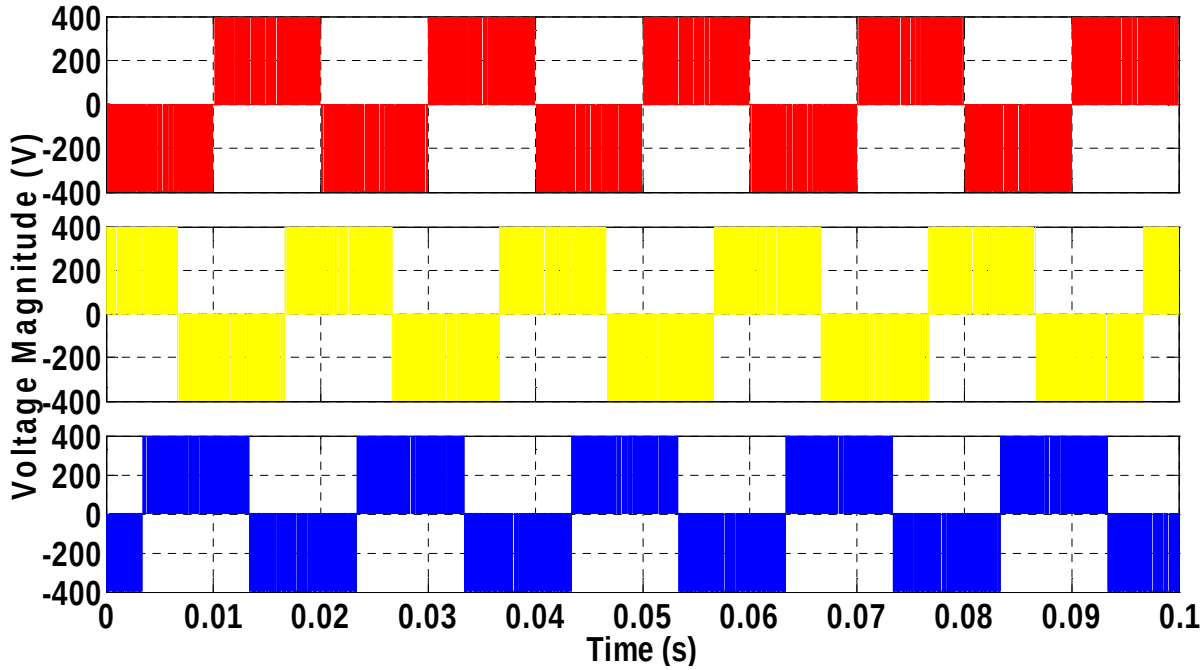

Figure A.6 Simulation result of three-phase two-level VSC.

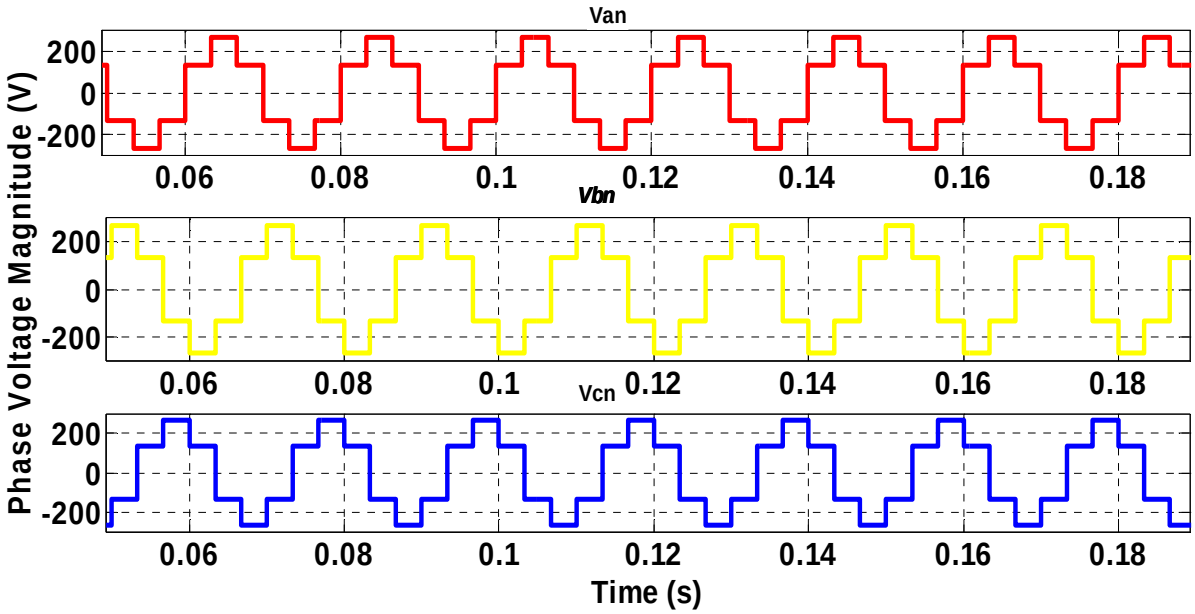

Figure A.7 Simulation result of Hybrid Cascaded H-bridges multilevel converter with single dc sources.

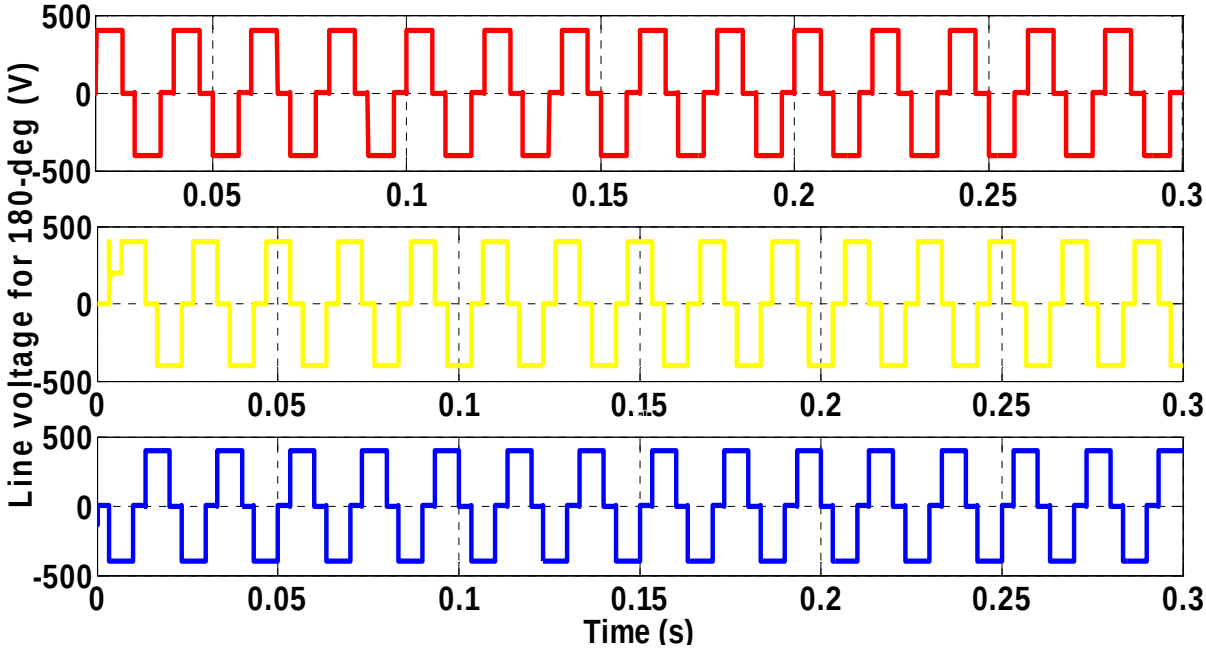

Figure A.8 Simulation result of line voltage for 180-degree mode.

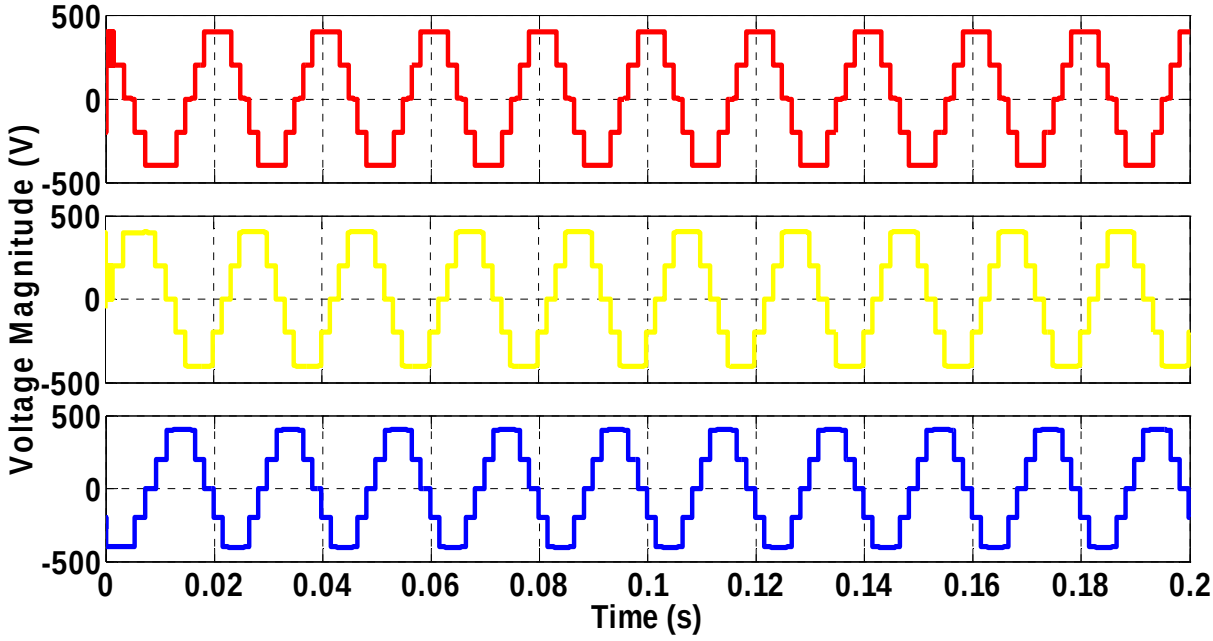

Figure A. 9 Simulation result of Phase voltage for 180-degree mode.

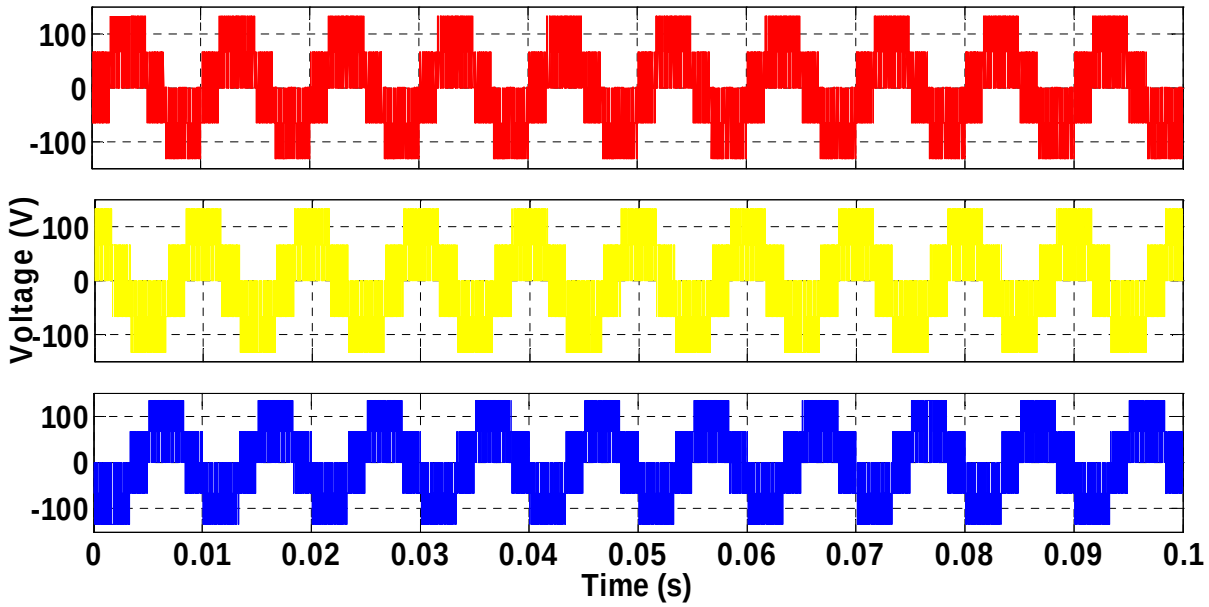

Figure A.10 Simulation result of Hybrid cascade multilevel with bottom three leg inverter.

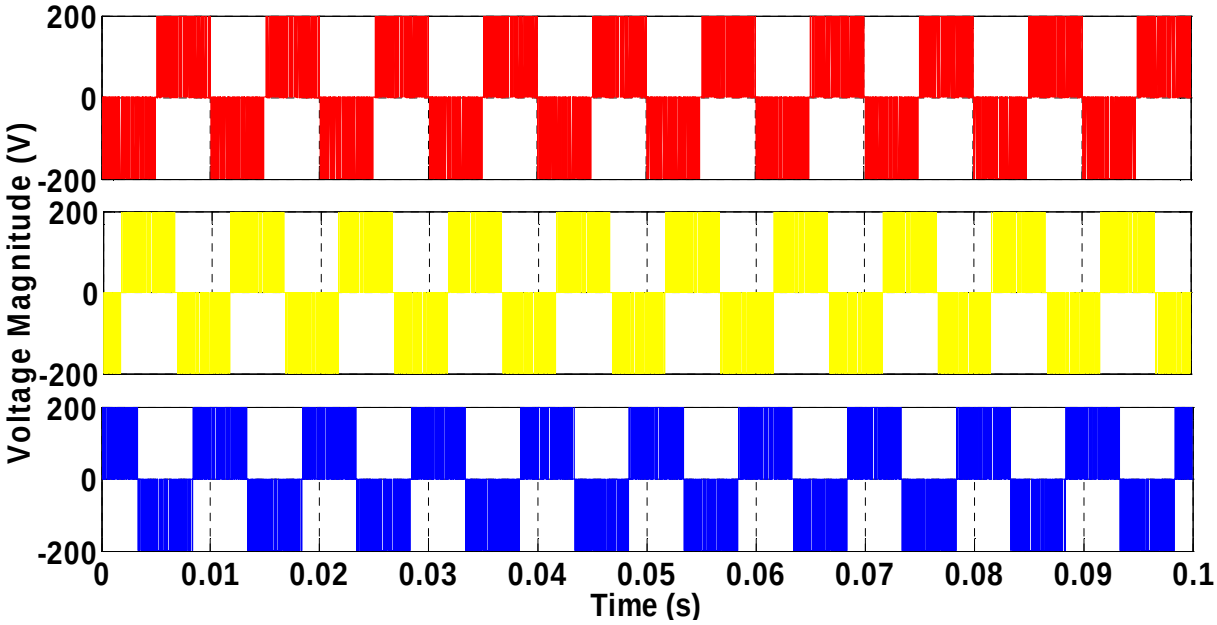

Figure A. 11 Simulation result of 120-degree mode.

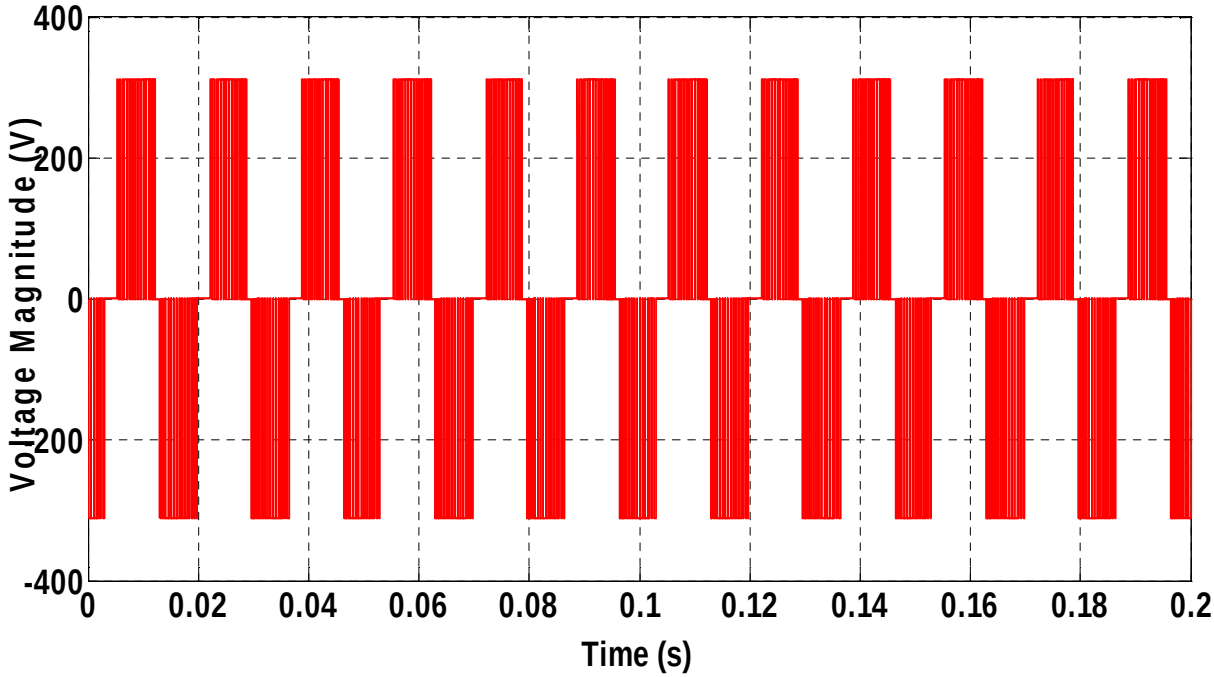

Figure A.12 Simulation result of Phase voltage for 180-degree mode.

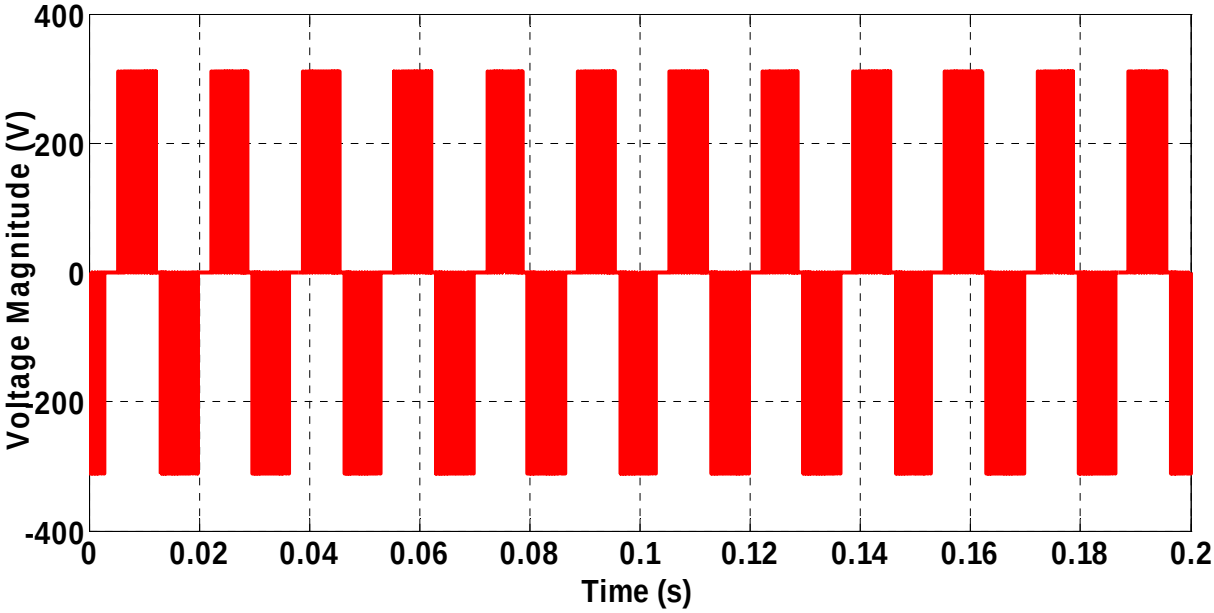

Figure A.13 Simulation result of single phase inverter with bipolar switching.

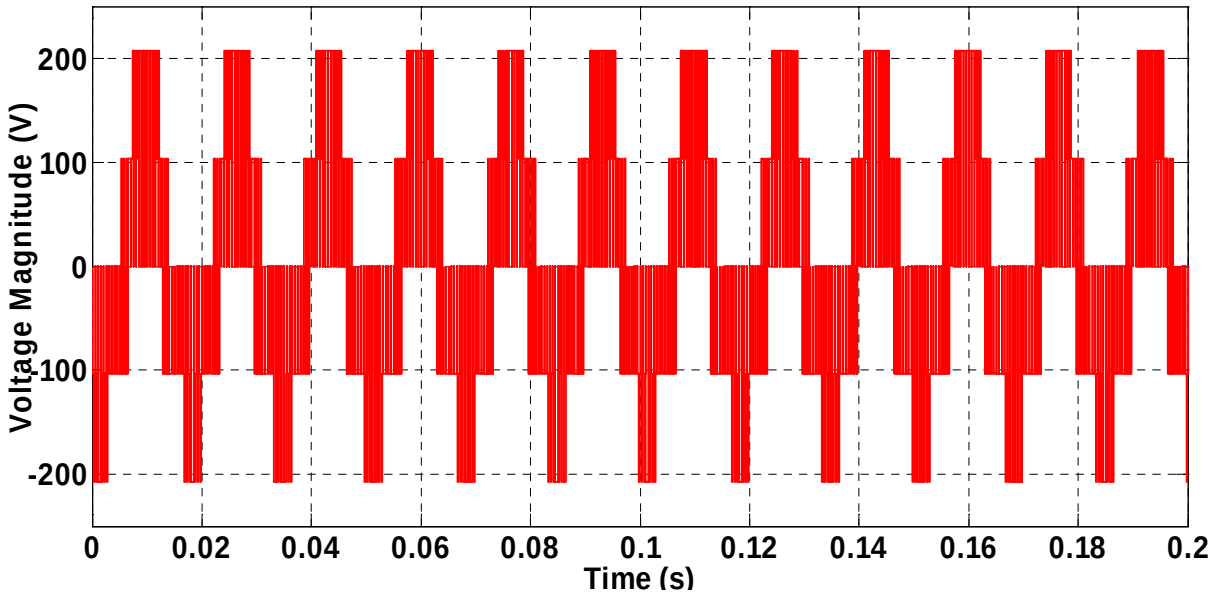

Figure A.14 Simulation result of single phase bridge inverter using IGBTs, with renewable source.

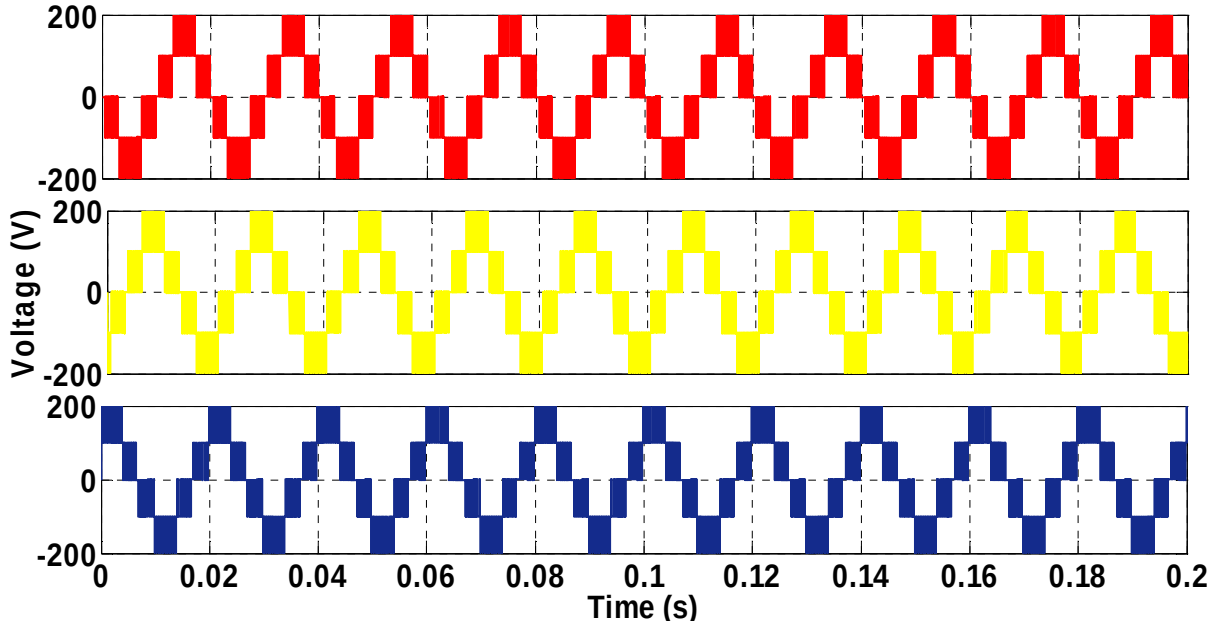

Figure A.15 Simulation result of cascade multilevel inverters with Single dc source by employing single phase transformers.

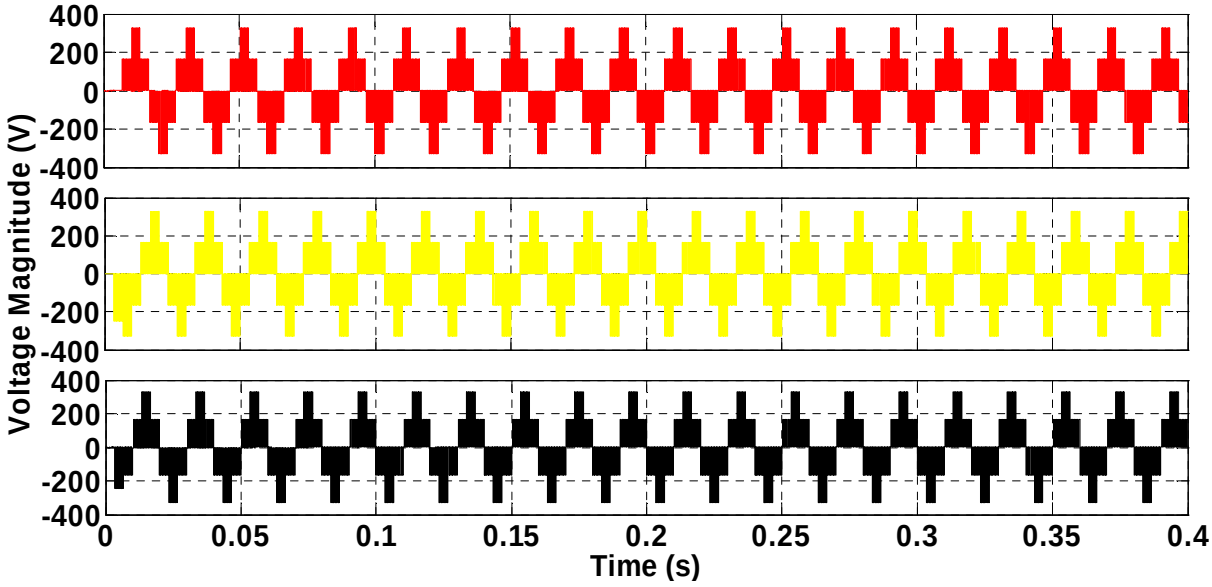

Figure A.16 Simulation result of cascade multilevel inverters with Single dc source by employing single phase transformers with minimum number of dc sources.

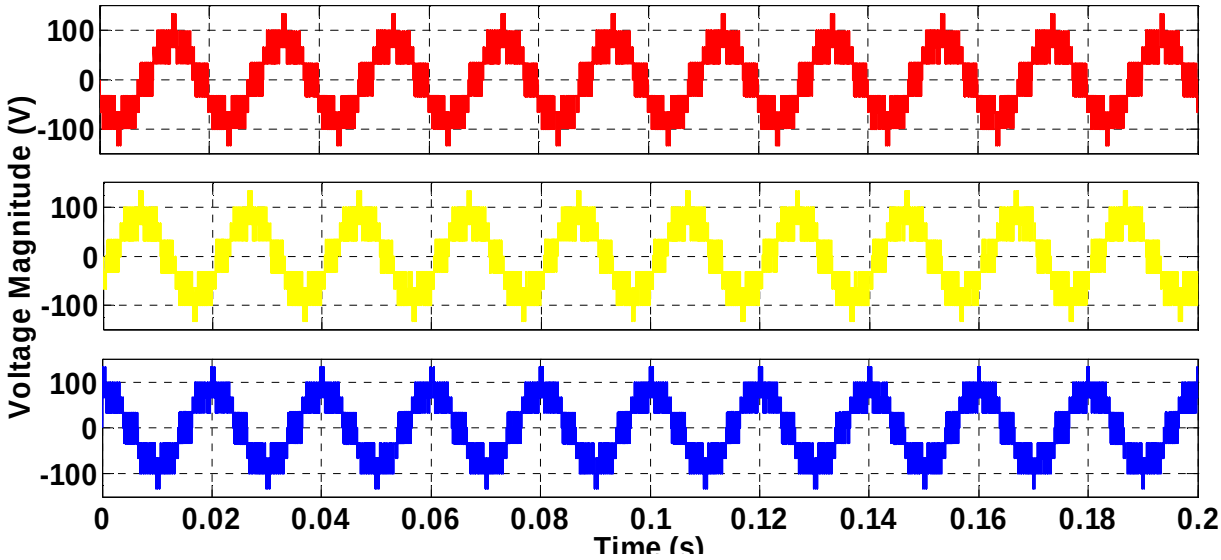

Figure A.17 Simulation result of Cascade multilevel inverter with Single dc source by employing cascade transformers

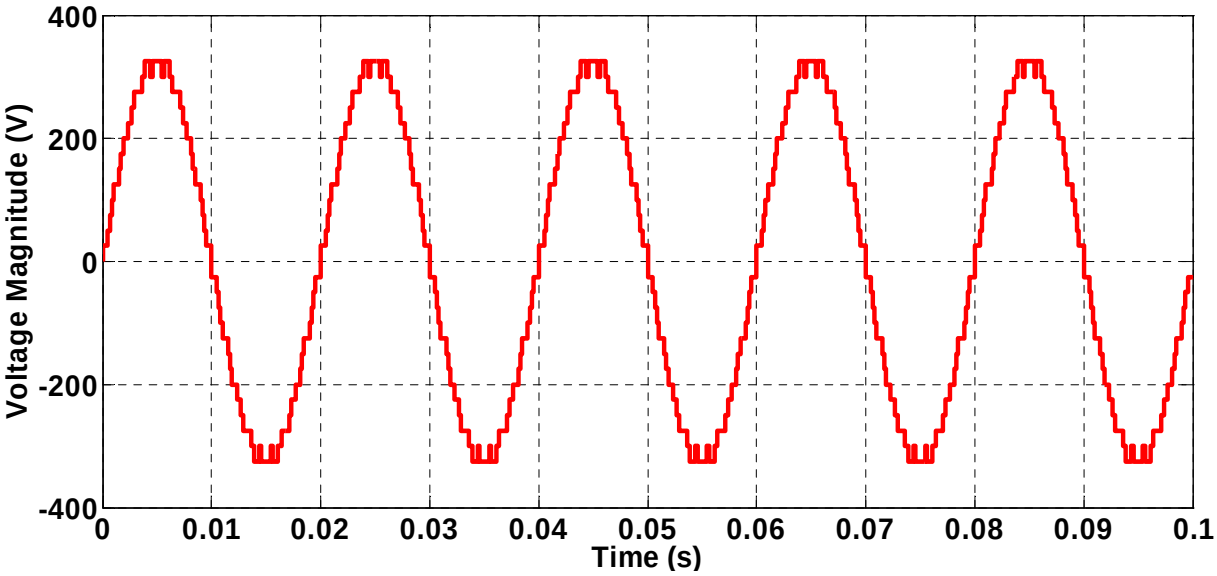

Figure A.18 Simulation result of Unequal dc source.

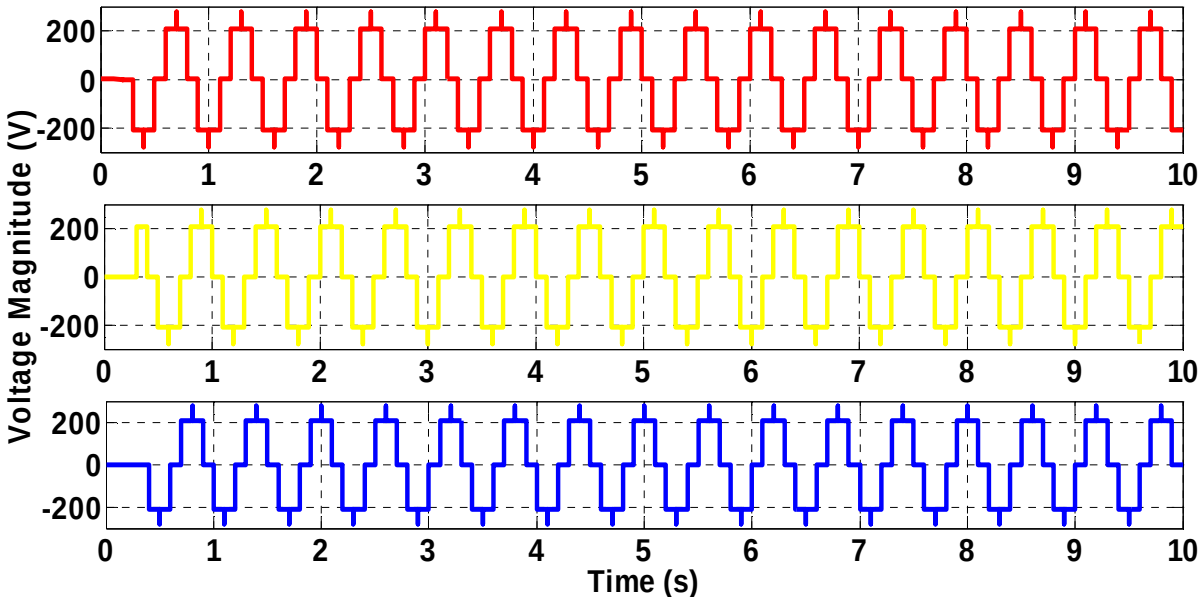

Figure A.19 Simulation result of 120-degree conduction

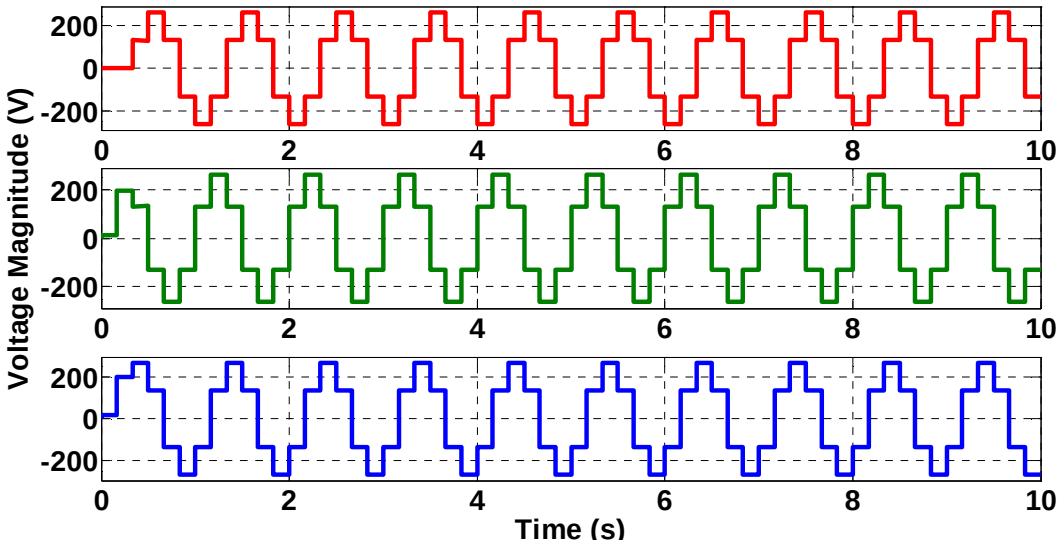

Figure A.20 Simulation result of Hybrid multilevel inverter with single PV-wind-PEMFCS dc-source.

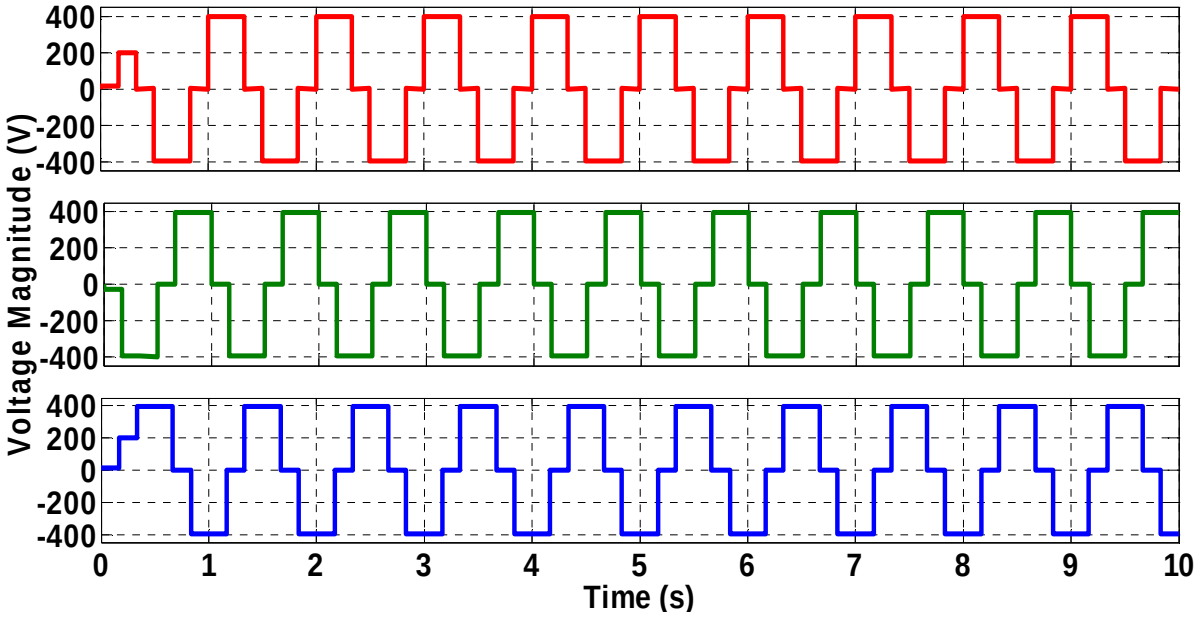

Figure A.21 Simulation result of 3-phase inverter with only PV input.

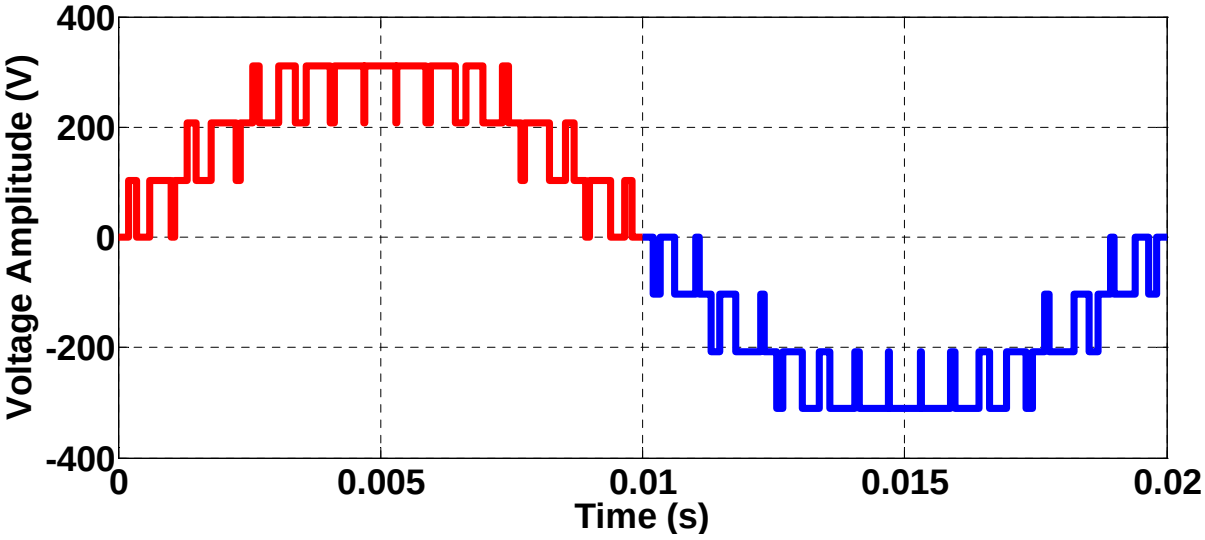

Figure A. a. 22 The output voltage waveform of the PWM switching

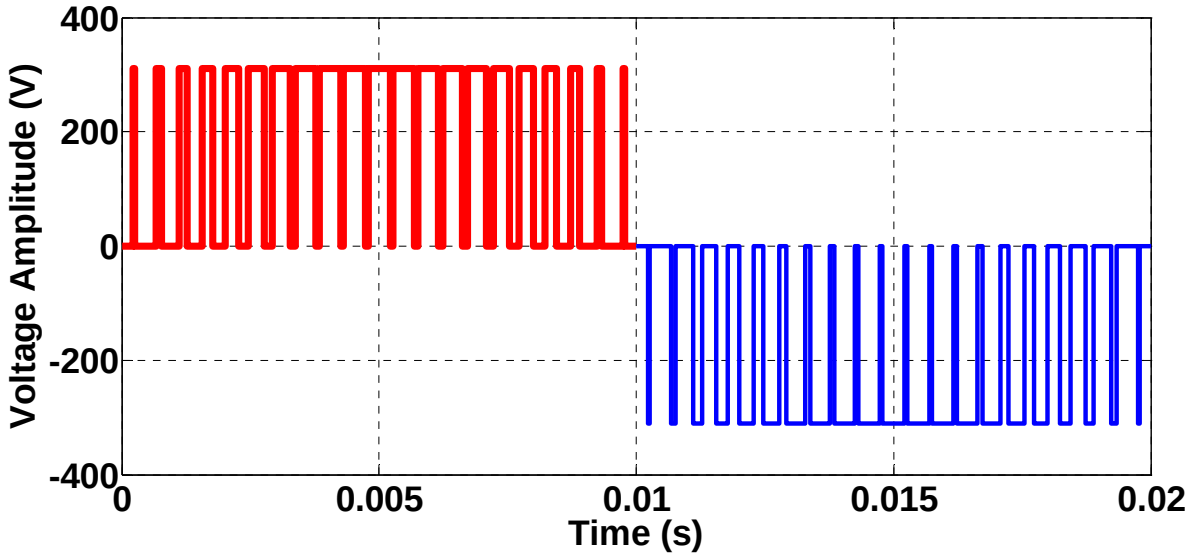

Figure A. b .22 The output voltage waveform of the PWM switching

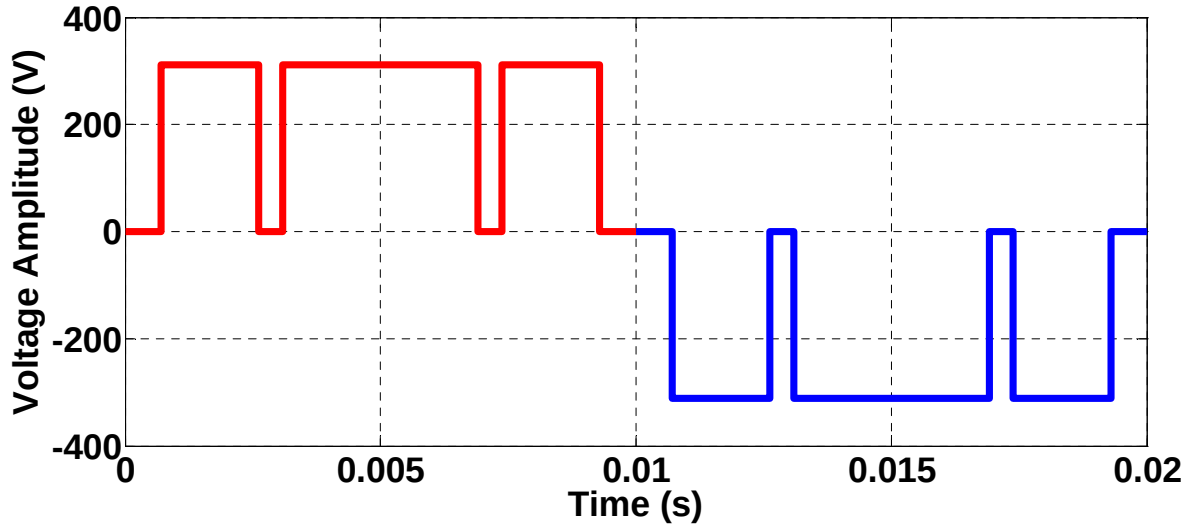

Figure A. c. 22 The output voltage waveform of the PWM unipolar switching

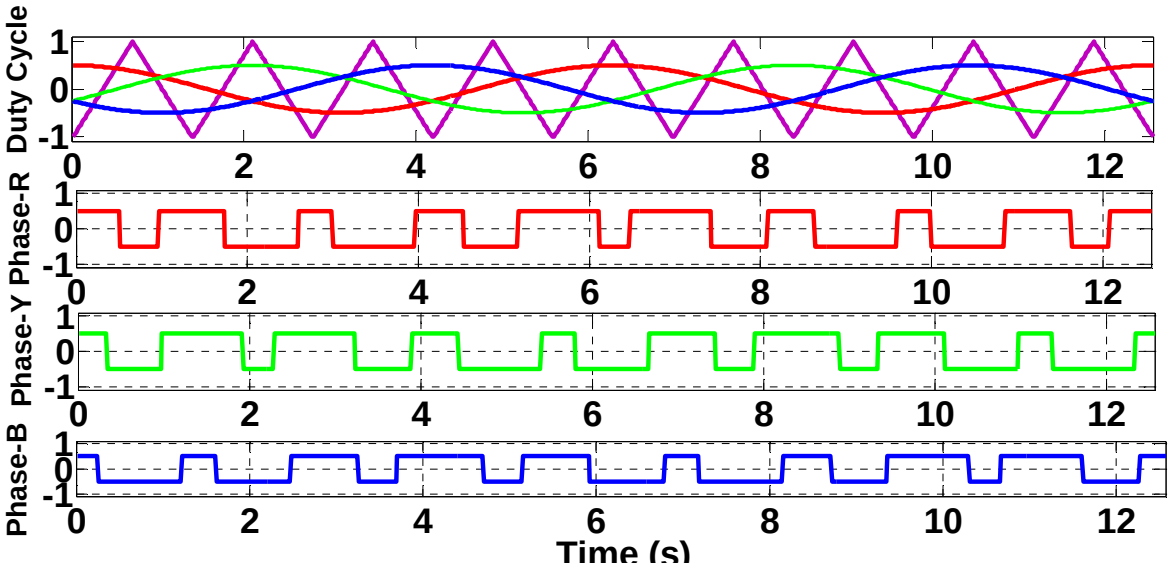

Figure A. a.23 The output voltage waveform of the three phase PWM switching

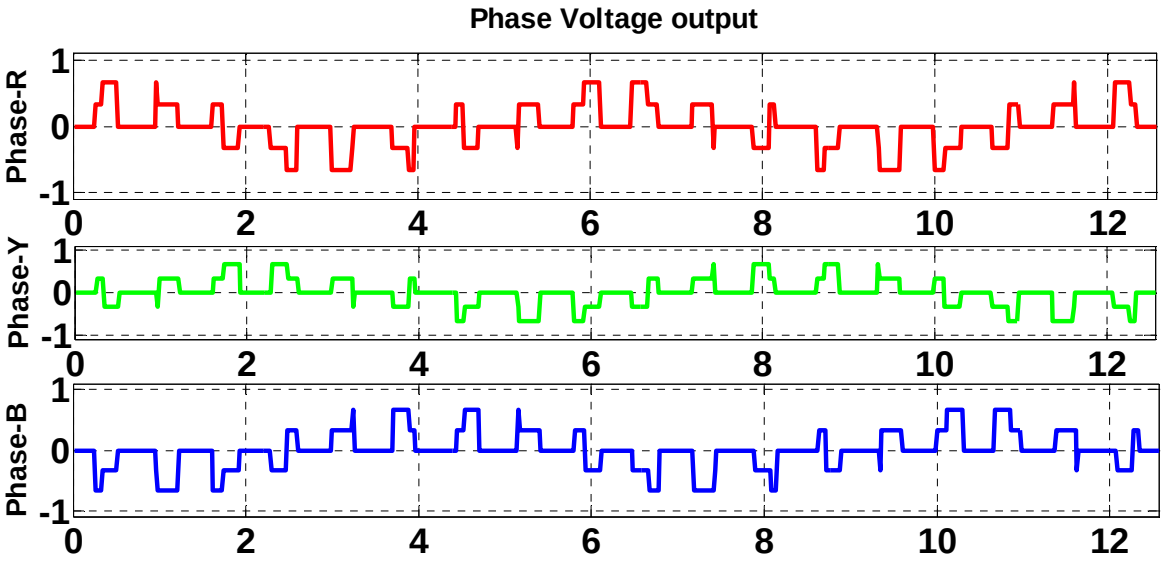

Figure A. b.23 The output phase voltage waveform of the three phase PWM switching

Table A.1 Switching angles and THD calculation for 180-degree conduction mode with different Modulation Index with 3-Switching angles (degrees).

MI	alpha1	alpha2	alpha3	THD	MI	alpha1	alpha2	alpha3	THD
0.02	59.6695	60.3311	89.7135	84.7343	0.52	51.46	69.098	82.7121	36.0165
0.03	59.5044	60.4968	89.5703	84.5492	0.53	51.2947	69.2961	82.5817	35.3158
0.06	59.0099	60.9951	89.1407	83.5588	0.54	51.1293	69.4962	82.4522	34.6349
0.07	58.8452	61.1616	88.9976	83.0871	0.55	50.9638	69.6986	82.3239	33.9712
0.08	58.6807	61.3282	88.8545	82.5471	0.56	50.7981	69.9034	82.1966	33.322
0.09	58.5162	61.4951	88.7114	81.9404	0.57	50.6323	70.1108	82.0706	32.6848
0.1	58.3518	61.6621	88.5684	81.269	0.58	50.4663	70.3211	81.9459	32.0568
0.11	58.1875	61.8294	88.4254	80.5352	0.59	50.3001	70.5344	81.8227	31.4354
0.12	58.0233	61.9969	88.2824	79.7414	0.6	50.1338	70.7512	81.7011	30.8179
0.13	57.8592	62.1646	88.1396	78.89	0.61	49.9672	70.9716	81.5813	30.2019
0.14	57.6951	62.3326	87.9968	77.9839	0.62	49.8005	71.1961	81.4635	29.5848
0.15	57.531	62.5009	87.854	77.026	0.63	49.6335	71.4251	81.3479	28.9644
0.16	57.367	62.6694	87.7113	76.0193	0.64	49.4663	71.6592	81.2347	28.3383
0.17	57.2031	62.8382	87.5687	74.9673	0.66	49.1312	72.1445	81.0169	27.0599
0.18	57.0392	63.0074	87.4262	73.8731	0.67	48.9633	72.3974	80.9129	26.4032
0.19	56.8753	63.1768	87.2838	72.7404	0.68	48.795	72.6582	80.8129	25.7319
0.21	56.5477	63.5166	86.9993	70.3737	0.69	48.6265	72.928	80.7174	25.0437
0.22	56.3839	63.6871	86.8572	69.1473	0.7	48.4576	73.2083	80.6271	24.3359
0.25	55.8927	64.2007	86.4317	65.342	0.71	48.2883	73.5007	80.5428	23.6056
0.26	55.729	64.3728	86.2902	64.0446	0.73	47.9485	74.1308	80.3969	22.0638
0.27	55.5653	64.5453	86.1488	62.7392	0.74	47.7779	74.4746	80.3384	21.2432
0.28	55.4016	64.7182	86.0076	61.4298	0.75	47.6067	74.8435	80.2924	20.3815
0.3	55.0741	65.0656	85.7257	58.8138	0.76	47.435	75.2437	80.2621	19.4708
0.32	54.7466	65.4152	85.4446	56.2262	0.77	47.2625	75.6845	80.2523	18.5002
0.33	54.5828	65.5909	85.3044	54.9517	0.78	47.0892	76.1799	80.2699	17.4559
0.36	54.0912	66.1217	84.8853	51.243	0.79	46.9149	76.7525	80.3263	16.3189
0.38	53.7633	66.4792	84.6074	48.893	0.8	46.7394	77.4445	80.4427	15.0641
0.39	53.5992	66.6591	84.4689	47.7614	0.82	46.3827	79.7936	81.1598	12.0568
0.4	53.4351	66.8399	84.3308	46.6611	0.85	14.0947	75.9148	86.4606	12.0352
0.42	53.1068	67.2042	84.0557	44.5588	0.87	14.4568	77.4901	86.6098	12.0073
0.46	52.4492	67.9455	83.511	40.7626	0.88	14.6442	78.432	86.7606	11.9031
0.49	51.9551	68.5147	83.1084	38.2612	0.91	15.2366	82.9179	88.0389	8.6862

Table A.2 Switching angles and THD calculation for 180-degree conduction mode with different Modulation Index with 4-Switching angles (degrees).

MI	alpha1	alpha2	alpha3	alpha4	THD	MI	alpha1	alpha2	alpha3	alpha4	THD
0.01	55.483	55.729	84.922	87.6488	364.855	0.48	48.6144	58.1706	68.097	89.2333	20.1854
0.02	55.289	55.777	83.61	87.1819	297.294	0.52	11.2099	60.494	77.078	84.4901	29.6727
0.03	55.109	55.838	82.687	86.9111	251.82	0.53	11.3053	60.6758	76.737	84.5409	29.5793
0.04	54.937	55.905	81.949	86.7336	218.258	0.54	11.4024	60.8555	76.407	84.5985	29.4537
0.05	54.772	55.976	81.322	86.6123	192.293	0.55	47.5164	57.5861	65.665	89.9594	19.1769
0.06	54.61	56.05	80.769	86.5291	171.598	0.56	11.6018	61.2088	75.775	84.7307	29.1143
0.07	54.452	56.125	80.269	86.4736	154.743	0.564	47.1661	57.2439	64.838	89.9985	19.3647
0.08	54.297	56.201	79.811	86.4393	140.779	0.57	46.9802	57.0282	64.39	89.9975	19.3703
0.09	54.144	56.279	79.384	86.4217	129.041	0.59	11.9119	61.723	74.877	84.9622	28.4119
0.1	53.992	56.357	78.984	86.4178	119.043	0.6	12.0179	61.89	74.587	85.0465	28.1319
0.11	53.843	56.435	78.604	86.4252	110.423	0.62	12.2335	62.2164	74.016	85.2238	27.5085
0.12	53.695	56.513	78.242	86.4421	102.905	0.608	45.5278	54.6435	60.932	89.9919	15.7568
0.13	53.548	56.592	77.896	86.4672	96.2726	0.62	44.701	53.0218	59.254	89.99	14.0425
0.14	53.402	56.67	77.561	86.4993	90.36	0.68	12.9047	63.1212	72.332	85.8096	25.1344
0.15	53.258	56.747	77.238	86.5376	85.0356	0.7	25.7084	40.9129	53.229	88.7416	14.4167
0.16	53.114	56.824	76.924	86.5814	80.196	0.71	13.2518	63.5132	71.472	86.1251	23.6337
0.17	52.971	56.901	76.619	86.63	75.7597	0.72	23.3242	42.4526	52.998	88.2154	14.7984
0.18	52.828	56.976	76.32	86.683	71.6627	0.73	22.5129	43.0905	52.882	88.0807	14.8399
0.19	52.687	57.051	76.028	86.7398	67.8544	0.74	21.817	43.6819	52.769	87.9878	14.7291
0.2	52.545	57.125	75.741	86.8002	64.2955	0.75	21.1997	44.2417	52.663	87.9246	14.5306
0.21	52.405	57.198	75.459	86.8638	60.9555	0.76	13.8453	64.0003	69.916	86.6756	20.572
0.22	52.265	57.27	75.181	86.9303	57.8105	0.77	20.1236	45.3067	52.479	87.8599	14.0221
0.24	51.985	57.409	74.635	87.0711	52.0378	0.78	14.088	64.0931	69.205	86.9032	19.1257
0.26	51.707	57.542	74.1	87.2211	46.8794	0.79	19.1881	46.3513	52.357	87.8524	13.4398
0.28	51.43	57.669	73.572	87.3789	42.2803	0.8	18.7569	46.8856	52.331	87.8643	13.1215
0.3	51.153	57.787	73.049	87.5435	38.2086	0.81	14.4601	64.0116	67.93	87.2526	16.6882
0.32	50.876	57.895	72.528	87.7142	34.6418	0.82	17.9475	48.032	52.393	87.9121	12.4403
0.34	50.6	57.993	72.006	87.8901	31.5561	0.83	17.5628	48.6798	52.514	87.9458	12.0962
0.36	50.322	58.078	71.481	88.0708	28.9209	0.84	17.1873	49.4193	52.735	87.9849	11.7722
0.38	50.044	58.148	70.95	88.2558	26.6959	0.85	14.9911	62.8127	65.177	87.7394	12.97
0.4	49.764	58.201	70.41	88.4447	24.8339	0.86	15.1458	61.9302	63.918	87.8688	12.0749
0.42	10.392	58.548	82.277	84.946	26.9385	0.87	15.3439	60.1923	61.82	88.0081	11.302

Table A.3 Switching angles and THD calculation for 180-degree conduction mode with different Modulation Index with 5-Switching angles (degrees).

MI	alpha1	alpha2	alpha3	alpha4	alpha5	THD	MI	alpha1	alpha2	alpha3	alpha4	alpha5	THD
0.01	9.8597	10.143	49.783	50.217	89.905	59.9894	0.46	7.8539	21.295	35.926	60.071	87.4135	21.066
0.03	49.7716	50.224	69.574	70.425	89.714	59.901	0.47	46.018	52.507	62.708	77.17	85.7631	35.397
0.04	9.4561	10.589	49.126	50.864	89.619	59.5184	0.48	7.9161	21.682	24.758	60.558	89.9358	15.829
0.06	49.5391	50.443	69.147	70.85	89.427	59.5418	0.49	45.826	52.517	62.325	77.558	85.6216	33.615
0.07	9.08	11.06	48.461	51.507	89.334	58.514	0.51	45.63	52.509	61.929	77.966	85.4901	31.8
0.08	49.382	50.587	68.861	71.133	89.237	59.1711	0.52	45.531	52.498	61.725	78.18	85.429	30.88
0.09	8.8453	11.387	48.012	51.935	89.147	57.5803	0.53	15.31	50.875	59.666	71.749	89.8667	13.569
0.11	49.1434	50.797	68.431	71.56	88.952	58.4224	0.54	45.328	52.459	61.303	78.63	85.3179	29.013
0.12	49.0631	50.866	68.286	71.702	88.857	58.1225	0.55	45.225	52.429	61.085	78.869	85.2691	28.065
0.14	48.9014	51.001	67.997	71.988	88.667	57.4489	0.56	45.12	52.393	60.862	79.12	85.2258	27.105
0.15	8.2262	12.435	46.632	53.212	88.596	53.8184	0.57	15.493	51.188	59.363	72.924	89.509	13.217
0.19	7.8922	13.193	45.676	54.064	88.245	50.8202	0.58	44.905	52.296	60.396	79.662	85.1597	25.143
0.2	48.4076	51.388	67.116	72.852	88.103	54.8663	0.59	44.794	52.234	60.153	79.959	85.1396	24.137
0.22	48.2402	51.509	66.818	73.143	87.917	53.8297	0.6	44.68	52.162	59.902	80.278	85.1307	23.109
0.24	7.5759	14.217	44.42	55.133	87.835	46.8793	0.61	44.564	52.078	59.642	80.626	85.1359	22.054
0.25	47.9866	51.684	66.366	73.585	87.639	52.1234	0.62	15.821	51.343	58.729	74.451	89.0972	13.467
0.26	47.9014	51.74	66.214	73.734	87.547	51.5163	0.63	44.319	51.869	59.091	81.442	85.2064	19.835
0.27	47.8158	51.795	66.06	73.883	87.455	50.8911	0.64	44.19	51.741	58.798	81.941	85.2873	18.65
0.28	47.7299	51.848	65.906	74.033	87.364	50.2481	0.65	16.074	51.278	58.19	75.428	88.8788	13.714
0.29	47.6436	51.9	65.751	74.184	87.274	49.5881	0.66	43.913	51.421	58.165	83.317	85.6385	16.056
0.3	7.3633	15.592	42.782	56.431	87.408	42.0216	0.67	16.27	51.147	57.752	76.125	88.7511	13.827
0.31	47.47	52	65.437	74.489	87.093	48.2188	0.68	16.379	51.05	57.505	76.493	88.6944	13.853
0.32	47.3826	52.047	65.279	74.643	87.004	47.5108	0.69	16.496	50.927	57.237	76.878	88.6437	13.854
0.33	47.2949	52.093	65.119	74.799	86.915	46.7878	0.7	16.623	50.774	56.945	77.284	88.6002	13.826
0.34	7.333	16.632	41.562	57.309	87.186	38.5107	0.71	16.762	50.588	56.627	77.716	88.5657	13.766
0.35	7.3402	16.913	41.234	57.531	87.141	37.5543	0.72	16.916	50.361	56.278	78.182	88.5426	13.671
0.36	47.0293	52.221	64.632	75.273	86.652	44.5353	0.73	17.088	50.084	55.894	78.693	88.5345	13.538
0.37	46.9399	52.259	64.467	75.434	86.566	43.7584	0.74	17.286	49.747	55.469	79.267	88.5473	13.353
0.39	46.7599	52.33	64.132	75.761	86.396	42.1685	0.75	17.519	49.332	54.992	79.932	88.5909	13.09
0.42	46.4861	52.418	63.615	76.269	86.149	39.7012	0.77	18.172	48.14	53.824	81.818	88.8762	11.986
0.44	46.3008	52.463	63.259	76.619	85.99	38.0064	0.78	18.694	47.218	53.07	83.549	89.327	11.116

Table A.4 Switching angles and THD calculation for 180-degree conduction mode with different Modulation Index with 7-Switching angles (degrees)

MI	alpha1	alpha2	alpha3	alpha4	alpha5	alpha6	alpha7	%THD
0.001	44.9957	45.0043	59.9917	60.1083	74.9883	75.0117	89.9928	60.0209
0.01	44.957	45.0426	59.917	60.1824	74.883	75.1169	89.9284	60.006
0.03	44.8697	45.1265	59.8494	60.2455	74.6487	75.3506	89.7852	59.8856
0.04	44.8404	45.4761	59.7607	60.3402	74.638	75.3489	89.7138	59.6144
0.05	44.7928	45.5978	59.7005	60.4801	74.6261	75.4417	89.6425	59.3862
0.06	44.7659	45.619	59.6937	60.5857	74.5961	75.7013	89.5706	59.4801
0.07	44.7205	45.6288	59.5073	60.6645	74.5781	75.8183	89.4992	59.2853
0.08	44.7178	45.6697	59.4179	60.7856	74.5163	76.7337	89.4295	58.4017
0.1	44.7021	45.7055	59.345	60.8971	74.3226	76.1699	89.2855	58.5241
0.13	44.6905	45.7174	58.9776	61.0236	74.2641	76.5232	89.0727	57.5016
0.14	44.6702	45.748	58.8358	61.1719	74.1098	77.3822	89.0112	55.122
0.19	44.5181	45.7254	58.7271	61.2558	73.9347	77.2379	88.9515	54.7001
0.2	44.5006	45.7855	58.7117	61.3901	73.9159	77.1336	88.811	50.209
0.23	43.9164	45.8507	57.9477	61.4726	73.8236	77.7236	88.7753	52.3008
0.24	43.8651	45.8801	57.8512	61.5791	73.7093	77.8465	88.7307	51.6381
0.25	43.8135	45.9088	57.7539	61.6548	73.6817	77.9702	88.72391	50.9512
0.27	43.7548	45.9767	57.6165	61.7213	73.4341	78.1922	88.71866	42.6871
0.29	43.7036	46.0149	57.5576	61.8973	73.2611	78.4732	87.9714	47.9703
0.32	43.6925	46.0845	57.4518	61.9637	72.9576	78.8615	87.8759	45.5039
0.34	43.636	46.1777	56.9163	61.9982	72.7376	78.5348	87.86521	33.7895
0.35	43.5778	46.1944	56.8377	62.0139	72.5402	79.2618	87.85862	42.8558
0.36	43.4221	46.262	56.7309	62.14598	72.4973	79.3985	87.75245	41.9354
0.37	43.4036	46.3387	56.666	62.2352	72.2287	79.213	87.63584	29.7945
0.38	43.3893	46.3932	56.5141	62.3442	72.053	79.6777	87.52039	40.0413
0.42	43.3169	46.4658	56.466	62.4317	71.8305	79.4618	87.41251	23.1747
0.45	43.2698	46.5524	56.3612	62.5392	71.6941	80.4388	87.30224	32.9183
0.46	43.1606	46.5957	56.2676	62.6496	71.5875	80.399	87.251	18.1642
0.47	42.9444	46.6278	56.1779	62.6509	71.3906	80.182	87.1472	17.0863
0.48	42.9399	46.6446	56.0254	62.6707	71.1969	80.1066	87.0345	16.1957
0.49	42.8471	46.694	55.9127	62.6859	71.0365	80.0382	86.9495	28.5656
0.52	42.7344	46.701	54.9342	62.6916	70.7785	79.9891	86.8656	17.632
0.53	42.6382	46.7389	53.9935	62.7041	70.4738	79.8519	86.6209	13.3235
0.54	42.5679	46.7797	53.9806	62.7189	70.1757	79.7937	86.5136	13.0944
0.55	42.433	46.786	53.9674	62.7206	70.0439	79.7568	86.4222	21.7898
0.56	41.9567	46.7801	53.8886	62.7385	69.7811	79.6349	86.3298	20.6466
0.57	41.8772	46.7938	53.7422	62.7455	69.5007	79.5419	86.2517	19.5031

0.58	41.8245	46.8144	53.6975	62.7597	68.9996	79.4645	86.1844	18.4314
0.59	41.7053	46.8216	53.5788	62.7602	68.5874	79.3876	86.0611	17.2195
0.6	41.4309	46.8351	53.4312	62.7823	68.3017	79.27769	85.9001	18.0802
0.61	41.3915	46.8715	53.3695	62.7977	68.2647	79.1867	85.861	17.8302
0.62	41.3899	46.6031	52.9045	62.8053	68.0862	79.1572	85.7007	13.7266
0.63	40.6016	46.5204	52.8422	62.8122	67.744	79.0017	85.6172	14.831
0.64	39.6016	46.5125	52.75749	62.8212	67.5919	78.9882	85.5199	16.8432
0.65	38.8951	46.3321	52.62947	62.8399	66.6014	78.7839	85.4259	13.2956
0.66	37.8033	45.8327	52.5335	62.8445	66.4969	78.5759	85.3245	14.8647
0.67	37.1319	45.0485	52.4818	62.8614	66.2756	78.4795	85.2596	13.701
0.68	36.958	44.7923	52.2155	62.8783	66.1988	78.4642	85.113	14.75
0.69	35.556	44.3987	52.1939	62.8862	66.0609	78.5553	85.1299	13.2899
0.7	34.9618	43.5525	52.0708	63.1382	65.8484	78.6771	85.1375	11.5955
0.71	33.8214	42.7609	50.875	63.1402	65.8298	78.7606	85.1465	14.3435
0.73	32.4183	41.7611	49.8472	63.1511	65.8362	78.8708	86.1582	13.9101
0.74	31.5234	40.768	49.6981	63.1602	65.9078	78.8807	85.2069	13.6446
0.75	30.6329	39.7796	49.3506	63.1722	66.7815	78.9942	85.2577	13.3468
0.76	29.7469	38.7962	48.1048	63.2876	66.76579	79.4118	85.3171	13.0171
0.77	28.8656	37.8181	46.6606	63.487	66.5373	79.5334	85.1069	12.6559
0.78	26.989	36.8453	44.1181	63.6911	66.4206	79.5614	85.1158	12.2637
0.79	25.1173	35.8782	42.5774	63.7009	66.3088	79.7945	85.1279	11.8409
0.8	24.8726	34.3413	41.1909	63.8037	66.2251	79.9762	85.1364	13.4262
0.81	23.3174	33.7199	39.7454	63.8579	67.9558	80.3559	85.1414	11.8339
0.82	22.6521	32.8694	38.4422	63.938	67.8184	80.5112	84.9192	10.0299
0.83	21.0065	31.8754	37.8691	64.0492	68.7304	80.6823	84.7686	9.8241
0.84	20.3839	30.5072	36.4809	64.1852	68.9949	80.9883	84.672	9.017
0.85	19.9988	29.4152	35.5773	64.3986	69.4578	81.573	84.5181	8.6987
0.86	18.167	28.2993	34.6531	64.7377	71.4695	81.6828	85.4209	8.084
0.87	17.8246	27.4005	33.0134	66.0854	72.5825	82.9787	85.5147	7.0379
0.88	16.5272	26.5007	31.8165	67.6621	73.5399	83.3808	85.6646	6.7982
0.89	15.7232	25.6235	30.9067	69.4163	74.5722	84.798	85.7177	6.1346
0.9	14.581	25.5008	29.9526	71.3465	75.9013	84.9466	86.869	5.5942
0.91	10.2069	23.9965	25.144	75.9189	76.8983	86.9516	89.9482	5.4963

Table A.5 For Bipolar 4-switching with different modulation index

MI	alpha1	alpha2	alpha3	alpha4	THD	MI	alpha1	alpha2	alpha3	alpha4	THD
0.105	21.005	38.5328	61.1938	79.301	139.198	0.455	23.3588	32.559	65.9929	77.9039	112.963
0.11	21.051	38.4612	61.2526	79.27	138.989	0.46	23.3656	32.4457	66.0767	77.9007	112.468
0.125	21.188	38.2452	61.4301	79.178	138.312	0.47	23.3742	32.2146	66.2462	77.8962	111.447
0.121	21.152	38.303	61.3826	79.202	138.499	0.48	23.3757	31.977	66.4184	77.8942	110.378
0.125	21.188	38.2452	61.4301	79.178	138.312	0.497	23.36	31.5566	66.7174	77.8967	108.425
0.13	21.233	38.1727	61.4896	79.148	138.07	0.515	23.3144	31.0865	67.0432	77.9072	106.117
0.135	21.278	38.1001	61.5494	79.118	137.82	0.52	23.2957	30.951	67.1354	77.9114	105.423
0.141	21.332	38.0126	61.6214	79.082	137.51	0.53	23.2498	30.6729	67.322	77.9216	103.954
0.145	21.368	37.9542	61.6696	79.058	137.298	0.548	23.1352	30.1473	67.6658	77.945	101.001
0.15	21.413	37.8808	61.7299	79.029	137.025	0.557	23.0608	29.8717	67.8415	77.9587	99.3541
0.155	21.457	37.8073	61.7905	79	136.746	0.566	22.9738	29.587	68.0196	77.9734	97.5829
0.156	21.466	37.7925	61.8027	78.994	136.689	0.57	22.9308	29.4575	68.0996	77.9802	96.7538
0.162	21.518	37.7039	61.8758	78.96	136.343	0.59	22.6734	28.7818	68.5067	78.0154	92.2111
0.168	21.571	37.6149	61.9491	78.925	135.987	0.6	22.5163	28.4261	68.7146	78.0327	89.6972
0.172	21.606	37.5553	61.9982	78.903	135.745	0.61	22.3391	28.0588	68.9252	78.0492	87.0407
0.18	21.675	37.4357	62.0969	78.858	135.248	0.62	22.1413	27.6802	69.1384	78.0642	84.2717
0.185	21.718	37.3606	62.1588	78.831	134.929	0.635	21.8053	27.0928	69.4627	78.0828	80.0102
0.193	21.786	37.2398	62.2584	78.787	134.407	0.64	21.6829	26.8923	69.5719	78.0876	78.5922
0.22	22.011	36.8263	62.5993	78.646	132.544	0.65	21.423	26.4853	69.7921	78.095	75.8169
0.228	22.075	36.702	62.7018	78.606	131.965	0.66	21.1437	26.0714	70.0143	78.0992	73.1932
0.23	22.092	36.6708	62.7275	78.596	131.819	0.67	20.8462	25.6522	70.2387	78.1001	70.8067
0.236	22.14	36.5767	62.8049	78.567	131.376	0.686	20.3361	24.9745	70.6024	78.0946	67.6648
0.24	22.171	36.5137	62.8567	78.547	131.077	0.687	20.0673	24.6341	70.7866	78.0891	66.7443
0.25	22.25	36.3552	62.9871	78.5	130.321	0.71	19.5063	23.9542	71.1607	78.0739	64.7949
0.26	22.327	36.195	63.1187	78.453	129.551	0.72	19.1425	23.5315	71.399	78.0627	64.2037
0.27	22.402	36.0331	63.2514	78.409	128.769	0.739	18.4296	22.7376	71.8641	78.0417	63.7088
0.275	22.44	35.9515	63.3183	78.387	128.374	0.74	18.3915	22.6962	71.8892	78.0408	63.6956
0.28	22.476	35.8695	63.3855	78.365	127.977	0.75	18.0068	22.2849	72.1428	78.0325	63.5769
0.29	22.549	35.7039	63.5208	78.324	127.175	0.763	17.4996	21.7574	72.4835	78.0278	63.3401
0.31	22.688	35.3666	63.7955	78.245	125.55	0.774	17.0652	21.3176	72.7839	78.0318	62.9355
0.32	22.755	35.1946	63.935	78.208	124.728	0.78	16.8265	21.0803	72.9533	78.0382	62.5994
0.33	22.819	35.0202	64.076	78.173	123.902	0.79	16.4259	20.6887	73.2461	78.0573	61.8193
0.34	22.881	34.8433	64.2186	78.139	123.07	0.807	15.7367	20.0328	73.7817	78.1225	59.7743
0.35	22.941	34.6636	64.3628	78.108	122.235	0.81	15.6139	19.9181	73.8823	78.1396	59.3135
0.36	22.998	34.4811	64.5087	78.078	121.396	0.827	14.9096	19.2728	74.4978	78.2787	56.1302
0.374	23.073	34.2203	64.7159	78.04	120.214	0.83	14.7835	19.1593	74.616	78.3125	55.4702
0.386	23.132	33.9915	64.8964	78.01	119.191	0.846	14.0984	18.5532	75.3131	78.5574	51.4989

0.39	23.151	33.9141	64.9572	78.001	118.849	0.85	13.9229	18.4006	75.5091	78.6399	50.4008
0.4	23.195	33.7179	65.1106	77.98	117.986	0.866	13.1953	17.7787	76.4185	79.0949	45.7252
0.42	23.271	33.3132	65.4235	77.944	116.226	0.876	12.7106	17.3729	77.1324	79.5247	42.7412
0.43	23.303	33.1041	65.5833	77.929	115.323	0.886	12.1886	16.9426	78.0258	80.1348	39.9751
0.442	23.334	32.8466	65.778	77.915	114.212	0.91	10.6103	15.6766	81.8923	83.331	36.382

Table A.6 For Bipolar 5-switching with different modulation index

MI	alpha1	alpha2	alpha3	alpha4	alpha5	%THD	MI	alpha1	alpha2	alpha3	alpha4	alpha5	%THD
0.1	18.257	18.647	61.098	78.8786	80.943	89.631	0.69	11.73	15.303	67.6548	72.729	86.7244	13.86
0.11	18.104	18.534	61.208	78.7689	81.039	88.226	0.71	11.56	15.268	67.8955	72.54	86.9203	13.298
0.114	18.044	18.49	61.251	78.7251	81.077	25.436	0.723	11.45	15.247	68.0547	72.42	87.0476	12.937
0.122	17.924	18.403	61.339	78.6376	81.154	86.333	0.73	11.39	15.237	68.1414	72.357	87.1161	12.744
0.13	17.807	18.319	61.426	78.5503	81.231	84.951	0.74	11.3	15.222	68.2668	72.267	87.2139	12.471
0.138	17.69	18.236	61.514	78.4632	81.308	83.477	0.755	11.18	15.203	68.4586	72.137	87.3605	12.067
0.146	17.602	18.214	61.505	78.3661	81.306	25.199	0.762	11.12	15.194	68.55	72.078	87.4289	11.881
0.148	17.548	18.135	61.623	78.3545	81.305	25.152	0.773	11.03	15.182	68.6965	71.988	87.5363	11.592
0.5	13.481	15.842	65.486	74.6338	84.857	19.167	0.78	10.97	15.174	68.7919	71.933	87.6046	11.411
0.51	13.383	15.804	65.598	74.5307	84.955	18.905	0.79	10.89	15.164	68.9318	71.858	87.7022	11.157
0.52	13.286	15.767	65.709	74.4278	85.054	18.639	0.814	10.7	15.144	69.2906	71.7	87.9362	10.564
0.53	13.189	15.731	65.821	74.3252	85.152	18.371	0.82	10.65	15.14	69.3874	71.668	87.9947	10.421
0.555	12.951	15.646	66.101	74.0696	85.398	17.688	0.833	10.55	15.132	69.6114	71.612	88.1214	10.117
0.56	12.904	15.63	66.157	74.0186	85.448	17.55	0.844	10.46	15.126	69.8219	71.586	88.2286	9.8667
0.573	12.782	15.589	66.304	73.8865	85.575	17.187	0.8455	10.45	15.125	69.8526	71.585	88.2432	9.0529
0.58	12.717	15.568	66.383	73.8155	85.644	16.991	0.8555	9.255	15.371	48.2949	49.504	88.4899	8.7673
0.59	12.625	15.539	66.496	73.7145	85.743	16.71	0.882	9.42	15.363	48.0961	49.047	88.6073	8.5796
0.62	12.35	15.457	66.838	73.4133	86.038	15.857	0.88	9.392	15.364	48.1418	49.136	88.5877	8.6098
0.632	12.242	15.427	66.976	73.2939	86.155	15.514	0.89	9.535	15.363	47.8331	48.614	88.6863	8.4645
0.646	12.117	15.394	67.138	73.1555	86.293	15.114	0.9	9.687	15.372	47.1674	47.736	88.7871	8.3428
0.67	11.905	15.342	67.418	72.9209	86.528	14.428	0.91	9.869	15.413	45.313	45.682	88.8972	8.2881

Table A.7 For Bipolar 6-switching with different modulation index

MI	alpha1	alpha2	alpha3	alpha4	alpha5	alpha6	THD	MI	alpha1	alpha2	alpha3	alpha4	alpha5	alpha6	THD
0.01	0.091	14.976	45.068	59.917	75.092	89.929	181.612	0.5	6.321	18.38	26.582	36.313	46.127	54.796	124.12
0.02	14.892	14.978	60.166	74.858	75.178	89.857	179.946	0.54	15.94	20.91	28.062	36.735	65.303	73.365	120.44
0.03	15.246	29.682	30.107	44.62	60.251	74.899	179.913	0.58	14.97	19.47	27.887	35.797	66.012	72.987	110.58
0.04	15.328	29.574	30.139	44.491	60.336	74.866	179.804	0.6	11.85	14.94	65.564	71.323	81.187	86.608	104.16
0.05	0.4568	14.883	45.337	59.584	75.463	89.645	179.445	0.61	14.43	18.79	27.855	35.339	66.373	72.788	99.887
0.06	15.49	29.354	30.196	44.23	60.508	74.803	179.423	0.65	13.7	17.94	27.852	34.731	66.867	72.52	94.997

0.08	15.65	29.131	30.244	43.964	60.683	74.742	179.186	0.66	13.51	17.73	27.855	34.578	66.993	72.454	92.42
0.1	15.809	28.901	30.283	43.692	60.86	74.684	178.832	0.67	13.32	17.53	27.86	34.424	67.121	72.389	89.984
0.12	1.105	14.743	45.803	58.993	76.117	89.16	176.519	0.68	13.13	17.33	27.865	34.27	67.25	72.325	87.68
0.14	1.2921	14.709	45.935	58.822	76.306	89.025	175.249	0.69	11.38	15.03	66.764	71.139	82.757	86.74	79.737
0.18	14.035	14.856	61.515	73.743	76.625	88.746	170.729	0.7	12.75	16.95	27.877	33.957	67.515	72.2	78.433
0.2	16.556	27.638	30.282	42.234	61.796	74.431	169.473	0.73	12.18	16.39	27.89	33.473	67.93	72.027	74.83
0.22	2.0498	14.596	46.457	58.128	77.072	88.497	168.301	0.74	11.12	15.08	67.613	71.221	84.046	87.23	73.263
0.27	13.558	14.826	62.299	73.14	77.472	88.157	159.569	0.75	11.07	15.09	67.811	71.265	84.382	87.406	69.81
0.32	13.295	14.822	62.745	72.816	77.959	87.846	151.809	0.76	11.61	15.86	27.887	32.965	68.378	71.882	68.96
0.33	17.19	25.464	29.612	40.045	63.142	74.151	151.141	0.78	11.22	15.52	27.869	32.606	68.705	71.811	68.029
0.34	17.204	25.26	29.527	39.865	63.251	74.126	150.471	0.8	10.84	15.19	27.83	32.225	69.066	71.773	67.293
0.35	5.0344	19.656	25.457	37.911	44.754	56.392	149.62	0.81	10.64	15.03	27.8	32.023	69.265	71.772	65.981
0.36	17.21	24.833	29.345	39.503	63.472	74.073	149.566	0.83	10.25	14.71	27.713	31.592	69.717	71.823	60.427
0.37	13.033	14.826	63.202	72.502	78.461	87.55	148.132	0.84	10.05	14.55	27.651	31.359	69.983	71.889	53.163
0.38	17.182	24.384	29.155	39.141	63.696	74.013	147.644	0.85	9.851	14.38	27.574	31.11	70.29	71.994	50.885
0.39	12.929	14.83	63.389	72.381	78.667	87.438	146.445	0.86	9.643	14.22	27.477	30.841	70.655	72.159	46.567
0.4	12.877	14.832	63.483	72.321	78.772	87.383	145.561	0.87	9.427	14.05	27.355	30.547	71.11	72.415	42.161
0.42	4.0177	14.511	47.685	56.29	79.113	87.333	142.123	0.88	9.199	13.87	27.198	30.216	71.713	72.822	40.585
0.44	12.669	14.845	63.866	72.087	79.2	87.173	135.8	0.89	8.945	13.66	26.988	29.826	72.594	73.511	37.669
0.46	16.687	22.425	28.429	37.727	64.607	73.692	129.149	0.9	8.728	14.2	26.618	29.275	45.152	45.897	34.436
0.48	16.469	21.918	28.285	37.389	64.838	73.59	128.581	0.91	8.144	12.95	25.967	28.275	77.543	78.205	30.223

Table A. 8 Switching angles for 120-degree mode of operation with 3-switching

MI	alpha1	alpha2	alpha3	THD	MI	alpha1	alpha2	alpha3	THD
0.003	59.95	60.0496	89.9141	127.3125	0.52	49.327	61.0514	69.373	21.8003
0.004	59.934	60.0661	89.8854	127.3036	0.54	48.3597	59.2537	67.2453	23.6974
0.005	59.917	60.0826	89.8568	127.2921	0.56	46.9497	56.604	64.6731	30.3107
0.007	59.884	60.1155	89.7995	127.2616	0.57	45.9679	54.8865	63.2476	29.8812
0.009	59.851	60.1484	89.7422	127.2209	0.58	44.7404	52.926	61.8005	26.514
0.01	59.834	60.1648	89.7135	127.1968	0.59	43.2673	50.8211	60.4239	23.6562
0.02	59.667	60.3285	89.4269	126.8167	0.6	41.6233	48.734	59.201	22.6027
0.03	59.499	60.491	89.1401	126.1884	0.61	39.9357	46.8242	58.1651	22.3582
0.05	59.16	60.8122	88.5657	124.2203	0.62	38.318	45.1829	57.2984	22.5674
0.07	58.817	61.1279	87.9893	121.3853	0.64	35.4925	42.7264	55.9158	23.5274
0.18	56.873	62.7368	84.7457	96.8568	0.65	34.2913	41.8415	55.3328	23.8932
0.19	56.691	62.8691	84.441	94.3913	0.66	33.21	41.1304	54.7921	24.3172
0.2	56.509	62.9983	84.134	91.9422	0.68	31.3319	40.0962	53.7866	25.0984
0.22	56.141	63.247	83.512	87.1088	0.7	29.7307	39.4188	52.8316	24.8077
0.24	55.77	63.4809	82.8779	82.3675	0.73	27.6641	38.8026	51.4187	22.3501
0.26	55.396	63.6976	82.2296	77.7081	0.8	23.6303	38.0607	47.8397	17.4284

0.29	54.826	63.9839	81.2245	70.8496	0.82	22.5661	37.8021	46.6309	16.7475
0.32	54.245	64.2121	80.1701	64.1954	0.84	21.5053	37.4044	45.2525	16.7072
0.34	53.85	64.3232	79.4323	59.9569	0.85	20.9684	37.1168	44.4691	17.0501
0.36	53.448	64.3934	78.6597	55.9474	0.86	20.4211	36.7389	43.5963	17.614
0.38	53.036	64.413	77.8444	52.1794	0.87	19.8559	36.2335	42.6027	18.259
0.4	52.612	64.3694	76.976	48.5618	0.88	18.6636	35.5969	41.683	12.0174
0.42	52.172	64.2454	76.041	44.8702	0.89	18.6123	34.5712	40.0288	18.576
0.44	51.711	64.0169	75.0206	40.7926	0.9	17.863	33.1446	38.233	17.5934
0.46	51.218	63.6495	73.889	36.0867	0.91	16.8862	30.9055	35.7933	15.5157
0.48	50.678	63.0921	72.6093	30.8277	0.92	15.2151	26.9516	32.1732	11.8768
0.5	50.065	62.2669	71.1289	25.5989	0.93	9.1406	17.6968	26.4431	16.224

Table A. 9 Switching angles for 120-degree mode of operation with 4-switching

MI	alpha1	alpha2	alpha3	alpha4	THD	MI	alpha1	alpha2	alpha3	alpha4	THD
0.001	54.7451	54.7679	79.007	79.046	110.6577	0.41	21.095	43.2762	59.4927	72.388	35.509
0.002	31.9925	32.0886	66.373	66.4425	140.7003	0.42	20.719	43.6891	59.3631	72.433	33.599
0.003	31.9685	32.1126	66.356	66.4598	140.6903	0.44	19.905	44.5971	59.1334	72.468	30.094
0.004	31.9445	32.1367	66.338	66.4772	140.6763	0.45	19.46	45.1051	59.0394	72.452	28.587
0.006	31.8964	32.1847	66.304	66.5118	140.6363	0.46	18.983	45.6613	58.9655	72.406	27.267
0.008	19.3201	19.6912	46.386	46.8458	188.0815	0.5	16.559	48.7507	59.1215	71.796	22.358
0.009	19.2969	19.7144	46.357	46.8745	188.0227	0.51	15.755	49.9347	59.4395	71.505	21.083
0.01	19.2737	19.7376	46.328	46.9032	187.957	0.53	13.901	53.3377	61.2098	71.021	24.788
0.02	31.5602	32.5213	66.06	66.7542	139.9103	0.54	13.11	55.3998	62.9856	71.319	29.691
0.04	54.2959	55.2051	78.234	79.8122	108.9965	0.55	12.651	57.0509	64.8775	72.159	29.614
0.05	30.8391	33.2439	65.537	67.2711	135.802	0.56	12.442	58.151	66.3955	73.187	27.641
0.06	30.5984	33.4855	65.362	67.4425	133.7042	0.58	12.348	59.4373	68.3012	75.042	27.542
0.07	30.3574	33.7275	65.187	67.6134	131.2727	0.6	12.415	60.2197	69.2931	76.495	28.456
0.09	29.8743	34.213	64.837	67.9535	125.5038	0.64	12.705	61.291	70.0145	78.642	28.863
0.1	29.6321	34.4568	64.662	68.1226	122.2219	0.66	12.884	61.7174	70.0446	79.497	28.506
0.11	29.3893	34.7013	64.487	68.2911	118.7165	0.69	13.177	62.2763	69.8513	80.624	27.356
0.12	29.146	34.9465	64.312	68.4588	115.0218	0.7	13.28	62.4435	69.7375	80.97	26.834
0.15	28.4113	35.6881	63.787	68.957	103.1714	0.71	13.384	62.6011	69.6022	81.304	26.255
0.17	27.9168	36.1883	63.437	69.2843	95.0236	0.72	13.491	62.7485	69.4464	81.628	25.627
0.21	26.913	37.2069	62.74	69.9241	79.5319	0.75	13.819	63.1184	68.8572	82.554	23.53
0.23	26.4015	37.7278	62.394	70.2349	72.7195	0.76	13.932	63.2116	68.6174	82.849	22.78
0.25	25.8818	38.2584	62.049	70.5381	66.7578	0.77	14.046	63.285	68.3525	83.14	22.012
0.26	25.6185	38.5279	61.878	70.6864	64.11	0.78	19.339	46.2525	52.6003	84.442	18.13
0.28	25.0834	39.0771	61.538	70.9755	59.4365	0.79	14.279	63.3541	67.7315	84.709	20.439
0.31	24.2555	39.9314	61.034	71.3858	53.6285	0.8	14.399	63.3357	67.3626	84.989	19.639
0.33	23.6821	40.527	60.705	71.6396	50.1814	0.81	14.52	63.2673	66.9411	84.266	18.836

0.34	23.3873	40.8346	60.543	71.7593	48.4841	0.82	17.72	48.5033	52.6892	84.635	16.333
0.35	23.0864	41.1499	60.383	71.8733	46.7667	0.83	14.772	62.8992	65.8614	84.817	17.266
0.37	22.4628	41.8076	60.071	72.0813	43.1965	0.84	14.906	62.5226	65.1285	85.093	16.552
0.38	22.138	42.1528	59.92	72.1735	41.3277	0.85	15.631	50.9497	53.6215	85.912	15.988
0.35	23.0864	41.1499	60.383	71.8733	46.7667	0.86	15.217	60.8243	62.7284	85.661	15.503
0.37	22.4628	41.8076	60.071	72.0813	43.1965	0.87	15.506	58.0117	59.6017	85.994	14.754

Table A.10 Switching angles for 120-degree mode of operation with 5-switching

MI	alpha1	alpha2	alpha3	alpha4	alpha5	THD
0.001	49.9925	50.0075	69.9858	70.0142	89.9809	90.0313
0.003	49.9773	50.0226	69.9574	70.0425	89.9427	90.0286
0.006	49.9546	50.0451	69.9148	70.0849	89.8854	90.0196
0.08	49.3723	50.5754	68.8338	71.1005	88.4669	87.9152
0.09	49.2906	50.6431	68.6835	71.2331	88.2737	87.363
0.1	49.2082	50.7096	68.5321	71.3644	88.0799	86.7508
0.17	48.6137	51.1424	67.4414	72.2459	86.7003	80.9299
0.2	48.3494	51.3074	66.9558	72.5994	86.0914	77.7245
0.21	48.26	51.3592	66.7912	72.7133	85.8853	76.5774
0.24	47.988	51.5041	66.2884	73.0412	85.2549	72.9306
0.25	47.8959	51.5485	66.1176	73.1453	85.0402	71.6532
0.27	47.7098	51.6311	65.7707	73.3444	84.6025	69.0162
0.29	47.5206	51.7045	65.416	73.5295	84.152	66.2781
0.3	47.4249	51.7373	65.2355	73.6159	83.9212	64.8731
0.33	47.1323	51.8185	64.6794	73.8456	83.2008	60.514
0.34	47.0328	51.8391	64.4885	73.9104	82.9497	59.0092
0.36	46.8303	51.8691	64.0972	74.0176	82.4267	55.907
0.37	46.7272	51.8778	63.8961	74.0582	82.153	54.3011
0.39	46.5162	51.8805	63.481	74.1066	81.5754	50.9484
0.4	46.4081	51.8735	63.2659	74.1111	81.2684	49.184
0.45	45.8262	51.7195	62.0803	73.8229	79.4526	38.9217
0.47	45.5608	51.5709	61.5219	73.4653	78.5118	33.7768
0.48	45.4151	51.4646	61.2106	73.1965	77.9637	30.9128
0.49	45.2562	51.3274	60.8679	72.8435	77.3444	27.8835
0.51	44.8713	50.902	60.0278	71.7605	75.7966	22.0149
0.52	44.616	50.555	59.4711	70.929	74.7949	20.2634
0.55	42.8882	47.7454	56.221	66.2423	70.3287	30.2271
0.56	41.3868	45.4777	54.3294	64.0789	68.5966	27.0381
0.59	35.6574	38.9709	50.684	60.1695	65.242	20.3089
0.62	32.1691	36.1715	48.8757	57.649	62.7301	25.6276
0.63	31.2899	35.5768	48.244	56.7061	61.8514	25.3578

0.64	30.4694	35.0333	47.5274	55.6622	60.9383	23.8698
0.65	29.672	34.4879	46.6892	54.5093	60.0009	21.8839
0.66	28.8671	33.8916	45.7012	53.2637	59.0637	20.4663
0.67	28.0296	33.2034	44.5603	51.9774	58.1643	20.0963
0.68	27.1463	32.405	43.3083	50.7391	57.3425	20.515
0.69	26.2239	31.5169	42.0304	49.6456	56.6237	21.7155
0.7	25.2877	30.5946	40.8175	48.7581	56.0092	23.5774
0.71	9.4427	20.5876	34.9858	65.8505	75.5515	23.4954
0.72	9.5935	20.7615	34.7128	66.1092	75.4025	23.4297
0.73	22.6781	28.1434	37.9298	47.2385	54.601	25.64
0.74	21.9199	27.5002	37.19	46.9906	54.2122	24.484
0.75	21.2183	26.9395	36.526	46.8175	53.8419	22.914
0.76	20.5676	26.4498	35.9196	46.6977	53.4822	21.2556
0.77	10.3701	21.5612	33.3319	67.4733	74.6941	22.5725
0.78	10.5298	21.7065	33.0488	67.7665	74.5673	22.3098
0.79	18.8574	25.2955	34.315	46.5186	52.4134	17.521
0.8	18.349	24.9836	33.8218	46.4864	52.0462	16.8888
0.81	17.8632	24.6951	33.3385	46.455	51.6664	16.5336
0.82	17.3962	24.4229	32.8601	46.4167	51.2687	16.3968
0.83	11.3499	22.3408	31.5602	69.4397	74.1215	20.5173
0.84	16.5038	23.9024	31.8994	46.2828	50.3901	16.5215
0.85	16.0714	23.6406	31.4069	46.1609	49.8861	16.6703
0.86	15.6429	23.367	30.8979	45.9741	49.3134	16.8219
0.87	15.2132	23.0699	30.3625	45.6847	48.6365	16.9547
0.88	14.7742	22.7302	29.784	45.2236	47.7912	17.0644
0.89	12.3845	22.7491	29.3182	73.2725	75.4406	15.8584
0.9	13.7765	21.7013	28.2888	43.0082	44.8806	17.0502
0.91	12.9566	20.3837	26.7645	39.7003	41.4639	14.8506

Table A. 11 Switching angles for 120-degree mode of operation with 6-switching

MI	alpha1	alpha2	alpha3	alpha4	alpha5	alpha6	THD
0.001	22.6737	22.7058	40.6287	40.6651	64.0484	64.072	117.2347
0.002	22.177	22.2354	40.1053	40.1782	64.6976	64.7782	117.0525
0.005	22.1332	22.2792	40.0505	40.2328	64.637	64.8387	117.0345
0.007	22.5774	22.8019	40.5196	40.7742	64.9775	64.1428	117.2025
0.008	22.0894	22.323	40.9957	40.2873	64.5764	64.8992	117.0011
0.009	22.8639	22.1583	40.3342	40.4925	64.4302	64.6739	100.1786
0.01	22.5291	22.8499	40.4651	40.8287	63.9421	64.1782	100.1682
0.04	22.0443	23.3274	39.9202	41.3754	63.5877	64.5318	99.1656
0.08	21.3906	23.957	39.1925	42.1087	63.1161	65.001	96.0098

0.1	21.0604	24.2686	38.8273	42.4781	62.8813	65.234	93.6951
0.13	20.5606	24.7314	38.2766	43.0368	62.5309	65.581	89.3818
0.15	20.2241	25.0364	37.9067	43.413	62.299	65.8102	85.9988
0.17	19.8845	25.3383	37.5338	43.7929	62.0689	66.0374	82.2596
0.2	19.704	25.3587	36.6381	43.1024	61.7332	66.1399	81.8435
0.21	19.1952	25.9301	36.7762	44.5663	61.6155	66.484	80.9113
0.26	18.3096	26.6382	35.7947	45.5674	61.067	67.0236	79.4336
0.27	18.1285	26.7738	35.5918	45.7736	60.9606	67.1283	78.0783
0.3	17.5755	27.1633	34.964	46.4076	60.6503	67.4345	77.0493
0.31	17.3874	27.2858	34.7468	46.625	60.5503	67.5335	76.7494
0.39	15.7818	28.0007	32.7323	48.5316	59.851	68.2467	34.5118
0.4	15.5622	28.0266	32.4165	48.8015	59.7828	68.3218	32.8896
0.41	15.3359	28.0247	32.0732	49.0825	59.7214	68.3922	31.3817
0.44	14.596	27.7378	34.7723	50.0206	59.5928	68.5631	27.5458
0.45	14.4521	27.9238	36.8058	50.8409	59.6689	68.2139	27.771
0.46	14.5009	27.0527	37.4387	50.7872	59.5823	68.6119	25.4449
0.48	14.7985	27.1429	38.9878	51.9018	59.7172	68.4636	23.2165
0.49	15.0097	28.6329	39.4325	53.1136	60.0157	67.9692	22.3107
0.61	16.6023	49.518	57.2105	71.679	77.0886	81.387	22.3263
0.62	16.6674	49.527	57.0796	71.9906	77.3247	81.8004	21.9583
0.63	16.7354	49.5275	56.94	72.3004	77.5249	82.1796	21.6959
0.64	16.8061	49.52	56.7923	72.6134	77.7015	82.5322	21.5265
0.65	16.8794	49.5044	56.637	72.9342	77.8646	82.8641	21.4313
0.67	17.0335	49.4481	56.3032	73.6171	78.1853	83.4835	21.3669
0.68	17.8172	48.9899	56.4917	73.3314	78.2795	84.4288	20.8415
0.69	17.4515	47.3304	56.3117	74.8561	78.7033	84.4022	20.1005
0.7	15.2863	46.2915	55.7397	74.8362	77.797	84.3598	21.1417
0.74	11.0196	42.9756	50.793	67.7919	70.1777	85.7303	17.4601
0.741	8.2849	40.7356	49.5055	66.8515	70.323	86.972	21.6707
0.82	7.3434	22.511	30.4319	68.1966	72.6906	87.9654	23.4087
0.84	7.3015	19.4158	24.7592	68.8343	72.5126	87.4206	19.1277
0.87	7.6095	17.0567	18.3676	70.0876	72.5422	87.1116	15.7326
0.88	7.3488	16.7036	18.6211	70.693	72.743	87.3488	14.7511
0.9	9.9432	17.3306	19.3133	72.9101	74.1828	87.8676	12.3052
0.91	10.0376	19.7229	19.9964	76.1255	77.1295	88.2699	11.1377

Table A.12 Switching angles for 120-degree mode of operation with 7-switching

MI	alpha1	alpha2	alpha3	alpha4	alpha5	alpha6	alpha7	THD
0.004	14.9532	15.0468	44.9361	45.0639	59.9671	60.0332	89.9427	90.0239
0.005	44.9785	45.0213	59.9585	60.0412	74.9414	75.0584	89.9284	90.0235

0.008	14.9065	15.0937	44.8724	45.128	59.9345	60.0668	89.8854	90.0007
0.009	44.9613	45.0383	59.9252	60.0741	74.8944	75.1049	89.8711	90.0051
0.01	14.8832	15.1171	44.8405	45.16	59.9183	60.0837	89.8568	89.9833
0.04	44.8245	45.1667	59.6623	60.3236	74.5258	75.4615	89.4266	89.5093
0.06	44.7336	45.2465	59.4883	60.4798	74.2839	75.6875	89.1391	88.8594
0.08	44.6407	45.3238	59.311	60.6321	74.0385	75.9102	88.8505	87.9554
0.1	13.8505	16.1834	43.423	46.6326	59.2827	60.9231	88.5671	85.2942
0.12	44.4491	45.4703	58.9463	60.9241	73.5372	76.3453	88.2689	85.4091
0.14	13.4074	16.6643	42.7982	47.3113	59.0701	61.3482	87.9934	80.9157
0.16	44.25	45.6051	58.568	61.1975	73.0202	76.7652	87.6783	81.9326
0.22	12.5792	17.6465	41.5404	48.7291	58.8299	62.3225	86.8474	68.6784
0.23	43.8837	45.8079	57.8714	61.6223	72.0702	77.4544	86.6094	73.8631
0.26	12.2161	18.1557	40.8969	49.4697	58.8336	62.8962	86.2791	61.184
0.27	12.1336	18.2862	40.7332	49.6574	58.8503	63.0518	86.1382	59.2007
0.29	43.5507	45.9406	57.2341	61.9154	71.1959	77.9788	85.633	65.272
0.31	11.8499	18.8267	40.061	50.4114	58.9846	63.7336	85.584	50.9504
0.32	43.3766	45.989	56.8985	62.029	70.7306	78.2056	85.1106	60.5056
0.33	43.3174	46.002	56.7837	62.0607	70.5703	78.274	84.9294	58.8556
0.3846	18.813	43.1467	52.9821	57.1952	65.5148	72.0907	89.9777	40.9297
0.35	11.6657	19.4117	39.3476	51.1462	59.219	64.5265	85.0568	42.508
0.36	11.6395	19.568	39.1599	51.3215	59.2889	64.7434	84.9322	40.4424
0.37	11.6224	19.7295	38.9674	51.4917	59.3613	64.9677	84.8117	38.423
0.38	11.6148	19.897	38.7693	51.6559	59.4346	65.1991	84.6961	36.4659
0.39	11.617	20.0713	38.5646	51.8131	59.5076	65.4371	84.5866	34.5878
0.41	11.6524	20.4465	38.1297	52.1029	59.6459	65.9317	84.392	31.13
0.42	42.7442	46.022	55.6567	62.1425	68.949	78.592	83.0093	42.7087
0.46	42.4485	45.9375	55.0595	59.2271	68.0394	78.3468	81.789	34.563
0.49	12.4214	23.6687	34.5125	52.7164	59.904	68.2412	85.3943	22.3129
0.5	42.0701	45.6888	54.2755	61.4098	66.7741	77.279	79.8207	24.9565
0.51	41.9369	45.5552	53.9949	61.1088	66.3064	76.6874	79.0444	22.2922
0.52	41.7586	45.3417	53.6189	60.6371	65.6807	75.8132	78.0318	20.2624
0.53	41.4723	44.9419	53.0251	59.8034	64.733	74.4787	76.6552	21.5592
0.54	40.8538	44.0016	51.851	58.1418	63.1272	72.4924	74.8189	28.4186
0.55	11.5912	20.112	37.8264	53.9973	59.857	68.7747	80.3724	19.787
0.56	11.8674	20.6784	37.2872	53.896	59.7691	69.1568	80.6235	19.9007
0.57	12.0655	21.0851	36.8781	53.8487	59.6834	69.4807	80.7415	19.8489
0.58	12.2284	21.4092	36.538	53.8222	59.5934	69.7781	80.7907	19.7587
0.59	12.373	21.6846	36.2386	53.8038	59.4967	70.0616	80.8005	19.6677
0.6	12.5074	21.9289	35.9654	53.7871	59.3923	70.3376	80.7864	19.5892
0.61	12.636	22.1521	35.7096	53.7687	59.2793	70.6098	80.7575	19.5284
0.62	5.8335	12.2985	29.8876	32.6976	43.2343	62.6678	72.1005	21.3098

0.63	6.0258	12.5535	29.4784	32.5575	42.9399	62.853	72.0531	21.4941
0.64	6.2041	12.7792	29.1185	32.47	42.6668	63.037	71.9859	21.5915
0.65	26.132	28.8831	38.3864	43.0368	51.1113	59.1519	62.6222	24.521
0.66	25.1942	28.0335	37.5149	42.478	50.6107	58.4859	61.9485	25.4049
0.67	13.3862	23.2815	34.3285	53.5213	58.3973	72.2812	80.5161	19.5739
0.68	13.5168	23.4539	34.1055	53.4441	58.2106	72.5826	80.4905	19.6352
0.69	7.0505	13.7869	18.6633	63.9661	71.5247	78.5801	87.6307	21.6045
0.7	22.2803	25.6748	34.915	40.9932	48.3139	55.3686	59.0721	19.6928
0.71	7.3212	13.9978	27.2221	32.495	40.9848	64.3379	71.2866	21.3297
0.72	20.9779	24.6018	33.51	39.8607	46.4573	53.4133	57.5568	18.6483
0.73	20.285	23.9677	32.6625	39.0508	45.3303	52.486	56.8759	20.94
0.74	7.7878	14.4338	26.548	32.6283	40.2919	64.9189	70.9479	21.0251
0.75	14.6222	24.7237	32.3633	52.3221	56.4046	75.3325	80.9581	19.2243
0.76	7.7633	13.814	19.013	65.2574	70.5864	79.9232	86.7942	18.5928
0.77	17.3325	21.0293	29.0808	35.834	41.5757	50.5632	55.059	23.6332
0.78	15.432	25.5816	30.8623	51.1305	55.1149	77.7468	82.6766	16.2917
0.79	16.0547	19.8486	27.7591	34.9498	40.4393	50.3456	54.4512	18.3077
0.8	15.491	19.3654	27.2064	34.634	39.961	50.3018	54.1655	15.9812
0.81	8.4077	13.9837	19.3115	66.2915	70.0109	80.9793	86.3069	15.1045
0.82	9.0748	15.4846	24.8378	32.9098	38.29	66.6679	70.1585	19.8703
0.83	14.036	18.2261	25.7983	33.9304	38.6688	50.2496	53.2915	13.1657
0.84	13.3584	17.0754	20.5298	50.31	53.0292	81.5648	85.9629	11.6819
0.85	13.2037	17.6294	24.9662	33.5254	37.8208	50.1776	52.6247	14.0978
0.86	9.7548	15.9504	23.9471	32.8004	37.0358	67.8953	70.084	18.7999
0.87	11.8327	15.4708	20.0432	50.2094	51.974	82.4967	85.9786	9.281
0.88	11.4033	15.1214	19.9867	50.0027	51.4486	82.8632	86.0367	8.7627
0.89	10.2894	16.2491	23.1625	32.3052	35.7122	69.701	70.9183	17.3312
0.9	11.2431	16.0995	22.7053	31.7772	34.9508	47.8883	48.814	16.8797
0.91	10.1174	14.2248	20.232	44.0477	44.8173	85.6717	87.6236	7.9591

Table A.13 Unipolar 60-degree modified phase voltage for 5-switching angles

MI	alpha1	alpha2	alpha3	alpha4	alpha5	THD
0.65	30.2692	34.4824	46.6878	54.5077	89.699	34.3169
0.67	43.2654	49.5999	54.7032	57.9805	87.574	24.6372
0.68	43.7032	51.3366	58.2971	60.6235	87.3148	31.8668
0.69	43.835	52.0267	60.4502	62.6	87.078	33.4459
0.7	43.8778	52.4161	61.8328	64.0317	86.8511	33.8064
0.71	43.8835	52.6885	62.7725	65.1074	86.6296	34.0647
0.72	43.8698	52.9047	63.4365	65.9483	86.4111	34.4002
0.73	43.8446	53.0894	63.9173	66.6281	86.1942	34.7961
0.74	43.8118	53.2548	64.2701	67.193	85.978	35.2112
0.75	43.7736	53.4072	64.53	67.6727	85.7618	35.6133
0.76	43.7314	53.5504	64.72	68.0875	85.545	35.9814
0.8	43.535	54.0668	65.0395	69.3227	84.6638	36.9314
0.81	43.4809	54.1863	65.0466	69.5584	84.4381	37.0223
0.82	43.4251	54.3028	65.0336	69.7726	84.2097	37.0539
0.83	43.3679	54.4166	65.0032	69.9676	83.9779	37.0271
0.85	43.2493	54.6363	64.8981	70.3063	83.5032	36.8038
0.87	43.1257	54.8456	64.7428	70.5828	83.0105	36.3636
0.88	43.0621	54.946	64.6485	70.6989	82.756	36.0655
0.9	42.9313	55.1376	64.4285	70.8867	82.2278	35.3181
0.92	42.7958	55.3145	64.1664	71.012	81.6683	34.3689
0.94	42.6552	55.4724	63.8585	71.0668	81.0695	33.2054
0.96	42.5089	55.6041	63.4957	71.0377	80.4204	31.7915
0.97	42.4333	55.6567	63.2887	70.9854	80.0725	30.9696
0.99	42.2759	55.724	62.807	70.787	79.318	29.0253
1	42.1933	55.7315	62.5219	70.6308	78.9052	27.8642
1.1	10.2213	13.4767	39.6099	63.8585	75.0177	15.4792
1.2	30.7011	35.8364	43.3412	63.9375	68.7203	15.1547
1.3	26.2376	34.1254	40.3797	63.8675	65.825	12.3809

The proposed multilevel inverter control was experimentally validated through hardware experimental set up as shown in Figure A.24 (a) and (b). In Figure A.24 (a) the hardware implementation of the MLI is shown and in Figure A.24 (b) the control hardware including the PV-panels for input of the inverter and MMT control unit is shown. In Figure A.24 (c) the output of the DVR for voltage sag is displayed and where the Figure A.24 (d) is shown for the control unit of the proposed system.

Figure A 24 Experimental validation set-up (a) MLI configuration (b) PV panel and control circuit for inverter input and MPPT (c) the output of the DVR (d) control unit of the proposed system

In Figure A.25 different wave forms are shown during three phase balanced voltage sag which is created at 50ms and cleared by DVR at 145ms. It is evident from Figure A.25 that the proposed control has acceptable dynamic response with low transients and the load voltage has almost remained constant during the fault period. In Figure A.26 shows different waveforms during three phase balanced voltage sag with nonlinear load created at 50ms and cleared by DVR at 150ms. It can be observed from Figure A.26 also that the proposed control has acceptable response with almost constant load voltage during the fault period.

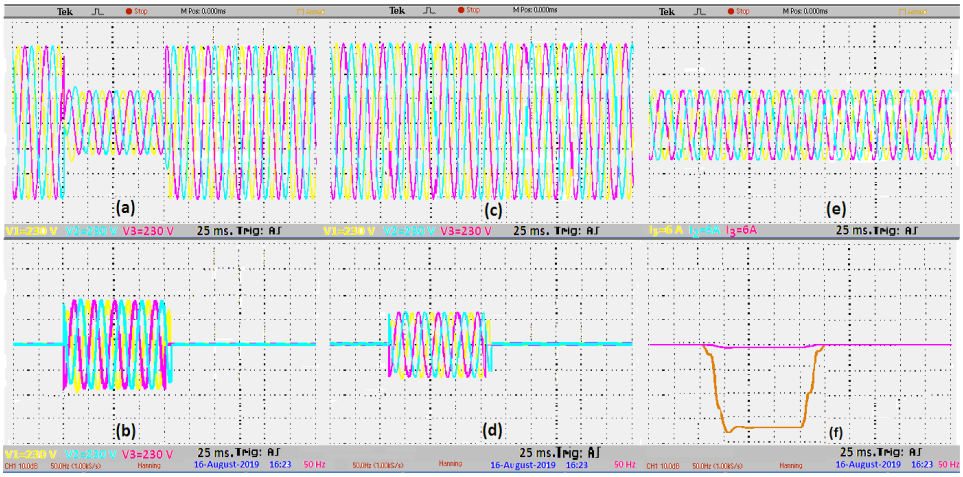

Figure A.25. Experimental waveforms for voltage sag with **linear** RL-load with balanced three-phase fault (a) three-phase source voltage during fault (Channel 1, 2 and 3: Y-axis: 75V/div., X-axis 25 msec/div.) (b) DVR injected voltage (Channel 1, 2 and 3: Y-axis: 35V/div., X-axis 25 msec/div.) (c) three-phase load voltage (Channel 1, 2 and 3: Y-axis: 75V/div., X-axis 25 msec/div.) (d) three-phase fault current (Channel 1, 2 and 3: Y-axis: 5A/div., X-axis 25 msec/div.) (e) three-phase load current (Channel 1, 2 and 3: Y-axis: 5A/div., X-axis 25 msec/div.) (f) active and reactive power (Channel 1, 2 and 3: Y-axis: ±20 W/div., X-axis 25 msec/div.)

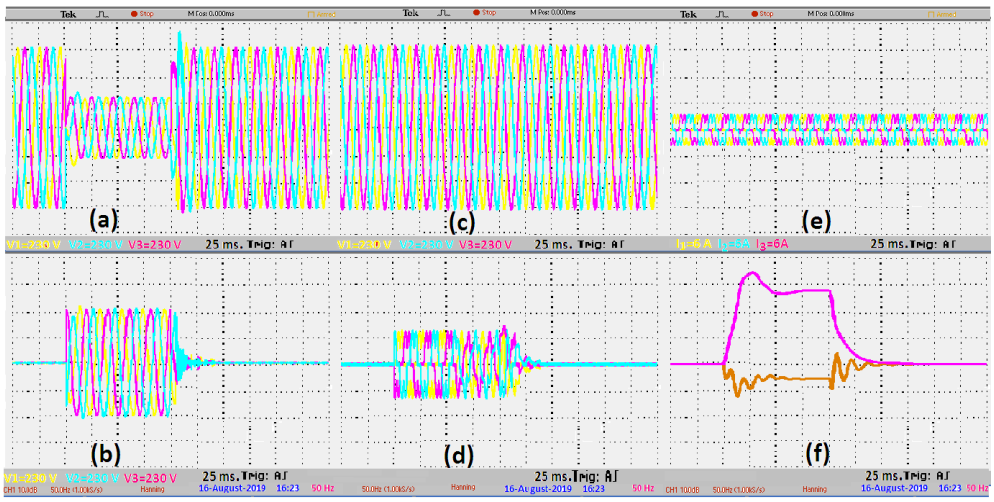

Figure A.26 DVR response for **nonlinear**-RL-load with balanced 3-phase and ground fault (a) three-phase balanced fault voltage (Channel 1, 2 and 3: Y-axis: 75V/div., X-axis 25 msec/div.) (b) DVR injection voltage (Channel 1, 2 and 3: Y-axis: 35V/div., X-axis 25 msec/div.) (c) three-phase load voltage (Channel 1, 2 and 3: Y-axis: 75V/div., X-axis 25 msec/div.) (d) three-phase fault current (Channel 1, 2 and 3: Y-axis: 5A/div., X-axis 25 msec/div.) (e) three phase load current (Channel 1, 2 and 3: Y-axis: 5A/div., X-axis 25 msec/div.) (f) active and reactive power (Channel 1, 2 and 3: Y-axis: ±20 W/div., X-axis 25 msec/div.)

In Figure A.27 (a) the per phase output voltage and current waveforms of the 15-level inverter are shown when connected to the system for compensation. The harmonic spectra for the load voltage with and without PV-DVR system are shown in Figures. A.27 (b) and (c) respectively. Inspection of Figures A.27 (b) and (c), shows the considerable improvements of harmonic spectra with the proposed control where the most of the higher order harmonics are eliminated.

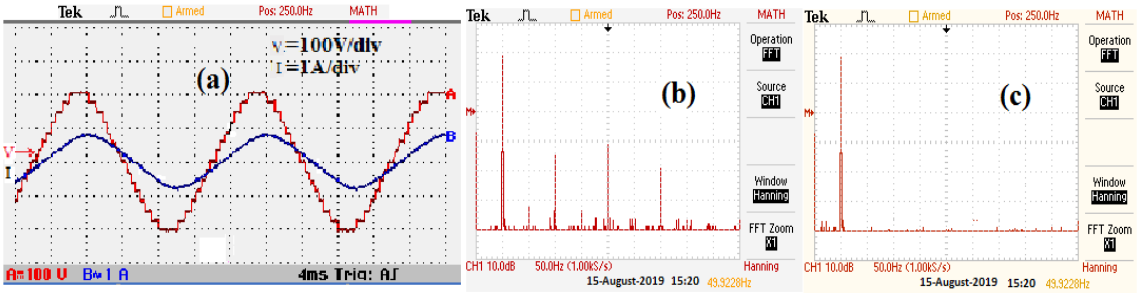

Figure A.27 Experimental harmonic spectra for (a) output voltage and current waveforms of the proposed15-level inverter for R=74 Ω, R=1mH (b) without PV-DVR and (c) with PV-DVR mode

Reference

[1] Ali Keyhani. Design of Smart Power Grid Renewable Energy Systems. Wiley-IEEE, ISBN-10: 1118978773, ISBN-13:978-1118978771, 22 Jul 2016.

[2] M. Shahidehpour, “Role of smart microgrid in a perfect power system,” IEEE Power Energy Soc. Gen. Meeting, 2010.

[3] N. Hatziargyriou, H. Asano, M.R. Iravani, and C. Marnay, “Microgrids: An overview of ongoing research, development and demonstration projects,” IEEE Power and Energy Mag., vol. 5, no. 4, Jul./Aug. 2007.

[4] S. Parhizi, H. Lotfi, A. Khodaei, and S. Bahramirad, “State of the Art in Research on Microgrids: A Review,” IEEE Access, vol. 3, pp. 890-925, July 2015.

[5] Downey, L. Dc microgrids. Darnell smart grid form, San Jose, CA. 10. 2010.

[6] Cetin, E., Yilanci, A., Ozturk, H. K., Colak, M., Kasikci, I., & Iplikci, S. A micro-dc power distribution system for a residential application energized by photovoltaicwind/ fuel cell hybrid energy systems. Energy and Buildings, 42, 2009.

[7] Joan Rocabert, Alvaro Luna, Frede Blaabjerg, and Pedro Rodr´ıguez. Control of Power Converters in AC Microgrids. IEEE TRANSACTIONS ON POWER ELECTRONICS, VOL. 27, NO. 11, NOVEMBER 2012.

[8] Xiong Liu, Peng Wang, and Poh Chiang Loh, “A Hybrid AC/DC Microgrid and Its Coordination Control,” IEEE Trans. Smart Grid, vol. 2, no. 2, pp. 278-286 June. 2011.

[9] Justo, J. J., Mwasilu, F., Lee, J., & Jung, J. W. Ac-micro-grids versus dc-micro-grids with distributed energy resources: A review. Renewable and Sustainable Energy Reviews, 24, 2013.

[10] R. Pena, J. C. Clare, G. M. Asher, “Doubly fed induction generator using back to back PWM converters and its application to variable speed wind energy generation,” in Proc. IEE Electr. Power Appl., vol. 143, no. 3, pp. 231-241, may 1996.

[11] D. P. Hohm, M. E. Ropp. “Comparative Study of Maximum Power Point Tracking Algorithms Using an Experimental, Programmable, Maximum Power Point Tracking Test Bed”, in IEEE, pp.1699-1702, 2000.

[12] D. Sera, R. Teodorescu, J. Hantschel, and M. Knoll. “Optimized maximum power pointtracker for fast-changing environmental conditions,” IEEE Trans. Ind. Electron., vol.55, no. 7, pp. 2629-2637, Jul. 2008.

[13] Math H.J. Bollen, Understanding Power Quality Problems, Voltage Sags and Interruptions, Willey India Pvt Ltd, ISSN 8126530391, 2011.

[14] G.Mehta and S. P. Singh, Power quality improvement through grid integration of renewable energy sources, IETE Journal of Research, vol. 59, no. 3, p. 210–218, 2013.

[15] Sood VK. HVDC and FACTS Controllers: Applications of Static Converters in Power Systems. Kluwer Academic Publishers 2004.

[16] Nkusi Emest. Flexible AC Transmission System (FACTS) Devices. ISBN-10: 3639853407, ISBN-13:9783639853407, AV Akademikerverlag, 10 August 2015.

[17] Kabilan Ramachandran, P. Suresh. Concept of FACTS (Flexible AC Transmission System). Laxmi Publications Pvt Ltd, ISBN: 9789384872298, 9384872296, 2016.

[18] Showkat Ahmad Dar. Flexible AC Transmission System. Onlinegatha, ISBN-10: 9385818732, ISBN-13: 978-9385818738, 2016.

[19] B. K. Bose, “Modern Power Electronics and AC Drives,” Prentice-Hall, Inc., New Delhi, 2002.

[20] Keith H. Sueker. Power Electronics Design: A Practitioner’s Guide. ISBN 0-7506-7927-1, TK7881.15.S84 2005, SciTech Publishing Inc, 2005.

[21] E. Acha, V.G. Agelidis, O. Anaya-Lara, T.J.E. Miller. Power Electronic Control in Electrical Systems. Newnes power engineering series. ISBN 0 7506 5126 1, 2002

[22] Fraidoon Mazda. Power Electronics Handbook. ISBN 0 7506 2926 6. An imprint of Elsevier Science, editions 1990, 1993, 1997.

[23] Muhammad H. Rashid. Power Electronics Handbook Devices, Circuits, and Applications. ISBN 978-0-12-382036-5, TK7881.15.P6733 2010, Elsevier Inc. Editions 2007, 2011.

[24] J. David Irwin. The Power Electronics Handbook. Industrial Electronics Series, CRC PRESS, Boca Raton London New York Washington, D.C., ISBN 0-8493-7336-0, TK7881.15 .P673 2001,2002.

[25] C.C. Marouchos. The Switching Function: analysis of power electronic circuit. DOI: 10.1049/PBCS017E, ISBN: 97808634135513, E-ISBN: 9781849190190, ID code 4444, IET, 2006.

[26] D. Grahame Holmes, Thomas A. Lipo. Pulse Width Modulation for Power Converters Principles and Practice. IEEE Series on Power Engineering, ISBN 0-471-20814-0, 2003.

[27] Fazel SS. Investigation and comparison of multi-level converters for medium voltage applications. Ph.D. Thesis, Berlin Technical University 2007.

[28] HATZIARGYRIOU N.D., MELIOPOULOS A.P.S., Distributed energy sources: technical challenges. Proc. IEEE PES Winter Meeting, New York, vol. 2, pp. 1017–1022, 2002.

[29] LASSETER R.H., Micro-grid. Proc. IEEE PES Winter Meeting, New York, vol. 1, pp. 305–308, 2002.

[30] Petersson, A., Harnefors, L., &Thiringer, T., "Evaluation of Current Conntrol Methods for Wind Turbines Using Doubly-Fed Induction Machines," IEEE Transactions on Power Electronics vol. 20, no. 1, 227–235 January 2005.

[31] J. Murphy, F. Turnbull, Power Electronics Control of AC Motors, Pergamon Press, 1988.

[32] Lingling Fan, Zhixin Miao, Subbaraya Yuvarajan, Rajesh Kavasseri, Hybrid modeling of DFIGs for wind energy conversion systems, Simulation Modelling Practice and Theory 18, 1032–1045, 2010.

[33] DUFFEY C.K., STRATFORD R.P., Update of harmonic standard IEEE-519: IEEE recommended practices and requirements for harmonic control in electric power systems, IEEE Trans. Ind. 25, (6), pp. 1025–1034, Appl., 1989.

[34] ENJETI P.N., ZIOGAS P.D., LINDSAY F., Programmed PWM techniques to eliminate harmonics: a critical evaluation, IEEE Trans. Ind. (2), pp. 302–316, Appl., 1990, 26.

[35] MAHROUS E.A., RAHIM N.A., HEW W.P., Three phase three level voltage source inverter with low based on the two level inverter topology, IET Electr. Power, 1, (4), pp. 637– 641, Appl., 2007.

[36] Jesmin F. Khan, Sharif M. A. Bhuiyan, Kazi M. Rahman, Gregory V. Murphy, Space vector PWM for a two-phase VSI. International Journal of Electrical Power and Energy Systems 51, 265-277, 2013.

[37] MOHAN N., UNDELAND T.M., ROBBINS W.P., Power electronics: converters, applications and design, Willy, New York, 3rd ed, 2003.

[38] P. Acharjee, S.K. Goswami, Expert algorithm based on adaptive particle swarm optimization for power flow analysis, Expert Syst. Appl. 36, 5151–5156, April 3, 2009.

[39] Erhan Butun, Tarik Erfidan, Satilmis Urgun, Improved power factor in a low-cost PWM single phase inverter using genetic algorithms, Energy conversion and Management 47, 1597-1609, 2006.

[40] J.A. Ghaeb, M.A.Smadi, M. Ababneh, Progressive decrement PWM algorithm for minimum mean square error inverter output voltage, Energy conversion and Management 52, 3309-3318, 2011.

[41] Sidney R.Bowes, Sukhminder sing Grewal, Novel Space-Vector-Based Harmonic Elimination Inverter Control, and IEEE Transactions on Industrial application, vol. 36, no. 2, March/April. 2000.

[42] Alinaghi Marzoughi, Hossein Imaneini, Amirhossein Moeini, An optimal selective harmonic mitigation technique for high power converters. International Journal of Electrical Power and Energy Systems 49, 34-39, 2013.

[43] K. Al-Othman, Nabil A. Ahmed, M. E. Alsharidah, Hanan A. AlMekhaizim, A hybrid real coded genetic algorithm- Pattern search approach for selective harmonic elimination of PWM AC/AC voltage controller. International Journal of Electrical Power and Energy Systems 44, 123-133, 2013.

[44] S.Yuvarajan, Lingling Fan, A doubly-fed induction generator-based wind generation system with quasi-sine rotor injection, Journal of Power Source 184, 325-330, 2008.

[45] Lingling Fan, Subbaraya, Rajesh Kavasseri, Harmonic Analysis of DFIG for a Wind Energy Conversion System, IEEE Transactions on Energy Conversion. vol. 25, no. 1, March. 2010.

[46] Yong Liao, Li Ran, Ghanim A. Putrus, Kenneth S. Smith, Evaluation of the effects of rotor harmonics in a Doubly- Fed Induction Generator With harmonic Induced Speed Ripple, IEEE Transactions on Energy Conversion, vol. 18, no. 4 ,December. 2003.

[47] J. Sun, H. Grotstollen, Solving nonlinear equations for selective harmonic eliminated PWM using predicted initial values, in: Proc. Int. Conf. Ind. Electro. Cont. Instrum. Automat, 259–264, 1992.

[48] Euzeli dos Santos, Edison R. da Silva . Advanced Power Electronics Converters: PWM Converters Processing AC Voltages (IEEE Press Series on Power Engineering). ISBN-13: 978-1118880944, ISBN-10: 1118880943, Nov 24, 2014.

[49] J.R. Wells, B.M. Nee, P.L. Chapman, P.T. Krein, Selective harmonic control: a general problem formulation and selected solutions, IEEE Trans. Power Electron. 20, 1337–1345, November 6, 2005.

[50] V.G. Agelidis, A. Balouktsis, C. Cosar, Multiple sets of solutions for harmonic elimination PWM bipolar.

[51] Waveforms: analysis and experimental verification, IEEE Trans. Power Electron. 21, 415–.421, March 2, 2006.

[52] Dan Simon, Biogeography Based Optimizations, IEEE Transactions on Evolutionary Computation, vol. 12, no. 6, December. 2008.

[53] Mohamed S.A. Dahidah, Vassilios G. Agelidis, Machavaram V. Rao. Hybrid genetic algorithm approach for selective harmonic control, Energy conversion and Management 49, 131-142, 2008.

[54] A.K.Al-Othman, Tamer H. Abdelhamid, Elimimination of harmonics multilevel inverters with non-equal dc sources using PSO, Energy conversion and Management 50, 756-764, 2009.

[55] A.I. Maywood, S. Wei, M.A. Rahman, A flexible way to generate PWM-SHE switching patterns using genetic algorithm, in: Proc. IEEE Appl. Power Electron. Conf., 1130–1134, 2001.

[56] B. Ozpineci, L.M. Tolbert, J.N. Chiasson, Harmonic optimization of multilevel converters using genetic algorithms, in: Proc. IEEE Power Electron. Spec. Conf., 3911–3916, 2004.

[57] Khaled El-Naggar, Tamer H. Abdelhamid, Selective harmonic elimination of new family of multilevel inverters using genetic algorithms, Energy conversion and Management 49, 89-95, 2008.

[58] J.C. Hernández, J. De la Cruz, B. Ogayar, Electrical protection for the grid-interconnection of photovoltaic-distributed Generation, Electric Power Systems Research 89, 85– 99, 2012.

[59] M.J. Ortega, J.C. Hernandez, O.G. Garcia, Measurement and assessment of power quality characteristics for photovoltaic systems: Harmonics, flicker, unbalance, and slow voltage variations, Electric Power Systems Research 96, 23– 35, 2013.

[60] Rup Narayan Ray, Debashis Chatterjee, Swapan Kumar Goswami, An application of PSO technique for harmonic elimination in a PWM inverter, Applied Soft Computing 9, 1315-1320, 2009.

[61] Alireza Hoseinpour, S. Masoud Barakati, Reza Ghazi, Harmonic reduction in wind turbine generators using a shunt Active Filter based on the proposed modulation technique. International Journal of Electrical Power and Energy Systems 43, 1401-1412, 2012.

[62] M.Valan Rajkumar, P. S. Manoharan, A Ravi, Simulation and experimental investigation of SVPWM technique on multilevel voltage source inverter for photovoltaic system. International Journal of Electrical Power and Energy Systems 52, 116-131, 2013.

[63] S. A. Azmi, G. P. Adam, K. H. Ahmed, S.J. Finney, and B. W. Williams, Grid Interfacing of Multi-megawatt Photovoltaic Inverters, IEEE transaction on Power Electronics, vol. 28, No. 6 June 2013.

[64] George J. Wakileh, Power System Harmonics, Fundamentals, Analysis and Filter Design, Springer, 2001.

[65] EN 50160. Voltage characteristics of electricity supplied by public distribution systems; 2004.

[66] CIGRE JWG C4.07, Power quality indices and objectives; 2004.

[67] IEC 61000-3-6: Assessment of emission limits for distorting loads in MV and HV power systems, technical report type 3, 1996.

[68] Heng Nian, Yu Quan, Jiabing Hub, Improved control strategy of DFIG-based wind power generation systems connected to a harmonically polluted network, Electric Power Systems Research 86 (2012) 84-97.

[69] E. G. Shehata, Gerges M. Salama, Direct power control of DFIGs based wind energy generation systems under distorted grid voltage conditions, International Journal of Electrical Power and Energy Systems 53 (2013) 956-966. 59

[70] Nashed, M. N., &Eskander, M. N., "Comparing the Quality of Power Generated from DFIG with Different Types of Rotor Converter," Journal of Electromagnetic Analysis and Applications, 4, 21-29, 2012.

[71] Krishna Sarker, Debashis Chatterjee, S. K. Goswami, "An optimized co-ordinated approach for harmonic minimization of Doubly Fed Induction Generator connected micro-grid system," International Journal of Electrical Power &Energy Systems, vol. 64, pages 58-70, January 2015.

[72] Paice, Derek A. Power Electronic Converter Harmonics, IEEE press, 1995.

[73] Dorin O. Neacsu. Switching Power Converters: Medium and High Power, Second Edition. ISBN-13: 978-1138075719, Mar 31, 2017.

[74] Adrian Ioinovici .Power Electronics and Energy Conversion Systems, Fundamentals and Hard-switching Converters. Volume 1, Wiley, ISBN-10: 0470710993, ISBN-13: 978-0470710999, Jun 10, 2013.

[75] Soo-Hyoung Lee, Jung-Wook Park. New Islanding Detection Method for Inverter- Based Distributed Generation Considering Its Switching Frequency. IEEE Trans. On industry application, Vol. 46, No. 5. 2010.

[76] Ion Boldea. Variable Speed Generators. ISBN-13: 978-0849357152,ISBN-10: 0849357152, CRC Press; 1 edition November 9, 2005.

[77] Christian Feltes , Advanced Fault Ride-through Control of DFIG Based Wind Turbines Including Grid Connection Via VSC-HVDC (Berichte aus der Energietechnik). Shaker Verlag GmbH, ISBN-13: 978-3844009712, May 1, 2012.

[78] Junwei Lu, Xiaojun Zhao, Sotoshi Yamada .Harmonic Balance Finite Element Method: Applications in Nonlinear Electromagnetics and Power Systems. Wiley-IEEE Press; 1 edition, ISBN-10: 1118975766, ISBN-13: 978-1118975763, October 3, 2016.

[79] Wells, J. R., Nee, B. M., Chapman, P.L., &Krein, P. T., "Selective harmonic control: a general problem formulation and selected solutions," IEEE Trans. Power Electron. 20 (6)), 1337–1345, November 2005.

[80] Agelidis, V.G., Balouktsis, A., &Cosar, C., "Multiple sets of solutions for harmonic elimination PWM bipolar waveforms: analysis and experimental verification," IEEE Trans. Power Electron. 21 (2), 415–421, March 2006.

[81] Tamer H. Abdelhamid and Khaled M. El-Nagger, "Optimal PWM control of a New Generalized Family of Multilevel Inverters," Electric Power Components and systems, 36: 73-92, 19 Dec 2007.

[82] Sundareswarn K., "Line Current Harmonic Elimination and Voltage Control of PWM AC/DC Converter Using a Hybrid Genetic Algorithm," Electric Power Components and systems, 35: 119-133, 23 Feb 2007.

[83] Islam Abdelqawee. A Selective Harmonic Elimination PWM Inverter Feeding Dynamic Loads. Noor Publishing, ISBN-10: 3330844647, ISBN-13: 978-3330844643, December 28, 2016.

[84] Wells J. R., Geng X., Chapman P. L., Krein P. T., & Nee B. M., "Modulation based harmonic elimination," IEEE Trans. Power Electron., 22, pp. 336-340, 2007.

[85] Mohamed Boutoubat, LakhdarMokrani, and Mohamed Machmoum, "Full Capability of Harmonic Current Mitigation for a Wind Energy System," Electric Power Components and systems, 42: 1743-1753, 20 Oct 2014.

[86] Jalal Amini, "Disturbance Rejection and Harmonics Reduction of Doubly Fed Induction Generator Based Wind Energy Conversion Systems," Electric Power Components and systems, 40: 1423-1444, 10 Sep 2012.

[87] Yujun Zheng and Xueqin Lu. Biogeography-Based Optimization: Algorithms and Applications. ISBN-13: 978-9811325854, ISBN-10: 9789811325854, Springer; 1st ed. 2019 edition ,September 15, 2018.

[88] Lingling Fan , Zhixin Miao . Modeling and Analysis of Doubly Fed Induction Generator Wind Energy Systems. Publisher: Academic Press; 1 edition, ISBN-10: 9780128029695, ISBN-13: 978-0128029695, ASIN: 0128029692, May 5, 2015.

[89] Ali Emadi .Handbook of Automotive Power Electronics and Motor Drives. ISBN-13: 978-0824723613, ISBN-10: 0824723619, Electrical and Computer Engineering ,25 May 2005.

[90] M. Lindholm and T. Rasmussen, "Harmonic analysis of doubly fed induction generators," in Proc. 5th Int. Conf. Power Electron. Drive Syst., vol. 2, pp. 837–841, Nov. 2003.

[91] Y. Baghouz and M. Azam, "Harmonic analysis of slip power recovery drives," IEEE Trans. Ind. Appl., vol. 28, no. 1, pp. 50–56, Jan./Feb. 1992.

[92] JawadFaiz, H. Barati and EyupAkpinar, "Harmonic analysis and performance improvement of slip energy recovery induction motor drives", IEEE Trans. POW. Elec., vol. 16, no. 3, pp. 410–417, May 2001.

[93] Qiuwei Wu, Yuanzhang Sun. Modeling and Modern Control of Wind Power (Wiley - IEEE) 1st Edition. Wiley-IEEE Press; 1 edition, ISBN-10: 9781119236269, ISBN-13: 978-1119236269, ASIN: 1119236266, February 5, 2018.

[94] Narain G. Hingoranl, Laszlo Gyugyi, Understanding FACTS Concepts and Technology of Flexible AC Transmission Systems. IEEE, IEEE PRESS, ISBN 0-7803-3455-8 IEEE Order No. peS'13 TK3148.H54 1999.

[95] K. R. Padiyar. FACTS CONTROLLERS IN POWER TRANSMISSION AND DISTRIBUTION. ISBN (13): 978-81-224-2541-3, ,Publishing For One World New Age International (P) Limited Publishers, 2007.

[96] Xiao-Ping Zhang, Christian Rehtanz, Bikash Pal. Flexible AC Transmission Systems: Modelling and Control. ISBN-10 3-540-30606-4, Springer Berlin Heidelberg New York, ISBN-13 978-3-540-30606-1 Springer Berlin Heidelberg New York, 2005, Springer-Verlag Berlin Heidelberg 2006.

[97] Enrique Acha, Claudio R. Fuerte-Esquivel, Hugo Ambriz-Pe´rez, Ce´sar Angeles-Camacho, FACTS Modelling and Simulation in Power Networks. John Wiley & Sons Ltd, The Atrium, Southern Gate, Chichester, West Sussex PO19 8SQ, England. ISBN 0-470-85271-2, 2004.

[98] Kalyan K. Sen, Mey Ling Sen. Introduction To Facts Controllers Theory, Modeling, and Applications. ISBN 978-0-470-47875-2 (cloth), TK3148.S46, Printed in the United States of America, IEEE Press, Published by John Wiley & Sons, Inc., Hoboken, New Jersey, 2009.

[99] R. M. Mathur and R. K. Varma, Thyristor-Based FACTS Controllers for Electrical Transmission Systems. New York: IEEE Press and Wiley, 2002.

[100] Y. H. Song and A. T. Johns, Flexible AC Transmission Systems (FACTS). London, The Institution Of Engineering And Technology, IEE Power Series, 30, ISBN: 9780852967713, 0852967713, UK: IEE, 1999.

[101] Akshay Kumar .DFIG-based Wind Power Conversion System Connected to Grid. GRIN Publishing, ISBN-10: 3656720290, ISBN-13: 978-3656720294, September 15, 2014.

[102] Om Prakash Bharti. Modeling and Control of DFIG-based Variable Speed Wind Turbine: DFIG-Based wind turbine. ISBN-10: 9783659279157, ISBN-13: 978-3659279157, ASIN: 3659279153, LAP LAMBERT Academic Publishing, October 17, 2012.

[103] Edgar N. Sanchez . Riemann Ruiz-Cruz . Doubly Fed Induction Generators: Control for Wind Energy .**ISBN-10:** 1498745849, **ISBN-13:** 978-1498745840. CRC Press; 1 edition, October 10, 2016.

[104] Francisco C. De La Rosa. Harmonics, Power Systems, and Smart Grids. CRC Press; 2 edition, ISBN-10: 1482243830, ISBN-13: 978-1482243833, Apr 20, 2015.

[105] R. N. Roy, D. Chatterjee, S. K. Goswami. Harmonic elimination in a multilevel inverter using the partical swarm optimization technique. IET power electron, Vol. 2. Lss. 6, pp. 646-652, 2009.

[106] Mude Kishore Naik .Development Of Svpwm Controller For Three Level Inverter. LAP LAMBERT Academic Publishing, ISBN-10: 9783659315077, ISBN-13: 978-3659315077, ASIN: 3659315079, December 28, 2012.

[107] Pedro Roncero-Sanchez, Enrique Acha. Dynamic Voltage Restorer Based on Flying Capacitor Multilevel Converter Operated by Repetitive Control IEEE Transactions on power delivery. Vol. 24, No. 2. April 2009.

[108] A. Ravi, P. S. Manoharan, J. Vijay Anand. Modeling and simulation of three phase multilevel inverter for grid connected photovoltaic system. Solar Energy 85, 2811-2818, 2011.

[109] Visscr A. J., Enslin J.H.R., Mouton H. T. Transformer less series sag compensation with a cascade multilevel inverter. IEEE Trans. Ind. Electron., 49, (4), pp. 824-831, 2002.

[110] Meyer C., Romaus C., DcDocker R. W. Five level neutral-point clamped inverter for a dyanamic voltage restorer. Proc. European Conf. on Power Electronics and Applications, 2005.

[111] M. Bollen. Understanding Power Quality Problems: Voltage Sag and Interruptions. New York: IEEE Press, 1999.

[112] T.H.E. Miller, Reactive Power Control in Electrical Systems, Book John Willy & Sons, Ins., Toronto, Canada, 1982.

[113] Abdul Balikci, Eyup Akpinar. A multilevel converter with reduced number of switches in STATCOM for load balancing. Electric Power Systems Research 123, 164-173,2015.

[114] Srinivas Bhaskar Karanki, Nagesh Geddada, Mahesh K. Mishra, Kalyan Kumar. A Modified Three-Phase Four-Wire UPQC Topology with Reduced DC-Link Voltage Rating. IEEE transaction on industrial electronics, vol. 60, No. 9 September 2013.

[115] Vinod Khadkikar. Enhancing Electric Power Quality Using UPQC: A Comprehensive Overview IEEE transaction on power electronics, vol. 27, No. 5 may 2012

[116] B. Han, B. Bae, H. Kim, S. Baek. Combined Operation of Unified Power- Quality Conditioner with Distributed Generation. IEEE Transaction on power delivery, Vol. 21, No. 1, March 2006.

[117] C. K. Sundarabalan, K. Selvi. Compensation of voltage disturbances using supported Dynamic Voltage Restorer. Electrical Power and Energy Systems 71, 77-92, 2015.

[118] Mostafa I. Marei, Ayman B. Eltantawy, Ahmed Abd El-Satter. An energy optimized control seheme for a transformerless DVR. Electric Power Systems Research 83,10-118, 2012.

[119] Ahmed M. Massoud, Shehab Ahmed, Prasad N. Enjeti, Barry W. Williams. Evaluation of a Multilevel Cascaded-Type Dynamic Voltage Restorer Employing Discontinuous Space Vector Modulation. IEEE transaction on industrial electronics, vol. 57, No. 7, July 2010.

[120] M. Ramasama, S. Thangavel. Experimental verification of PV based Dynamic Voltage Restorer (PV-DVR) with significant energy conservation. Electrical Power and Energy Systems 49, 296-307, 2013.

[121] Dan Simon, Evolutionary Optimization Algorithms. Wiley; 1 edition, ISBN-10: 0470937416, ISBN-13: 978-0470937419, April 29, 2013.

[122] N. Amutha, B. Kalyan Kumar. Improving fault ride-through capability of wind generation system using DVR. Electrical Power and Energy Systems, 46, 326-333, 2013.

[123] K.K. Matrawy, A. F. Mahrous, M. S. Youssef. Energy management and parametric optimization of an integrated PV solar house. Energy conversion and management, Volume 96, Pages 377-383, 15 May 2015.

[124] D. A. G. Vieira, L. S. M. Guedes, A. C. Lisboa, R.R. Saldanha. Formulations for hydroelectric energy production with optimality conditions. Energy conversion and management, Volume 89, Pages 781-788, 1 Januray 2015.

[125] P. Campo, T. Benitez, U. Lee, J. N. Chung. Modeling of biomass high temperature steam gasifier integrated with assisted solar energy and a micro gas turbine. Energy conversion and management, Volume 93, Pages 72-8315 March 2015.

[126] B. Kiran, R. Kumar, D. Deshmukh. Perspectives of microalgal biofuels as a renewable source of energy. Energy conversion and management, Volume 88, Pages 1228-1244, December 2014.

[127] F. Cao, H. Li, Q. Ma, L. Zhao. Design and simulation of a geothermal-solar combined chimney power plant. Energy conversion and management, Volume 84, Pages 186-195, August 2014.

[128] Sundarabalan CK, Selvi K. Compensation of voltage disturbances using PEMFC supported dynamic voltage restorer. Int J Electr Power Energy Syst, 71:77-92, 2015.

[129] Ali Ajami, M. Armaghan. Fixed speed wind fram operation improvement using current-source converter based UPQC. Energy conversion and management, Volume 58, Pages 10-18, June 2012,.

[130] N.H. Woodly, L. Morgan, and A. Sundaram, 'Experience with an inverter-based dynamic voltage restorer', IEEE Trans. Power Del., vol. 14, no. 3 pp. 1181-1186, Jul. 1999.

[131] Xinbo Ruan. Soft-Switching PWM Full-Bridge Converters: Topologies, Control, and Design. Wiley; ISBN-10: 1118702204, ISBN-13: 978-1118702208, Jun 23, 2014.

[132] Hussain Bassi. PWM Schemes with Two Switching Frequencies to Reduce THD. Noor Publishing, ISBN-10: 3330841567, ISBN-13: 978-3330841567, Dec 21, 2016.

[133] Teodorescu R, Beaabjerg F, Pedersen JK, Cengelci E, Sulistijo SU, Woo BO, et al. Multilevel converters-a survey. In: Proceedings on EPE conference; p. 2–11, 1999.

[134] K.S. Gayathri Devi, S. Arun, C. Sreeja. Comparative study on different five level inverter topologies. Electrical Power and Energy Systems 63, 363–372, 2014.

[135] Haiping Ma, Dan Simon. Evolutionary Computation with Biogeography-based Optimization (Metaheuristics Set). Wiley-ISTE; 1 edition, ISBN-10: 9781848218079, ISBN-13: 978-1848218079, ASIN: 1848218079, February 6, 2017.

[136] Brindha, R.; Kavita, R. “Harmonic optimization in seven level inverter employing hybrid BBO/MADS algorithm,” in International Conference on Inovations in Information, Embedded and Communication Systems (ICIIECS), March 2015.

[137] Kavita, R., Thottungal R. “WTHD minimization in hybrid multilevel inverter using biogeographical based optimization, Archives of Electrical Engineering, vol. 63, no 2, 187-196, 2014.

[138] Boualem Boukezata, Jean-Paul Gaubert, Abdelmadjid Chaoui, Mabrouk Hachemi. Predictive current control in multifunctional grid connected inverter interfaced by PV system. Solar Energy 139, 130-141, 2016.

[139] Zheng Zeng, Huan Yang, Rongxiang Zoh, Chong Cheng. Topologies and control strategies of multi-functional grid connected inverters for power quality enhancement: A comprehensive review. Renewable and Sustainable Energy Reviews 24, 223-270, 2013.

[140] Renata Carnieletto, Siddharth Suryanarayanan, Marcelo G Simões, Felix A. Farret. A multifunctional Sinsle-Phase Voltage Source Inverter in Perspective of the Smart Grid Initiative. Industry Applications Society Annual Meeting, IAS 2009, Pages: 1-7, 2009.

[141] M. Ramasamy, S. Thangavel. Experimental verification of PV based Dynamic Voltage Restorer (PV-DVR) with significant energy conservation. International journal of Electrical Power & Energy Systems, 46, 296-307, 2013.

[142] Taghzaded, H.; Hagh, M. T. Harmonic elimination of multilevel inverters using particle swarm optimization. IEEE International Symposium on Industrial Electronics, pp. 393-396, 2008.

[143] Jowder FAL. Design and analysis of dynamic voltage restorer for deep voltage sag and harmonic compensation. IET Gener Transm Distrib, 3:547-60, 2009.

[144] Manik Pradhan, Mahesh K. Mishra. Dual P-Q Theory based Energy Optimized Dynamic Voltage Restorer for Power Quality Improvement in Distribution System. IEEE Transactions on Industrial Electronics, DOI 10.1109/TIE.2018.2850009, Jun 1, 2018.

[145] Mohammad Farhadi Kangarlu, Ebrahim Babaei. A Generalized Cascaded Multilevel Inverter Using Series Connection of Sub-multilevel Inverters. IEEE Transactions on Power Electronics, VOL. 28, NO. 2, FEBRUARY 2013.

[146] Natarajan Prabaharan, Kaliannan Palanisamy. Analysis of cascaded H-bridge multilevel inverter configuration with double level circuit. IET Power Electronics, Vol. 10 Iss. 9, pp. 1023-1033, 2017.

[147] Raid Kadri, Horia Andrer, Jean-Paul Gaubert, Traian Ivanovici, Gerard Champenois, Paul Andrei. Modeling of the photovoltaic cell circuit parameters for optimum connection model and real-time emulator with partial shadow conditions. Energy 42, 57-67, 2012.

[148] A. Bouilouta, A Mellit, S. A. Kalogirou. New MPPT method for stand-alone photovoltaic systems operating under partially shaded conditions. Energy 55, 1172-1185, 2013.

[149] Krismadinata, Nasrudin Adb. Rahim, Hew Wooi Ping, Jeyraj Selvaraj. Photovoltaic module modeling using simulink/ matlab. Procedia Environment Sciences 17 , 537-546, 2013.

[150] Mehdi Dali, Jamel Belhadj, Xavier Roboam. Hybrid solar-wind system with battery storage operating in grid-connected and standalone mode: Control and energy management-Experimental investigation. Energy 35, 2587-2595, 2010.

[151] Roger C. Dugan , Mark F. F. Mcgranaghan , Surya Santoso, H. Wayne Beaty. Electrical Power Systems Quality. McGraw-Hill Education; 3 edition, ISBN-10: 0071761551, ISBN-13: 978-0071761550, 1 March 2012.

[152] H. Akagi. Trends in active power line conditioners. IEEE Trans. Power Electron., vol. 9, no. 3, pp. 263-268, May 1994.

[153] Arindam Ghosh, Amit Kumar Jindal, Avinash Joshi. A Unified Power Quality Conditioner for Voltage Regulation of Critical Load Bus. IEEE Power Engineering Society General Meeting, **ISBN:** 0-7803-8465-2 ,6-10 June 2004.

[154] Suresh Mikkili , Anup Kumar Panda .Power Quality Issues: Current Harmonics. CRC Press; 1st Edition, ASIN: B012VL32GO, 14 August 2015.

[155] Abdul Balikci, Eyup Akpinar. A multilevel converter with reduced number of switches in STATCOM for load balancing. Electric Power Systems Research 123, 164-173, 2015.

[156] L. Gyugyi, C. D. Schauder, S. L. Williams, T. R. Rietmen, D. R. Torgerson, A. Edris. The Unified Power Quality Controller: A New Approach to Power Transmission controller. IEEE Trans. Power Delivery, vol. 10, no. 2, Pp. 1085-1093, Apr.1995.

[157] C. K. Sundarabalan, K. Selvi. Compensation of voltage disturbances using supported Dynamic voltage Restorer. Electrical Power and Energy Systems 71, 77-92, 2015.

[158] Mostafa I. Marei, Ayman B. Eltantawy, Ahmed Abd El-Satter. An energy optimized control seheme for a transformerless DVR. Electric Power Systems Research 83, 10-118, 2012.

[159] Ahmed M. Massoud, Shehab Ahmed, Prasad N. Enjeti, Barry W. Williams. Evaluation of a Multilevel Cascaded-Type Dynamic voltage Restorer Employing Discontinuous Space Vector Modulation. IEEE transaction on industrial electronics, vol. 57, No. 7, July 2010.

[160] M. Ramasama, S. Thangavel. Experimental verification of PV based Dynamic Voltage Restorer (PV-DVR) with significant energy conservation. Electrical Power and Energy Systems 49, 296-307, 2013.

[161] Ahmed F. Zobaa , Shady Hossam Eldeen Abdel Aleem,Power Quality in Future Electrical Power Systems. Energy Engineering, The Institution of Engineering and Technology, ISBN-10: 1785611232, ISBN-13: 978-1785611230, March 24, 2017.

[162] Ali Ajami, Hossein Shokri, Ataollah Mokhberdoran. Parallel switch-based chopper circuit for DC capacitor voltage balancing in diode-clamped multilevel inverter. IET Power Electronics, Volume: 7, Issue: 3, 503 – 514, 2014.

[163] Muhammad Jafar ; Marta Molinas ; Takanori Isobe ; Ryuichi Shimada.Transformer-Less Series Reactive/Harmonic Compensation of Line-Commutated HVDC for Offshore Wind Power Integration. IEEE Transactions on Power Delivery, Volume: 29, Issue: 1 , 353 – 361, Feb. 2014.

[164] C.Bharatiraja, S. Jeevananthan, R. Latha. FPGA based practical implementation of NPC-MLI with SVPWM for an autonomous operation PV system with capacitor balancing. International Journal of Electrical Power & Energy Systems, Volume 61, 489-509, October 2014.

[165] J. Dionisio Barros, Fernando Silva. Multilevel Optimal Predictive Dynamic Voltage Restorer. IEEE transaction on industrial electronics, vol. 57, No. 8. August 2010.

[166] Fang Lin Luo , Hong Ye. Advanced DC/AC Inverters: Applications in Renewable Energy. Power Electronics, Electrical Engineering, Energy, and Nanotechnology, CRC Press; 1 edition, ISBN-10: 1466511354, January 22, 2013.

[167] M. Valan Rajkumar, P. S. Manoharan. FPGA based multilevel cascaded inverters with SVPWM algorithm for photovoltaic system. Solar Energy 87, 229-245, 2013.

[168] B. R. Lin, J. Y. Dong. New zero voltage switching DC-DC converter for renewable energy conversion systems. IET Power Electron., vol. 5, lss. 4, pp. 293-400, 2012.

[169] Yi-Ping Hsieh, Jiann-Fuh Chen, Tsorng-Juu Liang, Lung-Sheng Yang. A Novel High Step-Up DC-DC Converter for a Microgrid System. IEEE Transactions on power electronics. Vol. 26, No. 4. April 2011.

[170] Srinivas Bhaskar Karanki, Nagesh Geddada, Mahesh K. Mishra, Kalyan Kumar. A Modified Three-Phase Four-Wire UPQC Topology with Reduced DC-Link Voltage Rating. IEEE transaction on industrial electronics, vol. 60, No. 9 September 2013.

[171] Susarla Venkata Ananta Rama Sastry, K Srinivasa Ravi Kumar Power quality improvement using UPQC: Modeling and Simulation. LAP LAMBERT Academic Publishing, ISBN-10: 9783330079236, ISBN-13: 978-3330079236, ASIN: 3330079231, 25 April 2017.

[172] S. Tamalouzt, N. Benyahia, T. Rekioua, D. Rekioua, R. Abdessemed. Performances analysis of WT-DFIG with PV and fuel cell hybrid power sources system associated with hydrogen storage hybrid energy system. International journal hydrogen energy 41, 21006-21021, 2016.

Krishna Sarker